STUDIES ON THE APPLICATIONS OF THE TRIPLE-TO-DOUBLE COINCIDENCES RATIO METHOD FOR PRIMARY ACTIVITY STANDARDIZATION USING LIQUID SCINTILLATION COUNTING

CHAVDAR DUTSOV

A Dissertation
Submitted to the Department of Atomic Physics

Sofia University "St. Kliment Ohridski"

In Partial Fulfilment of the Requirements for the Degree of
Doctor of Philosophy

Under the Supervision of Assoc. Prof. Krasimir Mitev

Sofia, Bulgaria
July 2021

Studies on the applications of the Triple-to-Double Coincidences Ratio method for primary activity standardization using liquid scintillation counting

Chavdar Dutsov

SUPERVISOR:
Assoc. Prof. Krasimir Mitev

LOCATION:
Sofia University "St. Kliment Ohridski"
Department of Atomic Physics
Sofia, Bulgaria

TIME FRAME:
July 2018 – July 2021

ACKNOWLEDGEMENTS

Foremost, I would like to express my sincere gratitude to my supervisor Krasimir Mitev. He was a great mentor all the way from my first measurements of radon absorbing polymers on the RackBeta to the completion of this thesis. My university experience would not have been the same without his motivation, drive and passion for science.

I would like to pay my special regards to Phillipe Cassette for his guidance and ever fruitful discussions during my time at LNHB or over distance. I would also like to thank him for always encouraging me to try things I never did before, such as FPGA programming or PCB design. This work would not have been possible without him.

I would also like to thank Benoît Sabot for his help and support, and for being so pleasant to work with him.

My sincere regards must go to Valentin Jordanov. Though we did not have as much chances to work together as I would have liked, he was an inspiration and someone to look up to all throughout my time as a doctoral student.

I am very grateful to the team at LNHB, and especially Sylvie Pierre, Marie-Christine Lépy, Martin Loidl, Xavier Mougeot and Christophe Dulieu for all their positivity, encouragement and support during my stay there.

Many thanks also to my colleagues from Sofia University – Strahil Georgiev, Vladislav Todorov and Ivelina Dimitrova – for the friendly and cooperative working environment they help to create.

Thanks to Ivo Iliev, Tsvetelina Ivanova and Vasil Todorinov, my friends and also doctoral students at the time, for the always interesting discussions on physics, science and life in general.

The work on this thesis – from the initial data analysis to the final typesetting – was done using exclusively free & open source software. I would like to thank the community for building such powerful tools that everyone can benefit from.

I want to express my gratitude towards Boriana Chtirkova for always supporting me and being beside me all throughout my PhD – both when everything was going smoothly and in more challenging times.

Finally, I would like to thank my mother, Irina Zaharieva, for all her support during my studies and for giving me the opportunity to do what I love.

CONTENTS

ACRONYMS

SI	Système International d'unités/International System of Units
TDCR	triple-to-double coincidences ratio
LS	liquid scintillation
PMT	photomultiplier tube
EC	electron capture
FOM	figure of merit
C-TDCR	Compton coincidences and TDCR
ZoMBieS	zero model by using coincidence scintillation
CSET	Compton spectrometer efficiency tracing
CNET	CIEMAT/NIST efficiency tracing[1]
CdTe	cadmium telluride
CDT	common dead-time
IDT	individual dead-times
FWHM	full width at half-maximum
FPGA	field-programmable gate array
CFD	constant fraction discriminator
MAC_3	module d'acquisition de coïncidences triples
nanoTDCR	front-end digital pulse processing device for TDCR counting[2]
RCTD1	the French primary TDCR counter[3]
TDCR-SU	TDCR counter developed and operated at Sofia University
ICRU	International Commission on Radiation Units
DDEP	Decay Data Evaluation Project
BIPM	The International Bureau of Weights and Measures
LNHB	*Laboratoire National "Henri Becquerel"*
MIL	"Metrology of Ionizing Radiation" laboratory at Sofia University

1 The name comes from the two institutions that worked on the method – CIEMAT (Spain) and NIST (USA).
2 It is developed by Valentin Jordanov from the labZY company.
3 The acronym comes from the french *rapport de coïncidences triple à double* meaning triple to double coincidences ratio.

INTRODUCTION

METROLOGY is the science of measurement, embracing both experimental and theoretical determinations at any level of uncertainty in any field of science and technology[1]. It has its roots as far back as Ancient Egypt, where the success of the large construction projects of the time relied on consistent measurements. This was achieved by standard rods of equal length – the *royal cubit*, the earliest attested standard measure for length.

Throughout history the need to synchronize measurements was always present, and so, many local standards and units appeared and disappeared all over the world. However, up until the 18^{th} century there was no universal measurement system. This was changed in 1795 with the creation of the decimal-based metric system in France by the law "on weights and measures". It followed the newly formed definition of the *metre* as the length of one ten-millionth part of the distance from Earth's equator to its north pole – the first unit which in its determination was neither arbitrary nor related to any particular nation on the globe. The adoption of the metric system expanded with time, and, to ensure conformity between the different countries, the The International Bureau of Weights and Measures (BIPM) was formed [1].

The metric system has evolved into the International System of Units, abbreviated as SI from the French *Système International d'unités*. It consists of seven base units, which are the second (time, s), metre (length, m), kilogram (mass, kg), ampere (electric current, A), kelvin (thermodynamic temperature, K), mole (amount of substance, mol) and candela (luminous intensity, cd). As of 2019, the magnitude of all SI units are defined by exact numerical values for seven constants when expressed in terms of the corresponding SI units. These are the speed of light in vacuum c, the hyperfine transition frequency of caesium $\Delta\nu_{Cs}$, the Planck constant h, the elementary charge e, the Boltzmann constant k, the Avogadro constant N_A, and the luminous efficacy K_{cd}. Except the seven base units, there are 22 derived units with special names and symbols, which can also be used. One of these units is the unit for radioactivity – the becquerel Bq. It corresponds to the mean number of radioactive decays per unit time of a radioactive source. One becquerel is equal to one decay per second [1].

The becquerel can be regarded a special unit, due to the nature of the radioactive decay, which is the process by which unstable or excited nuclei lose energy by emission of one or more subatomic particles. There is a large variety of possibilities for the type of the emission resulting from a radioactive decay: β^+ and β^-, α-particles, neutrons, fission products, X-rays and γ-rays, Auger electrons and neutrinos. Some radioactive decays result in a single emission and some in a cascade of emissions, each of a different type. Of the possible particles, there are some that have electric charge and some that are

1 Source: BIPM website (Archived)

neutral. Their masses span from the massless photons and almost-massless neutrinos to the heavy α-particles and even heavier fission products. The effect of the emission on the surrounding medium can be felt from micrometers to hundreds of meters. Moreover, there is a huge variety in the radioactive isotopes themselves – from the lightest elements to the heaviest nuclei – which can be found in numerous chemical compounds and in all states of matter. For these reasons, there could be no single universal realization of the standard for the becquerel unit. Thus, the standardization techniques are usually specifically tailored to the radionuclide of interest.

One largely used measurement platform, however, is liquid scintillation (LS) counting since many radionuclides can be incorporated into a mixture with a liquid scintillator. This provides a 4π geometry for detecting the emitted radiation and significantly increases the detection efficiency. The exact variant of liquid scintillation detection technique used for primary standardization depends on the properties of the radionuclide. For γ-ray emitting radionuclides, coincidence methods can be used to determine the activity. For pure β, electron capture (EC) or mixed decays, the triple-to-double coincidences ratio (TDCR) method is applied, which uses ratios of measured coincidences to produce robust results. This is precisely the main focus of this thesis – the primary standardization of radioactivity using the TDCR method, what are some well known or newly discovered aspects of it, what difficulties are encountered and how they can be solved.

STRUCTURE OF THE DISSERTATION

The thesis is structured in three parts and twelve chapters. The first part serves as an overview of the field of radionuclide metrology using LS counting. The second and third parts contain the original work in the scope of the thesis. A short overview of the contents of each part is as follows:

In Part I, an overview of liquid scintillators and liquid scintillation counting in general are given. The emphasis is placed on radioactivity standardization methods and the TDCR method in particular.

Part II focuses on the time domain in LS counting and the distribution of the time intervals between detected scintillations in a LS detector in particular. First, a program, that has been developed for the analysis of digitizer list-mode data, is presented in Chapter 3. The following Chapter 4 describes a comparison of two algorithms to process coincidences and dead-times in a detector with three photomultiplier tubes (PMTs). Chapter 5 contains a derivation of the statistical distribution of the time intervals between detected prompt fluorescence events. The derived equations were verified using a dedicated Monte Carlo code, developed in the framework of the thesis and presented shortly in Appendix A. It is shown how this distribution could be used to estimate the detection efficiency in LS measurements using the free parameter model. The next chapter, Chapter 6, deals exclusively with experimental studies on the

derived equations and their application to real measurements. The possibility to use the newly developed theory to supplement standardizations using the TDCR method is discussed. Some applications of the time interval distributions to routine LS counting measurements are also shown.

Part III focuses on how the information from the distribution of the time intervals between detected events can be used in radionuclide metrology and the TDCR method in particular. Chapter 7 presents methods for precise measurements of the half-life of some nuclear excited states, namely the long-lived states in ^{57}Co and ^{237}Np, using LS counting and analysis of the resulting time distributions. The time information from LS measurements is utilized to develop an experimental method to evaluate the counting rate of accidental coincidences in a TDCR detector is presented in Chapter 8. Besides the experimental method, theoretical equations to evaluate the accidental coincidences are also developed and verified in the same study. Chapter 9 deals with the influence of the delayed fluorescence on the activity calculated by the TDCR method. The studies demonstrate the problems encountered in the standardization of low-energy emitters such as ^{3}H and ^{55}Fe. Chapter 10 shows the development and characterization of a new Compton coincidences and TDCR (C-TDCR) system for primary standardization of LS samples. The system was used to study the response of commercial liquid scintillators to electrons with energies in the range from 2 keV to 8 keV. The possibility to use this information in ^{3}H standardizations is also discussed. Chapter 11 outlines some practical applications of the TDCR method which are used in the "Metrology of Ionizing Radiation" laboratory at Sofia University to ensure metrological assurance of LS measurements.

Finally, Chapter 12 contains a brief summary of what has been presented in the thesis and highlights the important conclusions of the work. Some future directions for study are also stated. Additionally, some complementary information and measurements are shown in three appendices placed at the end of the thesis.

Part I

RADIONUCLIDE METROLOGY USING LIQUID SCINTILLATION COUNTING

1 LIQUID SCINTILLATION COUNTING

Liquid scintillation counting is the measurement of the activity of a radioactive material dissolved in a liquid scintillator by counting the rate of resulting light pulses. The solution is usually contained in glass or polyethylene vials, the common volumetric capacity being 20 ml. The scintillations coming from the vial are then measured on purposefully designed detectors called liquid scintillation (LS) counters. Most detectors are equipped with an optical chamber that houses the sample during measurement and photomultiplier tubes (PMTs), that register the scintillation events. The events are recorded for a certain time period and the counting rate of the sample is given as an output. The detection efficiency ε gives the relationship between the net (background corrected) counting rate n_0 and the activity A, where

$$A = \frac{n_0}{\varepsilon}. \tag{1.1}$$

As the radioactive source is practically within the active volume of the detector, the detection efficiency of LS measurements is relatively high. It is close to 100% for α-emitting radionuclides and for high-energy β-emitting radionuclides. However, it could be significantly lower for electron capture (EC) and low-energy β-emitters. For such radionuclides the detection efficiency ε must be known with high accuracy in order to calculate the activity of the source. A common way to measure the detection efficiency is to calibrate the detector with a source with activity that is known with low uncertainty and traceable to a primary standard. The calibration sources, however, are also measured by LS counting to determine their activity. As the efficiency in that case is unknown, a model of the light emission of the liquid scintillator and the detection of that light by the PMTs is necessary. Such a model was developed in the 1980s by Broda et al. and Malonda et al. [2, 3] based on previous works [4–6] and is called *the free parameter model*. It is the basis of all methods currently employed in the field of radionuclide metrology using LS counting[1].

LS counting is especially suited for the detection and measurement of activity of pure EC or β-emitters such as ^{3}H, ^{14}C, ^{55}Fe, ^{63}Ni and others[2]. Since the only emission from such nuclides is a charged particle, their decay cannot be detected from a more than a few centimeters if there is a medium between the source and detector. LS counting has the advantage in that regard as the radionuclide is dissolved in a solvent that absorbs the energy of the charged particles and transfers it to the scintillating molecules.

As usual in nature, the major advantage of LS counting comes with its own set of drawbacks. As the source is dissolved in the LS, the preparation technique plays a

1 The free parameter model is described in depth in Section 2.1.

2 A more comprehensive list can be found in the last paragraph of this chapter.

major role in what would be the detection efficiency. Taking ^{3}H for example, it usually comes in the form of tritiated water, i. e., water molecules in which one of the ^{2}H atoms is replaced with ^{3}H. In order to be possible to dissolve the water in the organic liquid, the scintillation cocktails usually contain some form of surfactant. Depending on the amount of water that is added to the liquid scintillator, its properties would change, which in turn affects the detection efficiency. Moreover, in practice, the water that is dissolved in the cocktail is taken from the environment and has to be purified beforehand. Even if a strict procedure is followed, small fluctuations in the preparation process will lead to LS samples with different detection efficiencies.

In this chapter a brief overview of all the components of a LS measurement will be given.

1.1 LIQUID SCINTILLATORS

Liquid scintillators are organic compounds that are developed to emit light when an ionizing particle interacts with them. Most organic scintillators of practical interest consist of aromatic molecules in which three of the valence electrons of carbon are hybridized in the sp^3 configuration and one p electron is left unchanged. The hybridized electron orbitals are also known as σ electrons and their bonds as σ bonds. This configuration of σ bonds forms the planar ring structure of benzene and other aromatic hydrocarbons. The unchanged p electron orbitals are symmetric with respect to the plane of the molecule and are called π electrons and their bonds – π bonds respectively [7].

The σ hybridized electron orbitals interact with each other in such a way as to produce localized C – H and C – C bonds. The π orbitals form delocalized molecular orbitals – six in the case of benzene (see Figure 1.1). Similar systems of delocalized π orbitals occur also in other aromatic molecules and their excited states are the reason for the luminescence of these molecules. Moreover, the individual molecules are loosely bound to one another by Van der Waals forces and due to that excitation in one molecular can be easily transferred to another. The effect of the energy transfer is important for liquid scintillators consisting of more than one type of molecule. In the two component systems a small amount of very efficient scintillator (primary fluorophore) is added to a large quantity of organic solvent. The solvent absorbs the bulk of the energy dissipated in the solution, and, through interactions between the molecules, the excitation energy can eventually reach one of the efficient scintillator's molecules which will lead to light emission with a high probability [8]. The emission spectra of the primary fluorophore is usually in the range of UV light, where the quantum efficiency of photomultiplier tubes is somewhat low. In order to improve the efficiency of light detection a small amount of secondary scintillator is also added that shifts the emission spectra to longer wavelengths. Such substances are called wavelength shifters and are added in concentrations that are an order of magnitude lower than that

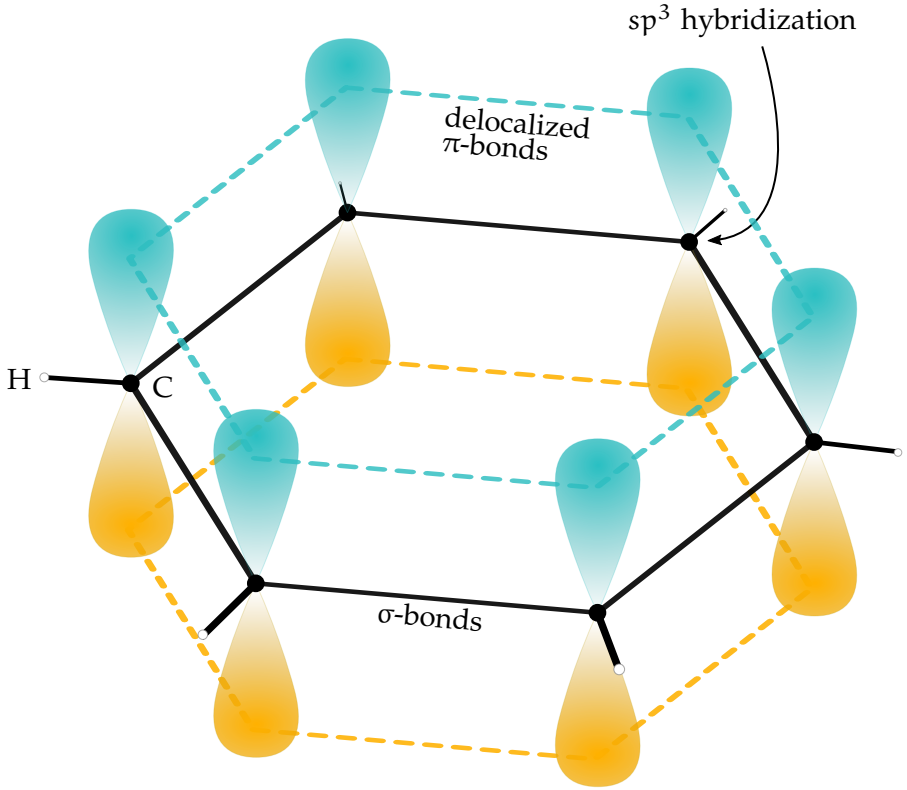

FIGURE 1.1: Schematic representation of a benzene molecule.

of the primary fluorophore. The energy transfer between the primary fluorophore and the wavelength shifter is purely radiative.

The path that the energy takes – from the kinetic energy of the charged particle passing through the scintillation cocktail to the luminescence photons emitted from it – is a complex one. In fact, only a small fraction of the kinetic energy of the particle is converted to fluorescent energy. The large remaining fraction is dissipated non-radiatively as vibrational excitations or heat. As a charged particle with sufficient energy passes through the mixture of scintillators, it leaves a trail of molecules with π electrons in their excited states. The concentrations of the primary fluorophore and the wavelength shifter are minuscule in comparison with the solvent thus it can be considered to a good approximation that the charged particle interacts only with the molecules of the solvent. The kinetic energy can be transferred to two types of excited states, singlet or triplet, which is the basis of the two main types of fluorescence light that is observed – prompt and delayed fluorescence.

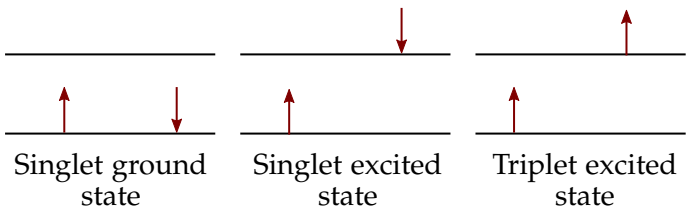

FIGURE 1.2: Electrons with paired (singlet) or unpaired (triplet) spins.

A singlet state (S_n) is a molecular electronic state in which all electron spins are paired, even on different energy levels. That is, the spin of an excited electron is still paired with that of the ground state electron. As per the Pauli exclusion principle, a pair of electrons on the same energy level must have opposite spins. In a triplet state the excited electron is not paired with the ground state electron and their spins are parallel. This is schematically shown in Figure 1.2. The origin of the term *singlet* comes from the field of spectroscopy, and it reflects that systems with net zero angular momentum emit photons with a single wavelength, i. e., a single line appear in the spectrum. This is opposed to double and triple lines in doublet and triplet states respectively.

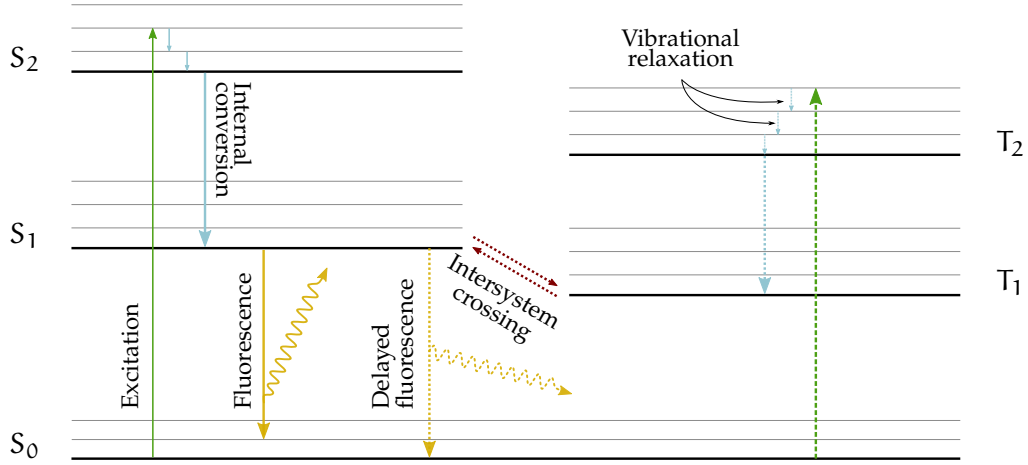

FIGURE 1.3: Schematic representation of the photoluminescence pathways. The solid lines show the path leading to prompt fluorescence and the dashed lines to delayed fluorescence.

The ratio of excited triplet states to excited singlet states, after the molecules of the solvent have absorbed the kinetic energy of the passing particle, is 3:1 as there are three times more available triplet states than singlet states. In a singlet state the spin quantum number of the system is $s = 0$, and thus, there is only one allowed value of the spin component, $m_s = 0$. In a triplet state $s = 1$ and so m_s could be -1, 0 or $+1$. The fluorescent molecules are usually excited in their higher excited S_n and T_n states, but they quickly recombine to S_1 and T_1 via internal conversion. It refers to a transition from a higher to a lower electronic state without the emission of a photon and the de-excitation energy is transformed into heat. The typical timescale of the process is 10^{-10} to 10^{-11} s. Internal conversion happens between states with the same multiplicity. The transitions between states of different multiplicity (e. g., $S_n \longleftrightarrow T_n$) are referred to as intersystem crossing [9].

Despite there being three times as much triplet compared to singlet states, the radiative emission from T states is much rarer than for S states, because the de-excitation from T_1 to S_1 is a forbidden transition. Molecules in the T_1 state can still emit light, after undergoing intersystem crossing to the S_1 state. This is illustrated in Figure 1.3.

Prompt fluorescence, or simply fluorescence, is the emission of a photon from the transition from the S_1 excited state to the S_0 ground state of a molecule. The life-

time of the S_1 state is in the order of a nanosecond to a few nanoseconds which is long in comparison with the life-time of the vibrational S_n states for the molecule. Their life-time is in the range of 10^{-12} s and so the molecule reaches thermodynamic equilibrium before the emission that occurs from the S_1 state. In other words, the energy from the charged particle can be transferred to any of the singlet energy states of the π electron $S_1, S_2, \cdots, S_n$, but the levels above S_1 undergo rapid and effective non-radiative transfers between adjacent excited states (internal converted). Thus, a molecular S_n state is quickly converted to an S_1 state via internal energy transfer between states and the dissipation of remaining vibrational energy [7].

In the context of liquid scintillation counting, in the 1950s, it was seen that prompt fluorescence cannot explain the total of scintillation light that was observed. According to Birks [7], Voltz [10] and Wright [11] it is necessary to consider another distinct component of the scintillation light. The second scintillation component results from de-excitation of S_1 states produced by T_1 states after intersystem crossing. The T_n states have a lower energy than the corresponding S_n states, due to the additional energy that is "contained" in the de-coupled spins. Thus, in order for the $T_1 \rightarrow S_1$ migration to happen, some amount of energy that corresponds to the difference in the energies of the two levels must be absorbed. Depending on the separation of the levels, this could be thermal energy, and this process is called *thermally activated delayed fluorescence*. It is the focus of ongoing research related to the manufacturing of highly efficient organic light emitting diodes [12–14]. In the more commonly used organic scintillators, the favored pathway is the triplet-triplet annihilation, i. e., bimolecular interaction between molecules in the lowest excited triplet state T_1 [7]. The probability for this process is usually lower than for the prompt fluorescence due to the need for the interaction of two molecules in the T_1 state. The lower probability leads also to a lower emission intensity. The process of triplet-triplet annihilation is also controlled by the diffusion of excited states and is slower than the exponential de-excitation of S_1, hence the name *delayed fluorescence*.

In fact, the picture described in Figure 1.3 is very simplified. Commonly used scintillators do not consist of only one specie (solvent), but also have a small amount of a highly efficient fluorescent molecule (primary fluorophore) with its excited states F_n. It is also possible to have some quantity of a quenching chemical Q that efficiently absorbs excitation energy. Thus, there are many possible pathways that the absorbed kinetic energy of the ionizing particle can take. Most of them ($\approx$ 99%) lead to the dissipation of the energy as heat. After the formation of the S_1 and T_1 states, at a timescale of a few ns, the main energy transfer phenomena, that present practical interest in the context of LS counting, can be summarized by the following equations[3]:

1. $S_1 \rightarrow S_0$ or $S_1 + S_0 \rightarrow S_0 + S_0$ — de-excitation of singlets
2. $S_1 + S_0 \rightarrow S_0 + S_1$ — energy migration in the solvent (can also involve excimer formation and dissociation [16])

3 They are the same mentioned by Voltz and Laustriat [15], but neglecting the reactions with low probability.

3. $S_1 + Q \rightarrow S_0 + Q$ chemical quenching of singlets
4. $T_1 \rightarrow S_0$ de-excitation of triplets
5. $T_1 + Q \rightarrow S_0 + Q$ chemical quenching of triplets
6. $T_1 + T_1 \rightarrow S_1 + S_0$ annihilation triplet-triplet creating a singlet state
7. $T_1 + T_1 \rightarrow T_1 + S_0$ annihilation triplet-triplet
8. $S_1 + F_0 \rightarrow F_1 + S_0$ energy transfer to the fluorescent molecule (Förster process)
9. $F_1 \rightarrow F_0 + h\nu$ de-excitation of the fluorescent molecule and light emission

Inside a LS cocktail, the distribution of solvent molecules in their ground state S_0, molecules of the primary fluorophore F_0 and molecules of the quencher Q is homogeneous. This is not the case for the excited states S_1 and T_1. They are localized in small volumes around the track of the particle, especially at time scales of about 10^{-10} s. At this stage, the higher excited states S_2, S_3, ..., S_n can interact with one-another and recombine non-radiatively [16]. According to Voltz and Laustriat [15], no significant bimolecular $S_1 + S_1 \rightarrow S_0 + S_0$ happen in that time period[4]. The recombination process of closely formed excited states is termed *ionization quenching*, and its prominence depends on the local concentration of excitations – the higher the concentration, the more likely it becomes. This introduces a dependence of the light output of the scintillator on the stopping power of the particle. The ionization quenching phenomenon is central to LS measurements and will be discussed in-depth later.

It should be noted that this ionization quenching phenomenon is not the same for T_1 species. For them the bimolecular reaction 7. is favored by the local concentration of F_1 states. This reaction is in competition with 6. which causes delayed fluorescence. That is, for increased density of triplet excited states, the quenching of triplet states becomes stronger, but, at the same time, the probability for triplet–triplet interaction increases. Birks [7], noticed that: "The ionization quenching mainly affects the intensity of the fast scintillation component, and has much less effect on the intensity of the slow component". This implies that the ionization quenching is not similar for the singlets and triplets states.

The typical lifetime of S_1 states is a few nanoseconds. This is much shorter than the lifetime of T_1 states, typically a few hundreds of ns, depending on the nature of the solvent. The lifetime of F_1 states is lower than a ns and generally the quantum yield of equation 9. is high. The primary fluorescent molecule is very efficient and its radiative de-excitation probability is close to one. The time dependence of the intensity of the two scintillation components will be discussed in the next paragraphs.

4 The main argument supporting this assertion is that the ionization quenching does not affect S_1 lifetime.

1.1.1 *Time dependence of the scintillation intensity*

The intensity of fluorescence in a single component scintillator decreases exponentially with time following the law [7]:

$$I = I_0 e^{-t/\tau}, \tag{1.2}$$

where I_0 is the initial light output at time $t = 0$ and τ is the fluorescence life-time. The time dependence of the scintillation intensity of delayed fluorescence is significantly more complex than that of the prompt as it is controlled by the diffusion process of triplet states. A schematic representation of the time dependence of the two scintillation components is shown in Figure 1.4.

Most scintillators of practical interest are two or three component systems with a solvent, primary fluorophore and a wavelength shifter. For such systems the simple exponential decay law from equation (1.2) will be an approximation. The scintillation emission for the more complex systems has a finite rise time, due to the speed of the energy transfer between the solvent and fluorophore. For a binary system the prompt fluorescence scintillation intensity with time $I_p^{(b)}(t)$ is given by [7]:

$$I_p^{(b)}(t) = n_0 \frac{a_{sf}^{(r)}/\tau_s^{(r)} + 1/\tau_{sf}}{1/\tau_s - 1/\tau_f} \left(e^{-t/\tau_f} - e^{-t/\tau_s} \right), \tag{1.3}$$

where n_0 is the initial number of excited solvent molecules, τ_f is the radiative decay time of the fluorophore, τ_s is the non-radiative decay time of the solvent, τ_{sf} is the non-radiative energy transfer time between the solvent and fluor, $\tau_s^{(r)}$ is the natural radiative life-time of the solvent and $a_{sf}^{(r)}$ is the probability that the emission of the solvent will be absorbed by the fluorophore. The overall shape of equation (1.3) is an exponential decay with a finite rise time, governed by the non-radiative decay time of the solvent. The rise and decay time of the two component system depends on the solvent and fluor molecules. For the common combination DIN + PPO[5] the rise time is in the order of 1 ns and the decay time between 2.5 and 7 ns [17].

Probably, the most comprehensive attempts to quantify the intensity of the delayed component with time can be found in the work of King & Voltz [19]. In this work the time dependence of delayed fluorescence is modeled with a diffusion kinetic equation describing the local density of delayed singlet states $c_s'(r,t)$:

$$\frac{\delta c_s'(r,t)}{\delta t} = D_s \nabla_r^2 c_s'(r,t) - \frac{1}{\tau_s} c_s'(r,t) + k_u c_T^2(r,t), \tag{1.4}$$

where the term $k_u c_T^2(r,t)$ describes the production of delayed singlet states by the bimolecular interaction between two T_1 states. The equation is solved with the initial condition that $c_s'(r,0) = 0$. The initial distribution of the triplet states is derived for two cases: one for particles with low stopping power for which the ionizations are far apart and there is no interaction between them and two for particles with high linear energy

5 DIN + PPO stands for the mixture of diisopropyl naphthalene and 2,5-diphenyloxazole

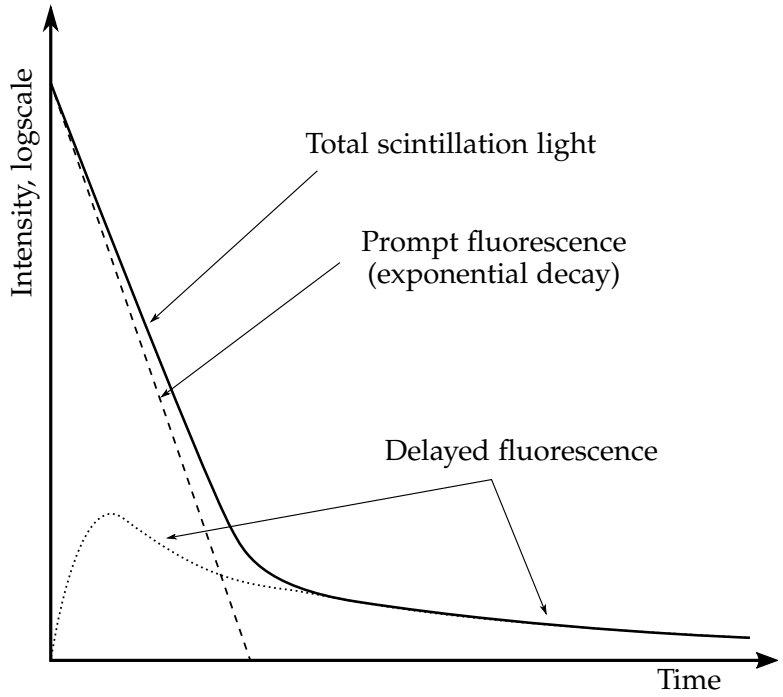

FIGURE 1.4: Schematic representation of the prompt and delayed emissions to the total scintillation light. Figure adapted from [18].

transfer for which the created ionizations are close to each other. The former case is considered for electrons and the latter for α-particles and heavy ions. The solution of equation (1.4) is derived after assumptions for Gaussian distribution of the excited states along the particle track and for time t long enough so that the triplet relaxation in the track is mainly diffusion controlled – i. e., after the triplet-triplet annihilation seizes to be the dominant process. The solution given in the work of King & Voltz is:

$$I'(t) = C\frac{N_T(0)}{\left\{1+\frac{t_d}{\sqrt{2}t_{tt}}\left[1-\left(1+\frac{t}{t_d}\right)^{-\frac{1}{2}}\right]\right\}^2\left(1+\frac{t}{t_d}\right)^{\frac{3}{2}}}, \tag{1.5}$$

where t_d is the delayed fluorescence decay time, $N_T(0)$ is the initial concentration of triplet states and t_{tt} is the triplet-triplet annihilation relaxation time. Since t_{tt} is inversely proportional to dE/dx, for particles with low stopping power it could be reasonable to assume that $\frac{t_d}{\sqrt{2}t_{tt}}\left[1-\left(1+\frac{t}{t_d}\right)^{-\frac{1}{2}}\right] \ll 1$. Under such assumptions the equation is reduced to:

$$I'(t) = \frac{M}{(1+t/t_d)^{\frac{3}{2}}}. \tag{1.6}$$

It should be stressed, however, that this simplification should be reasonable only for t that is long enough so that effects of the initial conditions are negligible. This excludes the finite rise time of the delayed scintillation light.

1.1.2 *Ionization quenching*

The density of the excitations produced in the scintillator depends on the linear energy transfer of the particle. The higher the stopping power is, the higher the excitation density. This leads to decreased efficiency of the scintillator, an effect known as "ionization quenching", which is similar in all types of organic scintillators [7]. Due to it, the light output of the scintillator depends on the linear energy transfer of the particles – it is highest for high-energy electrons and lowest for α-particles and heavy nuclei. Moreover, for a given particle, the intensity of the emitted light changes non-linearly with the energy. There are a few attempts to describe the ionization quenching behaviour with respect to the energy and type of particle.

The most widely used model is a semi-empirical formula proposed by Birks and is known as Birks' law [7]:

$$\frac{dI}{dx} = \frac{\eta_0 \frac{dE}{dx}}{1 + kB \frac{dE}{dx}}, \tag{1.7}$$

where x is the range of the particle in the scintillator, dE/dx is the particle's stopping power, η_0 is the absolute scintillation efficiency, which is the ratio of the sum of energies of all photons emitted during the scintillation event to the energy released in the cocktail. The specific density of the ionized and excited molecules along the trajectory of the particle is $kB\frac{dE}{dx}$, where kB is the ionization quenching parameter and is measured in units cm/MeV or µm/MeV. Birks' law for the ionization quenching was proposed as a description of the intensity of the prompt fluorescence. According to Birks, the ionization quenching has much less effect on the intensity of the slow component (see section 3.5 in [7]).

Equation (1.7) was generalized by Chou, introducing a term proportional to the square of the stopping power [20]:

$$\frac{dI}{dx} = A\frac{dE}{dx}\left[1 + B\frac{dE}{dx} + C\left(\frac{dE}{dx}\right)^2\right]^{-1}. \tag{1.8}$$

Another expression was also proposed by Wright with the form [11]:

$$\frac{dI}{dx} = \frac{A}{2B}\ln\left[1 + 2B\frac{dE}{dx}\right]^{-1}. \tag{1.9}$$

These equations were proposed for the description of the prompt fluorescence component, largely disregarding the delayed fluorescence. An attempt to describe both scintillation components was done by Voltz et al. The total scintillation intensity with respect to the stopping power of electrons is given as [10]:

$$\frac{dI}{dx} = \eta_s\left[\frac{1}{W_s}\frac{dE}{dx}e^{-B_s\frac{dE}{dx}} + \alpha\frac{\Phi_t}{W_t}\frac{dE}{dx}e^{-B_t\Phi_t\frac{dE}{dx}}\right], \tag{1.10}$$

where W_s and W_t are the mean energies required to produce a singlet S_1 and a triplet T_1 states, respectively. B_s and B_t are quenching parameters for the prompt and delayed

fluorescence and Φ_t is the part of the energy lost by the ionizing particle, per unit path length, to activate triplet states of molecules that will participate in a triplet-triplet interaction. Generally, the first summation term of the equation deals with the prompt fluorescence and the second with the delayed fluorescence.

Equation (1.10) presents great interest as the expansion in powers of $B_s \frac{dE}{dx}$, up to the second order, resembles greatly the other proposed equations (1.7), (1.9) and (1.8). Thus, it leads to similar results for the prompt fluorescence, but it also adds a description of the delayed fluorescence. All equations, except for (1.7), are rarely used in practice, because they introduce more unknown parameters. Thus, albeit possibly recognizing only a part of the scintillation light, Birks' law is the most commonly adopted model describing the non-linearity of organic scintillators.

The fluorescence yield of the scintillator according to Birks' law is given by

$$L(E) = \eta_0 \int_0^E \frac{dE}{1 + kB(dE/dx)} = \eta_0 E Q(E), \tag{1.11}$$

where $Q(E)$ is the ionization quenching function

$$Q(E) = \frac{1}{E} \int_0^E \frac{dE}{1 + kB(dE/dx)}. \tag{1.12}$$

There are some problems which arise when calculating Birks' ionization quenching function: the choice of an optimal value of the ionization quenching parameter kB, calculation of the values of the stopping power for energies under 1 keV and the lack of precise knowledge of the atomic composition and density of the used scintillator, which are necessary for the calculation of the stopping power dE/dx.

The stopping power can be regarded as the force that acts on charged particles due to its electromagnetic interactions with the surrounding matter that results in a loss of the particle's energy [21, 22]. dE/dx is defined as the average energy dissipated by an ionizing particle per unit path length in a medium [23]. The stopping power of a particle in a given material, in the case where its energy transfers are smaller than some cut-off value W_c, can be calculated using the Bethe formula [24]:

$$\frac{dE}{dx} = \frac{2\pi r_e^2 mc^2}{u} \frac{\rho}{\beta^2} \frac{Z}{A} z^2 \left[\ln\left(\frac{2mc^2 \beta^2 W_c}{(1-\beta^2) I^2} - \beta^2 \right) \right], \tag{1.13}$$

where ρ denotes the density of the material in units $g\,cm^{-3}$, $u = 1.6605655 \times 10^{-24}$ is the atomic mass unit, r_e is the classical electron radius, mc^2 is the rest mass of the electron, β is the velocity of the particle divided by the velocity of light, z is the projectile charge, and I is the mean excitation energy of the medium. The equation is valid when the velocity of the projectile is large compared to the velocities of the atomic electrons [25].

For electrons and positrons the stopping power in units $MeV\,cm^{-1}$ can be calculated using the formula given in the International Commission on Radiation Units (ICRU) report №37 [25]:

$$\frac{dE}{dx} = \frac{2\pi r_e^2 mc^2}{u} \frac{\rho}{\beta^2} \frac{Z}{A} \left[\ln(E/I)^2 + \ln(1 - \tau/2) + F^-(\tau) - \delta \right], \tag{1.14}$$

where τ is the ration of the kinetic energy of the electron E to its rest mass, δ is a density-effect correction which accounts for the reduction of the stopping power due to the polarization of the medium. Here $F^-(\tau)$ is given by:

$$F^-(\tau) = (1-\beta^2)\left[1 + r^2/8 - (2r+1)\ln 2\right]. \tag{1.15}$$

TABLE 1.1: Compositions of some commercial scintillators produced by Perkin Elmer [26].

Cocktail	C	H	N	O	P	S	Na	Density g cm^{-3}	Z/A	Molecular weight
UltimaGold	16.81	24.54	0.040	1.52	0.11	0.02	0.02	0.98	0.5459	255.76
UltimaGold XR	18.11	29.80	0.035	2.83	0.11	0.03	0.03	0.99	0.5476	297.98
UltimaGold AB	18.67	28.49	0.010	2.53	0.01	0.00	0.00	0.98	0.5485	293.47
UltimaGold LLT	18.57	28.43	0.010	2.56	0.01	0.00	0.00	0.98	0.5486	292.68
InstaGel Plus	18.53	30.93	0.006	3.90	0.00	0.00	0.00	0.95	0.5490	315.71
HionicFluor	10.83	18.77	0.060	1.97	0.18	0.04	0.04	0.95	0.5449	188.87

Important parameters in equation (1.14) are the Z/A ratio and density ρ of the medium. One practical problems is that if commercial LS cocktails are used, and such is usually the case, the exact chemical composition is a trade secret. Fortunately, some information is given by the manufacturers or can be found in the literature [27]. The elemental composition for some commonly used cocktails produced by Perkin Elmer are given in Table 1.1.

1.2 PHOTOMULTIPLIER TUBES

Another important component of the LS counting system is the detector of the fluorescence light. Many kinds of light sensors exist, but the best suited for low-intensity and low-noise applications, such as LS counting, is the photomultiplier tube (PMT). A PMT is a vacuum tube that consists of a transparent window, a photocathode, focusing electrodes, an electron multiplier and an anode [28]. The PMT is probably the most important part of any LS detector system. It converts incident photons into electrical signals via the following processes: photons pass through the transparent window and excite electrons in the photocathode which are emitted in the vacuum; the photoelectrons are accelerated by the potential difference between the cathode and anode; they are focused by the focusing electrodes onto the first dynode, where they are multiplied via secondary electron emission; this process repeats at every dynode step; at the final step, the secondary electrons that are emitted by the last dynode are collected at the anode. A schematic representation of the construction of a PMT is shown in Figure 1.5.

PMTs have several important characteristics, in the context of LS counting, such as the photocathode and window materials, the quantum efficiency, the current amplification

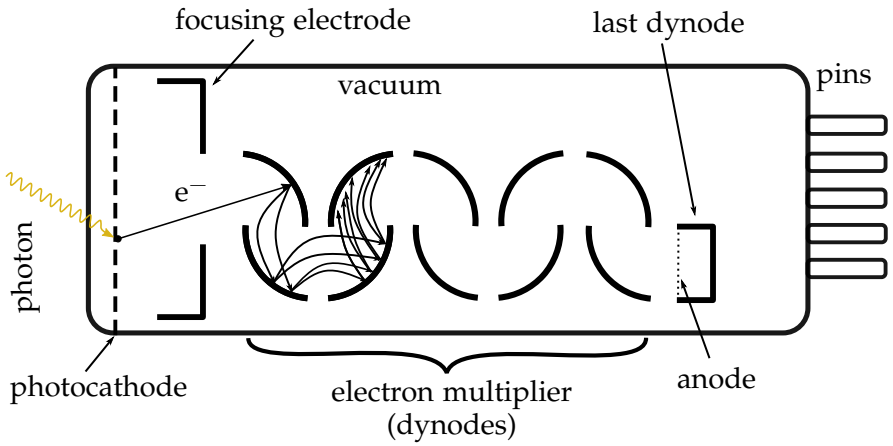

FIGURE 1.5: Schematic representation of a construction of a PMT.

(gain), the dark current and the time characteristics. Photocathodes are usually made of compound semiconductors which consist of alkali metals with a low work function [28]. An overview of the kinds of photocathodes currently employed in practical applications is given in [28]. The most commonly used window material is borosilicate glass. The preferred type for LS counting is that which contains reduced amount of potassium, which has a long-lived radioactive isotope – ^{40}K. More specialized UV transmitting window materials are required for the purpose of detection of Čerenkov light. The quantum efficiency ε_q is the ratio of the number of photoelectrons emitted from the photocathode to the number of incident photons. It is generally expressed as percent and typical values for PMTs used in LS applications are between 20% and 40%. Generally, the higher the quantum efficiency, the better – especially in the case of three-PMT systems, where the probability to register a triple coincidence is proportional to ε_q^3.

The amount of light that has to be detected in most LS counting applications is very low – in the order of a few photons per keV energy released in the cocktail. Therefore, single photon sensitivity is preferred in conventional LS counting. It is mandatory, however, for its application to radioactivity metrology, as the used models assume that the detection efficiency for single photons is not zero and that 100% of the photoelectrons produce a detectable signal, i. e., significantly above the noise level. Thus, the gain of PMTs used for metrological applications must be as high as possible ($> 10^6$), while keeping the dark current and electrical noise low. The threshold of the electronics that analyzes the PMT signals should be set in such a way that the electrical noise is minimized while still preserving 100% of the single photoelectron signal. This is achievable with PMTs that have a good separation between the two [29].

Often, when a pulse from a PMT is observed, it is followed by a series of smaller parasitic pulses called *afterpulses*. They can be due to light that is emitted from one of the dynodes that reaches the photocathode and produces further photoelectrons. Another possible origin of afterpulses is the residual gas sometimes found in PMTs, which can be ionized by the passage of electrons. The positive ions that are formed can drift in the reverse direction and interact with the photocathode, thereby causing

a new electron avalanche. In practice, in order to prevent the detection of afterpulses, a dead-time of at least 10 µs is imposed after each detected signal or at the end of each coincidence window. For the same reason, within a coincidence window in a multple-PMT detector, only the first event that is detected from a given PMT is regarded and all others are being ignored.

The important time characteristics of PMTs are the rise time, fall time and transient time spread. Generally, the PMT is a photodetector with an exceptionally fast time response. The rise time of a typical PMT pulse is in the order of 1–2 ns and the fall time is two to three times larger than that [28]. The transient time spread is the distribution of the time of generation of PMT pulses with respect to the single photons that generate them. The typical full width at half-maximum (FWHM) for that distribution is 300 – 500 ps. The time characteristics of the used PMTs are usually of no concern in conventional LS counting, but are very relevant when the precise timing of events is required[6].

1.3 LIQUID SCINTILLATION COUNTERS

LS counters are detection systems consisting of two or more PMTs that are housed in an optical chamber and are targeted towards a LS vial containing the sample of interest. The optical chamber is a housing with reflective inner walls that is used to focus as much of the light that is emitted from the sample as possible into the opening windows of the PMTs, and, at the same time, to keep off ambient light so that it does not interfere with the measurement.

As PMTs working in single photon mode are relatively noisy detectors, the signals coming from a single PMT are not guaranteed to be connected to a scintillation burst within the sample. For example, there may be also signals due to the termionic emission of electrons from the photocathode. However, the scintillation light emitted by the scintillator is isotropically distributed, and there are in the order of 10 photons per 1 keV energy released in the cocktail. Thus, there is a probability that the scintillation light produced by an ionizing particle is detected simultaneously by the PMTs in the system. Due to the finite decay constant of scintillation light, this detection will not be simultaneous, but will be separated by some time. This requires that a certain time interval is selected as the maximum interval between two events, for which they are still considered to be coming from the same decay event. This time interval is known as *coincidence resolving time* or *coincidence window*. In the framework of primary radioactivity measurements using LS counting, the selection of the coincidence window is not a trivial task[7].

6 An example when PMTs with low transient time spread are needed will be given in Chapter 6.
7 Special attention to the problem is given in Chapter 9.

1.4 APPLICATIONS OF LIQUID SCINTILLATION COUNTING

LS counting is a powerful technique for the measurement of ionizing radiation with various practical applications. It finds use in many areas such as: radioactivity survey in the environment or in nuclear facilities [30], radionuclides standardization [27], high energy and neutrino physics [31], ^{14}C dating [32], marine studies [33], environmental studies and monitoring [4].

There are several methods for standardization of the activity of radioisotopes that employ LS counting. The $4\pi\beta - \gamma$ coincidence counting is a standardization method which could be used for nuclides that have both β and γ emissions. However, it cannot be used for pure β emitting radionuclides and requires a relatively sophisticated setup with two different kinds of detectors. The CIEMAT/NIST efficiency tracing (CNET) method, can be applied for the standardization of many nuclides and can be done on a commercial LS counter. However, it is not purely a primary method as it relies on a tracer nuclide, usually ^{3}H, whose activity was determined beforehand by TDCR counting. The TDCR method has been developed for the direct activity measurement of β and EC radionuclides, including the radionuclides decaying towards the ground level of the daughter [27]. It uses a statistical model which is applied to the counting rate data from a LS system with three PMTs. These three methods can be used for the standardization of the activity of many radioisotopes including, but not limited to: ^{3}H [34], ^{11}C [35], ^{14}C [36], ^{18}F [37, 38], ^{22}Na [39], ^{32}P [40], ^{33}P [41], ^{35}S [42], ^{41}Ca [43], ^{63}Ni [44, 45], ^{64}Cu [46], ^{55}Fe [47], ^{59}Fe, [48], ^{67}Ga [49], ^{68}Ge/^{68}Ga [50], ^{89}Sr [51], ^{87}Y [49], ^{90}Y [52], ^{90}Sr/^{90}Y [53], ^{99}Tc [54], ^{99m}Tc [55], ^{106}Rh [51], ^{109}Cd [56, 57], ^{110m}Ag [58], ^{123m}Te [59], ^{124}Sb [60], ^{124}I [61], ^{129}I [62], ^{131}I [48, 60], ^{134}Cs [63, 64], ^{139}Ce [65], ^{153}Sm [66, 67], ^{177}Lu [68], ^{186}Re [69, 70], ^{188}W/^{188}Re [71], ^{204}Tl [72], ^{210}Po [73], ^{222}Rn [74], ^{223}Ra [75, 76], ^{224}Ra [77], ^{238}Pu [78]. ^{241}Pu [45] and ^{241}Am [60, 79]. [8]

8 The list is not intended to be exhaustive.

2

RADIONUCLIDE METROLOGY USING LIQUID SCINTILLATION COUNTING

THE detection efficiency for high-energy β-emitters and α-emitters in liquid scintillation counting can be assumed to be 100% for all practical purposes [80]. This is not the case of low-energy β-emitters and some EC nuclides, where the detection efficiency is less than 100% and can vary with measurement conditions. In order to perform a precise absolute measurement of the activity of the source, the detection efficiency must be known with high accuracy. It can be calculated by the use of one particular model called the "free parameter" model, which is based on the statistical description of phenomena occurring in the LS counter and is described hereafter.

2.1 THE FREE PARAMETER MODEL IN LS

As a result of radioactive decay inside the liquid scintillation cocktail, an amount of energy E is released, and the expected mean number of emitted photons can be expressed as [27]:

$$\bar{m} = \frac{\eta_0 Q(E) E}{h\nu}, \tag{2.1}$$

where $h\nu$ is the mean photon energy and η_0 is the absolute scintillation efficiency. The function $Q(E)$ takes into account that the fraction of the deposited energy that is converted into scintillation light is not constant with the deposited energy, i. e., the scintillator has non-linear response. If we assume that the number of emitted photons is distributed according to the Poisson distribution with a mean value $\bar{m}$, the number of photons m emitted per decay is also Poisson distributed [27]:

$$p(m, \bar{m}) = \frac{\bar{m}^m}{m!} e^{-\bar{m}}. \tag{2.2}$$

Assume first, that there is one PMT that is used to register the scintillation light. The emission of m photons from the scintillator leads to the detection of $\bar{n}$ photons by the PMT on average, i. e., emission of $\bar{n}$ photoelectrons from its photocathode. Here $\bar{n}$ can be expressed by:

$$\bar{n} = \bar{m} \varepsilon_q \mu \xi, \tag{2.3}$$

where ξ is a factor that takes into account the geometrical efficiency of the PMTs, ε_q is the quantum efficiency of the PMT and μ is the spectral matching factor between the

fluorescence spectrum of the scintillator and the absorption spectrum of the photocathode. The mean number of photoelectrons $\bar{n}$ produced by the emission of a particle with energy E in the cocktail can be calculated from equations (2.1) and (2.3):

$$\bar{n} = \bar{m}\phi = \frac{\eta_0 \xi \varepsilon_q \mu}{h\nu} Q(E)\, E, \tag{2.4}$$

where ϕ is the total efficiency of the PMT and is equal to the product of ξ, ε_q and μ. The quantity of interest is the probability to detect a measurable signal, i. e., production of at least one photoelectron, if there are $\bar{m}$ photons emitted by the sample. The photoelectric process in the photocathode can be described by the binomial distribution [27]:

$$b(n; m, \varepsilon_q \mu \xi) = \frac{m!}{n!(m-n)!} (\varepsilon_q \mu \xi)^m (1 - \varepsilon_q \mu \xi)^{m-n}, \tag{2.5}$$

where $b(n; m, \varepsilon_q \mu \xi)$ is the probability that m incident photons on the photocathode lead to the emission of exactly n photoelectrons given that the quantum and geometrical efficiency of the photomultiplier tube is $\varepsilon_q \mu \xi$. We can express the probability for emission of at least one photoelectron from the probability of emission of exactly zero photoelectrons [27]:

$$p_e(m) = 1 - b(0; m, \varepsilon_q \mu \xi) = 1 - (1 - \varepsilon_q \mu \xi)^m, \tag{2.6}$$

The probability P_E, then, to detect a scintillation event in the case of $\bar{m}$ emitted photons on average is given by:

$$\begin{aligned} P_E &= \sum_{m=0}^{\infty} p(m, \bar{m}) \left[1 - (1 - \varepsilon_q \mu)^m\right] \\ &= 1 - \sum_{m=0}^{\infty} \frac{\bar{m}^m}{m!} e^{-\bar{m}} (1 - \varepsilon_q \mu)^m \\ &= 1 - \left\{ \sum_{m=0}^{\infty} \frac{[\bar{m}(1 - \varepsilon_q \mu \xi)]^m e^{-\bar{m}(1-\varepsilon_q \mu \xi)}}{m!} \right\} \frac{e^{-\bar{m}}}{e^{-\bar{m}(1-\varepsilon_q \mu \xi)}} \\ &= 1 - e^{-\bar{m}} e^{\bar{m}(1-\varepsilon_q \mu \xi)} = 1 - e^{-\bar{m}\varepsilon_q \mu \xi} = 1 - e^{-\bar{n}} \end{aligned} \tag{2.7}$$

Thus, a cascade of three random processes abiding to: Poisson distribution (2.2), binomial distribution (2.5) and multinomial distribution (2.8), can be resumed by only using Poisson statistics for the mean number of photons emitted in the cocktail $p(m, \bar{m})$ [27].

In the case of a detector with R photomultipliers, the number of photons incident on each photomultiplier form a set $\{m_i\}$ which fulfills the criteria $m = m_1 + m_2 + \cdots + m_R$. The probability P_d, for a given set $\{m_i\}$ to occur, is given by the multinomial distribution [27]:

$$P_d = \frac{1}{R^m} \frac{m!}{m_1! m_2! \cdots m_R!}. \tag{2.8}$$

Combining equation (2.8) with the probability of the formation of a pulse from a given type P_x, we get the probability of m photons creating a detectable pulse:

$$\begin{aligned} P_R(m) &= P_d P_x \\ &= \frac{m!}{R^m} \sum_{m_1=0}^{m} \sum_{m_2=0}^{m-m_1} \cdots \sum_{m-m_1-\cdots-m_{R-2}}^{m_R} \frac{P_x}{m_1!m_2!\cdots m_{R-1}!(m-m_1-\cdots-m_{R-1})!} \end{aligned} \tag{2.9}$$

The probability for the formation of different types of pulses P_x, when there are n incident photons on the photomultipliers, can be computed using equation (2.6). For example, for two photomultipliers, A and B, working in coincidence, the probability for the formation of a coincident impulse P_x^{AB} with m_A photons reaching PMT A and $m_B = m - m_A$ photons reaching PMT B is:

$$\begin{aligned} P_x^{AB} &= p_e(m_A)p_e(m_B) \\ &= p_e(m_A)p_e(m-m_A) \\ &= (1-(1-\varepsilon_q\mu\xi)^{m_A})\,(1-(1-\varepsilon_q\mu\xi)^{m-m_A}) \end{aligned} \tag{2.10}$$

Let us examine more thoroughly the case of a detector with two photomultipliers, A and B, working in coincidence. In this case P_x is given by equation (2.10). Substituting in equation (2.9) we get the detection efficiency for a coincidence pulse with n incident photons on the photocathodes of the two PMTs:

$$P_R^{AB} = \frac{m!}{2^m} \sum_{m_A=0}^{n} \frac{(1-p_0^{m_A})(1-p_0^{m-m_A})}{m_A!(m-m_A)!}, \tag{2.11}$$

where $p_0 = 1-\varepsilon_q\mu\xi$ is the probability of emission of zero photoelectrons if there is a photon incident on the photocathode. The detection probability P in the case of two PMTs in coincidence is given by:

$$P_{AB} = P_E = \sum_{m=1}^{\infty} \frac{p(m,\bar{m})}{2^m} \sum_{m_A=0}^{m} \binom{m}{m_A} (1-p_0^{m_A})(1-p_0^{m-m_A}) \tag{2.12}$$

Developing the brackets in the second sum in (2.12) we get:

$$P_{AB} = \sum_{m=1}^{\infty} \frac{p(m,\bar{m})}{2^m} \sum_{m_A=0}^{m} \binom{m}{m_A} (1-p_0^{m_A}-p_0^{m-m_A}+p_0^{m}) \tag{2.13}$$

For the calculation of the finite sums we use the binomial formula:

$$(x+y)^n = \sum_{k=0}^{n} \binom{n}{k} x^k y^{n-k} \tag{2.14}$$

We can separate equation (2.13) into four sums for which we get [81]:

$$\begin{aligned}
&\sum_{m_A=0}^{m}\binom{m}{m_A} = 2^m \\
&\sum_{m_A=0}^{m}\binom{m}{m_A} p_0^{m_A} 1^{m-m_A} = (1+p_0)^m = (2-\varepsilon_q\mu\xi)^m = 2^m\left(1-\frac{\varepsilon_q\mu\xi}{2}\right)^m \\
&\sum_{m_A=0}^{m}\binom{m}{m_A} p_0^{m-m_A} 1^{m_A} = (1+p_0)^m = (2-\varepsilon_q\mu\xi)^m = 2^m\left(1-\frac{\varepsilon_q\mu\xi}{2}\right)^m \\
&\sum_{m_A=0}^{m}\binom{m}{m_A} p_0^{m} = 2^m p_0^m = 2^m(1-\varepsilon_q\mu\xi)^m
\end{aligned} \tag{2.15}$$

If we substitute the calculated finite sums in the right-hand member of equation (2.13) we can derive the probability of counting P_{AB} for two PMTs in coincidence:

$$\begin{aligned}
P_{AB} &= \sum_{m=0}^{\infty}\frac{\bar{m}^m}{m!}e^{\bar{m}}\left\{1-2\left(1-\frac{\varepsilon_q\mu}{2}\right)^m+(1-\varepsilon_q\mu)^n\right\} = \\
&= \sum_{m=0}^{\infty}\frac{\bar{m}^m}{m!}e^{-\bar{m}} - \sum_{m=0}^{\infty}2\frac{\bar{m}^m}{m!}e^{-\bar{m}}\left(1-\frac{\varepsilon_q\mu}{2}\right)^m + \sum_{m=0}^{\infty}\frac{\bar{m}^m}{m!}e^{-\bar{m}}(1-\varepsilon_q\mu)^m = \\
&= 1-2e^{-\bar{m}}e^{\bar{m}(1-\varepsilon_q\mu/2)}\sum_{m=0}^{\infty}p(m,\bar{m}(1-\varepsilon_q\mu/2)+e^{-\bar{m}}e^{\bar{m}1-\varepsilon_q\mu}\sum_{m=0}^{\infty}p(m,\bar{m}(1-\varepsilon_q\mu) = \\
&= 1-2e^{-\bar{m}+\bar{m}\left(1-\frac{\varepsilon_q\mu}{2}\right)}+e^{-\bar{m}+\bar{m}(1-\varepsilon_q\mu)} = 1-2e^{-\bar{m}\varepsilon_q\mu/2}-e^{-\bar{m}\varepsilon_q\mu} = \\
&= \left(1-e^{-\frac{\bar{m}\varepsilon_q\mu}{2}}\right)^2 = \left(1-e^{-\frac{\bar{n}}{2}}\right)^2
\end{aligned} \tag{2.16}$$

Equations (2.16) and (2.7) can be derived by the assumption of pure Poisson process describing the statistics of photoelectrons without considering a binomial distribution [81]. The counting probability of various kinds of pulses, created by monoenergetic particles, are summarized in Table 2.1.

Using equations (2.7) and (2.16), the detection probability P of a LS counter with R identical PMTs becomes

$$P = 1-e^{-\bar{n}/R}, \tag{2.17}$$

where the mean number of photoelectrons created in *all* R PMTs is given by:

$$\bar{n} = EQ(E)\varphi. \tag{2.18}$$

The free parameter φ introduced in (2.18) is the average effective energy (after taking into account the ionization quenching function) that is needed to create a photoelectron at the photocathode of the PMT:

$$\varphi = \frac{\bar{n}}{EQ(E)} = \frac{L\xi\varepsilon_q\mu}{h\nu}. \tag{2.19}$$

The free parameter is very frequently referred to as figure of merit (FOM). The probability of counting P is a function of the FOM φ and the energy of the particle. To ensure the validity of the assumption that the detection probability follows a Poissonian distribution, the detector must be constructed in such a way that the detection probability of one photoelectron is not zero. To achieve this in practice, the position of the discriminator thresholds of each PMT must be just below the single-photoelectron peak. Also, the geometrical efficiency of the PMTs should be constant for the entire volume of the sample, i. e., the detection efficiency is the same irregardless of where in the volume of the sample does a decay occur. This problem is addressed in [82].

TABLE 2.1: Detection probability for various kinds of pulses caused by monoenergetic particles in a detector with R photomultipliers with identical and non-identical response. The Poisson non-detection probability is $p_0 = e^{-\bar{n}/R}$. The signals are either from a single PMT (no coincidence), from two PMTs (with or without coincidence) or from three PMTs (no coincidence, double coincidence or triple coincidence)

R	Signal mode	Coincidence	Probability of counting $P(E, \varphi)$
			Identical PMTs, $p_A = p_B = p_C = p_0$
1	A	None	$1 - p_0$
2	A; B	None	$1 - p_0$
	AB	Double	$(1 - p_0)^2$
3	A; B; C	None	$1 - p_0$
	AB; BC; AC	Double	$(1 - p_0)^2$
	T	Triple	$(1 - p_0)^3$
			Non-identical PMTs, $p_A \neq p_B \neq p_C$
1	A	None	$1 - p_A$
2	A; B	None	$(1 - p_A); (1 - p_B)$
	AB	Double	$(1 - p_A)(1 - p_B)$
3	A; B; C	None	$(1 - p_A); (1 - p_B); (1 - p_C)$
	AB; BC; AC	Double	$(1 - p_A)(1 - p_B); (1 - p_A)(1 - p_C); (1 - p_B)(1 - p_C)$
	AB + BC + AC	D_3^*	$(1 - p_A)(1 - p_B) + (1 - p_A)(1 - p_C) +$ $+(1 - p_B)(1 - p_C) - 2(1 - p_A)(1 - p_B)(1 - p_C)$
	T	Triple	$(1 - p_A)(1 - p_B)(1 - p_C)$

* Logical sum of double coincidences

2.1.1 *Calculation of detection efficiency*

The detection efficiency of the LS counter ϕ is a function of the FOM and depends on the type of disintegration of the radionuclide. In the case of pure β-emitters ε is the product of the counting probability $P(E, \varphi)$ of a given pulse (taken from table 2.1) and the normalized β-spectrum $S(E)$, integrated over the entire decay energy range [27]:

$$\phi(\varphi) = \int_0^{E_{max}} S(E)P(E, \varphi)dE, \tag{2.20}$$

where E_{max} is the maximum energy of the β particle.

EC radionuclides decay along multiple paths and have more complex decay schemes. In the case of these radionuclides, the counting efficiency ε is calculated as the sum of products of intensities $I(E_j)$ and the probability of counting $P(E_j, \phi)$ of a given type of signal (taken from Table 2.1) at certain energy E_j. The summation is performed over the entire discrete energy spectrum with k energies E_j [27]:

$$\phi(\varphi) = \sum_{j=0}^{k} I(E_j)P(E_j, \varphi). \tag{2.21}$$

2.1.2 *Calculation of energy spectra*

An important part of the calculation of the detection efficiency is the spectrum of the deposited in the cocktail energy. It is composed of the electrons emitted from the decay process of the initial isotope or from rearrangement processes in the shell of the daughter atom. Additionally, photons, that are emitted as a result of the decay process, can transfer energy to the scintillator via Compton scattering and photoelectric effect. For photons with energies higher than 1.022 MeV, electron-positron pairs can also be produced. It should be emphasized here that, in certain cases, the deposited energy spectrum may not correspond to the emission spectrum. This could happen, for example, when X-ray or γ photons escape the volume of the scintillator, or are scattered and deposit only a part of their energy. Another source of difference is for high-energy β-particles, which have a long stopping path, and can interact only partially with the scintillator before leaving it.

For β^- or β^+ transitions, the probability for an electron emission with energy $W = 1 + E/m_0c^2$ is given by [27]:

$$N(W)dW = \frac{g^2}{2\pi^3}\sqrt{W^2-1}W(W_0 - W)^2F(Z, W)(1 + \delta_R(W, Z))C(W)dW, \tag{2.22}$$

where g is the coupling constant of the weak interaction, $F(Z, W)$ is the Fermi function, $\delta_E(W, Z)$ accounts for radiative corrections, Z is the atomic number of the daughter nucleus and W_0 is the maximum energy. $C(W)$ is the shape factor function. Equation 2.22 can be evaluated using the SPEBETA code by Ph. Cassette [83]. A more sophisticated calculation that includes screening corrections is included in the BetaShape code by X.

Mougeot [84]. Beta-spectra calculated by the code can be found on-line on the Decay Data Evaluation Project (DDEP) website [85]. The importance of the β-spectrum shape for the TDCR method is difficult to overestimate. A critical analysis of the subject is given in the studies by K. Kossert and X. Mougeot [53, 86].

In the EC process a vacancy in the shell of the daughter atom is produces. This is then followed by a rearrangement of the electrons that may lead to the ejections of Auger electrons. The X- or γ-rays that are emitted can also interact with the scintillator and produce secondary electrons. When calculating the detection efficiency of EC emitters, the continuous β-spectrum must be replaced by a sum of all possibilities of Auger electrons and photon interactions. The contribution of the latter is calculated with the aid of Monte Carlo procedures. There are different atomic rearrangement models that were developed in order to compute the counting efficiency of EC nuclides. A good summary of models can be found in [27]. Advancements towards high-precision calculation of EC decays can be found in [87].

Excluding pure β-emitters, the radioactive decays are usually accompanied by one or more photon emissions. Low-energy X-rays of a few keV are usually easily fully absorbed within the scintillator [27]. For higher energies the Compton scattering becomes more probable and the fraction of the total energy that gets deposited within the sample reduces. In any case, the effect of multiple secondary electrons with energies $E_1 + E_2 + \cdots + E_n = E$ is not the same as the effect of a single electron with energy E, due to the non-linearity of the scintillator. The correct effective deposited energy would have to be weighted by the ionization quenching function for each electron energy, i. e., $E_{eff}^{(1)} = EQ(E)$ and $E_{eff}^{(n)} = E_1 Q(E_1) + E_2 Q(E_2) + \cdots + E_n Q(E_n)$.

The effective deposited energy in the case of photon interactions can be calculated with the aid of Monte Carlo procedures. In this case, the detection efficiency starts to depend on the size and shape of the sample, as this controls the probability to absorb X- or γ-rays. No such dependence would exist for low-energy β-emissions. For high energy electrons, however, the possibility for the escape of β-particles, before they have deposited all their energy in the sample must be considered. This can again be modeled using Monte Carlo methods. In the case of high-energy electrons, the corrections that must be introduced are less necessary as the detection efficiency would be close to one [88]. It should be noted here, that in the cases where emissions escape the sample, the transport in the surroundings of the LS vial must also be simulated with the Monte Carlo code due to the possibility of backscattered photons or electrons.

2.2 THE TRIPLE-TO-DOUBLE COINCIDENCES RATIO METHOD

The triple-to-double coincidences ratio (TDCR) method is a LS counting method that is used to calculate the average number of detected photons from a scintillating sample. The technique relies on the free parameter model for a three-PMT detector to make the link between the measured scintillations and the detection efficiency. A specialized

analyzer system is required for the application of the TDCR method. The system must allow the counting of double coincidence pulses (AB, BC and AC) and triple coincidence pulses (T).

2.2.1 *Detection efficiency of a three-PMT detector*

The theoretical counting efficiencies in a $R = 3$ PMT system can be calculated by substituting the appropriate counting probability $P(E, \varphi)$ from Table 2.1 in equation (2.19) and are the following:

$$\phi_2 = \int_0^{E_{max}} S(E) \left(1 - e^{-\bar{n}/3}\right)^2 dE, \tag{2.23}$$

for two PMTs working in coincidence and

$$\phi_T = \int_0^{E_{max}} S(E) \left(1 - e^{-\bar{n}/3}\right)^3 dE, \tag{2.24}$$

for three PMTs working in coincidence. The logical sum of double coincidences is calculated as [27]:

$$\phi_D = \int_0^{E_{max}} S(E) \left[3\left(1 - e^{-\varphi E Q(E)/3}\right)^2 - 2\left(1 - e^{-\varphi E Q(E)/3}\right)^3\right] dE \tag{2.25}$$

The ratio of the triple coincidences counting efficiency to the logical sum of double coincidences counting efficiency is expressed as [27]:

$$\frac{\phi_T}{\phi_D} = \frac{\int_0^{E_{max}} S(E) \left(1 - e^{-\varphi E Q(E)/3}\right)^3 dE}{\int_0^{E_{max}} S(E) \left[3\left(1 - e^{-\varphi E Q(E)/3}\right)^2 - 2\left(1 - e^{-\varphi E Q(E)/3}\right)^3\right] dE}, \tag{2.26}$$

where $S(E)$ is the normalized spectrum of the energy transferred to the liquid scintillation cocktail, which includes β-particles, photoelectrons and Compton electrons, coming from X-ray and γ-ray interactions in the cocktail, and Auger and conversion electrons. $Q(E)$ is the ionization quenching correction factor (1.12), E_{max} is the maximum β-particle energy and φ is the FOM. The logical sum of the double coincidences is defined as:

$$D = AB \vee BC \vee AC, \tag{2.27}$$

where $\vee$ is the logical or operator, and the number of D coincidences can be obtained from the double and triple coincidences as:

$$D = AB + BC + AC - 2T. \tag{2.28}$$

For a large number of detected events, the ratio of the triple coincidence counting rate to the logical sum of double coincidences counting rate T/D converges towards the

ratio of counting efficiencies ϕ_T/ϕ_D [27]. The left-hand side of the expression for the ratio of the triple coincidences efficiency to the logical sum of double coincidences efficiency (2.26) can be obtained experimentally and the right-hand side can be calculated theoretically if $S(E)$ is known and the value of kB in (1.12) is assumed.

Equation (2.26) is valid under the assumption of identical PMTs, but in a real counter this assumption is rarely true. In that case a set of three equations has to be solved [27]:

$$\begin{aligned}
\frac{\phi_T}{\phi_{AB}} &= \frac{\int_0^{E_{max}} S(E)\left(1-e^{-\varphi_A EQ(E)}\right)\left(1-e^{-\varphi_B EQ(E)}\right)\left(1-e^{-\varphi_C EQ(E)}\right)dE}{\int_0^{E_{max}} S(E)\left(1-e^{-\varphi_A EQ(E)}\right)\left(1-e^{-\varphi_B EQ(E)}\right)dE},\\
\frac{\phi_T}{\phi_{BC}} &= \frac{\int_0^{E_{max}} S(E)\left(1-e^{-\varphi_A EQ(E)}\right)\left(1-e^{-\varphi_B EQ(E)}\right)\left(1-e^{-\varphi_C EQ(E)}\right)dE}{\int_0^{E_{max}} S(E)\left(1-e^{-\varphi_B EQ(E)}\right)\left(1-e^{-\varphi_C EQ(E)}\right)dE},\\
\frac{\phi_T}{\phi_{AC}} &= \frac{\int_0^{E_{max}} S(E)\left(1-e^{-\varphi_A EQ(E)}\right)\left(1-e^{-\varphi_B EQ(E)}\right)\left(1-e^{-\varphi_C EQ(E)}\right)dE}{\int_0^{E_{max}} S(E)\left(1-e^{-\varphi_A EQ(E)}\right)\left(1-e^{-\varphi_C EQ(E)}\right)dE},
\end{aligned} \tag{2.29}$$

where φ_A, φ_B and φ_C are the FOMs of each PMT and $\varphi_A + \varphi_B + \varphi_C = \varphi$. Similar to the situation with identical PMTs, here the experimental ratios T/AB, T/BC and T/AC converge towards the theoretical counting efficiency ratios ϕ_T/ϕ_{AB}, ϕ_T/ϕ_{BC} and ϕ_T/ϕ_{AC} when the number of detected events is large. The values of the FOMs in equations (2.29) can be found using a Downhill Simplex algorithm [89], where the function to be minimized is the squared sum of differences between the theoretical and experimental ratios:

$$\Delta = \left(\frac{\phi_T}{\phi_{AB}} - \frac{T}{AB}\right)^2 + \left(\frac{\phi_T}{\phi_{BC}} - \frac{T}{BC}\right)^2 + \left(\frac{\phi_T}{\phi_{AC}} - \frac{T}{AC}\right)^2. \tag{2.30}$$

The minimization of the equation gives the values of the FOMs (φ_A, φ_B and φ_C) for a given kB value. The counting efficiency for a given coincidence type (double coincidence, triple coincidence, etc.) can be calculated using Table 2.1 and equation (2.19). The activity can be determined using the calculated counting efficiency and the counting rate for that coincidence type. As most information is contained in the logical sum of the double coincidences D, the activity A is often expressed as:

$$A = \frac{D}{\phi_D(kB, \varphi_A, \varphi_B, \varphi_C)}. \tag{2.31}$$

Depending on the radionuclide, equation (2.30) can have one solution, in the case of pure β-emitters, and three solutions, in the case of EC radionuclides [27]. In the cases where the equation has three solutions, the counting efficiency must be varied experimentally to determine on which part of the curve does the experimental TDCR lie.

Counting efficiencies calculated with the TDCR model are dependent on the choice of the kB parameter, which is the only adjustable parameter in the model. For high

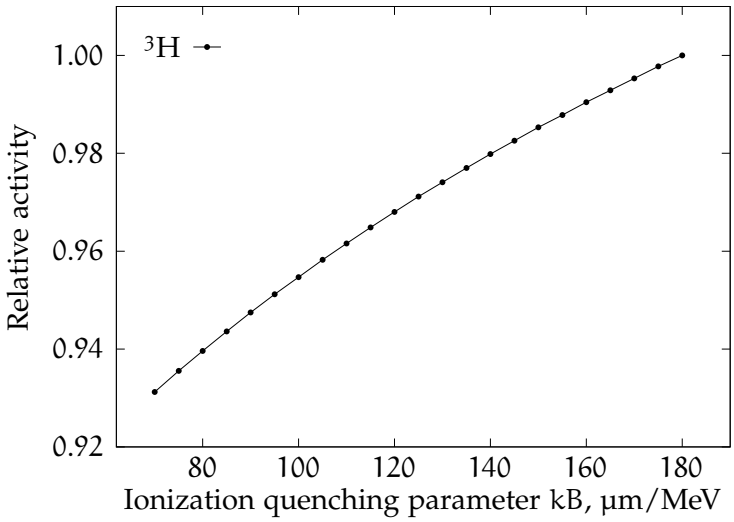

FIGURE 2.1: Influence of the kB parameter on the calculated activity using the TDCR model in the case of ^{3}H. All other parameters, such as the FOM, are kept the same.

energy β-emitters (over a few hundred keV), the influence of the chosen value of the kB parameter is negligible [27]. For radionuclides emitting low energy electrons (for example ^{3}H), the differences in the activities calculated with different kB values are significant. The dependence of the estimated activity of ^{3}H on the value of the kB parameter is illustrated on Figure 2.1.

Due to the specific requirements of the TDCR model, the use of specially designed LS counters, vials and multichannel analyzers is necessary.

2.2.2 *Practical aspects of the TDCR method*

There are some practical considerations which need to be taken for the proper application of the TDCR model. Special requirements exist for the liquid scintillation vials which need to be used as well as for the construction of the three PMT detector system.

LIQUID SCINTILLATION VIALS The main purpose of the liquid scintillation vials is to securely store the radioactive sample and cocktail and provide safe and stable handling. The most common types of vials used in liquid scintillation counting are plastic (polyethylene) vials and glass vials with low potassium content and a standard volume of 20 ml. The light output from plastic vials is higher than the one from clear glass vials due to their diffusive surface, which suppresses effects like total internal reflection and refraction [90]. The main drawback of plastic vials is the shorter long-term stability of the cocktail, which is caused mainly because it diffuses in the vial walls. There is no such effect in glass vials, but significant light trapping can occur due to the large difference in refractive indices between glass and air; this causes total internal reflection of some of the emitted light, which causes problems with the application of the TDCR model. It causes reduction of the total amount of light, emitted from the vial,

thus reducing the detection efficiency, and it has a different probability of occurring depending on the location of the scintillation event inside the vial. The latter effect creates a dependency between the mean number of photons emitted from the vial and the location of the scintillation, which violates one of the primary assumptions of the TDCR model that the number of photons reaching the photocathodes of the PMTs follow a Poisson distribution with a mean value which is constant for the entire volume. A compromise can be achieved by using clear glass vials plastered with diffusive tape, or by creating diffusive glass vials by sandblasting or etching [80].

LIQUID SCINTILLATION COUNTERS The number of emitted photons in a liquid scintillation event is low in the case of low-energy β-emitters. This requires the use of very optimized optics and sensitive photomultipliers with high quantum efficiency of the photocathode. Quantum efficiency is defined as number of photoelectrons emitted from the photocathode divided by the number of incident photons and its range is from 20% to 40% [91]. As the TDCR model assumes non-zero detection probability for single photons, the PMTs must have good separation of the single electron peak from the noise peak for a proper adjustment of the analyzer's threshold. This requires the use of high-gain photodetectors with high peak-to-valley ratio on the single photon peak [29].

Considering that the signal from the phototubes is a few nanoseconds long, the electronics and signal processing unit of the detector must be able to process fast pulses. To reduce the effect of thermal noise in the PMTs, the analyzer of the detector must be able to detect coincident signal between the different PMTs. The usual duration of the coincident window (the maximum elapsed time between two pulses for which they are considered coincident) is between 40 ns and 200 ns[1].

When a photomultiplier tube is operated in a pulse detection mode, as in LS counting, random pulses with small amplitudes following the signal output pulse may be observed. They are called afterpulses and often disturb the accurate counting of signals. There are two types of afterpulses: very short delay ones (several nanoseconds), caused by elastic scattering of electrons from the first dynode, and long delay ones, caused by positive ions created by the ionization of residual gases in the volume of the PMT [28]. The latter are following the signal after a delay in the order of microseconds, due to the slower movement of the heavier positive ions. To ensure the correct counting of scintillation pulses, the electronics of the LS detector must have a dead-time unit, which adds a dead-time period after each detected pulse to avoid false coincidences. The duration of the dead-time period is a few tens of microseconds. It is mandatory that the dead-time is from the extending type [27], that is whenever a pulse comes during a dead-time period, the period timer is set to zero and starts again. This ensures that every detected event will be preceded by an event free period. Precise knowledge of the dead-time is also important when measuring radionuclides with very short half-life

1 In fact, the choice of the proper coincidence resolving time was found to be non-trivial and the whole of Chapter 9 is dedicated to this problem.

daughter products in their decay chain (e. g., ^{214}Po in the decay chain of ^{222}Rn with a half-life 160 µs). If the short-lived product has a half-life that is similar to the dead-time of the detector, a significant amount of its decays would occur during the dead-time and will not be registered. By knowing the dead-time period with high precision, it is possible to make corrections when calculating the activity.

In order to implement the TDCR model, a specialized 3-PMT counter is needed. The three PMTs are positioned symmetrically around the vial at equal 120° angles. If the PMTs are identical, the simplified equations (2.24) and (2.25) can be used, but due to the high cost of matched PMTs, this is usually not the case. In non-identical PMT systems, the proper detection efficiency can be calculated using the system of equations (2.29).

A relationship exists between the single signals and those in coincidence, which allows the formulation of two balance equations [92]:

$$A + B + C = T + D + S, \tag{2.32}$$

$$AB + BC + AC = 2T + D. \tag{2.33}$$

To compute the equations, the detector must store information of the non-coincident signals (A, B, C), the logical sum of the non-coincident signals (S), the double coincidence signals (AB, BC, AC), the logical sum of the double coincidence signals (D) and the triple coincidence signals (T). Fulfillment of the balance equations on each acquisition run is a good indicator of the proper operation of the detector system [29].

CODE FOR THE IMPLEMENTATION OF THE TDCR MODEL The determination of efficiency using the TDCR model requires the numerical integration of equations (1.12) and (2.29), the minimization of (2.30) and the computation of electron stopping powers. A specialized computer code has been developed to perform the calculations required by the TDCR method. TDCR18 is an application devoted to the calculation of detection efficiencies and FOM of three-PMT LS counters for β-radionuclides. It is similar to the older version TDCR07c, which can be found on-line [93]. The code, developed by Ph. Cassette (LNHB), is used in some parts throughout this work to implement the TDCR method. The physical models used in the program are:

- Poisson statistics (2.7) for the light emission from the liquid scintillator
- Birks' law (1.7) for the non-linearity of the scintillator,
- ICRU n°37 formula [25] over 100 eV and linear extrapolation to zero under 100 eV for the stopping powers of the electrons in the LS cocktail,
- Optionally uses the stopping power dataset provided by Tan & Xia [94],
- β-spectra calculated using the SPEBETA program [83].

The program uses the radionuclide atomic number and atomic mass, and the density and Z/A ratio of the LS cocktail as an input after which it presents various options for

calculation to the user. One of the options is to calculate the detection efficiencies from the three values of individual triple-to-double coincidence ratios (T/AB, T/BC, T/AC), when the asymmetry of the phototubes is not negligible. The program calculates the detection efficiency for each of the three double coincidences (ε_{AB}, ε_{BC}, ε_{AC}) and gives the relative quantum efficiencies of each PMT. A detailed explanation of the code can be found in [93].

DETECTION EFFICIENCY VARIATION The TDCR model provides means to calculate the detection efficiency of the detector system for given measurement conditions and for a given radionuclide. Changing the measurement conditions would not change the activity of the sample, except, of course, accidentally dropping it on the floor and breaking the vial. If the TDCR model, including the choice of kB parameter, is correct, the calculated activity of the measured sample should be independent of the variations in the detection efficiency. That is, the activity calculated at detection efficiency 0.2 should be the same as the activity calculated at detection efficiency 0.5 and at 1.0. This premise is the basis of the efficiency variation method. By making consecutive measurements of the same LS sample under different conditions, the detection efficiency will vary.

In a properly designed counter, the detection efficiency is always optimal, so the only way to vary the detection efficiency is to decrease it. There are several ways to decrease the detection efficiency of a LS counter: defocusing the photomultiplier tubes, decreasing the light output of the source by coaxial filters or by creating a set of quenched sources. There are indications that the three methods could be equivalent [80], however, data from the framework of this thesis shows a significant difference between the use of grey filters and chemical quenching[2].

After performing measurements under different conditions, the activity of the sample is calculated for different values of the ionization quenching parameter kB. The kB value that results in the least variation of the calculated activity among the various measurements is chosen as the "optimal". In this sense, the ionization quenching parameter kB in Birks' formula (1.12) is an external parameter for the TDCR model. The kB parameter characterizes the LS cocktail and, in the ideal case, it should be independent of the detection system. Due to the fact that it is the only variable parameter in the TDCR model, the choice of an optimal kB value may depend on the detection system parameters (geometry of the detector, vial type, cocktail volume, etc.)[3].

The detection efficiency variation method is the go-to method to determine the kB parameter in the practice of radionuclide metrology using LS counting. The method is illustrated on Figure 2.2. In this example, a ^{3}H source in a toluene based LS cocktail was measured with a set of optical filters with different transparency. The activity was calculated using different values of the ionization quenching parameter kB. It is important to note that the optimal value for kB is chosen solely on the logic that the calculated activity of the source should be independent of the detection efficiency.

2 The results from a comparison of the two methods are shown in Chapter 9.

3 These deficiencies of the detection efficiency variation method are discussed in Chapter 9.

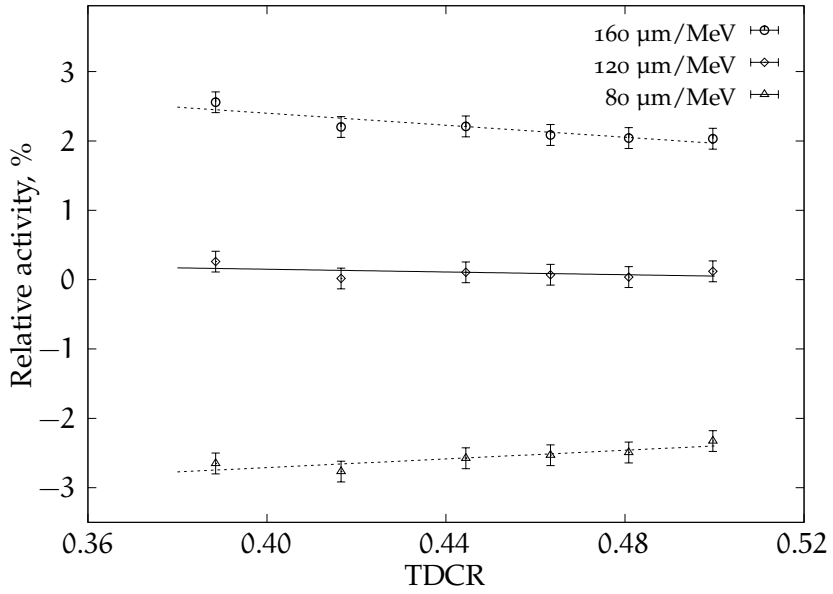

FIGURE 2.2: Calculated activity as a function of the TDCR at different kB values - high, optimal and low. A ^{3}H sample in a diffusive vial was used. The efficiency was varied using mesh filters with different density

The choice of the kB parameter is very important for the correct calculation of the activity of low-energy emitters like ^{3}H as shown in Figure 2.1. For the measurement of high-energy radionuclides, the influence of the kB is less pronounced. This can be explained by the fact that the non-linearity of the light emission of the LS cocktail depends mainly on the non-linearity of the linear energy transfer of the electrons passing through the matter with energies less than 20 keV [80]. The light produced by higher energy β-emitters comes mainly from higher energy electrons, for which the linear energy transfer is constant.

Detection efficiency variation is also necessary in those situations where, as said previously, one TDCR value corresponds to more than one detection efficiency. The only possibility in such a case is to vary the detection efficiency, and thus the TDCR value, to determine on which point on the curve does the correct detection efficiency lie.

2.3 THE COMPTON COINCIDENCES METHOD

The weak point of activity standardization methods that use the free parameter model is the lack of precise knowledge of the non-linearity of the scintillator. To an extent it can be described by semi-empirical functions, like Birks' formula, but still there is some uncertainty due to the unkown parameters. Perhaps, the best solution to the problem is to replace the non-linearity equations with an experimentally measured light ouput of the scinitllator. Such measurements can be performed using the Compton coincidences method.

The Compton coincidences method is a technique to study the response of scinitllators in the 1 – 20 keV energy range. It was initially developed by M. N. Péron and P. Cassette [95, 96]. The basic premise is that a collimated external source of mono-energetic γ-rays is placed such that the photon beam passes through the LS vial containing the scintillator that is studied. Most of the γ-rays undergo Compton scattering and produce a Compton electron inside the cocktail. The scattered γ-ray can interact with the γ-detector and knowing its energy it is possible to calculate the energy deposited in the cocktail by the Compton electron from the energy conservation law. In the initial design, the relative light output of the scintillator is determined by analyzing the energy spectrum of a single PMT [95]. Both the LS and γ-ray detection parts of the system are connected in coincidence. With the appropriate analyzing electronics it is possible to study the LS response in coincidence with events in the γ-channel, for a series of narrow slices in the γ-spectrum. This is equivalent to having a source of monoenergetic electrons with a known energy that is adjustable in a certain range. The energy of the virtual source depends on the energy gate in the γ-spectrum. A schematic drawing of the Compton coincidences setup is shown in Figure 2.3.

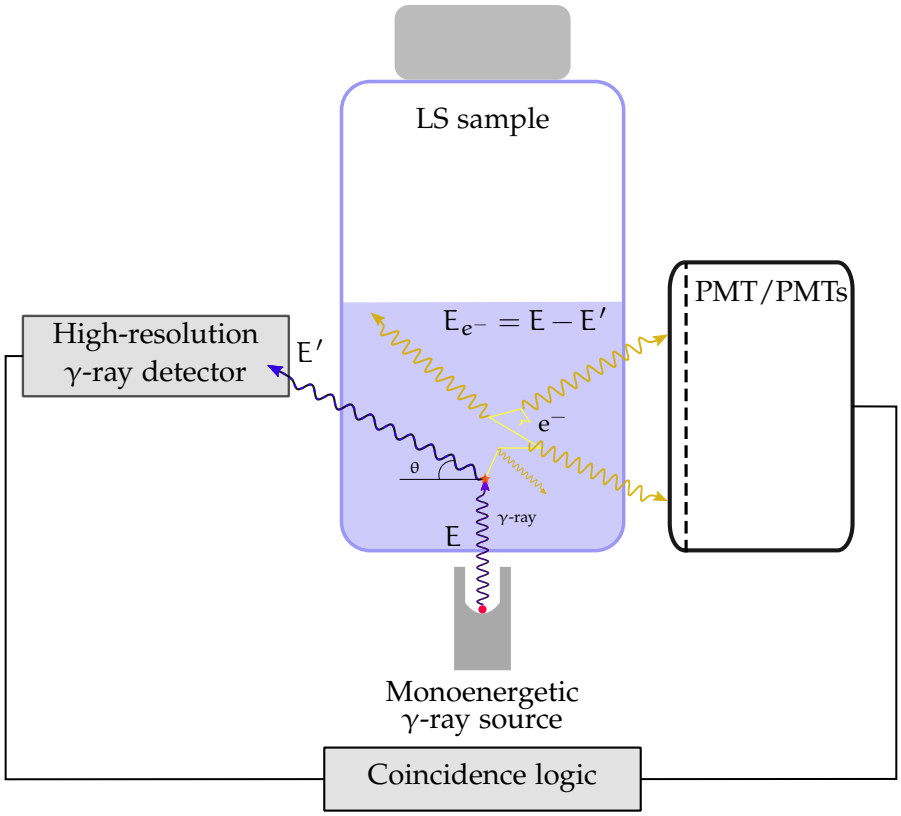

FIGURE 2.3: Schematic representation of a Compton coincidences system. The energy of the electron that is deposited in the cocktail can be determined from the energy of the scattered γ-ray.

The initial premise was expanded in 2008 by P. Cassette and Phuc Do, by replacing the single PMT with a TDCR detector [97]. The use of a three-PMT system allows the direct calculation of the mean number of detected photons for a monoenergetic source.

It is derived from the non-detection probability, i. e., the probability to detect 0 photons if there are $\bar{n}$ dectected on average. For absorbed energy E the detection efficiency in PMT X is [97]:

$$\varepsilon_X = 1 - e^{-\frac{\bar{n}}{3}}, \quad X = A, B, C. \tag{2.34}$$

For two PMTs X and Y or three PMTs T in coincidence the detection efficiency ε_{XY} is [97]:

$$\varepsilon_{XY} = \left(1 - e^{-\frac{\bar{n}_X}{3}}\right)\left(1 - e^{-\frac{\bar{n}_Y}{3}}\right), \quad XY = AB,\ BC,\ AC. \tag{2.35}$$

$$\varepsilon_T = \left(1 - e^{-\frac{\bar{n}_A}{3}}\right)\left(1 - e^{-\frac{\bar{n}_B}{3}}\right)\left(1 - e^{-\frac{\bar{n}_C}{3}}\right) \tag{2.36}$$

Finally, from the ratio of the efficiency for triple to the efficiency for double coincidences, one can obtain the mean number of detected photons per PMT $\bar{n}_A$, $\bar{n}_B$ and $\bar{n}_C$:

$$\bar{n}_Z = -3 \ln\left(1 - \frac{\varepsilon_T}{\varepsilon_{XY}}\right) = -3 \ln\left(1 - \frac{T}{XY}\right), \quad Z = C, A, B, \tag{2.37}$$

where it is assumed that, for a high number of detected events, the ratio of the detected triple to double coincidences tends towards the ratio of efficiencies.

The method implicitly assumes that there is no correlation between any pair of PMTs, i. e., irregardles of the position of the decay inside the sample, the number of photons reaching each PMT is equal on average. This may not be true for samples in clear glass vials due to the possibility of total internal reflection. For samples in diffusive glass or polyethylene vials the assumption should be reasonable. Equation (2.37) is useful only if the double and triple detection efficiencies are not close to 100%. This implies electron energies in the range up to 10 – 20 keV. This is not a severe limitation, however, as this range is the most interesting when studying the scinitllator non-linearity.

The Compton coincidences method with a TDCR detector can be used in two ways as a primary activity measurement method: the *Compton spectrometer efficiency tracing* (CSET) method proposed by Ph. Cassette and Phuc Do [97] and application of the TDCR method with a measured non-linearity function of the scinitllator, again proposed in the same article (hereafter referred to as Compton coincidences and TDCR or simply C-TDCR). The latter approach was implemented as the *zero model by using coincidence scintillation* (ZoMBieS) method by Bignell et al. [98].

COMPTON SPECTROMETER EFFICIENCY TRACING The CSET is a method that bears resemblance to the CNET method [99]. In the latter, the tracer is a ^{3}H source with known activity. This is associated with many problems, such as the long-term stability of the solution or the need to replace the tracer in time as ^{3}H decays with 12.32 years half-life. Note here, that the activity of this ^{3}H source must be standardized by another method and the only possibility thus far is the TDCR method.

The premise behind the CSET is that the ^{3}H tracer is replaced by Compton electrons produced by the external monoenergetic γ-ray source. By considering only LS events which are in coincidence with the Compton spectrometer it is possible to create a

virtual source inside the sample with a known energy spectrum. The light output of the scinitllator, in terms of mean number of photons detected per keV of energy absorbed in the scinitllator, can be deduced from the measurement of the virtual source. The virtual source is then removed and the source of interest is measured. The detection efficiency of the source to be measured can be deduced from the previously determined light yield [97].

ZERO MODEL BY USING COINCIDENCE SCINTILLATION The ZoMBieS method was developed in order to circumvent the usage of semi-empirical equation that describes the light output of the scintillator. The method uses a three PMT TDCR counter and a γ-ray detector connected in coincidence. The type of coincidence (double or triple) in the TDCR detector produced by each electron is also recorded. The light output of the scintillator can be obtained from the triple to double coincidences ratio analytically under an assumption for a mono-energetic source [97]. Thus, the relative light output of the scintillator can be obtained as a function of the energy deposited by the Compton electrons.

Part II

THE TIME DOMAIN OF LIQUID SCINTILLATION COUNTING

3

ANALYSIS OF DIGITIZED LIST-MODE DATA

Analog acquisition systems in LS counting have some often sought advantages over their digital equivalents. Once build, they are usually stable in time and easy to use. Because they are relatively difficult to build and to make changes after, they are seldom configured in practice and once set up for operation, they are rarely changed again. These qualities are perfect for more routine measurements or when stability has a high priority. However, digital acquisition, and especially waveform digitization and off-line storage, has the edge in some circumstances – especially when exploring new ways in which the detector system could be used.

By using a fast digitizer it is possible to record the timestamp, energy of each signal coming from a PMT or γ-detector in a LS system. The recording is usually done in the storage of a computer and can be analyzed off-line indefinite number of times. This allows the use and comparison of various analysis algorithms on the same set of signals. Having off-line recordings of measurements also gives the possibility to re-process the obtained data differently when new data or knowledge becomes available. For these and other advantages, almost all measurements performed within this thesis were performed with a four channel 1 GS/s CAEN DT5751 digitizer. It has the ability to save the pulse area and timestamp of all incoming PMT pulses into a *list-mode* file for later analysis. To process the data a dedicated home-made software (hereafter referred to as LIST_MODE_ANALYSIS) was developed.

3.1 THE LIST_MODE_ANALYSIS PROGRAM

The LIST_MODE_ANALYSIS is a program that can read CAEN digitizer list-mode files, analyze them using coincidence counting logics and output counting rates and energy or time domain spectra. It is developped in the framework of this thesis, and is intended to be used with a two or three PMT LS detector or a LS detector in coincidence with a γ detector. The program is written in the Rust programming language, which is a strongly-typed system programming language with similar syntax and performance as C++, but has the advantage of being memory safe without using garbage collection.

The PMTs of a LS system are highly sensitive detectors that are very efficient in discerning even single photons. One drawback, however, is the large amount of noise events that can also be observed: uncorrelated events such as thermal noise or noise in the cables and electronics and correlated events such as afterpulses. Thus, single PMTs are not reliable and coincidence between two or more PMTs is looked for in order to discriminate between noise events and true scintillations from the sample. To define the coincidences, at the base of the operation of the LIST_MODE_ANALYSIS program

sits the coincidence counting logic. There are two such logics that were developed for 3-PMT LS detectors – the common dead-time logic used in the MAC_3[1] TDCR acquisition module [100], and the individual dead-times logic developed for the front-end digital pulse processing device for TDCR counting (nanoTDCR) [101]. An early version of the LIST_MODE_ANALYSIS software could use both algorithms, and it was used to perform a comparison of the two. The results from the comparison, as well as more information about the counting algorithms, can be found in Chapter 4. Because of the results from the comparison and the general ease of use of the common dead-time logic, it was selected as the main algorithm for defining coincidences.

The common dead-time logic states that whenever an event is registered in a given channel, a dead-time window that is common for all three channels will be triggered. At the same moment a common coincidence window will also be opened. The dead-time window is in the order of 10 µs and the coincidence window is in the order of a few tens or a few hundreds of nanoseconds. The coincidence window is defined as the time after the first event that opened it in which more events will be considered. After the coincidence window is over, the dead-time window remains open. The dead-time is of the extending type and so all events that fall within the window reset it, i. e., the dead-time window is opened anew. This ensures that before an event is registered, the time that has passed from a previous detected event is at least the width of a one dead-time window. Only after the end of the dead-time window a detected event can start a new coincidence window.

Only the first registered event in a given channel (*primary event*) is considered and all other events in the same channel are ignored for the duration of the coincidence window. This is again necessary due to the occurrence of unwanted afterpulses that follow the main pulse. Within a coincidence window the channel, energy and timestamp of the primary events are recorded. The timestamps, relative to the start of the coincidence window, can be used to construct the spectra of the time differences Δt_i for each coincidence channel $i = AB, BC, AC, D$ or T. The energies can be used to discriminate coincidences using predefined gates, e. g., register only events in coincidence with a certain energy deposited in the γ-channel.

3.2 FLOW OF THE PROGRAM

There are three main modes of operation of the LIST_MODE_ANALYSIS program:

1. obtain the single and coincidence counting rates in the various channels
2. obtain the time distribution of events within a coincidence channel
3. obtain the counting rates in all channels as a function of the energy deposited in the γ channel.

1 The abbreviation comes from the french *module d'acquisition de coïncidences triples* or module for the acquisition of triple coincidences.

LIST_MODE_ANALYSIS: MODE 1 In the first mode the program simply applies the common dead-time logic with user defined coincidence window and dead-time window widths and increments the coincidence counters appropriately. It also monitors the live-time of the system and the end of a run through the data the program reports the counting rates in each channel. This mode is used for more basic LS measurement where timing data is not needed. In this mode, the software also has the ability to record only LS events which are in coincidence with an event within a specified energy window in the γ channel. The latter is especially useful when applying the CSET technique described in Section 2.3.

LIST_MODE_ANALYSIS: MODE 2 The second mode of operation is more involved and it works as follows: The user inputs the path to the CAEN list-mode files, the coincidence window width and the dead-time window duration. The user also selects the coincidence channel for which the time distribution will be constructed (AB, BC, AC, D or T). The reference and secondary single channels must be also chosen, if a double coincidence channel is selected. For example, consider the case when channel A is selected as a reference, channel C as a secondary and the AC time distribution is requested. If C triggers after A the recorded time difference will be positive and if C triggers before A it will be negative.

At the end of each coincidence window, the coincidence counters are incremented appropriately and the histogram $h^{(i)}$ for the selected by the user time distribution is incremented. If the time distribution for the D channel is required and there is a D event during the coincidence resolving time, the histogram bin corresponding to a time difference Δt between the second and the first arriving primary events is recorded. If the selected time distribution is for the T channel, the histogram bin corresponding to the time difference between the third and first arriving primary events is recorded, only if there is a triple coincidence during the coincidence resolving time.

If the selected time distribution is for one of the double coincidence channels AB, BC or AC, it must be noted that some of these events are also T events. If there is a double coincidence from the requested type and there is no T coincidence during the coincidence resolving time, the time difference that is recorded in the histogram is the time between the secondary and reference channels. If there is a T coincidence during the coincidence resolving time, the recorded time difference will be that of the T event. A graphic depiction of the same logic used for the calculation of the different Δt_i can be seen in Figure 3.1.

After the analysis of all files is completed, the LIST_MODE_ANALYSIS code outputs the histogram of the time differences for the user-selected coincidence channel. The histogram has a user selectable bin width. The time differences Δt_i described above are defined in such a way that the histograms $h^{(i)}$ fulfill the following criteria:

$$n^{(i)}(\tau) = \frac{1}{L} \sum_{t=0}^{\tau/b} h_t^{(i)}, \tag{3.1}$$

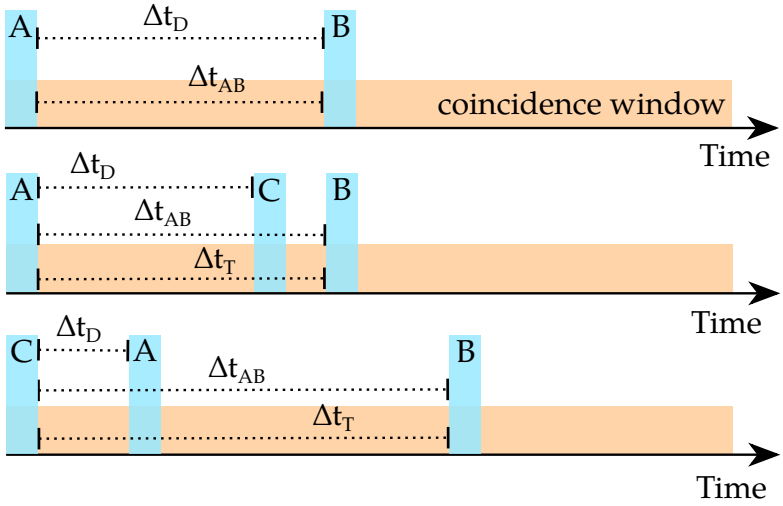

FIGURE 3.1: Time differences between the first and last primary events in the AB, D and T channels. Note that all T coincidences are a subset of the AB coincidences. Thus, in the third case, the C event is the first primary event in both the AB and T channels.

where $n^{(i)}$ is the counting rate that would be reported by a *Mode 1* measurement with coincidence resolving time τ and live-time L. The histograms $h^{(i)}$ give the opportunity to study the counting rate for a given channel as a function of the coincidence resolving time with a single measurement. It should be noted that the construction of the histogram of time differences between only two channels is relatively straightforward and such histograms were shown in previous publications [102]. The time differences in a three PMT systems are more involved, however, and the selection logic described above was first developed for the LIST_MODE_ANALYSIS code.

For the proper analysis of time distributions it is usually also necessary to perform a correction for accidental coincidences. The method for correction for is described in detail in Chapter 8. It is based on the analysis of the time distribution in a given coincidence channel. The underlying assumption is that coincidences of primary events separated by several microseconds in time are accidental. By analyzing the time distribution in the region where the rate of occurrence of true coincidences is negligible, the contribution of the accidental coincidences can be estimated. The measured time distribution $f_i(t)$ is the sum of the distribution of true events $f_{true}(t)$ and the distribution of the accidental coincidences, where $t = \Delta t$. As the accidental coincidences are formed by uncorrelated events and if their occurrence is a Poisson process, then their distribution in time is exponential, which gives:

$$f(t) = f_{true}(t) + a_0 e^{-\lambda t}, \tag{3.2}$$

where a_0 are the accidental coincidences at time zero and λ is the rate of coincidence events.

The parameters of the distribution can then be determined by a fit in the region where the contribution of the true coincidences can be assumed negligible. The contribution of the accidental coincidences in the i^{th} channel in a given bin can then be calculated as:

$$a_t^{(i)} = a_0 e^{a_1 t} \tag{3.3}$$

where a_0 and a_1 are the parameters of the fit of the time interval distribution. In the LIST_MODE_ANALYSIS software the fit is done using time distribution data between 2 µs and 3 µs. This interval was found to contain negligible contribution from true coincidences. The counting rate of the true coincidence in a given coincidence channel i is then determined as:

$$n_{true}^{(i)}(\tau) = \frac{1}{L} \sum_{t=0}^{\tau/b} \left[h_t^{(i)} - a_t^{(i)} \right]. \tag{3.4}$$

At the end of a *Mode 2* analysis, both the $h_t^{(i)}$ and $(h_t^{(i)} - a_t^{(i)})$ histograms are reported by the software.

The second mode of operation was used in the studies in Chapter 8 to develop methods for correction for accidental coincidences. It was also used for studying the effect of the coincidence resolving time on TDCR activity measurements, described in Chapter 9. In Chapter 7, the half-life of some nuclear excited states is measured by analysis of the time distributions of coincidences between LS events and a γ channel.

LIST_MODE_ANALYSIS: MODE 3 The third mode of operation was specifically developed for analysis needed for the application of the C-TDCR method. An overview of the method is given in Section 2.3. This mode is used only with a two or three PMT LS system in coincidence with a γ detector. At the start of the analysis, an empty 2D array with size N : M is initialized, where N is the number of energy channels in the γ spectrum and M are the number of LS-γ coincidence channels (19 in total). If there is a coincidence between a LS channel and the γ channel, the array cell that corresponds to the γ energy and the LS-γ coincidence is incremented. When the entirety of the files are analyzed, the software outputs the 2D array from which the number of events in each coincidence channel can be obtained as a function of the γ channel energy.

3.3 PRACTICAL USAGE

Besides the three main modes of operation, the LIST_MODE_ANALYSIS program has a number of options that can be used to filter specific events or to manipulate the input and output. The software does not have a graphical user interface and it is operated within the command line with a set of options. A full list of the options is given in the Appendix in listing C.1. The source code of the program is published on https://gitlab.com/cdutsov/cdt_logic.

4

COMPARISON OF COINCIDENCE COUNTING ALGORITHMS

For the proper working of a LS counting system, it is important to force an artificial dead-time after each detected signal [100]. The purpose of this practice is to eliminate the chance for the detection of PMT afterpulses. There are two types of dead-time that could be imposed – non-extending and extending type. The former has a fixed duration after each detected signal and the latter is imposed after a signal and is then extended by each subsequent signal that falls within the dead-time. The extending type dead-time is favored in LS counting as it ensures that at least some minimum amount of time, given by the dead-time base duration, has passed between one detected signal and the previous.

In a single PMT LS system the dead-time logic is simple, but in a two or three PMT system there can be a number of ways in which the dead-time can be applied to the various channels. In TDCR counting there are two ways currently in use in which dead-time is imposed. The common dead-time (CDT) counting logic states that an incoming pulse in either channel of the TDCR detector will trigger the dead-time counter for all three channels. The individual dead-times (IDT) counting logic states that an incoming pulse in a given channel will trigger the dead-time counter for that channel only. The other two channels will remain open and could accept new signals. Some example sequences of events and the response of each counting logic are shown in Figure 4.1.

The CDT counting logic is implemented in the analog circuits of commonly used MAC_3 TDCR counting module [100] and the IDT counting logic was recently designed for use in the nanoTDCR counting device [101], which is based on field-programmable gate array (FPGA) technology. While the CDT logic is widely used and well tested, the IDT offers potential improvements in TDCR counting and thus a comprehensive comparison of the two logics is necessary. In this chapter, the performance of the two TDCR counting logics is compared with three different experimental setups and a dedicated Monte Carlo code for simulation of TDCR events. The performed studies are also presented in [103].

4.1 EXPERIMENTAL SETUPS

In order to perform a systematic comparison between the CDT and IDT counting logics, three different experimental setups were used. To have results that are independent of the used hardware, a dedicated Monte Carlo code for the simulation of TDCR events, was used as well. A brief description of each experimental setup and the Monte Carlo code is given hereafter.

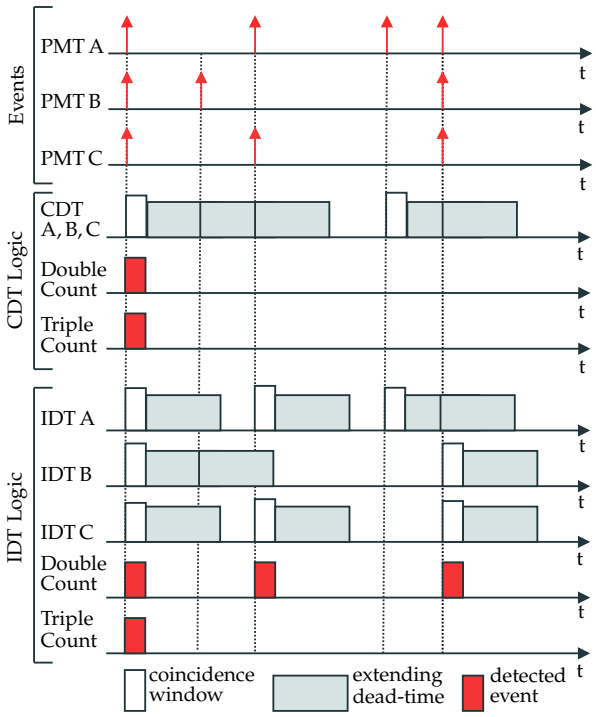

FIGURE 4.1: Comparison of the IDT and CDT counting logics in the case of double and triple coincidences. The IDT counting logic could misclassify triple events as double events, but has much lower double coincidence dead-time.

4.1.1 *RCTD1-MAC3-CAEN desktop digitizer*

The first experimental setup was realized on the French primary TDCR counter (RCTD1). The read-out chain of the RCTD1 consists of an amplifier (CAEN Mod. N978) and a constant fraction discriminator (CFD). The CFD is a Canberra 2126Q with four channels. The digital outputs of the CFD were connected both to the MAC3 module and a CAEN DT5751 desktop digitizer with 1 GHz sampling rate (Figure 4.2). The digitizer has the option to record the time of arrival of the incoming pulses in each TDCR channel in list-mode files. The data files were processed off-line by the LIST_MODE_ANALYSIS computer code, which is described in Chapter 3. Initial versions of the code had the option to obtain the coincidence counting rates when using both the CDT and IDT counting algorithms. The MAC3 is widely used and well tested and thus it was used as a reference to which the digitizer data could be compared.

4.1.2 *Experimental setup 2: RCTD1, MAC3 and nanoTDCR*

The second experimental setup again includes the RCTD1 detector system. This time, the CAEN digitizer was replaced by a nanoTDCR device. Both the nanoTDCR and the MAC3 module were directly connected to the logical outputs of the CFD. A simplified schematic of the setup is shown in Figure 4.3. This setup was used for the measurement of four ^{3}H and three ^{90}Sr/^{90}Y sources. With this experimental setup the real-life

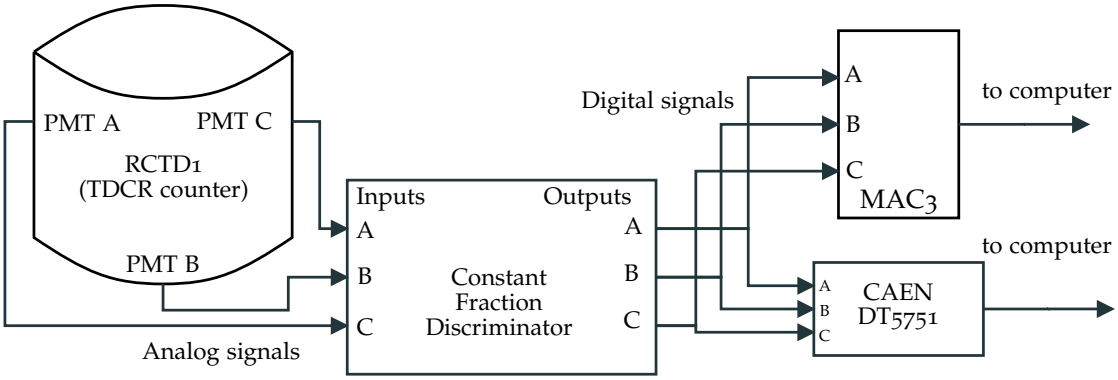

FIGURE 4.2: Schematic of system 1

implementation of both counting logics, CDT implemented in the MAC3 and the IDT implemented in the nanoTDCR, can be compared. By taking the digital outputs of the CFD, all possible differences in the analog signal processing parts of the MAC3 and nanoTDCR are eliminated. This ensures that any differences between the two can come only from statistical fluctuations due to the number of recorded events or differences in the behavior of the two counting logics. A limit of the system is that the two counting systems cannot be started and stopped at exactly the same time and thus they do not count precisely the same set of pulses. Nevertheless, a significant overlap between the pulses that they detect can still be achieved.

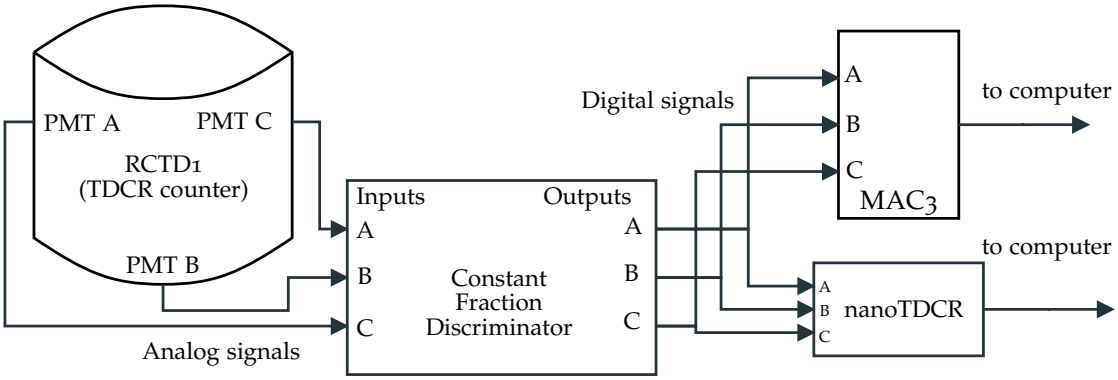

FIGURE 4.3: Schematic of system 2

4.1.3 *Experimental setup 3: CDT and IDT implementation in the FPGA of the nanoTDCR*

The nanoTDCR device is an FPGA based device and thus very versatile and easily extensible. It is capable of simultaneous measurements using two different dead-time base durations and two different coincidence resolving times. This feature turns one measurement with the nanoTDCR into four distinct measurements, each having one of two dead-time base durations and one of two coincidence windows. Moreover, the two dead-time analyzing logics can follow a different counting algorithm, i. e., one with the CDT and one with IDT. Using this opion, one algorithm can be selected for two of the

measurement channels and the other algorithm for the remaining channels. This makes it possibile to compare the two counting logics with simultaneously occuring signals on the same hardware.

For the third experimental setup, a nanoTDCR device was connected directly to the PMTs of the TDCR counter developed and operated at Sofia University (TDCR-SU) [104]. The two possibile coincidence windows of the nanoTDCR where set to 40 ns and 100 ns respectively. Both dead-time base durations were set to 50 µs, but one using the CDT and the other the IDT counting algorithm. With this setup, four pure β-emitters: ^{3}H, ^{14}C, ^{63}Ni, ^{90}Sr/^{90}Y and five ^{222}Rn LS-sources were measured. The activity of the ^{222}Rn sources varies from 60 Bq to 3000 Bq.

The α-emitter ^{222}Rn has four short-lived daughters: ^{218}Po and ^{214}Po – α-emitters and ^{214}Pb and ^{214}Bi – high-energy β-emitters. The daughter nuclide ^{214}Po is of particular interest when comparing the performance of the CDT and IDT algorithms because it can decay during the imposed dead-time of the counter, due to its very short half-life of 165 µs. The logical sum of double coincidences detection efficiency is practically 100% for the α-particles and very close to 100% for the β-particles in the decay chain of ^{222}Rn. Thus, in the standardization of ^{222}Rn via LS counting, the most important factor for calculation of the detection efficiency is the the correction for decay of ^{214}Po during the dead-time of the system [74].

4.1.4 *Simulation: Monte Carlo generated events processed by CDT and IDT counting logics*

In order to have more flexibility and information when comparing the two counting algorithms a Monte Carlo code which simulates the time sequence of PMT detection events in a TDCR measurement was used. The code was developed by Krasimir Mitev for the purposes of this study and is described shortly in [103]. It was also the inspiration for the code described in Appendix A.

The input of the program is the activity and measured counting rates (A, B, C, AB, BC, AC, ABC) from a real measurement of a source. Additionally, the user can add noise counting rates to each PMT. Another important input of the code is the time distribution of scintillation events. In this work, the input time distribution was determined by connecting a time-to-amplitude converter (TAC) to two of the output channels of a TDCR counter. The channels are used as start and stop triggers for the TAC and a measurement of a ^{3}H source was performed. The obtained distribution is approximated well with a sum of a Voigt profile and an exponentially modified Gaussian distribution (see the solid line in Figure 4.4). The so fitted time distribution was then used in all ^{3}H simulations as a function from which the Monte Carlo code samples the timing of individual events. The code outputs the generated single, double and triple coincidence counting rates. It can also output the raw timestamps of each generated event, which can be then fed into the LIST_MODE_ANALYSIS analysis program. It can be used to obtain the distribution of the time intervals between two PMTs. If the Monte Carlo and

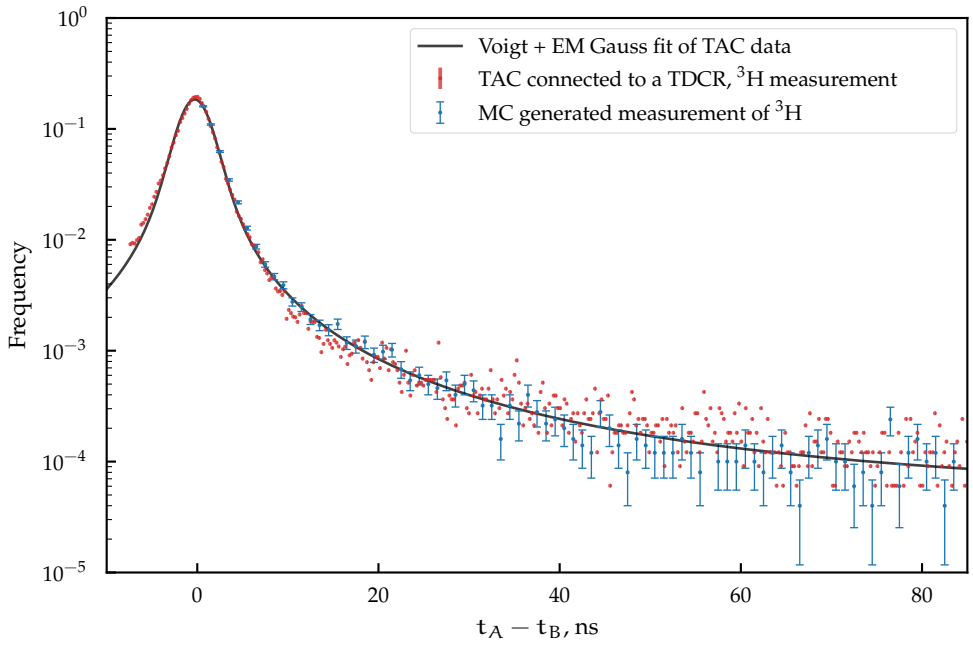

FIGURE 4.4: A TAC measurement of the time interval distribution between events from a ^{3}H source in a TDCR counter (red) and time distribution between Monte Carlo generated events (blue)

LIST_MODE_ANALYSIS codes work correctly, the obtained time distribution should be the same as the one at the input. To illustrate the performance of the Monte Carlo code the input and output time distributions are shown in Figure 4.4. The input is the experimental time from the TAC and the output is the distribution of the time intervals between events in PMTs A and B obtained from the Monte Carlo generated list-mode file analyzed with the LIST_MODE_ANALYSIS program. There is an excellent agreement between the two distributions. The comparison serves to demonstrate that the used Monte Carlo code generates realistic time interval distribution between events in a TDCR counter.

After the validation, the Monte Carlo code was used to generate list-mode files with a time distribution of events corresponding to a ^{3}H source. The data was generated for a wide range of activities. The files were analyzed using the LIST_MODE_ANALYSIS program once using the CDT logic and once using the IDT logic. The artificially generated sequences of events provide a base to which the counting rates that obtained using the two counting algorithms can be compared. The Monte Carlo simulations also provide the opportunity to test the counting logics with a very wide range of activities, which is difficult to achieve in practice.

4.2 RESULTS FROM THE COMPARISON

4.2.1 *Results from experimental setup 1: RCTD1 – MAC3 – CAEN desktop digitizer*

Using the first experimental setup nine ^{3}H sources with activities from 1200 Bq to 47 kBq and nine ^{90}Sr/^{90}Y sources with activities from 920 Bq to 14.5 kBq were measured simultaneously with the two counting systems. The coincidence resolving time of the MAC3 module is 40 ns and the dead-time base duration is 50 µs. The same parameters are used in the LIST_MODE_ANALYSIS code that applies the CDT and IDT counting algorithms. Ten consecutive measurements were performed on each source using the MAC3 module with 60 s acquisition time for ^{3}H and 30 s acquisition time for ^{90}Sr/^{90}Y. The digitizer acquisition time was set to 600 s and 300 s for the ^{3}H and ^{90}Sr/^{90}Y measurements respectively. The activities of the samples were calculated from the obtained coincidence counting rates using the TDCR07c program [93] using the same TDCR model parameters (kB value, cocktail density and elemental composition). The specific activities of the sources from the MAC3 data and the digitizer data using the two counting algorithms are shown in Figure 4.5 for ^{3}H and in Figure 4.6 for ^{90}Sr/^{90}Y. Note the break in the y axis in the figures.

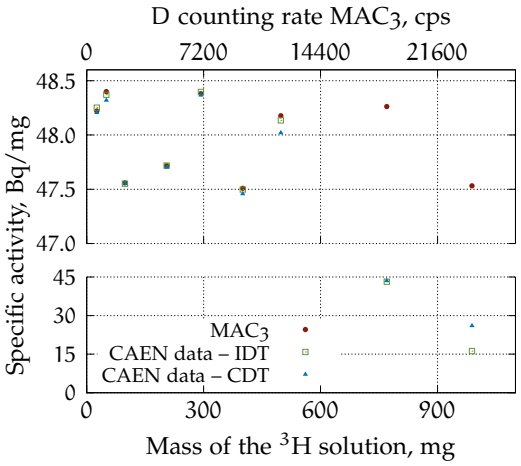

FIGURE 4.5: Specific activity of the ^{3}H sources with experimental setup 1.

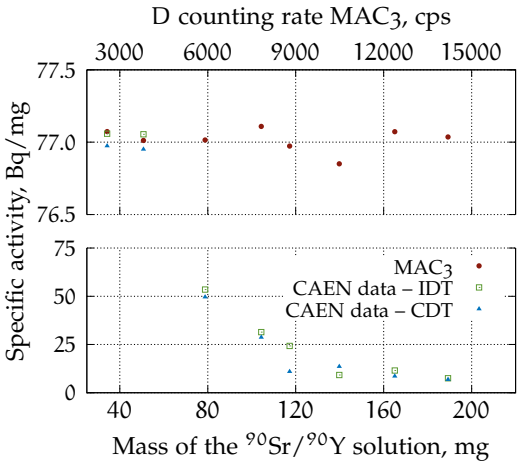

FIGURE 4.6: Specific activity of the ^{90}Sr/^{90}Y sources with experimental setup 1.

We observed that there is a sharp drop in the counting rates obtained with the CAEN DT5751 compared to the MAC3 counting rates. It was later found out that the specific computer that was connected to the digitizer was unable to write all the incoming events to the hard disk drive at counting rates higher than around 30 kcps for ^{3}H and 4 kcps for ^{90}Sr/^{90}Y. The lower limit for the latter comes from the much higher number of photons detected on average due to the much higher mean energy of the β spectrum. The more photons, the more data must be recorded in the memory of the computer. In all later considerations in this chapter concerning the CAEN digitizer measurements only the results where the digitizer was able to record all incoming data were used. The problem was eliminated in all further studies using the digitizer.

The difference between the IDT results (X_{IDT}) and the CDT results (X_{CDT}) is calculated as:

$$\Delta = \frac{X_{CDT} - X_{IDT}}{X_{IDT}} \times 100\%. \tag{4.1}$$

If we consider only the measurements where the digitizer was able to record all incoming events, we see that the activities obtained with the two counting algorithms agree within 0.20% for the ^{3}H measurements and within 0.27% for the ^{90}Sr/^{90}Y measurements (see Figure 4.2). The results from this experiment show that the two counting algorithms return very similar results. Nevertheless, this setup did not allow the study of very high counting rates, where lie both the possible benefits of the IDT algorithm and the possible differences between CDT and IDT.

4.2.2 *Results from experimental setup 2: RCTD1 − MAC3 − nanoTDCR*

Four of the ^{3}H sources (activities from 4.7 kBq to 47 kBq) and three of the ^{90}Sr/^{90}Y sources (activities from 900 Bq to 8 kBq) were chosen to be measured on the second experimental setup. The coincidence window of the MAC$_3$ module and the nanoTDCR device was set to 40 ns and the dead-time base duration to 50 µs in all measurements. The high-voltage of the RCTD1 is automatically set on and off in accordance with the MAC$_3$ acquisition. Therefore, it is necessary that the nanoTDCR counting time is shorter than the MAC$_3$ counting time to ensure that the high-voltage of the detector is on. To achieve that, the acquisition time of the MAC$_3$ was set to 60 s in the live time counter and that of the nanoTDCR to 60 s in the real time counter. This leads to slightly shorter counting times with the nanoTDCR, thereby increasing the uncertainty in these measurements in comparison with the MAC$_3$.

The results from the comparison of the acquisition systems are shown in Table 4.1. The activities of the sources were calculated using the TDCR07c code. The same kB parameter and cocktail data was used to analyze both data sets. The average and the statistical uncertainty of each quantity of interest for a given source are calculated from a set of ten measurements.

The direct comparison shows excellent agreement between the nanoTDCR implementing the IDT counting algorithm, and the MAC$_3$ implementing the CDT counting algorithm. The differences in calculated activity are less than 0.15% for all four measurements of ^{3}H samples with activities from 4.5 kBq and 46 kBq and less than 0.25% for the three measurements of ^{90}Sr/^{90}Y with activities from 900 Bq to 8 kBq.

4.2.3 *Results from experimental setup 3: CDT and IDT implemented in the FPGA of nanoTDCR*

Five sources containing ^{3}H, ^{14}C, ^{63}Ni, ^{90}Sr/^{90}Y and ^{222}Rn in UltimaGold LLT liquid scintillation cocktail were measured using the TDCR-SU detector and nanoTDCR counting device. The nanoTDCR was set to acquire simultaneous CDT and IDT counting measure-

Nuclide	MAC3 Activity, Bq	nanoTDCR Activity, Bq	MAC3 and nanoTDCR difference			
			D	T	Efficiency	Activity
^{3}H	4591(23)	4596(19)	0.38%	0.61%	0.25%	0.11%
	13896(22)	13892(48)	0.14%	0.32%	0.17%	-0.03%
	23265(61)	23297(96)	0.24%	0.34%	0.10%	0.14%
	46184(48)	46240(120)	0.12%	0.12%	-0.01%	0.12%
^{90}Sr/^{90}Y	915(1)	913(2)	0.06%	0.08%	0.18%	-0.20%
	3877(3)	3878(5)	0.05%	0.02%	0.01%	0.04%
	7987(4)	8007(26)	0.14%	-0.06%	-0.17%	0.25%

TABLE 4.1: Comparison of the counting rates, calculated efficiency and activity with the second experimental setup.

ments. The dead-time base duration was set to 50 µs and the coincidence resolving time to 40 ns. Using the TDCR07c program the activities of the pure β sources were calculated from the ratios T/AB, T/BC and T/AC obtained with the two counting algorithms. The average and the standard deviation σ for the quantities of interest for each measured source were calculated from a set of ten measurements. The results are shown in Table 4.2.

Nuclide	CDT Activity, Bq	IDT Activity, Bq	CDT and IDT difference			
			D	T	Efficiency	Activity
^{3}H	871.80(30)	871.80(30)	0.00%	0.00%	−0.01%	0.01%
^{14}C	2327.0(30)	2325.2(30)	0.02%	0.00%	−0.01%	0.04%
^{63}Ni	2110.5(10)	2109.5(10)	0.04%	0.00%	−0.03%	0.07%
^{90}Sr/^{90}Y	3010.2(26)	3009.7(25)	0.01%	0.00%	−0.01%	0.01%
^{222}Rn	3050.9(42)	3039.0(45)	0.21%	0.00%	−0.18%	0.39%
	1825.1(16)	1818.0(14)	0.21%	0.00%	−0.18%	0.40%
	1016.8(10)	1013.0(10)	0.20%	0.00%	−0.17%	0.38%
	147.06(50)	146.41(60)	0.23%	0.00%	−0.21%	0.44%
	60.62(30)	60.31(30)	0.25%	0.00%	−0.24%	0.51%

TABLE 4.2: Comparison results with experimental system №3 – CDT and IDT implemented in the FPGA of the nanoTDCR.

An excellent agreement between the IDT and the CDT counting results is observed for the measurements of ^{3}H, ^{14}C, ^{63}Ni and ^{90}Sr/^{90}Y. The difference in the double

coincidences counting rates is less than 0.05% in all measured samples and no difference is observed in the triple coincidence counting rates. The differences in the calculated activities between the IDT and the CDT are less than 0.07%.

The detection efficiency for the ^{222}Rn source was calculated using a dedicated computer code. It assumes 100% detection efficiency for the α emissions and applies the TDCR model for the two β emissions in the ^{222}Rn decay chain. Most importantly, it applies a correction for the decay of ^{214}Po during the dead-time imposed by ^{214}Bi. The code was developed by Ph. Cassette[1], and a more complete description is to be given elsewhere. The corrected counting rate R_0 of ^{214}Po is calculated in the following way:

$$R_0 = Re^{-\lambda\tau}, \tag{4.2}$$

where the experimentally measured ^{214}Po counting rate is R, λ is the ^{214}Po decay constant and τ is the dead-time base duration. In the case of the IDT logic the dead-time for the D channel is smaller than that for the CDT logic. As no specific correction for IDT exists so far, the same correction was used for both methods. It is possible that differences in the activity calculated by the two methods are due to the need for a different dead-time correction. Differences up to 0.51% between the two counting logics were observed in the ^{222}Rn experiments. The differences are in the double coincidence counting rate estimates which propagate to the estimates of the activity. The most likely explanation for this effect is the possibility of the IDT logic to misclassify T events as D events. This can be seen well in Figure 4.1. Looking at the IDT logic, there exists the possibility of a single event to trigger the dead time in one channel. In this case, the other two channels will remain open. If a triple event is registered during the dead-time of the channel that registered the single, then the two open channels would register a double. The channel that is in dead-time would extend its dead-time and will not register an event.

4.2.4 *Simulation results: Monte Carlo simulation of ^{3}H measurements*

The Monte Carlo code was used to generate list-mode files of ^{3}H measurements with activities up to 200 kBq. The output data of the code was processed using the LIST_MODE_ANALYSIS program. The dead-time base duration and the coincidence window for both counting logics were the same – 50 µs and 40 ns respectively. The coincidence counting rates (CDT or IDT) were compared to the reference coincidence counting rates of the Monte Carlo summary file. The ratio of the CDT to Monte Carlo and the IDT to Monte Carlo double and triple counting rates is shown in Figure 4.7. The difference in double coincidences counting rates is less than 0.07% in all measured samples and between the triple coincidences counting rates are less than 0.16%. However, the two algorithms do not agree well with the Monte Carlo reference counting rates. The differences are within 0.36% in the D channel and up to 1.2% in the T channel

1 The code was recieved in a private communication.

(Figure 4.7, middle). A possible explanation for these deviations is the very short 40 ns coincidence window for ^{3}H. This problem is expanded upon in Chapter 9.

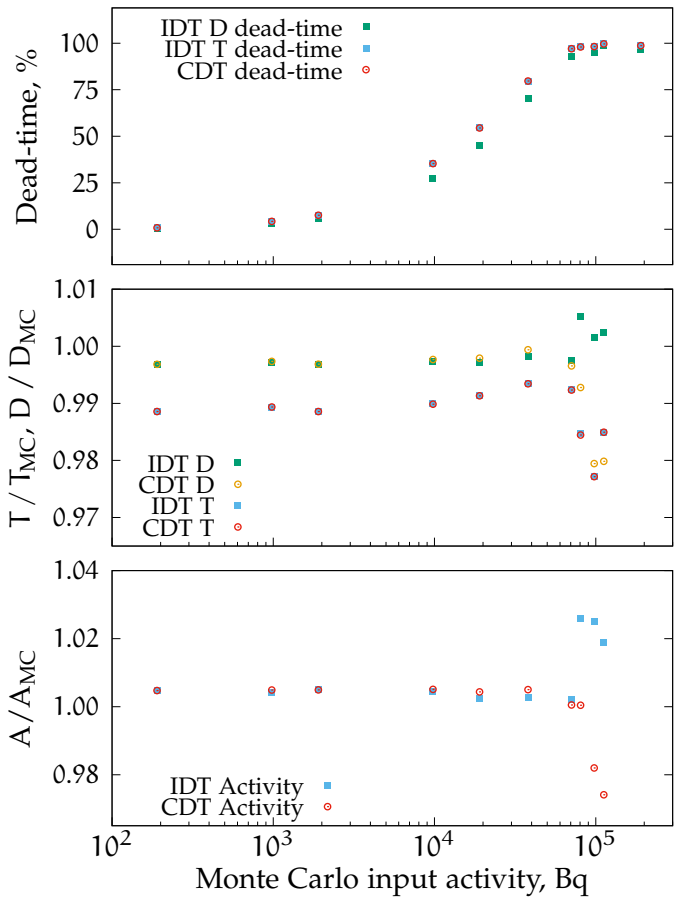

FIGURE 4.7: Comparison between the two counting algrorithms and the Monte Carlo reference counting rates and activities for a simulated ^{3}H measurement.

The TDCR07c program was used to calculate the activity and the same cocktail density, composition and kB parameters were used in all calculations. The ratio of the activities calculated with the CDT and the IDT counting logics to the activity calculated from the raw Monte Carlo counting rates is shown in Figure 4.7 (bottom). Although a significant amount of the triple coincidences were missed by the two algorithms due to the short coincidence window, the TDCR model compensates for some of the losses. There is an excellent agreement between the two for ^{3}H activities up to 80 kBq.

The IDT counting algorithm has an advantage as in this case it results in the same coincidence counting rates and calculated activities, but with a significant reduction in the D dead-time (see Figure 4.7, top). For example, for 9700 Bq activity the D dead-time of the IDT logic is 28.8% and the dead-time of the CDT logic is 38.8%. This leads to 16.3% increase in the D live-time for IDT logic compared to CDT logic. The increase in the live-time is 36.4% at 19 kBq and 81.5% at 38 kBq.

In order to study the influence of the effect of coincidence window on the TDCR results, the first five ^{3}H Monte Carlo generated measurements were processed with

100 ns coincidence window								
D count rate, cps			T count rate, cps			Activity, Bq		
MC data	IDT bias	CDT bias	MC data	IDT bias	CDT bias	MC data	IDT bias	CDT bias
95.19	−0.35%	−0.34%	43.72	−1.24%	−1.24%	189.88	0.48%	0.48%
491.01	−0.28%	−0.27%	225.58	−1.07%	−1.07%	979.08	0.44%	0.50%
16.26	−0.31%	−0.31%	437.11	−1.15%	−1.15%	1901.95	0.51%	0.49%
4915.73	−0.26%	−0.23%	2256.30	−1.01%	−1.01%	9809.87	0.46%	0.51%
9522.37	−0.29%	−0.21%	4368.84	−0.87%	−0.87%	19014.31	0.25%	0.43%
200 ns coincidence window								
D count rate, cps			T count rate, cps			Activity, Bq		
MC data	IDT bias	CDT bias	MC data	IDT bias	CDT bias	MC data	IDT bias	CDT bias
95.30	−0.15%	−0.16%	43.67	−0.59%	−0.59%	190.52	0.25%	0.25%
491.61	−0.11%	−0.12%	226.01	−0.55%	−0.55%	979.89	0.29%	0.28%
952.69	−0.19%	−0.17%	437.11	−0.62%	−0.62%	979.89	0.29%	0.28%
4916.44	−0.05%	−0.07%	2256.06	−0.45%	−0.45%	9813.26	0.33%	0.31%
9520.00	0.03%	0.11%	4368.84	−0.24%	−0.25%	19014.31	0.23%	0.39%
300 ns coincidence window								
D count rate, cps			T count rate, cps			Activity, Bq		
MC data	IDT bias	CDT bias	MC data	IDT bias	CDT bias	MC data	IDT bias	CDT bias
95.40	−0.16%	−0.16%	43.83	−0.60%	−0.60%	190.18	0.26%	0.23%
492.73	−0.19%	−0.18%	226.85	−0.57%	−0.57%	980.74	0.19%	0.20%
952.01	−0.17%	−0.15%	437.73	−0.48%	−0.49%	1897.56	0.10%	0.13%
4915.25	−0.05%	0.00%	2255.75	−0.32%	−0.32%	9808.92	0.21%	0.32%
9523.22	−0.13%	−0.04%	4368.16	−0.28%	−0.28%	19019.81	0.01%	0.18%

TABLE 4.3: Tests of the influence of the coincidence resolving time on two counting algorithms. The bias is calculated relative to the Monte Carlo reference.

100 ns, 200 ns and 300 ns coincidence windows. The bias of both the CDT and the IDT counting logics against the Monte Carlo ground truth is calculated as in equation 4.1. The results are shown in Table 4.3 and show that with the increase of the coincidence window the differences between the Monte Carlo data and the estimated D and T counting rates, efficiencies and activities tend to decrease. This is true for both the CDT and the IDT estimates. These results imply that 40 ns coincidence window duration is too short for ^{3}H measurements and it seems that 200 ns or even 300 ns coincidence windows would be a better choice. This phenomenon is expanded upon in Chapter 9 and in [105].

CONCLUSIONS

A comprehensive experimental comparison of the IDT and the CDT counting logics was performed. The results were backed up by analysis of artificially generated sequences of events by means of Monte Carlo simulations. An excellent agreement was observed between the two counting logics for measurements of the pure β-emitting radionuclides

^{3}H, ^{14}C, ^{63}Ni and ^{90}Sr/^{90}Y. In the case of ^{222}Rn however, there are differences up to 0.51% in the ^{222}Rn activities calculated by the two counting logics. The differences are in the double coincidence counting rate estimates which propagate to the estimates of the activity. The most probable reason was identified as the misclassification of T events as D events by the IDT logic, which could happen in certain cases. Due to this, and its general complexity, the IDT logic was excluded in the LIST_MODE_ANALYSIS code after this study.

The analysis of the Monte Carlo simulated measurements of ^{3}H indicate an excellent agreement between the two methods. The observed differences are less than 0.11% for activity up to 38 kBq. The IDT counting algorithm seems to have an advantage in this particular case as it results in the same counting rates and calculated activities, but with a significantly reduced dead-time in the D channel. The performed simulations also indicate that a 40 ns coincidence resolving time is insufficient for ^{3}H measurements as the measured counting rates are significantly lower that the ones generated by the Monte Carlo code. Better agreements can be achieved with 200 ns or even 300 ns coincidence window. The last discovery paved the way for the quest for finding the optimal resolving time (Chapter 9) and the evaluation of accidental coincidences (Chapter 8) which is necessary for the use of long coincidence windows. The findings in this study were published in [103].

5 THE TIMING OF DETECTED PROMPT SCINTILLATION EVENTS

Due to the finite life-time of the excited states of the fluorescent molecule, the scintillation photons are emitted in different times with respect to the moment of radioactive decay. This moment is however unknown in a typical LS measurement as radioactive decay is a stochastic process. Therefore, there is no reference time to which the time of emission of individual scintillation events could be linked to. What is realistically measurable with a LS counting system, however, is the distribution of the time intervals between signals from two PMTs, i. e., one giving the reference time and the other giving a stop signal. The signals themselves are the product of detected scintillation photons. The distribution is based on the probability density of the time difference between the detected signals in each of the two PMTs. This difference is given by the cross-correlation operation which is usually used in the field of signal processing, thus, for the sake of simplicity, this distribution will be hereafter called the *cross-correlation distribution*. The purpose of this chapter is to present a theoretical model of the cross-correlation distribution, derived after initial assumptions about the nature of the light emission and detection processes.

There are several questions regarding the cross-correlation distribution that this thesis aims to answer:

- Can the distribution of accidental coincidences be distinguished from the distribution of true coincidences?
- What is the necessary coincidence window with that needs to be used in order not to miss true coincidences?
- Can the information contained in the time distribution of scintillation events be used to calculate the mean number of detected photons, thus contributing to and improving current activity standardization methods?
- What are the ratios of detected prompt and delayed fluorescence events to the total detected? Do these ratios depend on the scintillator, nuclide, coincidence window and other parameters?

Finding answers to these questions requires first a proper understanding of how the detected scintillation events are distributed in time in regard to one another. The second necessity is the development of a good model of this time distribution.

When the time of detection of a PMT signal is considered it concerns only the first photon detected in that PMT within the coincidence window (primary event). This is done in order to ensure that only true signals are considered and PMT afterpulses are

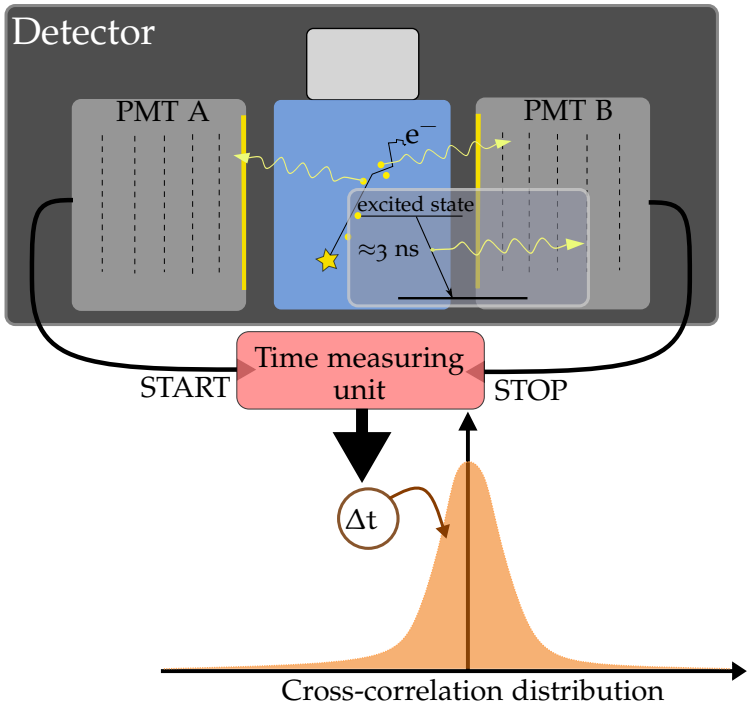

FIGURE 5.1: A schematic illustration of the acquisition of the cross-correlation distribution.

ignored. Considering the timing of the primary events only is adequate, as the primary event forms the rising edge of the PMT signal and its timestamp is recorded by the analyzing electronics. Note that, when deriving the cross-correlation distribution, we will assume that the time of emission of a photon is the same as the time that it hits the photocathode of a PMT. This assumption is reasonable as the distance between the center of the scinitllation vial and the photocathode is less than two centimeters. This corresponds to roughly 100 ps with the speed of light.

Considering a two PMT LS detector, there is a sequence of events that can be followed from the initial decay of a radionuclide withing the scintillator to the detection of a primary event by the electronics. It is shown schematically in Figure 5.1. We will limit the discussion to β-emitters, but the logic would be similar for the other types of radionuclides. Following a radioactive decay, an electron with a given energy E is released into the liquid scintillator. The charged particle gradually loses its energy in interactions with the molecules of the scintillator, creating a total of N excited states in the process. Most of the excited states will de-excite non-radiatively, but a fraction will produce scintillation photons. Of these photons some will be absorbed by the scintillator and some will be lost in the walls of the optical chamber. A part of the emitted photons can reach the photocathodes of the PMTs. The photocathodes usually have a quantum efficiency between 20% and 40% thus not all photons that reach them will produce photoelectrons by the photoelectric effect. In practice, the PMTs that are used are such that even a single photoelectron produces a measurable signal with practically 100% probability. Following the sequence of events, an electron depositing energy E in the scintillator will result in N excited states of which n will be detected by the detector –

k of those in one PMT and $(n-k)$ in the other. The time interval between two primary events will, in fact, be the time between the first from k photons detected in one PMT and the first from $(n-k)$ photons detected in the other PMT.

The quantity of interest in this work is the cross-correlation distribution $D(\Delta t)$ of the time intervals between the primary events in a two PMT detection system.

5.1 DISTRIBUTION OF THE TIME INTERVALS BETWEEN PRIMARY EVENTS

Consider the case where an electron with energy E is absorbed by the scintillator and produces n excited states $x_1, x_2, \ldots, x_n$ that will all emit photons that will be detected. Let the probability (p_i) for each state to de-excite at a given time t is an exponential distribution with a decay constant λ:

$$p_i(t) = \lambda e^{-\lambda t}. \tag{5.1}$$

The function of interest here is the distribution of the time of emission from the state that de-excites first, as that state will form the rising edge of the detector signal and will serve as the start or stop in the timing circuit. The probability for the state x_1 to be the first de-exciting is the probability of x_1 to de-excite at moment t and all the other states to de-excite after it:

$$p_{x1}(t) = \lambda e^{-\lambda t}\left[\int_t^\infty \lambda e^{-\lambda t} dt\right]^{n-1} = \lambda e^{-n\lambda t}, \tag{5.2}$$

where the second term is the probability of all other states to de-excite after x_1. The probability of the first photon arriving at time t from any of the n states is then:

$$P_i(t) = p_{x1} + p_{x2} + \ldots + p_{xn} = n\lambda e^{-n\lambda t}, \tag{5.3}$$

where i denotes one of the PMTs. A schematic illustration of this logic is given in Figure 5.2.

For a detector system with two PMTs the total number of detected photons n will be the sum of k detected in the one PMT and $n-k$ detected in the other. If the two PMTs are denoted with A and B, and if the first emitted photon is assumed to be the first to be detected, then, according to equation (5.3), the probability for detection of the first photon at a time t_A in PMT A or t_B in PMT B will be:

$$\begin{aligned} P_A(t_A) &= k\lambda e^{-k\lambda t_A} \\ P_B(t_B) &= (n-k)\lambda e^{-(n-k)\lambda t_B} \end{aligned} \tag{5.4}$$

In the following subsections the probability density function (pdf) $P_{AB}(t_A - t_B)$ will be developed.

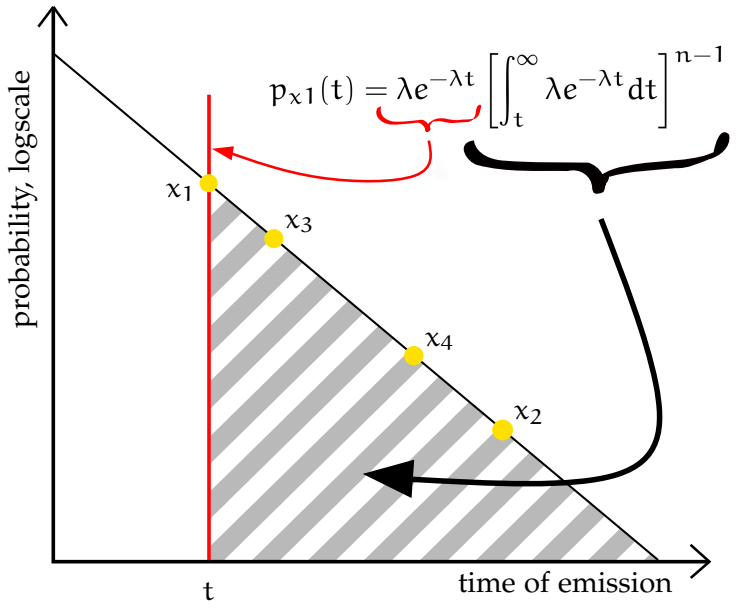

FIGURE 5.2: A schematic illustration of the probability density function of the emission time of the first from n emitted photons. It is equivalent to the probability of a state to de-excite at a time t multiplied by the probability of all other states to de-excite at a later moment.

5.1.1 *Probability density function of the time between two exponentially distributed random variables*

Let X and Y be two exponentially distributed random variables. The pdf of X is $\tau e^{-\tau x}$ and the pdf of Y is $\mu e^{-\mu x}$. The joint pdf of X and Y is:

$$P_{X,Y}(x, y) = \tau\mu e^{-\tau x} e^{-\mu y} \tag{5.5}$$

Let $Z = Y - X$. The function of interest is the pdf of Z. First, the cumulative distribution function of Z is $F_Z(z)$, i. e., the probability that $Z \leqslant z$, thus the question is what is the probability that $Y - X \leqslant z$. For a given z, x and y must satisfy the condition $y - x = z$. This can be calculated using the following integral. First, integrate equation (5.5) with respect to y, and then with respect to x. Note that y travels from 0 to $x + z$, and x travels from 0 to infinity. Thus,

$$P(Z \leqslant x) = \int_0^\infty \tau e^{-\tau x} \left(\int_{y=0}^{x+z} \mu e^{-\mu y} \, dy \right) dx. \tag{5.6}$$

The inner integral is $1 - e^{-\mu(x+z)}$. The equation can then be solved for x:

$$\begin{aligned} P(Z \leqslant z) &= \int_0^\infty \left(\tau e^{-\tau x} - \tau e^{-\mu z} e^{-(\tau+\mu)x} \right) dx \\ &= 1 - \frac{\tau}{\tau + \mu} e^{-\mu z}, \end{aligned} \tag{5.7}$$

which gives the comulative distribution function of the difference of two exponentially distributed random variables. For the pdf $f_Z(z)$ of Z, the cumulative distribution function can be differentiated and the result is:

$$f_Z(z) = \frac{\tau\mu}{\tau+\mu} e^{-\mu z}, \quad \text{for } z \geqslant 0. \tag{5.8}$$

Note here, that equation (5.8) only deals with positive values of z. For negative z the expression is similar, but the argument in the exponent will be positive τ. Equation (5.8) gives the pdf of the time of arrival between two exponentially distributed random variables with different decay parameters μ and τ.

5.1.2 *Probability density function of the time between primary events*

Now consider the case where there are n photons, each of them having an exponential distribution in time of the type $\lambda e^{\lambda t}$. These n photons are all detected by a system with a two PMTs, PMT A and PMT B. Let PMT A be the reference PMT, which will give the start signal and let PMT B be the secondary PMT, which will give the stop signal. The distribution of the time interval between the first photon that hits the secondary PMT and the first photon that hits the primary PMT will be derived hereafter.

If there are a total of k photons incoming on the primary PMT, the time of detection of the primary event, according to (5.3) is

$$P_A(t_A) = k\lambda e^{-k\lambda t_A},$$

where $k\tau$ is the effective decay constant that the PMT observes. Similarly, for the secondary PMT there are $(n-k)$ detected photons and the time distribution of the primary event is

$$P_B(t_B) = (n-k)\lambda e^{-(n-k)\lambda t_B},$$

where $(n-k)\lambda$ is the effective decay constant that is observed by the secondary PMT.

Substituting $\tau = k\lambda$ and $\mu = m\lambda$ in (5.8), the pdf of the time between the primary events in the two PMTs $Q_{AB}(\Delta t_{AB})$, where one PMT detected k photons and the other detected $(n-k)$ photons, is:

$$Q_{AB}(\Delta t_{AB}) = \frac{k(n-k)}{n} \tau e^{-(n-k)\lambda\Delta t_{AB}}, \quad \text{valid for } t \geqslant 0, \tag{5.9}$$

where $\Delta t_{AB} = t_A - t_B$.

Now consider a simplified source of light which emits exactly n number of photons every time it is activated, and they are detected by a two PMT system. The probability, then, to have k number of detected photons in the primary PMT and $(n-k)$ number of photons in the secondary PMT can be calculated by the binomial distribution as:

$$B(n,k) = \frac{n!}{k!(n-k)!}\, \varepsilon_A^k\, \varepsilon_B^{n-k} \tag{5.10}$$

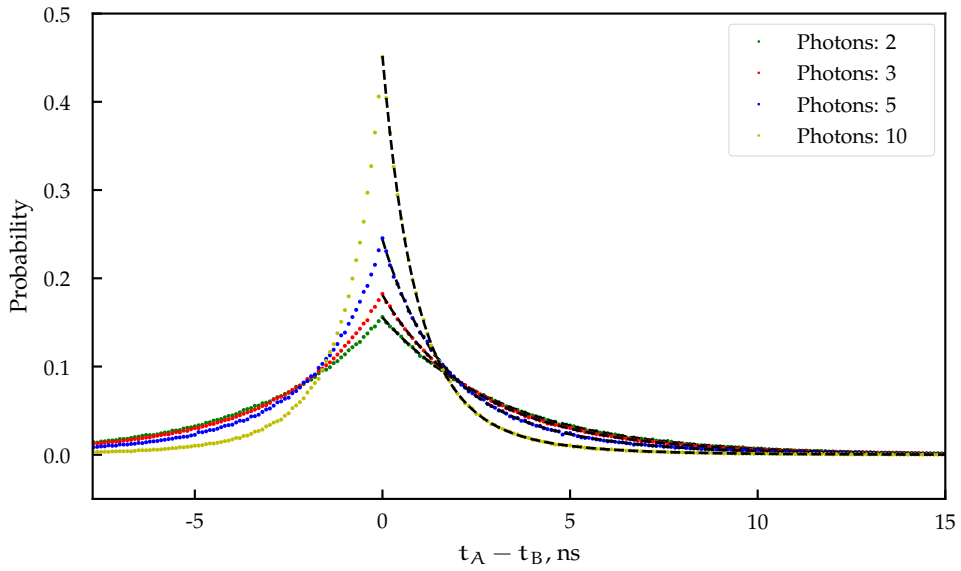

FIGURE 5.3: Histogram of the difference between the primary events in PMT B and PMT A. The figure is in linear scale. The black line is the theoretical model according to equation 5.11.

Combining equations (5.9) and (5.10) and summing over all possible combinations the pdf $S_{AB}(t_{AB})$ of the time difference Δt between the primary events is obtained:

$$S_{AB}(\Delta t_{AB}) = \frac{1}{C}\sum_{k=1}^{n-1}\frac{n!}{k!(n-k)!}\,\varepsilon_A^k\,\varepsilon_B^{n-k}\,\frac{k(n-k)}{n}\tau e^{-(n-k)\tau t}, \quad \text{valid for } t \geqslant 0. \tag{5.11}$$

Note that, the summing of k is from 1 to $n-1$. That must be so, because events with 0 photons in either PMT will not result in a detected coincidence. Because of that, the equation is also not normalized. The normalization factor C is equal to:

$$C = \sum_{k=1}^{n-1}\frac{n!}{k!(n-k)!}\,\varepsilon_A^k\,\varepsilon_B^{n-k}, \tag{5.12}$$

or the sum of probabilities for detected events.

VALIDATION OF THE EQUATIONS In order to test whether equation (5.11) gives correct results, the Monte Carlo code described in Appendix A is used. A small modification is included to remove the Poisson distributed number of photons for a given energy and substitute it with user selectable fixed number of photons produced in every decay event. The comparison can also serve as a visualization of the distribution for various parameters.

The code was used to simulate measurements with 2, 3, 5 and 10 photons. The obtained histograms are plotted alongside the normalized equation (5.11) with the same parameters. The results from the comparison of the analytical equation and the Monte Carlo simulation are shown in Figure 5.3. An excellent agreement between the analytical function and the Monte Carlo simulated histogram can be observed. Note

that, equation (5.11) describes only events where PMT A gives the start signal and PMT B the stop signal. The symmetric case will be described later. It is interesting to note how the shape of the distribution changes with the change in number of detected photons. When increasing the total number of detected events, the height of the distribution increases and it becomes narrower.

5.1.3 *Response function of the detector*

What should also be modelled when describing the distribution of the time between detections of primary events is the response function of the detector. For large time differences of tens of nanoseconds it would be negligible, but it plays a major role if very short time intervals are considered. The time response of the PMTs and associated electronics is assumed to be described by a Gaussian function of the type:

$$G(t;\mu_i,\sigma_i) = \frac{1}{\sqrt{2\pi}\sigma_i} exp\left(-\frac{(t-\mu_i)^2}{2{\sigma_i}^2}\right), \tag{5.13}$$

where $i = A, B$ for the two PMTs. It is also assumed that the response function of the detector applies to the primary event only, i. e., the first photon that produces a photoelectron in the PMT is the first event that is registered by the electronics. This model is adequate as the rearrangement of signals from individual photons in the PMT would be unlikely and the major contribution to the uncertainty in the final recorded timestamp comes from the analyzing electronics. With this assumption, the probability PG_i to regster a pulse with a timestamp t_i, which corresponds to the detection of the first event in one of the PMTs, becomes:

$$\begin{aligned} PG_A(t_A;n,k,\lambda,\mu_A,\sigma_A) &= P_A(t_A;n,k,\lambda) * G_A(t;\mu_A,\sigma_A), \\ PG_B(t_B;n,k,\lambda,\mu_A,\sigma_A) &= P_B(t_B;n,k,\lambda) * G_B(t;\mu_B,\sigma_B), \end{aligned} \tag{5.14}$$

where $*$ indicates convolution.

Here we are interested in the probability to obtain a time difference $\Delta t_{AB} = t_A - t_B$ between the pulses from PMTs A and B, which is given by the cross-correlation of $PG_A(t)$ and $PG_B(t)$. Similarly, the time differences between B and A, $\Delta t_{BA} = t_B - t_A$, is given by the cross-correlation of $PG_B(t)$ and $PG_A(t)$.

$$\begin{aligned} PG_{AB}(\Delta t) &= PG_A(t_A) \star PG_B(t_B), \\ PG_{BA}(\Delta t) &= PG_B(t_B) \star PG_A(t_A), \end{aligned} \tag{5.15}$$

where $\star$ denotes the cross-correlation operator. The sum of the distributions PG_{AB} and PG_{BA} will be referred to as the cross-correlation distribution between PMTs A and B. Noting that the cross-correlation of functions $f(t)$ and $g(t)$ is equivalent to the convolution of $f(t)$ with $g(-t)$, one also gets:

$$\begin{aligned} PG_{AB}(\Delta t) &= PG_A(t_A) * PG_B(-t_B), \\ PG_{BA}(\Delta t) &= PG_B(t_B) * PG_A(-t_A). \end{aligned} \tag{5.16}$$

Then, substituting equations (5.14) in (5.16) and using the associativity of the convolution operator, the equations can be written as:

$$\begin{aligned} PG_{AB}(\Delta t_{AB}) &= (P_A(t_A) * P_B(-t_B)) * (G_A(t_A) * G_B(-t_B)), \\ PG_{BA}(\Delta t_{BA}) &= (P_B(t_B) * P_A(-t_A)) * (G_A(t_B) * G_A(-t_A)). \end{aligned} \tag{5.17}$$

In order to simplify the notation, it is useful to define $\Delta t = \Delta t_{AB} = -\Delta t_{BA}$. Explicitly, the distribution $P_{AB}(\Delta t; n, k, \lambda) = P_A(t_A) * P_B(-t_B)$ is given by:

$$P_{AB}(\Delta t; n, k, \lambda) = \begin{cases} \frac{k(n-k)}{n}\lambda e^{-(n-k)\lambda\Delta t}, & \text{for } \Delta t \geqslant 0, \\ 0, & \text{for } \Delta t \leqslant 0. \end{cases} \tag{5.18}$$

Similarly, for $P_{BA}(\Delta t; n, k, \lambda) = P_B(t_B) * P_A(-t_A)$:

$$P_{BA}(\Delta t; n, k, \lambda) = \begin{cases} 0, & \text{for } \Delta t \geqslant 0, \\ \frac{k(n-k)}{n}\lambda e^{-k\lambda\Delta t}, & \text{for } \Delta t \leqslant 0. \end{cases} \tag{5.19}$$

Noting that the convolution of two Gaussian distributions is also a Gaussian distribution and that $G(-t; \mu, \sigma) = G(t; -\mu, \sigma)$, one gets:

$$\begin{aligned} G_{AB}(\Delta t; \mu, \sigma) &= G_A(t_A; \mu_A, \sigma_A) * G_B(t_B; -\mu_B, \sigma_B), \\ G_{BA}(\Delta t; \mu, \sigma) &= G_B(t_B; -\mu_B, \sigma_B) * G_A(t_A; \mu_A, \sigma_A), \end{aligned} \tag{5.20}$$

with $\mu = \mu_A - \mu_B$ and $\sigma^2 = \sigma_A^2 + \sigma_B^2$. Finally, for the cross-correlation distributions $PG_{AB}(t)$ and $PG_{BA}(t)$, the following equations are obtained:

$$PG_{AB}(\Delta t; n, k, \lambda, \mu, \sigma) = P_{AB}(\Delta t; n, k, \lambda) * G_{AB}(\Delta t; \mu, \sigma) \tag{5.21}$$

$$PG_{BA}(\Delta t; n, k, \lambda, \mu, \sigma) = P_{BA}(\Delta t; n, k, \lambda) * G_{BA}(\Delta t; -\mu, \sigma), \tag{5.22}$$

The convolution of an exponential distribution of the type $f(x) = \tau e^{-\tau x}$ and a Gaussian distribution is the exponentially modified Gaussian distribution with the form:

$$EMG(t; \tau, \mu, \sigma) = \frac{\tau}{2} e^{\frac{\tau}{2}(2\mu + \tau\sigma^2 - 2t)} \operatorname{erfc}\left(\frac{\mu + \tau\sigma^2 - t}{\sqrt{2}\sigma}\right), \tag{5.23}$$

where erfc denotes the complementary error function $\operatorname{erfc}(x) = 1 - \operatorname{erf}(x)$. In order to evaluate the convolutions in (5.21) and (5.22), the following substitutions can be made: $t = \Delta t$ and $\tau = k\lambda$ in the case of PG_{AB} and $t = -\Delta t$ and $\tau = (n-k)\lambda$ in the case of PG_{BA}. The total distribution of the time intervals Δt then becomes:

$$\begin{aligned} \Xi(\Delta t; n, k, \lambda, \mu, \sigma) = \frac{1}{n}\Big(& k\ EMG_{AB}\left(\Delta t; (n-k)\lambda, \mu, \sigma\right) \\ & + (n-k)\ EMG_{BA}\left(-\Delta t; k\lambda, -\mu, \sigma\right)\Big). \end{aligned} \tag{5.24}$$

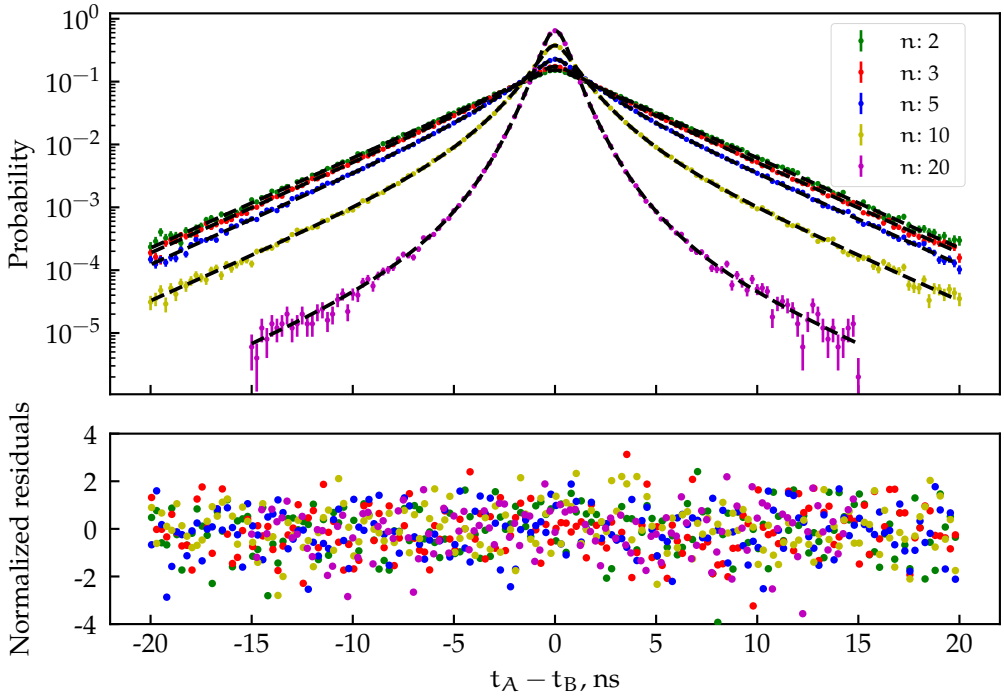

FIGURE 5.4: Histogram of the difference between primary events in PMT B and PMT A. The black line is the theoretical model calculated using equation 5.25.

5.1.4 *Binomial statistics of the number of detected events*

The probability to detect exactly k photons in one PMT and $m = n - k$ in the other out of n detected photons per ionizing particle is given by the binomial distribution. Thus, summing over all possible n and k pairs one obtains the cross-correlation distribution between two PMTs for a fixed number of exactly n detected photons:

$$B(\Delta t; n, \lambda, \varepsilon_A, \varepsilon_B, \mu, \sigma) = \sum_{k=1}^{n-1} \binom{n}{k} \varepsilon_A^k \varepsilon_B^{n-k} \Xi(\Delta t; n, k, \lambda, \mu, \sigma), \tag{5.25}$$

where ε_A and ε_B are the relative efficiencies of the PMTs which satisfy the equality $\varepsilon_A + \varepsilon_B = 1$. It should be noted that the binomial coefficients are summed from 1 to $n - 1$, because events with zero hits in either PMT will not result in a detected coincidence.

The validity of equation 5.25 was tested using the Monte Carlo code. The program was used to simulate an artificial measurement in which each decay produces exactly n detected photons, i.e., no Poisson statistics for the average number of detected photons. The Gaussian jitter of the PMTs is set to 0.6 ns and the decay time of the scintillator to 4 ns. The analytical time distribution was calculated using equation (5.25) with the same parameters. The comparison is shown in Figure 5.4. Excellent agreement was found between the theoretical model and the Monte Carlo simulation.

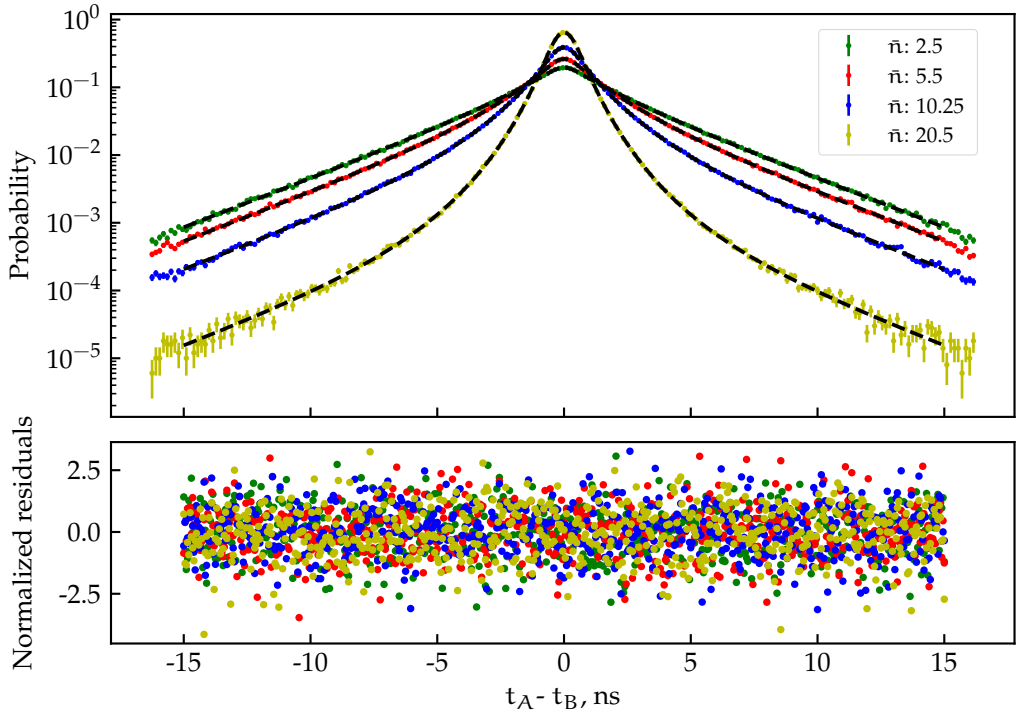

FIGURE 5.5: Histogram of the difference between the primary events in PMT B and PMT A. The black lines are the calculations with the theoretical model given in equation 5.26.

5.1.5 *Poisson statistics of the number of detected events*

In a real situation the number of excited states for a deposited energy E will not be a fixed number n, but will follow a Poisson distribution with a mean number $\bar{n}$. By summing through all possible n we obtain:

$$\Pi(\Delta t; \bar{n}, \lambda, \varepsilon_A, \varepsilon_B, \mu, \sigma) = \sum_{n=2}^{\infty} \sum_{k=1}^{n-1} \frac{\bar{n}^n}{n!} e^{-\bar{n}} \binom{n}{k} \varepsilon_A^k \varepsilon_B^{n-k} \Xi(\Delta t; n, k, \lambda, \mu, \sigma), \quad (5.26)$$

The validity of equation (5.26) was also tested using the Monte Carlo code. The program was used to simulate an artificial measurement of a monoenergetic source with a constant mean number of detected photons. The Gaussian jitter of the PMTs is set to 0.6 ns and the decay time of the scintillator to 4 ns. The analytical time distribution was calculated using equation (5.26) with the same parameters. The comparison is shown in Figure 5.5. Excellent agreement was found between the theoretical model and the Monte Carlo simulation. It is interesting to note that the slope of the long tailing is independent of the number of photons, because, after a long enough time, all exponents die out, and what is left are only the exponents which correspond to 1 photon per PMT.

5.2 THE CROSS CORRELATION DISTRIBUTION AND THE FREE PARAMETER MODEL

Equation (5.26) is sufficient to describe the cross-correlation distribution that would result in the case of mono-energetic electrons. If the source is a β-emitting radionuclide, then its β-spectrum must be taken into account. Introducing the spectrum of the deposited energy in the scintillator $S(E)$, the final cross-correlation distribution becomes:

$$D(\Delta t;\varphi,\lambda,\varepsilon_A,\varepsilon_B,\mu,\sigma) = \frac{1}{L}\underbrace{\int_0^{E_{max}} S(E)}_{\text{Energy spectrum}}\underbrace{\sum_2^{\infty}\frac{(\bar{n}(E;\varphi))^n}{n!}e^{-\bar{n}(E;\varphi)}}_{\text{Poisson statistics}}$$
$$\underbrace{\sum_{k=1}^{n-1}\binom{n}{k}\varepsilon_A^k\varepsilon_B^{n-k}}_{\text{Combinatorial term}}\underbrace{\Xi(\Delta t;n,k,\lambda,\mu,\sigma)}_{\text{Cross-correlation}}\,dE, \quad (5.27)$$

where E_{max} is the maximum energy in the particle spectrum $S(E)$, μ is the difference in the static time delay of the two PMTs and σ is the quadratic sum of the standard deviation of the Gaussian time jitters in the two PMTs. L is a normalization coefficient equal to the probability of all detected events:

$$L = \int_0^{E_{max}} S(E)\sum_2^{\infty}\frac{(\bar{n}(E;\varphi))^n}{n!}e^{-\bar{n}(E;\varphi)}\sum_{k=1}^{n-1}\binom{n}{k}\varepsilon_A^k\varepsilon_B^{n-k}\,dE, \quad (5.28)$$

which is necessary because events with less than one detected photon per PMT will not lead to coincidence and will not be detected. The Poisson distribution accounts for the probability to have n detected photons in a given decay if there are $\bar{n}$ photons detected on average for a particular energy. The mean number of detected photons $\bar{n}$ with respect to the deposited energy in the cocktail E can be obtained as[1].

$$\bar{n}(E;\varphi) = EQ(E)\varphi, \quad (5.29)$$

where $Q(E)$ is a factor that takes into account the ionization quenching and is dependent on the energy of the particle as well as on the stopping power of the particle in the scintillator. The parameter φ is the figure of merit (FOM) and it is equal to the mean number of detected photons per keV of effective energy released into the scintillator - i. e., after taking into account ionization quenching. The most widely used description of the ionization quenching function $Q(E)$ is given by Birks' semi-empirical equation (1.12).

The cross-correlation term $\Xi(\Delta t)$ gives the probability to have a given Δt between the first photon from k total detected in one PMT and the first photon from $(n-k)$ total detected in the other PMT. It is given by $\Xi(\Delta t;n,k,\lambda,\mu,\sigma)$ (explicitly given in equation (5.1.3)) and is a sum of two exponentially modified Gaussian distributions. The parameters μ and σ are the Gaussian centroid and standard deviation, respectively

1 See equation (2.18) in Section 2.1 for a derivation.

and τ is the decay constant of the exponential distribution. The two terms in the sum in equation (5.1.3), EMG_{AB} and EMG_{BA}, consider the two cases $t_A - t_B \geqslant 0$ and $t_A - t_B \leqslant 0$.

One of the parameters that determine the cross-correlation distribution, as shown in equation (5.2), is the FOM φ. Thus, if the decay constant of the scintillator λ and the parameters of the response function of the system (μ, σ, ε) are known, then φ is the only free parameter left. If the derived model describes the timing properties of the detected scintillation events, then the FOM can be estimated from the experimentally obtained cross-correlation distribution. The FOM is a key parameter as it is used to calculate the detection efficiency and, from it, the activity of the sample. The detection efficiency for coincidences in a two PMT system ϕ_{AB} is given by the free parameter model in LS counting [106]:

$$\phi_{AB} = \int_0^{E_{max}} S(E) \left(1 - e^{\frac{-\bar{n}(E;\varphi)}{2}}\right)^2 dE, \tag{5.30}$$

where the factor 2 stays for the number of PMTs in the system. The only parameter here that needs to be determined in order to calculate the detection efficiency is φ. A similar equation is derived for a three PMT system and is shown in Section 2.1. By knowing the detection efficiency, the activity of the sample A is calculated as:

$$A = \frac{n_{AB}}{\phi_{AB}}, \tag{5.31}$$

where n_{AB} is the net (background corrected) counting rate of the two PMTs in coincidence. The value of φ can also be used to determine the average number of detected photons $\bar{n}$ in the case of measurements of nuclides with an energy spectrum $S(E)$:

$$\bar{n} = \int_0^{E_{max}} S(E)\, EQ(E)\varphi \, dE. \tag{5.32}$$

The correct calculation of the energy spectrum $S(E)$ is very important for the radionuclide standardization by LS counting and for many β-emitters the reliability of the β-spectra calculation was carefully evaluated [107, 108]. For a given energy spectrum and ionization quenching function, the relationship between the FOM and the average number of detected photons $\bar{n}$ is unambiguous so, the knowledge of either φ or $\bar{n}$ is sufficient to determine the detection efficiency and thus the activity of the sample.

Equations 5.2 and 5.28 are for two PMT counting systems. Similar equations can be derived also for three PMT systems, considering that probability to have k photons in PMT A, m photons in PMT B and $l = n - k - m$ in PMT C can be calculated by the multinomial distribution. Thus, the equivalent of equation (5.2) for a three PMT system is:

$$D'(\Delta t; \varphi, \lambda, \varepsilon, \mu, \sigma) = \frac{1}{L'} \int_0^{E_{max}} S(E) \sum_2^{\infty} \frac{(\bar{n}(E;\varphi))^n}{n!} e^{-\bar{n}(E;\varphi)} \sum_{k=1}^{n-1} \sum_{m=1}^{n-k} \frac{n!}{k!m!l!} \varepsilon_A^k \varepsilon_B^m \varepsilon_C^l \, \Xi(\Delta t; k, m, \lambda, \mu, \sigma) \, dE,$$

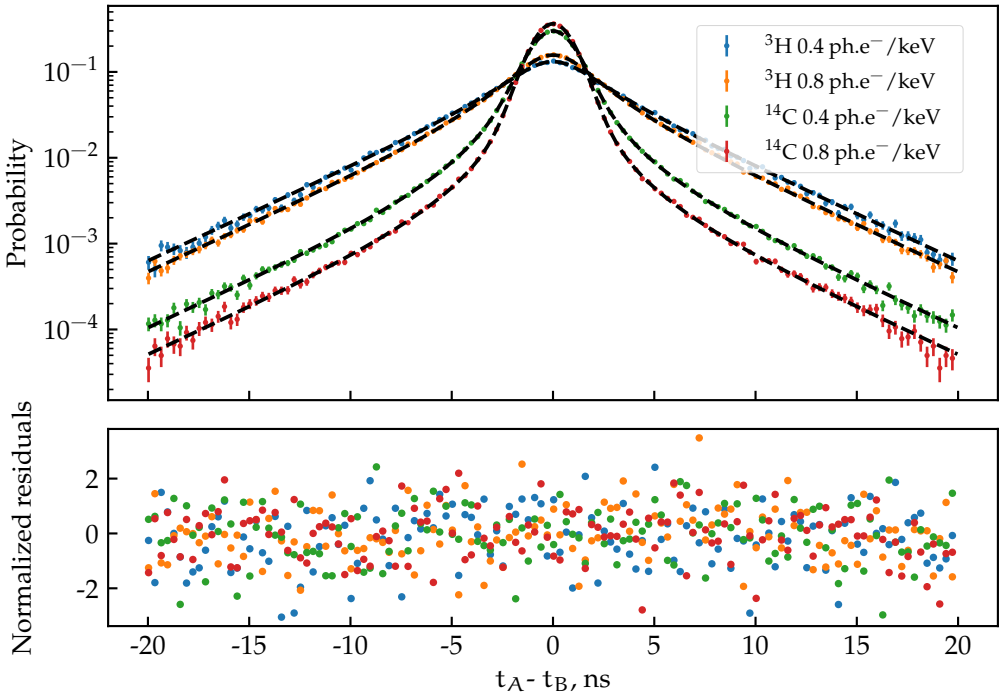

FIGURE 5.6: Cross-correlation distributions of ^{14}C and ^{3}H simulated using a Monte Carlo code for two different values of φ.

(5.33)

where ε_A, ε_B and ε_C are the measured relative efficiencies of the PMTs and L' is the normalization constant given by:

$$L' = \int_0^{E_{max}} S(E) \sum_2^{\infty} \frac{(\bar{n}(E;\varphi))^n}{n!} e^{-\bar{n}(E;\varphi)} \sum_{k=1}^{n-1} \sum_{m=1}^{n-k} \frac{n!}{k!m!l!} \varepsilon_A^k \varepsilon_B^m \varepsilon_C^l \, dE \tag{5.34}$$

5.3 DISCUSSION ON THE CROSS-CORRELATION DISTRIBUTION

Several assumptions were made in order to derive the cross-correlation distribution. Firstly, the decay of prompt fluorescence is assumed to be purely exponential. This assumption may hold poorly in the case of a two or a three component liquid scintillation cocktail. In multicomponent systems the energy of the ionizing particles is dissipated predominantly in the solvent. The solvent itself does not emit light, however, and its excitation energy is transferred non-radiatively to the primary fluorophore. The transfer of energy is rapid, but the time it takes may be similar to the decay time of the primary fluorescent molecule. If the case is such, the simple exponential equation (5.1) cannot be used and a term accounting for the finite rise time of the scintillation signal should be added. This would however overcomplicate the model and an analytical equation of the cross-correlation distribution cannot be derived. This limitation of the model must

be kept in mind when it is applied to fit real measurement data from a two component scintillator.

The second important assumption that was made in order to derive equation (5.2) is that the time jitter of the recorded timestamps of incoming photons is Gaussian with a constant standard deviation σ and centroid μ. The timestamp of a PMT signal is given by the analyzing electronics. In the simplest case it corresponds to the moment in which the signal crosses a predefined threshold. Due to the differences in the amplitudes and thus in the slopes of the rising edges of the incoming signals the recorded timestamp will depend on the amplitudes of the signal. This will introduce a dependence of the parameters of the response function of the detector, μ and σ, on the amplitude of the signal. Moreover, the timing of steeper rising edges is more precise, therefore, the higher the amplitude of the signal the lower the σ of the Gaussian distribution will be. Both effects can be significantly minimized with the use of a constant fraction discriminator and thresholds that are as low as possible.

A third challenge before the derived cross-correlation distribution is that it models the prompt fluorescence only. In real scintillators, however, there is oftentimes a non-negligible contribution of delayed fluorescence to the overall scintillation light. Moreover, it is possible that delayed photons overlap in time with prompt photons, thus they cannot be discriminated by the choice of a specific coincidence window. Even if the time dependence of the intensity of delayed fluorescence is known, there would be a significant difficulty to incorporate it into the derived cross-correlation distribution. The start signals could be either from prompt or delayed photons and the stop signals as well. Including delayed fluorescence would lead to a highly complex model with many unknown parameters and would be difficult to use in practice.

When deriving the cross-correlation distribution, it was assumed that the time of emission of a photon is the same as the time that it hits the photocathode of a PMT. This assumption is reasonable as the flight time of photons between the center of the scinitllation vial and the photocathode is in the order of 100 ps, and the timing resolution set by the PMTs and analyzing electronics is larger than that. However, the time spread due to the flight time of scinitllation photons should be accounted for if the timing resolution of the detector is improved significantly.

There are several interesting observations that can be made when looking at the cross-correlation equation (5.2) and Figures 5.5 and 5.6. What can be noticed first is that with increasing average number of detected photons, the distribution becomes narrower, with less pronounced tails, and more peaked. What we expect to see is a relationship between some of the parameters of the distribution, e. g., the height or the kurtosis, and the average number of photons.[2]

Another interesting possibility is to see whether equation (5.2) describes the cross-correlation distribution of real measurements in a satisfactory manner. If so, it could be used to fit experimental histograms, which would allow the estimation of the parameters

2 This is explored in Chapter 6.

of the scintillator (λ), of the detection system (σ, μ) and, most importantly, the FOM of the measurement (φ). The knowledge of the FOM and the ionization quenching function is enough to calculate the detection efficiency for the given measurement and thus the activity of the sample. The same two unknowns are required for the TDCR method to calculate the activity. Thus, if possible to estimate the FOM from a cross-correlation measurement it would be also possible to calculate the activity of the sample similarly to the TDCR method. This possibility is explored more in-depth in Chapter 6.

The final determination of the activity using the cross-correlation method relies on the free parameter model. The latter is also the basis of the TDCR method for primary activity calculation. Due to that, both methods rely on the correct description of the light output of the scintillator with respect to the deposited energy and, therefore, both will be very sensitive to the used ionization quenching function. This is especially true when dealing with low-energy emitters such as ^{3}H.

6

ESTIMATION OF THE DETECTION EFFICIENCY USING TIME DOMAIN INFORMATION

In the preceding chapter it was shown that the overall shape of the cross-correlation distribution depends on the mean number of detected photons and on the spectrum of the deposited in the scintillator energy. This is especially visible in Figure 5.6, where the distribution is calculated in the case of ^{3}H and ^{14}C for two different values of the figure of merit. The Monte Carlo simulations show that with increasing average number of photons, i. e., increased detection efficiency, the cross-correlation distribution becomes more narrow and peaks higher. It seems reasonable to think that by analyzing an experimental distribution one would be able to calculate the detection efficiency in a given measurement. Such possibility is explored in this chapter.

In the following sections, the correlation between some superficial parameters of the experimental cross-correlation distribution and the detection efficiency is explored. The possibility to fit the analytical equation, derived in Chapter 5, to measurement data and obtain the FOM is also examined. The approach is compared with the already established TDCR method described in Section 2.2.

6.1 CROSS-CORRELATION SPECTRA OF MONOENERGETIC ELECTRONS

In order to study the properties of the cross-correlation distribution, experimental spectra were acquired using the Compton coincidences method. The method uses a three PMT TDCR counter and a γ-ray detector connected in coincidence. A collimated external source of mono-energetic gamma-rays is placed such that the photon beam passes through the LS-vial containing the scintillator that is studied. Most of the γ-rays undergo Compton scattering and produce a Compton electron inside the cocktail. The scattered γ-ray can interact with the γ detector and knowing its energy it is possible to calculate the energy deposited in the cocktail by the Compton electron from the energy conservation law. The method is described in more detail in Section 2.3.

In the current study the Compton coincidences detector that was used was the one developed at *Laboratoire National "Henri Becquerel"* (LNHB)[1]. The detector consists of three Hamamatsu R7600-200 square form factor PMTs [91] and a cadmium telluride (CdTe) γ-ray detector. The PMTs are placed in a 3D printed housing which hosts an optical chamber that is optimized for light collection and is covered with reflective foil with 98% reflectivity in the visible spectrum. The outputs of the PMTs are connected to a

1 The French primary radionuclide metrology institute.

CAEN DT5751 digitizer [109] with 1 ns timing resolution. An external 77 MBq ^{241}Am source was used as a mono-energetic source of 59.54 keV γ-rays. The source was filtered in order to remove the lower energy X-rays of ^{237}Np. This setup allows to study the response of the scintillator to electrons with energies from 2.5 keV to 8.5 keV in 270 eV steps. The same setup was also used in the studies presented in Chapter 10 and a more thorough description of the setup is given there.

The outputs of the three PMTs and the CdTe detector were all connected to the same digitizer mentioned above. The timestamps and energies of each event were recorded in list-mode files and were analyzed off-line using the LIST_MODE_ANALYSIS program described in Chapter 3. The software was used to obtain the cross-correlation distributions for a number of deposited energies in the scintillator.

By using the Compton coincidences method it is possible to study the shape of the cross-correlation distribution for monoenergetic electrons with known energies. This removes some of the complexity of the distribution associated with the particle spectrum and ionization quenching phenomena.

The setup was used to measure the cross-correlation distributions with respect to the deposited energy in four different LS cocktails: UltimaGold, UltimaGold LLT, HionicFluor and a home-made Toluene+PPO. The results for UltimaGold and UltimaGold LLT are shown in Figures 6.1 and 6.2, respectively. The results from the other two cocktails were omitted in the main text and are shown in the Appendix in Figures C.1 and C.2.

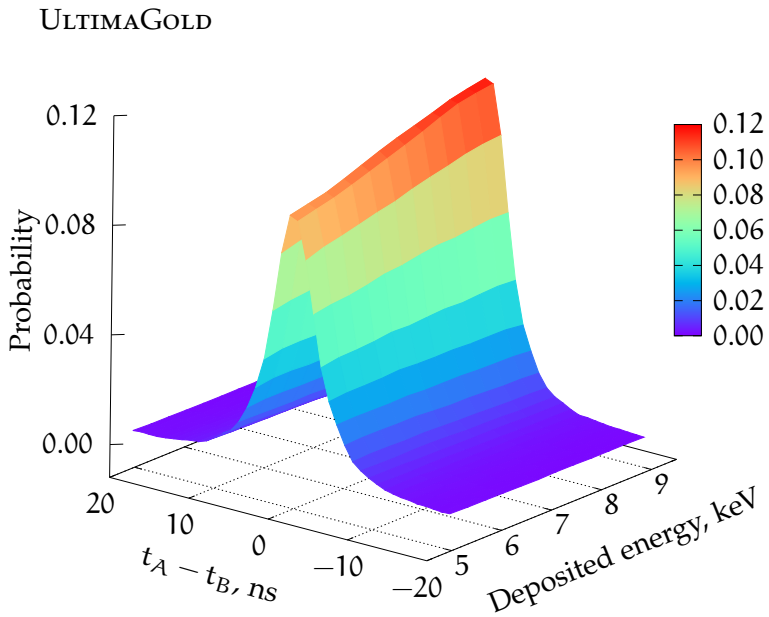

FIGURE 6.1: Cross-correlation spectra $D(\Delta t)$ of UltimaGold LS cocktail acquired by the Compton coincidences method.

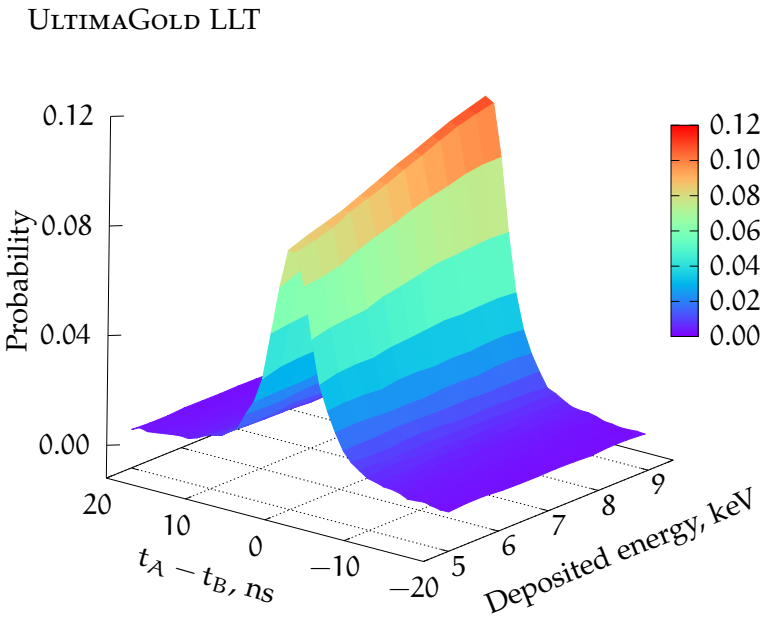

FIGURE 6.2: Cross-correlation spectra $D(\Delta t)$ of UltimaGold LLT LS cocktail acquired by the Compton coincidences method.

The results show that, with increasing deposited in the cocktail energy, the height of the cross-correlation distribution also increases. As shown in Chapter 10, the energy of the Compton electrons and the average number of detected by the LS system photons are closely related. Thus, there exists a correlation between the height of the distribution and the detection efficiency. This correlation will be explored in the subsequent section.

6.2 HEIGHT OF THE CROSS-CORRELATION SPECTRUM

The height of the cross-correlation spectrum seems to be an important parameter that could be used to characterize the distribution as a whole, i. e., outside the fundamental parameters: λ, σ, μ, etc. Thus, it would be valuable to derive an analytical equation that connects the fundamental parameters with the height of the resulting distribution. The maximum of the cross-correlation distribution is located at $\Delta t = \mu$, and so the height H_0 is given by:

$$H_0 = D(\Delta t = \mu; \varphi, \lambda, \epsilon_A, \epsilon_B, \mu, \sigma). \tag{6.1}$$

Note that for PMTs with the same static time delay μ equals zero and the maximum is located at $\Delta t = 0$.

By substituting $\Delta t = \mu$ in equation (5.2) it would be possible to derive the link between H_0 and the parameters of the distribution. Due to the complexity of the cross-correlation distribution, however, this task is difficult, and it may not even be possible analytically. Before falling back to numerical methods, it is, nevertheless, interesting to

derive this connection in a more simplified case. By considering only the monoenergetic case, ignoring the Gaussian response function of the detectors and substituting $\Delta t = \mu$ the resulting cross-correlation distribution can be written as:

$$\Pi(\Delta t = \mu; \bar{n}, \lambda, \epsilon) = \frac{1}{C} \sum_{2}^{\infty} \sum_{k=1}^{n-1} \frac{\bar{n}^n}{n!} e^{-\bar{n}} \binom{n}{k} \varepsilon^k (1-\varepsilon)^{n-k} \frac{k(n-k)}{n} \lambda, \tag{6.2}$$

where $\varepsilon = \varepsilon_A = 1 - \varepsilon_B$ and C is a normalization coefficient. The binomial distribution can be calculated first:

$$\begin{aligned}
B(\mu) &= \sum_{k=1}^{n-1} \binom{n}{k} \varepsilon^k (1-\varepsilon)^{n-k} \frac{k(n-k)}{n} \lambda \\
&= \sum_{k=1}^{n-1} \binom{n-1}{k} \varepsilon^k (1-\varepsilon)^{n-k} k\lambda \\
&= \sum_{k=1}^{m} \binom{m}{k} \varepsilon^k (1-\varepsilon)^{m-k+1} k\lambda, && \text{where } m = n-1 \\
&= (1-\varepsilon)\lambda \underbrace{\sum_{k=1}^{m} \binom{m}{k} \varepsilon^k (1-\varepsilon)^{m-k} k}_{\text{expected value of the binomial } m\varepsilon} \\
&= \varepsilon(1-\varepsilon)\lambda m, && \text{substituting back } n = m-1 \\
&= \varepsilon(1-\varepsilon)\lambda(n-1).
\end{aligned} \tag{6.3}$$

Substituting the result in equation (6.2) the Poisson distribution can be calculated also:

$$\begin{aligned}
\Pi(\mu) &= \sum_{2}^{\infty} \frac{\bar{n}}{n!} e^{\bar{n}} \underbrace{\varepsilon(1-\varepsilon)\lambda(n-1)}_{\text{constant term}} \\
&= \varepsilon(1-\varepsilon)\lambda \sum_{n=2}^{\infty} \frac{\bar{n}}{n!} e^{\bar{n}} (n-1) \\
&= \varepsilon(1-\varepsilon)\lambda \sum_{l=1}^{\infty} \frac{\bar{n}}{(l+1)!} e^{\bar{n}} \left[(l+1)-1\right], && \text{where } l = n-1 \\
&= \varepsilon(1-\varepsilon)\lambda \left(\sum_{l=1}^{\infty} \frac{\bar{n}^l}{l!} e^{-\bar{n}} - e^{-\bar{n}} \sum_{l=1}^{\infty} \frac{\bar{n}^{l+1}}{(l+1)!} \right), && \text{where } m = l+1 \\
&= \varepsilon(1-\varepsilon)\lambda \left(\bar{n} - e^{-\bar{n}} \sum_{m=1}^{\infty} \frac{\bar{n}^m}{m!} \right) \\
&= \varepsilon(1-\varepsilon)\lambda \left(\bar{n} - e^{-\bar{n}} (e^{\bar{n}} - 1) \right) \\
&= \varepsilon(1-\varepsilon)\lambda \left(\bar{n} + e^{-\bar{n}} - 1 \right))
\end{aligned} \tag{6.4}$$

The final result gives the relationship between the height of the cross-correlation distribution and the underlying parameters $\bar{n}$ and λ in this simplified case. Equation (6.4) cannot be used in practice, because it is not normalized. The normalization is required

because events with less than one detected photon per PMT would not be registered. It is equal to the reciprocal of the sum of the probabilities for all detected events, or:

$$\frac{1}{C} = \sum_{n=2}^{\infty} \sum_{k=1}^{n-1} \binom{n}{k} \varepsilon^k \varepsilon^{n-k} = e^{-\bar{n}} - e^{-\bar{n}\varepsilon} - e^{-\bar{n}(1-\varepsilon)} + 1. \tag{6.5}$$

Finally, combining equations (6.5) and (6.4), the height of the cross-correlation distribution H_0 in the simplified case of a monoenergetic source and no gaussian jitter is:

$$H_0 = \frac{\varepsilon(1-\varepsilon)\lambda\left(\bar{n} + e^{-\bar{n}} - 1\right)}{e^{-\bar{n}} - e^{-\bar{n}\varepsilon} - e^{-\bar{n}(1-\varepsilon)} + 1} \tag{6.6}$$

To visualize the result, as well as to validate it, the Monte Carlo code was used to simulate measurements corresponding to a zero gaussian jitter. The decay constant λ was set to 0.3 ns^{-1} and the relative PMT efficiencies were set to be equal. The simulations were performed for various mean number of detected photons and the height of the cross-correlation distribution was obtained in each case. It is taken as the probability in the bin corresponding to $\Delta t = 0$. As the bin size for the histograms of Monte Carlo data can be very narrow (10 ps in this case), this is an adequate approximation. The results are shown in Figure 6.3. Equation (6.6) was calculated with the same ε and λ parameters. There is an excellent agreement between the simulations and the analytical equation.

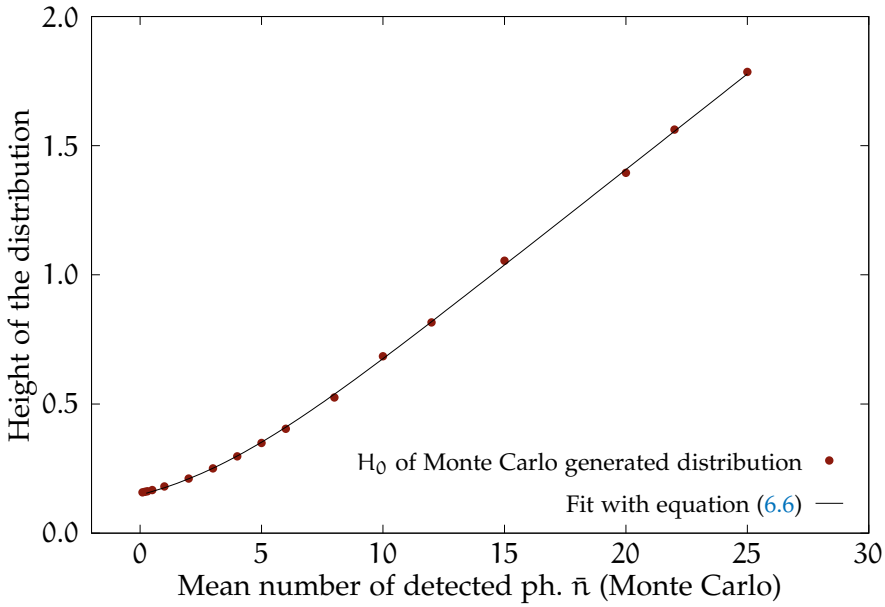

FIGURE 6.3: Height of Monte Carlo generated cross-correlation distributions without a Gaussian jitter. The line is calculated analytically using equation (6.6).

Despite being and important first step, equation (6.6) is valid for a too simplified case and may not be of practical interest. However, an analytical description of $H_0(\bar{n})$ that includes the response function of the detector and the deposited energy spectrum, would be very difficult to derive. Nevertheless, it is possible to calculate it numerically.

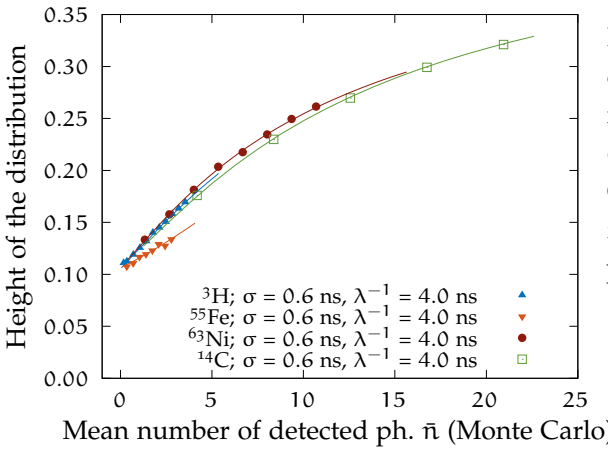

FIGURE 6.4: Height of the normalized cross-correlation spectra as a function of the mean number of detected photons. The data points are generated by the Monte Carlo code and the lines are calculated from the analytical equation with the same parameters at $\Delta t = \mu$.

This can be done by calculating $D(\Delta t = \mu; \varphi, \lambda, \varepsilon, \sigma, \mu)$ for a number of parameters φ and then interpolating the data points. To illustrate the approach, the Monte Carlo code was used to generate a number of measurements for ^{3}H, ^{55}Fe, ^{14}C and ^{63}Ni with a wide range of FOM parameters. In all cases the λ and σ parameters were 4.0 s^{-1} and 0.6 ns respectively. The PMT efficiencies were set to be equal. The height of the resulting cross-correlation distributions as a function of $\bar{n}$ is shown in Figure 6.4. The lines were calculated using the analytical equation (5.2) for the same parameters at a series of φ and at $\Delta t = \mu$. The mean number of photons were calculated from φ using (2.18).

There are some interesting observations that can be made when analyzing equation (6.6) and Figure 6.3. Firstly, for a high enough number of detected photons, the relationship between H_0 and $\bar{n}$ becomes linear, if the gaussian response function of the detector is not considered. This could be of interest in routine LS measurements and is explored further in Section 6.5. Another note is that the height H_0 does not tend to zero for zero mean number of detected photons. The explanation is that the number of detected photons in a given coincidence event must be at least two – one photon per PMT. Thus, even at very low average number of detected photons, the mean number of photons in a coincidence event tends to two. In a more realistic scenario, however, the relationship for high mean number of detected photons would not be linear due to the gaussian response function of the detector (see Figure 6.4). For increasing $\bar{n}$ the height of the distribution will tend to some value that corresponds to the height of the gaussian distribution. Thus, what is expected in real measurements is to have some portion of $H_0(\bar{n})$ that is linear, and it would tend to some minimal value for low $\bar{n}$ and to some maximum value for high $\bar{n}$. What can also be noted from Figure 6.4 is that for ^{3}H and ^{55}Fe the range of $\bar{n}$ is such that falls in the region where the influence of the response function of the detector is still insignificant and $H_0(\bar{n})$ is close to linear.

6.3 EXPERIMENTAL STUDIES ON THE HEIGHT OF THE CROSS-CORRELATION DISTRIBUTION

In order to further investigate the relationship between the height of the cross-correlation distribution and the mean number of detected photons, spectra of the EC nuclide ^{55}Fe and the pure β-emitters ^{3}H, ^{63}Ni and ^{14}C were acquired on a TDCR detector. The sources were prepared in UltimaGold LS cocktail using diffusive (sandblasted) glass vials. A ^{3}H in Toluene+PPO cocktail LS source was also measured. These nuclides were chosen to cover a wide range of mean number of detected photons and detection efficiencies. ^{55}Fe could be considered close to monoenergetic with a mean deposited energy E_{mean} ≈ 5.5 keV. ^{3}H (E_{mean} = 5.68 keV) is a low-energy β-emitter and the typical mean number of detected photons is around two, which results in a detection efficiency of roughly 50% for the logical sum of double coincidences. ^{63}Ni has 17.43 keV mean energy of the β-spectrum, and a 75% detection efficiency is commonly observed when it is measured on a TDCR counter. ^{14}C (E_{mean} = 49.16 keV) results in approximately 20 detected photons per decay and its detection efficiency is usually above 90%

The cross-correlation distributions were acquired using the same detector used for the Compton coincidences studies, but without an external γ-ray source. The digitized data was analyzed using the LIST_MODE_ANALYSIS software and the time distribution between two of the three PMTs of the system was obtained. The LS sources were also measured with a set of optical grey filters in order to obtain cross-correlation distributions of the same sample with different detection efficiencies.

Figure 6.5 depicts the cross-correlation distributions of all samples without filters. The experimental distributions are obtained by normalization of the measured cross-correlation spectra on the total number of events in the spectrum. The results in the figure confirm the aforementioned theoretical and experimental findings that higher energy deposited in the cocktail leads to more peaked and less tailed cross-correlation distribution. This phenomenon was also observed previously by other authors [102].

Figure 6.6 shows the height of the cross-correlation distribution of all measurements of the nuclides, including those with grey filters. The mean number of detected photons was obtained from the FOM obtained with the TDCR method and equation (2.18). The height of the distribution is taken as the probability in the bin corresponding to $\Delta t = \mu$. The bin size in the measurements is 1 ns, thus the obtained height corresponds to the average of the distribution within the bin. This was accounted for later when height was evaluated using the analytical equation.

The experimental results show that for a small mean number of detected photons $\bar{n}$ the height of the cross-correlation distribution H_0, depends almost linearly on $\bar{n}$. For large $\bar{n}$ the response function of the detector leads to a non-linear behaviour. The actual dependence can be found numerically by fixing $\Delta t = \mu$ in equation (5.2) and varying the parameters λ and σ. To account for the experimental bin size when calculating the height using the analytical equation, the distribution was evaluated in 10 points within ±0.5 ns around μ and average was taken as the height H_0. The quantum efficiencies

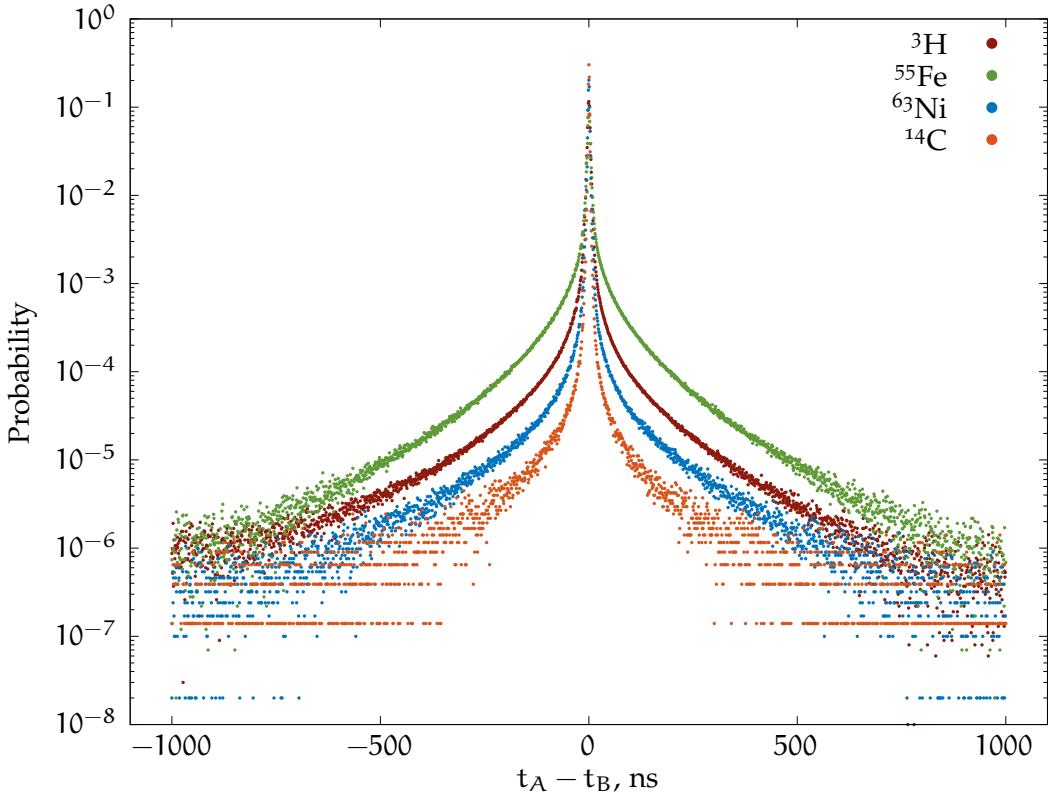

FIGURE 6.5: Cross-correlation spectra of ^{55}Fe, ^{3}H, ^{14}C and ^{63}Ni

of the PMTs are assumed to be identical and the μ parameter is calculated as the mean of the cross-correlation distributions. The two other free parameters, the λ and σ were varied until a satisfactory fit was achieved. The obtained parameters and fitted curves are shown in Figure 6.6.

It should be noted there that the fit of λ and σ seems to *guess* some expectations about those parameters. For example, the optimal decay constant for Toluene+PPO is 1.87 ns^{-1}, significantly lower than the ≈ 4 ns^{-1} decay constant obtained for UltimaGold. This is expected as it is known that the Toluene cocktail is much faster and its decay constant should be close to 2 ns^{-1}. Another observation is that the optimal σ parameters are different for ^{63}Ni and ^{14}C compared to ^{3}H and ^{55}Fe. To an extent, that is to be expected as both ^{63}Ni and ^{14}C have higher mean energy of the β-spectrum and so produce more light in the scintillator. This would lead to a steeper rising edge of the PMT signals and a more precise timestamp from the digitizer.

These results show that, for a given radionuclide, knowing the decay constant of the scintillator λ and the parameters of the detection system (ε, μ, σ), it is possible to obtain the average number of detected photons $\bar{n}$. Then it is straightforward to calculate the detection efficiency of the measurement using equation (5.30). Thus, the activity of the measured sample can be deduced from the height of the cross correlation distribution. There is a certain advantage here over the TDCR method as only a two PMT system is needed. A disadvantage, however, is the need to know the response function of the detector σ and the decay constant of the scintillator λ to a good precision.

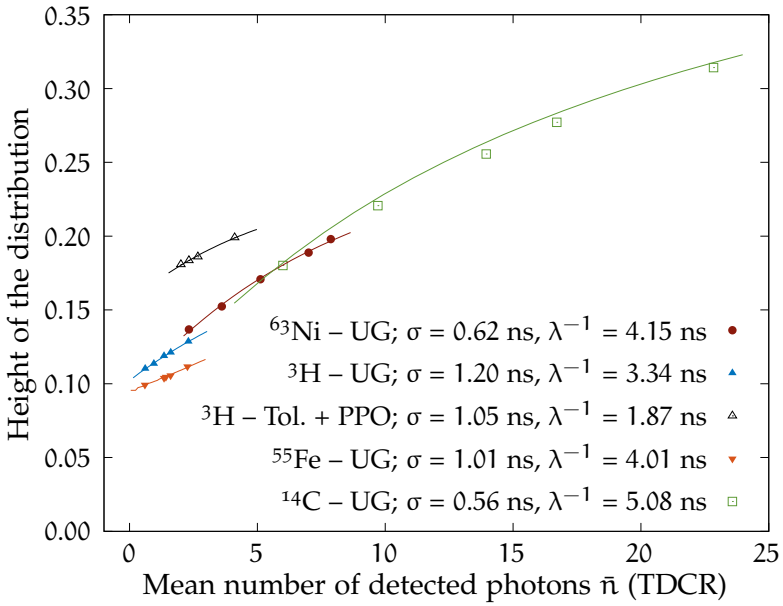

FIGURE 6.6: Height of the normalized cross-correlation spectra as a function of the mean number of detected photons. The data points measurements of ^{3}H, ^{55}Fe, ^{63}Ni and ^{14}C in UltimaGold and ^{3}H in Toluene+PPO cocktails. The fit is done with the analytical equation at $\Delta t = \mu$ in order to obtain the optimal λ and σ parameters.

6.4 CROSS-CORRELATIONS AND TDCR COUNTING

The TDCR method allows to estimate the FOM from a LS counting measurement with a three PMT system. The cross-correlation approach allows the determination of the same parameter for a two PMT system. It is, therefore, interesting to compare the FOM values obtained with the two methods.

The TDCR method is based on a model that provides a statistical description of the physical phenomena occurring in the LS counting system. The principle and development of the model is summarized in Section 2.2. With the TDCR method one can obtain the detection efficiency of the detector from the ratio of the triple to double coincidences. Under the assumption of three identical PMTs the ratio of the detection efficiency in the T channel to that in the D channel is [27]:

$$\frac{\Phi_T}{\Phi_D} = \frac{\int_0^{E_{max}} S(E)\left(1-e^{-\bar{n}(E;\varphi)/3}\right)^3 dE}{\int_0^{E_{max}} S(E)\left[3\left(1-e^{-\bar{n}(E;\varphi)/3}\right)^2 - 2\left(1-e^{-\bar{n}(E;\varphi)/3}\right)^3\right] dE}, \tag{6.7}$$

where $\bar{n}$ is the average number of photons detected for energy E deposited in the cocktail, and is the same parameter defined in equation (2.18), that is used in the cross-correlation method. Note that in this case the number of PMTs is equal to 3 and thus the factor in the denominator in the argument of the exponent. For a large number of detected events the ratio of the T to D coincidences tends towards the ratio of the detection efficiencies or $T/D = \Phi_T/\Phi_D$. The free parameter φ can then be obtained by

minimizing the squared difference between the two ratios. In the case of non-identical PMTs a set of three equations must be used, including the relative efficiencies of the three PMTs (see Section 2.2, equation (2.29)). The equations are used to optimize the three free parameters of the system $\varphi_A = \varepsilon_A \varphi$, $\varphi_B = \varepsilon_B \varphi$ and $\varphi_C = \varepsilon_C \varphi$.

A direct way to extract the parameters of the measurement φ, λ, σ and μ within the cross-correlation approach is to fit the experimental cross-correlation distribution with the function $D(\Delta t; \varphi, \lambda, \epsilon_A, \epsilon_B, \mu, \sigma)$ given explicitly in equation (5.2). One setback before the cross-correlation method can be applied however, is that the parameters φ and λ are highly correlated. This was explored with fits of Monte Carlo generated data in Appendix B. Thus, in order to obtain the correct φ, it is necessary to fix the correct λ or vice versa. Generally, the fast decay constant of the scintillator can be obtained by other methods, for example by time-correlated single photon counting [110]. The parameters concerning the measurement system can be estimated by careful characterization of the time response of PMTs and their relative quantum efficiencies. This is how we envision a state-of-the-art application of the cross-correlation method.

Another approach that could be used is to fix the φ parameter from a TDCR measurement and thus obtain the decay constant of the given scintillator. Once obtained, it could be used for other measurements with the same scintillation cocktail.

In order to compare the two methods the miniTDCR detector, operated in Sofia University, was used. The outputs of the detector were connected to a CAEN DT5751 digitizer. The off-line analysis of the data allows the application of both the TDCR and cross-correlation techniques using the same data. This is a significant advantage as the figure of merit and PMT efficiencies obtained by the two methods can be compared directly and in theory should be exactly the same. With this system, measurements of ^{3}H and ^{14}C LS-samples in a Toluene+PPO scintillator were performed. Both samples were measured without and with grey filters with transparencies from 90% to 60% The use of grey filters allows the change of φ without changing the parameters associated with the LS cocktail and nuclide. The FOM of the measurement without a filter was determined from the analysis of the data according to the TDCR method. The value was then used to determine the decay constant λ for this cocktail and the rest of the cross-correlation spectra were fitted with a fixed λ.

An example can be given with the ^{3}H measurements and the same technique was applied for the ^{14}C study. The cross-correlation spectrum of PMTs B and C was obtained using the LIST_MODE_ANALYSIS program. These two PMTs were selected due to their almost identical quantum efficiencies and gain. Note here that the FOM for a pair of PMTs, for example B and C, is $\varphi_{BC} = \varphi(\varepsilon_B + \varepsilon_C)$, where φ is the FOM from the TDCR measurement. The cross-correlation spectrum was taken within $\pm$20 ns from the centroid. This was done in order to reduce the influence of the delayed fluorescence as it seems to dominate after approximately 10 ns. The list-mode files obtained during the ^{3}H measurement without filter were also analyzed with the LIST_MODE_ANALYSIS program according to the TDCR method. The coincidence window of the analysis code was set to 20 ns to match the cross-correlation measurements. The relative quantum

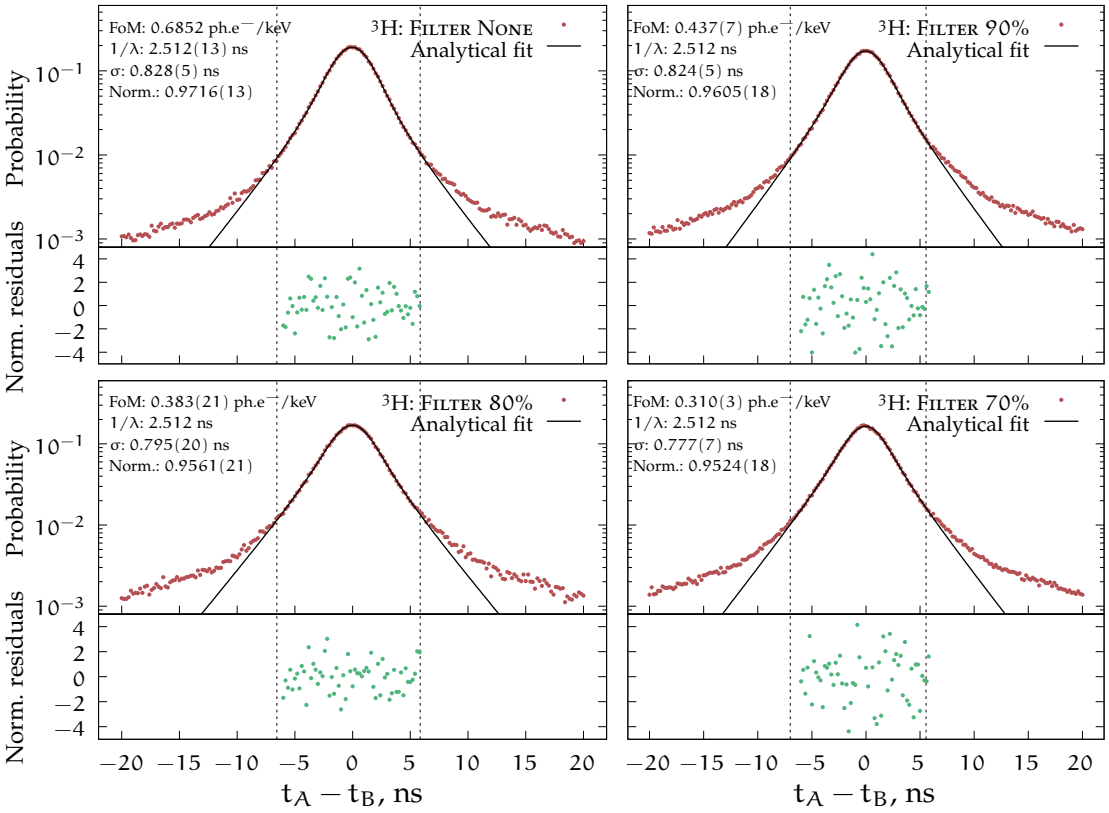

FIGURE 6.7: Cross-correlation spectra of a ^{3}H sample with varying levels of grey filters. Top left: without filter, top right: filter with 90% transparency, bottom left: filter with 80% transparency, bottom right: filter with 70% transparency. The spectra are fitted with equation (5.2). The normalized residuals are in units of standard deviations. The values in brackets are the uncertainties as reported by the fitting algorithm. The parameters, for which the values are given without uncertainties were fixed during the fitting.

efficiencies (ε_A, ε_B and ε_C) of the three PMTs were obtained as well as the FOM φ, using a dedicated calculation code [93].

The experimental cross-correlation spectra were fitted using equation (5.2) by fixing the value of the FOM to 0.685 ph.e$^-$/keV, as obtained from the TDCR method, and leaving all other parameters free. The fit was performed on data between -6 and 6 ns as the cross-correlation spectrum seems to be significantly affected by delayed fluorescence for larger time differences. The data and fit for the ^{3}H case are shown in Figure (6.7) in the top left sub-figure. The quality of the fit is good as most residuals lie within two standard deviations. Notice that a normalization parameter (*Norm.*) is multiplying equation (5.2) in order to accommodate the fact that not all of the cross-correlation spectrum can be explained by the prompt fluorescence only. From this measurement the prompt fluorescence decay time λ of the scintillator was determined to be $1/\lambda = 2.512(13)$ ns. This decay time was then used in all subsequent analysis of measurements of the ^{3}H sample.

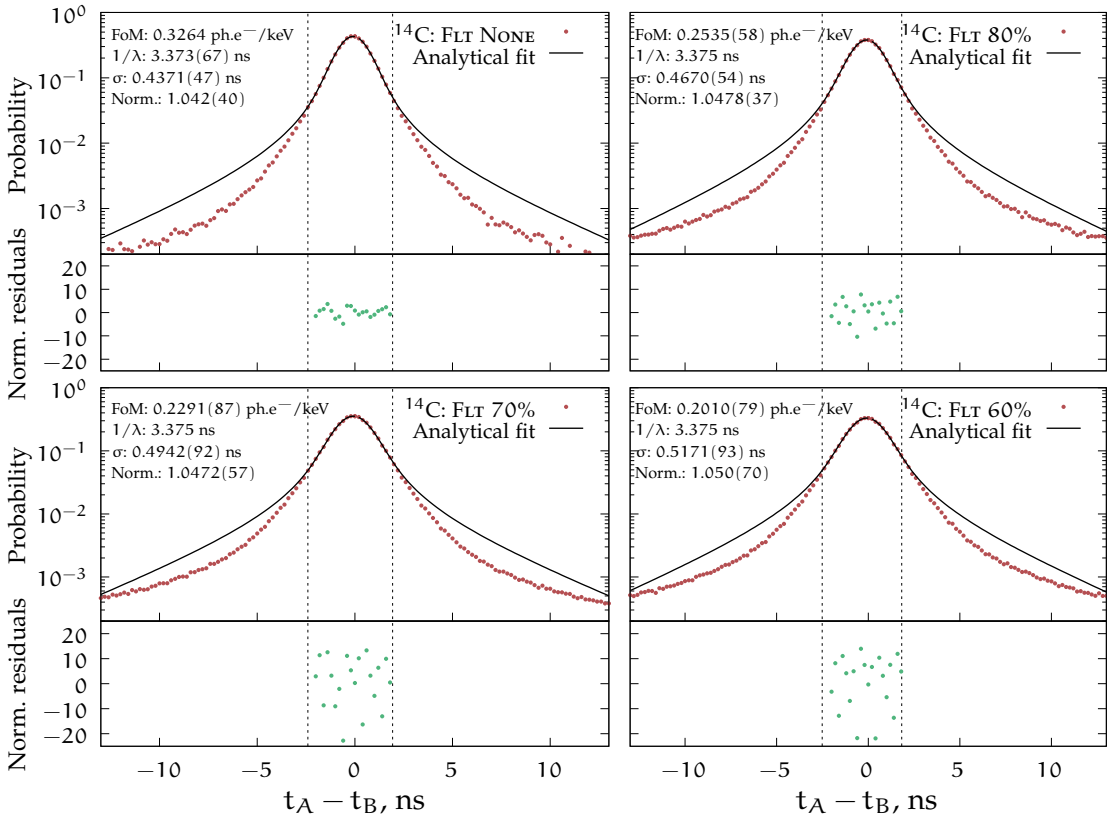

Figure 6.8: Cross-correlation spectra of a ^{14}C LS-source in toluene+PPO cocktail. All experimental spectra are fitted with equation (5.2) with a fixed λ and normalization parameters.

The same technique was used for the measurements of ^{14}C. For that cocktail the decay constant is $1/\lambda = 3.373(67)$ ns. It was obtained from the fit of the cross-correlation equation with a FOM taken from the TDCR method. The results for ^{14}C are shown in Figure 6.8.

Due to the much larger average number of photons in the case of ^{14}C compared to ^{3}H, the cross-correlation distribution is significantly narrower – 67% of all events in the distribution fall in the interval between ± 1 ns and 91% fall within ± 2 ns. For ^{3}H the intervals are ± 2.5 and ± 5 for 67% and 91% respectively. The range that can be successfully fitted by equation (5.2) was found to be ± 2 ns. The events outside this range seem to be significantly affected by the delayed fluorescence. The dispersion of the residuals seems to be considerably larger than for the ^{3}H measurements. This could be due to the much narrower time distribution for which minor non-linearities in the bin widths could play a role. Such effects are not included in the uncertainty of the value in each bin which is estimated as the square root of the number of events in the bin.

The comparison between the TDCR and cross-correlation estimated FOM values is shown in Table 6.1. The FOM parameters obtained with the two measurement methods agree well within the estimated uncertainties. The results indicate that, with a good knowledge of the prompt fluorescence decay constant, the cross-correlation method

^{3}H: φ, ph.e^{-}/keV			^{14}C: φ, ph.e^{-}/keV		
Filter	Cross-corr.	TDCR	Filter	Cross-corr.	TDCR
None	—	0.685(20)	None	—	0.326(6)
90%	0.437(7)	0.434(13)	80%	0.254(6)	0.267(4)
80%	0.383(21)	0.370(11)	70%	0.229(9)	0.233(4)
70%	0.310(3)	0.312(9)	60%	0.201(8)	0.191(3)

TABLE 6.1: Comparison of the FOM obtained by cross-correlation and TDCR measurements with various levels of grey filters for ^{3}H and ^{14}C LS sources.

provides reliable estimation of the FOM. It should be noted here, that the uncertainty associated with the cross-correlation method is only the uncertainty of the FOM parameter as reported from the fitting algorithm. In order for the method to be used in practice, a full uncertainty budget will be required. This will be explored in the future.

The TDCR method relies on the accurate description of the relative light output of the scintillator with respect to the deposited energy. This is commonly done with Birks' ionization quenching formula (see equation 1.12). As the method uses the triple and double coincidence counting rates to calculate the efficiency it is necessary to select coincidence windows that are wide enough to include all correlated events, otherwise a bias may be introduced in the measurement. For too short coincidence windows the loss of triple coincidences will be higher than the loss of double coincidences and a biased efficiency will be obtained. Increased coincidence resolving time would increase the contribution of delayed fluorescence to the overall scintillation light, thus the simple ionization quenching formula proposed by Birks to describe the ionization quenching of prompt fluorescence cannot be used. These issues of the TDCR method will be discussed in length in Chapter 9, but it can be summarized that the choice of coincidence resolving time for TDCR measurements is still an open problem. The cross-correlation method could be helpful in that regard as it allows considering only the events due to the prompt fluorescence. That way the ionization quenching formula proposed by Birks should describe the light output of the scintillator accurately. This could possibly lead to an improvement in the detection efficiency calculation for low-energy nuclides where the proper knowledge of the light output as a function of the deposited energy is critical. Further studes will be conducted in order to focus on this aspect of the cross-correlation method.

6.5 CROSS-CORRELATIONS AND CONVENTIONAL LIQUID SCINTILLATION ANALYSIS

The methods presented in the previous two sections demonstrate the potential for primary activity measurements without the need to do calibration measurements. This would be possible if the parameters of the detection system and LS cocktail are known beforehand. These methods, however, require complex calculations which may not be practical for all applications. The methods also depend on measurement of the cross-correlation distribution with very high resolution in the order of a few hundred picoseconds. Therefore, it is worth searching for a correlation between a parameter of the cross-correlation distribution and a parameter that can be used to calculate the detection efficiency. The connection between two such parameters that was already explored is between the height of the cross-correlation distribution and the figure of merit.

6.5.1 *The height of the cross-correlation distribution as a function of the FOM*

In order to study more simplified ways in which the height of the cross-correlation distribution can be used as a proxy for the detection efficiency, the same measurement data as in Section 6.3 was used. The data consists of measurements of ^{3}H, ^{55}Fe, ^{63}Ni and ^{14}C in UltimaGold LS cocktail. The time distributions are obtained with 1 ns bin size. For a bin size of such width, it should not be considered that the value of the probability at the bin corresponding to $\Delta t = \mu$ gives the height, or at least not to a good precision. This is especially true for ^{63}Ni and ^{14}C, where the cross-correlation distributions are very narrow and the first derivative is large in the region of the peak.

In order to improve the accuracy, the height of the distribution H_0 is determined by fitting the cross-correlation data in the range $[-3\text{ ns}, 3\text{ ns}]$ with a Voigt profile. The height is then taken as the value of the fitted function at $\Delta t = \mu$. By testing various functions it was determined that the Voigt profile describes well experimental distributions in a narrow range around the peak. Moreover, this function is convenient as it can be easily found in many commonly used curve fitting programs.

Figure 6.9 (top left) shows the cross-correlation distributions in the case of the ^{3}H sample measured as is and with various grey filters. The distributions were fitted with the Voigt profile and the height was taken as the value of the fit at $\Delta t = \mu$. The FOM of these measurements was also obtained, using the TDCR method. The relationship between the height and the FOM is shown in Figure 6.9 (top right). There is an excellent linear relation between H_0 and the FOM. Similar results were obtained in the case of ^{55}Fe, which are shown in the same figure (bottom left and bottom right). It should be noted that the linearity is conserved over a very wide range of FOM values, which covers most of what can be obtained in practice, i. e., both large and small detection efficiencies.

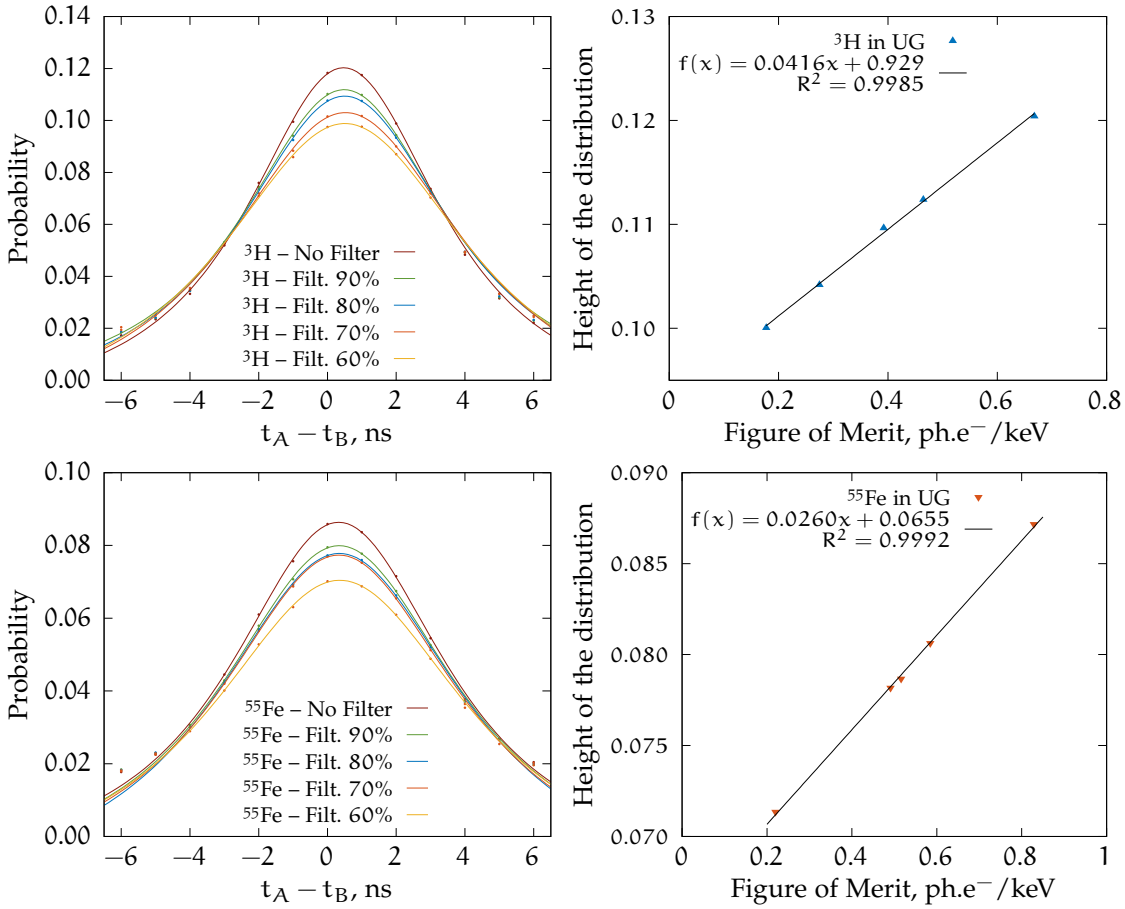

FIGURE 6.9: Cross-correlation studies with ^{3}H and ^{55}Fe in UltimaGold cocktail and various levels of grey filters. The cross-correlation spectra (left) are fitted within ±3 ns with a Voigt profile in order to evaluate the height of the distribution.

This linear relationship could be very useful in practice. For example, a method could be devised in which a calibration source in a given LS cocktail and vial is used. The $H_0(\varphi)$ relationship can be obtained for this source with cross-correlation measurements with a set of filters. This function can then be used to construct the inverse $\varphi(H_0)$, which can later be used to find the FOM in a given measurement if the height of the cross-correlation distribution is known.

This linear dependence is not seen for the ^{63}Ni and ^{14}C samples, where the influence of the response function of the detection system can be felt more clearly. The non-linearity of $H_0(\varphi)$ can be seen in Figure 6.10 and also from the studies in the previous section. The same non-linearity can be observed in the $H_0(\bar{n})$ relationship also. However, these dependencies are still close to linear, thus it could be beneficial to try to scale the height with another parameter that depends on the width of the distribution, which in turn is closely related to the detector's response. One such parameter that was found to be useful is the FWHM.

The same cross-correlation spectra of all sources with and without grey filters were taken and the H_0/FWHM was calculated. The FWHM was evaluated after the experi-

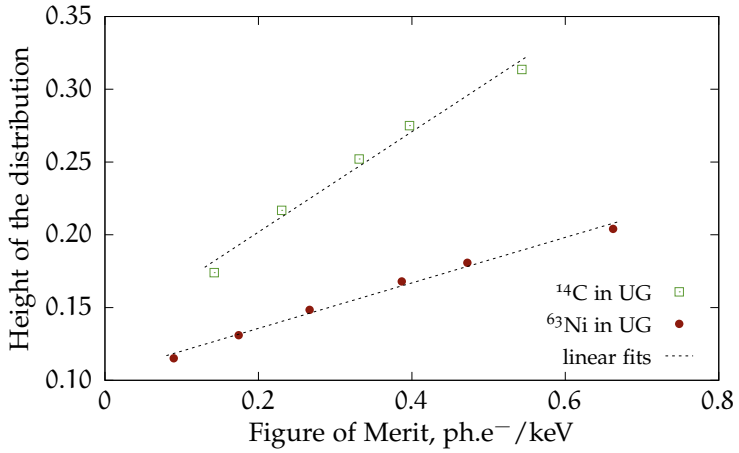

FIGURE 6.10: Cross-correlation studies with ^{63}Ni and ^{14}C in UltimaGold cocktail and various levels of grey filters. The cross-correlation spectra are fitted within ±3 ns with a Voigt profile in order to evaluate the height of the distribution.

mental spectrum was interpolated using a cubic spline. The results from the experiment are shown in Figure 6.11. The results show good linear relationship between the scaled height of the distribution and the mean number of detected photons $\bar{n}$ parameter. The figure can be compared with the $H_0(\varphi)$ shown in Figure 6.6.

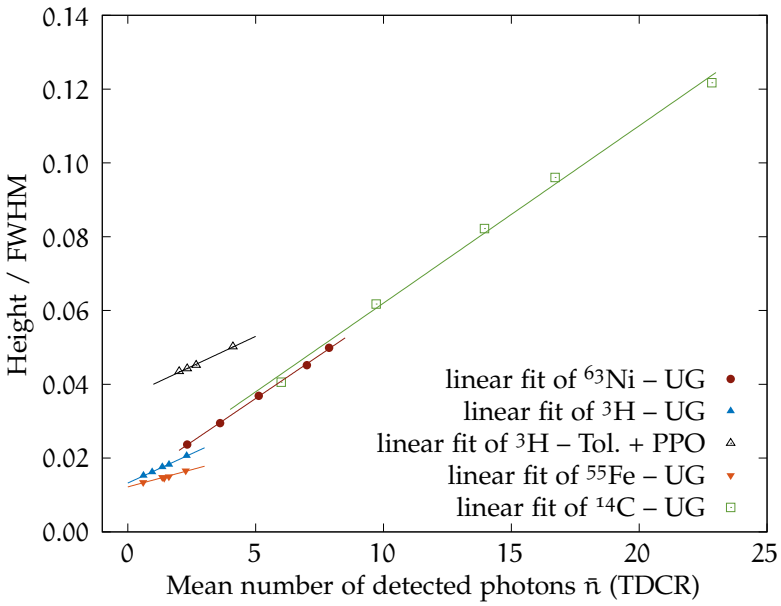

FIGURE 6.11: Scaled height of the cross-correlation distribution H_0/FWHM as a function of the $\bar{n}$. The data points are from measurements of various LS-sources and the average number of photons is calculated from the TDCR model.

6.5.2 *Relationship between the height and the TDCR parameter*

A commonly used approach in routine liquid scintillation analysis is to determine the detection efficiency from a quenching indicator using predetermined quench curves. There are many quenching indicators depending on the manufacturer of the LS analyzer, but they all rely on the analysis of the pulse-height spectrum of the sample acquired with an external γ source. A recent study [111] has shown that the TDCR value can also be used as a quench indicating parameter. Here we present results of TDCR measurements of ^{3}H and ^{55}Fe in UltimaGold cocktail with efficiency variation performed by means of grey filters. The results indicate that there is a linear relation between the height of the cross-correlation distribution H_0 (equation (6.1)) and the measured TDCR value in a very large interval (Figure 6.12).

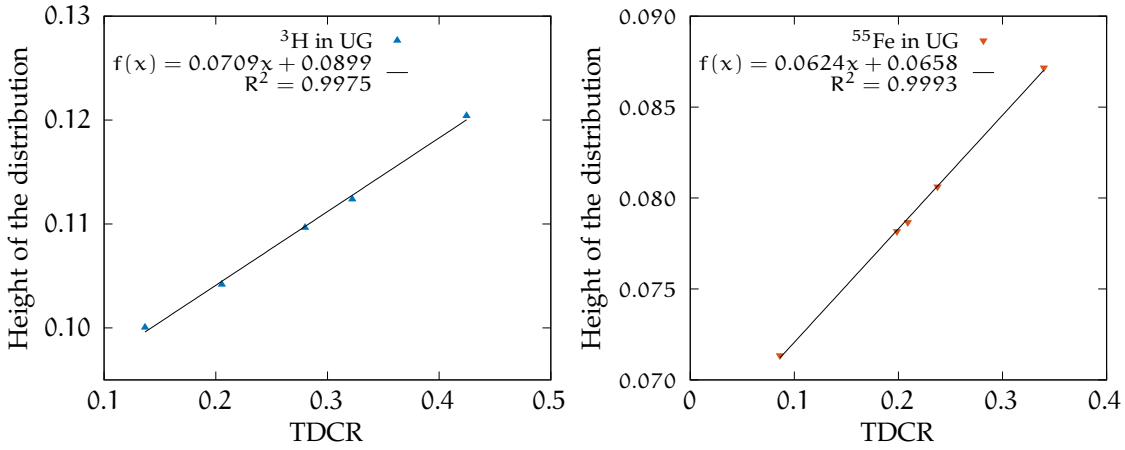

FIGURE 6.12: Height of the cross-correlation distribution (H_0) as a function of the TDCR value for ^{3}H (left) and ^{55}Fe (right) sources in UltimaGold cocktail.

6.5.3 *Kurtosis of the cross-correlation distribution*

Similar to the height, the tails of the distribution also depend on the FOM. It is thus also interesting to consider the relationship between the shape and contribution of the tails to the whole distribution. In order to characterize them it is possible to use the fourth moment of the cross-correlation distribution, the kurtosis K:

$$K = \mathbb{E}\left[\left(\frac{\Delta t - \overline{\Delta t}}{\sigma_D}\right)^4\right] \tag{6.8}$$

where $\overline{\Delta t}$ and σ_D are the mean and the standard deviation of the cross-correlation distribution and $\mathbb{E}$ stands for the expected value. The reasoning behind using the fourth moment of the distribution is that it is very sensitive to the tails.

Good linear relations are observed between the kurtosis and the mean number of detected photons (Figure 6.13). Note that, the experimental points for $K(\bar{n})$ seem to

belong to the same line for all β-emitting nuclides in UltimaGold cocktail except for ^{55}Fe.

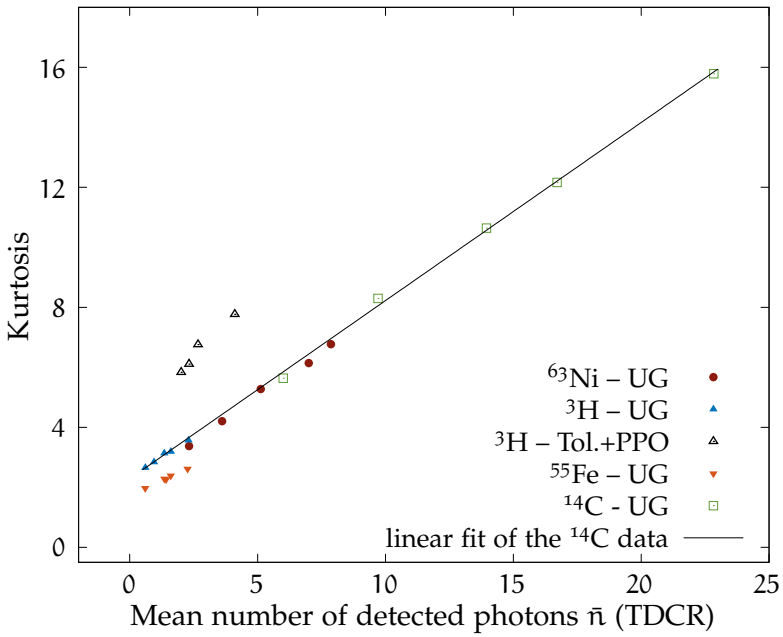

FIGURE 6.13: Kurtosis of the cross-correlation spectra – the data points are measurement results and the linear fit is performed on the ^{14}C data and extrapolated.

SUMMARY OF PART II

SUMMARY The main focus of the second part of the thesis falls on the studies of the distribution of light detection events. The LIST_MODE_ANALYSIS software for the off-line processing of CAEN digitizer data was presented in Chapter 3. The main contribution of the code is the definition of the time interval distributions not only for two channels in coincidence, but also for the logical sum of double coincidences and for the triple coincidences. Another main feature of the program is that all signals that are considered are subject to the same coincidence window and dead-time logical rules. This includes the case when the time distribution histograms are constructed. The dead-time logic that was chosen for the LIST_MODE_ANALYSIS code is the common dead-time logic. Its performance was compared to the recently proposed individual dead-times counting algorithm. The comparison was presented in Chapter 4. The IDT logic seems to lead to a reduced dead-time of the system when measurements of high activity ^{3}H sources are performed. It also shows very similar performance as the CDT in ^{63}Ni, ^{14}C and ^{90}Sr/^{90}Y measurements for activities in the range of 2 to 3 kBq. While having some benefits, the improvements in performance of the IDT logic seem to be at the expense of misclassification, in rare cases, of T events as D events. This was especially evident in ^{222}Rn measurements, where the ^{222}Rn activity obtained with IDT counting rates is 0.4% higher than with CDT counting rates. The results of the comparison were published in the journal *Applied Radiation and Isotopes* [103].

The comparison of the counting algorithms was performed also on artificially generated time sequences of events using a Monte Carlo code, which samples the timing of detected scintillations from a pre-measured time interval distribution. This code also served as an inspiration to develop another Monte Carlo simulation program that uses physical assumptions about the time dependence of the scintillation light of the prompt and delayed fluorescence and of the time response function of a LS detector. The latter code, described in Appendix A, outputs digitizer-like list-mode data that can be analyzed by the LIST_MODE_ANALYSIS program. The time distributions that were obtained from Monte Carlo simulation data were compared to real measurements and an excellent agreement was obtained.

The exploration of the time interval distributions were continued further in chapters 5 and 6. Firstly, an analytical model of the cross-correlation distribution of prompt fluorescence was developed. The various steps in the derivation were validated through comparisons with the Monte Carlo code. The final equation gives identical results as the Monte Carlo simulation in the case of a nuclide with a given energy spectrum, a LS cocktail with a given prompt decay constant and a detector system with given relative PMT efficiencies, static delays and standard deviations of the Gaussian time jitter.

As the analytical equation depends on the FOM of the measurement, it was postulated that it could be used to fit experimental data and be used to obtain the detection efficiency of a two PMT system. However, the complexity of the theoretical equation required a fast computer code for its calculation. Such code was developed in the framework of this thesis, and it is presented in Appendix B. The code was optimized to be as fast as possible, and it can be used to fit measurement data with the analytical equation in order to extract the underlying parameters.

The main result in this part is the study of the applications of the cross-correlation distribution. It was shown that the height of the distribution could be used to calculate the mean number of detected photons, if the parameters of the scintillator and detection system are known. Attempts were made to fit the analytical cross-correlation distribution directly to experimental data. Very good results were observed for ^{3}H and satisfactory results were observed for ^{14}C. These studies demonstrate that if the decay constant of the prompt component of the scintillator is known, it is possible to estimate the FOM of the measurement, and from it the detection efficiency. These results are an important first step towards the use of the cross-correlation distribution for primary activity measurements.

The use of cross-correlation data in routine LS analysis was also explored. It was shown that the height of the experimental distribution depends linearly on the FOM for the low-energy emitters ^{3}H and ^{55}Fe. This would allow to record the height as a function of the FOM for a calibration source and then use this information in subsequent measurements of unknown sources. The relationship between the height scaled to the FWHM and the mean number of detected photons was shown to be linear for all studied nuclides. The possibility to characterize the distribution using its kurtosis was also explored by plotting it with respect to the mean number of detected photons. The results show that, under certain conditions, the same linear relationship is observed for ^{3}H, ^{63}Ni and ^{14}C when in the same LS cocktail.

CHALLENGES There are several challenges in front of the successful application of the cross-correlation method for primary activity standardization by LS counting. Perhaps the largest obstacle is in the form of the delayed scintillation component. Thus far there does not seem to be a reliable model of its timing properties and attempts to describe it include many unknown parameters. Moreover, it is diffusion controlled and its emission rate depends on the temperature of the scintillator. As will be shown in Chapter 9, the delayed fluorescence is also problematic for the TDCR method. In this regard, it would be beneficial to develop LS cocktails with less pronounced delayed component.

Another challenge would be that the rise time of the prompt scintillation component is not included in the analytical model (equation 5.2). For some cocktail it is possible that this rise time is a significant fraction of the decay time and would influence the overall shape of the cross-correlation distribution. The inclusion of another exponent to

describe the scintillation rise time can be done, but it would not permit the analytical evaluation of the cross-correlation between the responses of the two PMTs.

From experimental point of view, high-quality PMTs have to be used for cross-correlation measurements, i. e., high quantum efficiency and single photon sensitivity. In addition, matched PMTs with similar efficiencies and timing response would be preferable. The analysis of the time of arrival of PMT signals requires fast digitizers with constant fraction discrimination or fast circuits with timing resolution better than 200 ps. The time-response properties of the system, described by λ, μ and σ in the cross-correlation distribution $D(\Delta t; \varphi, \lambda, \epsilon_A, \epsilon_B, \mu, \sigma)$, have to be carefully characterized. The parameters μ and σ are specific to the detector system and depend on the PMTs and the associated electronics. The decay constant λ is a property of the LS sample. Unfortunately, the decay constant λ and the figure of merit φ cannot be determined from a single fit of the cross-correlation distribution because they are strongly correlated. The solution is to use additional measurements, as it is done in this work, or to use other techniques, such as time-correlated single photon counting, to determine the decay constant λ. The latter option is very promising as it allows completely independent determination of λ for a particular LS sample and thus will largely facilitate the determination of the FOM. This approach will be explored in future studies.

From a theoretical point of view, a challenge in front of the cross-correlation method as a method for primary activity measurement is that it determines the mean number of detected photons or the FOM. In order to go from detected photons to detection efficiency one is obliged to go through the free parameter model. Thus, the cross-correlation method inherits all the deficiencies of the free parameter model, such as the unknowns in the light output as a function of the deposited energy. The same problems, however, apply to all other currently used methods in radionuclide metrology using LS counting, e. g., TDCR and CNET. In this regard, it is possible that the cross-correlation method gives new information that could be used to reduce the uncertainties associated with the free parameter model.

Finally, a full uncertainty budget of the detection efficiency derived from the cross-correlation method should be established for the application of this method in radionuclide metrology. Currently, only the fit uncertainty was considered, but in order to be precise, many other contributions would have to be considered, such as: the effect of the digitizer's finite sampling rate, the walk of the constant fraction discriminator, the influence of temperature on the decay constants, the influence of delayed fluorescence, uncertainty in the β-spectrum, uncertainties associated with the non-linearity of the light output of the scintillator with respect to the deposited energy and possibly others.

The challenges in front of the application of cross-correlation data to more routine LS measurements seem to be quite fewer. The preliminary results described in this part seem to suggest that the height of the cross-correlation distribution could be used as a proxy for the detection efficiency if the detection system is calibrated beforehand.

Part III

APPLICATIONS OF THE TIME DISTRIBUTIONS IN METROLOGY

7

MEASUREMENT OF THE HALF-LIFE OF SOME EXCITED NUCLEAR STATES BY LS COUNTING

Liquid scintillation counting has some specific features compared to other detection methods, namely the 4π detection geometry and the practically 100% detection efficiency for energies over 40 keV [23]. Due to these factors the method is well suited for measurements of the half-life of radioisotopes. In recent years it was successfully used for the accurate determination of a multitude of half-lives, e. g., the very long-lived ^{147}Sm (1.08×10^{11} years) [112], ^{176}Lu (3.8×10^{10} y) [113] and ^{10}Be (1.4×10^{6} y) [114] or the short-lived ^{212}Pb (10.64 h) [115] and ^{214}Po (3.7 µs) [116]. The measurement technique allows the determination of half-lives which range from several microseconds to 10^{11} years.

These properties of LS detectors could be also useful for the study of excited nuclear states, especially in short-lived nuclides, where lower detection efficiency would require long measurement times which may not be achievable. Moreover, due to the fast response of organic scintillators (typically a few ns, depending on the scintillator) and PMTs (typically 1.3 ns rise time), the timing of scintillation events could be very precise. Thus, it is a useful method for fast timing measurements in the nanosecond range.

In this chapter the LS method is shown to be a useful tool for the study of the half-life of some nuclear isomeric states. Two measurement techniques are proposed: one which utilizes a 3-PMT LS counter equipped with additional gamma detector and a CAEN digitizer and another with a 2-PMT LS detector – without the use of a γ channel. We analyze the time interval distributions between the events in the different channels of the system and demonstrate that these could be used for accurate determination of the half-lives of some excited states in certain nuclides.

7.1 MEASUREMENT SYSTEMS

Two experimental systems were used in this study. The first experimental system is the TDCR portable device developed at LNHB for primary measurement of activity of LS–samples. The same device was used in chapters 8, 9 and 10. It consists of a three PMT LS detector and a 5 mm x 5 mm x 1 mm CdTe X-ray detector. The PMTs in the LS system are square, small form-factor Hamamatsu R7600-200 tubes with 350 ps FWHM transient time spread [91]. The solid state detector is an AmpTek XR-100CdTe with a PX2T power supply and shaping amplifier [117].

The three PMTs are positioned in a 120° geometry around a standard 20 ml liquid scintillation vial. The vial is placed in a 3D printed optical chamber made with PLA[1] plastic. The chamber is covered with reflective polymer foil with 98.5% reflectivity across the visible spectrum (Enhanced specular reflector foil by 3M). The CdTe detector is placed as close as possible to the vial, in order to achieve maximum geometrical efficiency and between two of the three PMTs (as shown schematically in Figure 7.1).

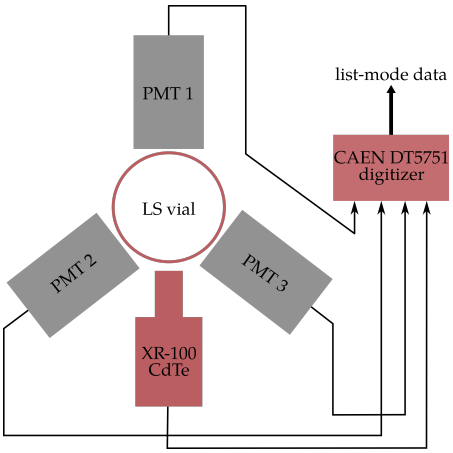

FIGURE 7.1: Simplified schematic of the three-PMT LS detector and the CdTe γ-detector.

The three PMT channels and the amplified and shaped output of the CdTe detector are connected to a CAEN DT5751 desktop digitizer [109] with 1 GS/s sampling rate. The signals of the three PMTs and the CdTe detector are digitized. A timestamp of the arrival times as well as the peak area are recorded for each event in a file for off-line analysis.

The second experimental system is an in-house developed LS detector with two XP2020Q PMTs looking from opposite sides at a standard 20 ml LS sample. The vial is placed in a 3D printed optical chamber which is optimized for fast light collection. Both PMTs are directly connected to the DT5751 digitizer and the incoming events are recorded in a list mode file. This system was used for the LS–LS coincidences measurements and to obtain the half-lives of the excited states without the use of the gamma channel.

The two detector systems were used to measure LS–sources of ^{57}Co and ^{241}Am in UltimaGold cocktails in standard 20 ml glass vials covered with diffusive tape. The latter is done in order to reduce the total internal reflection and trapping of light inside the sample. Both sources contain approximately 100 µl water.

Due to the higher delay of the CdTe detector, the PMT channels in the 3-PMT detector are delayed by 4 µs using the software. This value was determined by measuring the ^{241}Am LS–source and changing the delay until a maximum coincidence counting rate is reached between the LS and γ channels with a 40 ns coincidence window.

1 Polylactic acid – a common material used in 3D printig.

7.2 DECAY CURVE ANALYSIS

When analyzing the time interval distributions, depending on the measurement conditions, it is possible that the observed decay constant differs from the true decay constant of the excited state. Such a problem could arise when there is a large probability for uncorrelated events to serve as stop signals. This was first described by Radeloff et al. and they have proposed that a bi-exponential equation is needed in such cases to accurately describe the observed decay curve. The equation is the following [118]:

$$N_{total}(t)dt = Ae^{-(N_2+\lambda)t}dt + Be^{-N_2 t}dt, \tag{7.1}$$

where $N_{total}(t)dt$ is the number of detected events per unit time, λ is the decay constant of the excited state and N_2 is the counting rate in the channel of the transition depopulating the excited state. The second term in the sum accounts for contribution of the accidental coincidences and background signals to the observed time interval distribution. The first term is an exponential decay with a modified decay constant in order to account for uncorrelated events that serve as a stop signal. This behaviour was found to be significant for measurements of half-lives in the order of a second.

The highest single counting rate and the largest half-life studied in this work are for the 14.4 keV level of ^{57}Fe, so if the effect is significant it will be most pronounced in this measurement. The counting rate in the stop channel is $N_2 = 1.3 \times 10^3$ s^{-1} and the decay constant of the excited state is $\lambda = 7.094 \times 10^6$ s^{-1}. The difference between the apparent decay constant and the true one is 0.02%. As this is negligible compared to the other uncertainty factors a single exponent with λ as an argument was used to fit all obtained time distributions.

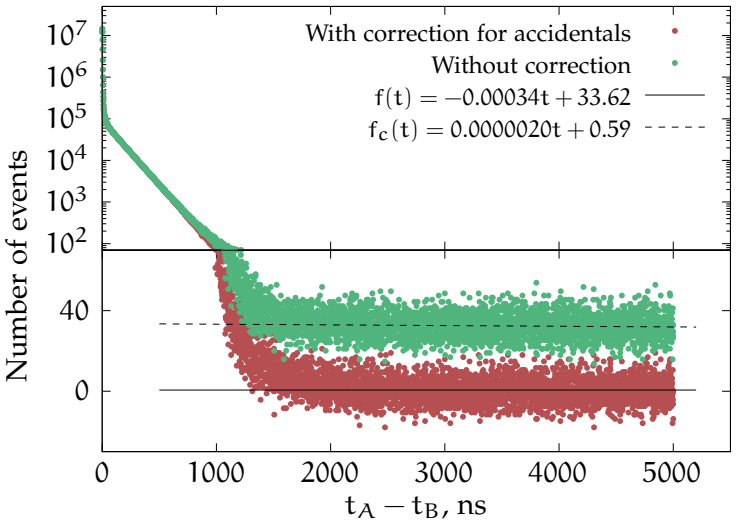

FIGURE 7.2: Time interval distribution of a ^{57}Co source without and with correction for accidental coincidences. The points between 3 µs and 5 µs were considered for the linear fits.

However, the accurate determination of the half-life necessitates that the plateau that is formed by the accidental coincidences is taken into account. In equation (7.1) this is

done via the second term in the sum. In this study all time interval distributions are corrected for accidental coincidences according to the experimental method described in Chapter 8. The distribution is obtained for a large enough window that includes all correlated coincidences as well as a part of the distribution which contains only accidental coincidences. The distribution of the accidental coincidences is approximated with a linear function and the accidental coincidences are subtracted from the observed time interval distribution to produce the distribution of the true coincidences. The approximation with a linear function is valid in the studied cases as the counting rate is low enough. The procedure is illustrated in Figure 7.2. The time interval distribution of a ^{57}Fe LS-source with start and stop signals from an LS detector is shown before and after subtraction of the contribution of the accidental coincidences.

The obtained time interval distributions are fitted with the non-linear least squares Levenberg-Marquardt algorithm using `gnuplot` [119]. The number of events per bin is in all cases more than 30, and so we can assume that the statistical fluctuations have a Gaussian distribution. The standard deviation of the number of detected events in each bin is calculated as the square root of the number of events in the bin, thus assuming Poisson statistics. The uncertainty of each data point is taken into account in the fitting algorithm.

7.3 HALF-LIFE MEASUREMENTS OF EXCITED STATES IN FE-57

^{57}Co decays via EC to the 136.5 keV excited level of ^{57}Fe with 99.8% probability (shown in Figure 7.3). The decay is detected in the liquid scintillator by the X-ray and Auger electron emissions. The time for the rearrangement of electrons after the EC is in the order of 10^{-16} s and thus this process is considered to be instant compared to the studied half-lives [120]. The energy released in the scintillator after the EC is in the range from 5.4 to 7.1 keV. The detection efficiency for a double coincidence in the LS detector for such energies is around 50%.

The second excited level of ^{57}Fe transitions to the ground level with 10.65% probability or to the first excited level with 85.5% probability with a half-life of around 8.6 ns (see Figure 7.3). The 2 – 0 transition can be detected in the scintillator by the 129.4 – 136.5 keV conversion electrons, produced with about 4% intensity, or it can be detected by the gamma emission due to the transition $\gamma_{2,0}$(Fe) = 136.5 keV which directly interacts with the scintillator by Compton scattering or photoelectric effect. Similarly to the previous transition, the 2 – 1 transition can be detected by the 115 – 122 keV conversion electrons, produced with about 4% intensity, or by the gamma emission due to the transition $\gamma_{2,1}$(Fe) = 122 keV. Finally, the first excited level has a 98 ns half-life and the 1 – 0 transition can be detected from the 7.3 – 14.4 keV conversion electrons or gamma emission due to the transition $\gamma_{1,0}$(Fe) = 14.4 keV. With the analysis of this decay scheme and the properties of this specific LS–gamma detector, there are a few possible start – stop combinations from the available events:

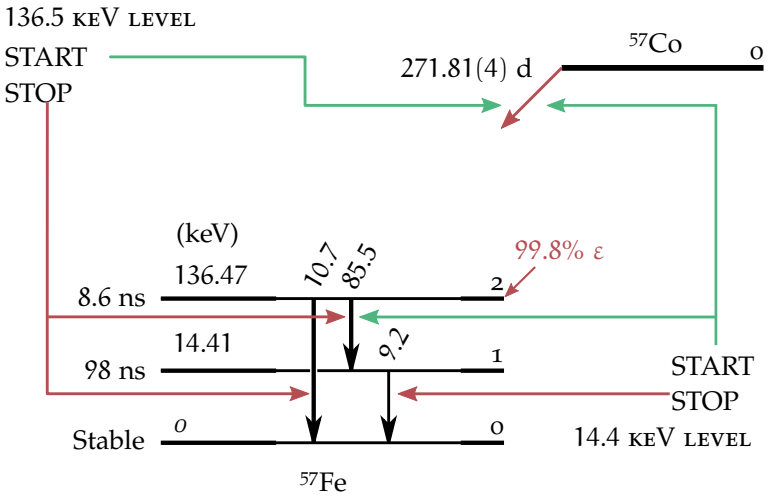

FIGURE 7.3: A simplified decay scheme of ^{57}Co. Only transitions with intensities above 0.2% are shown. The START and STOP signals that were used to study the half-lives of the two excited states are also shown. Data and figure taken from [121].

1. EC is detected (START) and $\gamma_{2,0}$(Fe) is detected (STOP). Such coincidences were used to study the half-life of the 2nd excited state.

2. EC is detected (START) and $\gamma_{2,1}$(Fe) is detected (STOP). In this case $\gamma_{1,0}$(Fe) would be within the dead time of the detector. These coincidences were also used to study the half-life of the 2nd excited state.

3. EC is not detected; $\gamma_{2,1}$(Fe) is detected (START) and $\gamma_{1,0}$(Fe) is detected (STOP). This was used to study the half-life of the 1st excited state.

4. EC is detected (START), $\gamma_{2,1}$(Fe) is not detected (low probability) and $\gamma_{1,0}$(Fe) is detected (STOP). Such coincidences were also used to study the half-life of the 1st excited state.

The various start and stop possibilities are shown in Figure 7.3.

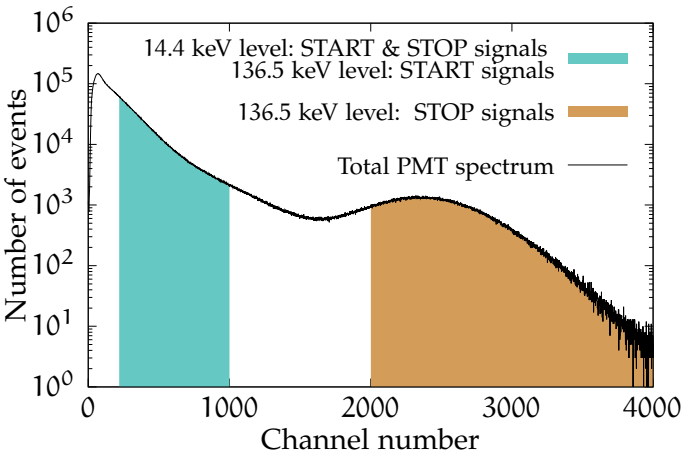

FIGURE 7.4: Spectrum of the ^{57}Co LS–sample obtained with the 2-PMT system. For the study of the 14.4 keV level the START and STOP signals are taken from the lower energy part of the spectrum. For the study of the 136.5 keV level the low energy events are used as START and the high energy events are used as STOP.

7.3.1 14.4 *keV level of Fe-57 using LS–LS coincidences*

A 60-hour-long measurement of a 5 kBq ^{57}Co LS–source was performed using the 3 PMT TDCR-γ detection system. This system was preferred over the 2-PMT system in order to directly compare results with LS–γ coincidences on the same list-mode data. The obtained list-mode files were analyzed using the dedicated software; two of the PMT channels were constrained to include only events with medium energy - i.e. removing single photon events and the high-energy 122 – 136 keV interactions. Removal of the single photon events is done in order to remove spurious events and delayed fluorescence coming from the cocktail. The energy spectrum and the part of the events which were considered for this study are shown in Figure 7.4. Even after selecting only a part of the energy spectrum that excludes the high energy events all coming from the 2nd excited state of ^{57}Fe there is a non-zero probability to detect events from this state because of Compton scattered electrons from the $\gamma_{2,0}$(Fe) and $\gamma_{2,1}$(Fe) transitions. Such events will distort the decay curve of the 1st excited state as they can serve as both start and stop signals. However, after ten half-lives of the 8.6 ns level, or about 90 ns, only events from the 14.4 keV level can be detected as a stop signal due to its significantly longer life-time compared to the other transitions.

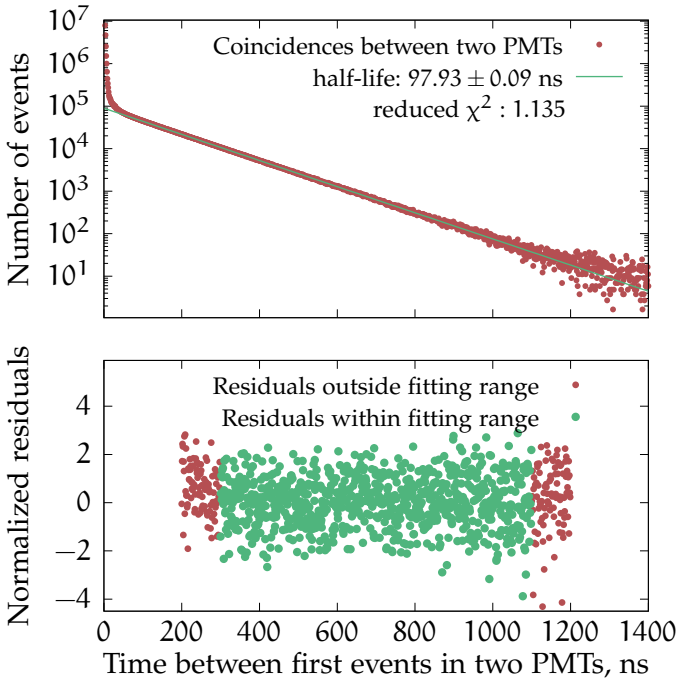

FIGURE 7.5: LS–LS coincidences measurements of the 14.4 keV level of ^{57}Fe. The start signal is given by a low energy event in one PMT and a low energy event in the other PMT. The time interval distribution is obtained with the TDCR detector. The normalized residuals are in units of number of standard deviations.

Another effect that has to be considered is that the Compton scattered electrons produced from the $\gamma_{2,1}$(Fe) transition interacting with the cocktail can act as a start signal. Due to the 8.6 ns half-life of the 2nd excited state they cannot be considered to be instantaneous after the decay. This leads to a sum of two exponential distributions: first a rise time equal to the decay time of the 2nd excited state and second an exponential decay with the decay constant of the 1st excited state. After a sufficient time the effect

of the rise time is negligible and only the decay time of the 2nd excited state will be observed.

The time interval distribution between the first events in the two PMTs within the selected energy range is shown in Figure 7.5. The total number of coincidence events in the presented measurement is 10^8. The time distribution was fitted with an exponential decay and the points considered in the fit are between 300 and 1100 ns. The obtained half-life is 97.93(9) ns, where the uncertainty is the statistical uncertainty reported by the fitting algorithm. The residuals are well grouped within $\pm 2\sigma$. Some residuals outside the fit boundaries are also shown in order to illustrate that the quality of the fit is preserved also at wider range.

7.3.2 14.4 *keV level of Fe-57 using LS–γ coincidences*

The same list-mode ^{57}Co measurement was used in order to study the LS–γ coincidences. In this case the start signal is given by an event in the 136.47 keV peak in the CdTe detector and the stop by a low-energy event in the LS (excluding the single photon peak). The time interval distribution is displayed in Figure 7.6. The fit is performed between 250 ns and 450 ns with an exponential function. The obtained half-life is 97.8(28) ns, where the uncertainty is only the statistical uncertainty reported by the fitting algorithm. Due to the low geometrical efficiency of the γ-channel detector, it is difficult to obtain the same precision for the same measurement time as with the LS–LS coincidences method.

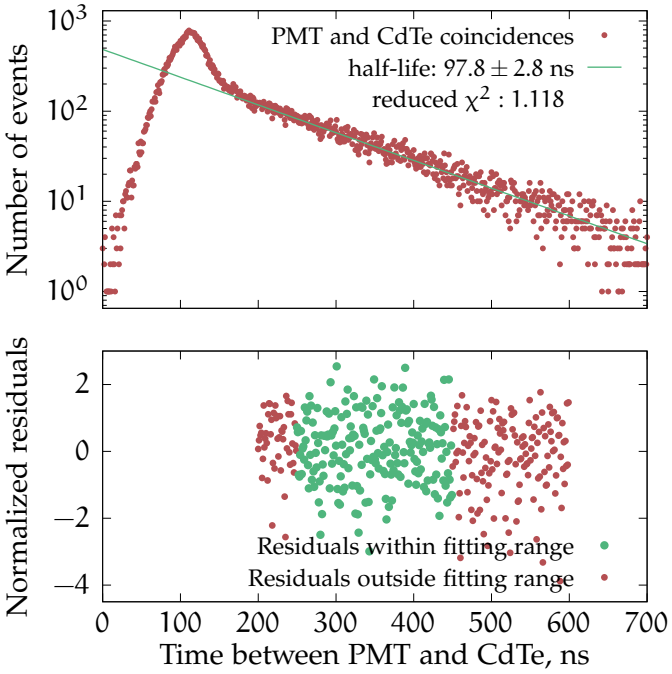

FIGURE 7.6: ^{57}Co LS–γ coincidences. Start signal is given by the 136 keV peak in the CdTe and the stop is given by a low-energy PMT event. The normalized residuals are in units of number of standard deviations.

7.3.3 136.5 *keV level of Fe-57 using LS–LS coincidences*

The half-life of the 136.5 keV excited state was determined from LS–LS coincidences using the 2-PMT detector by triggering on medium-energy events in one PMT as a start signal and using the 122-136 keV peaks for a stop signal in another PMT. The spectrum of the events considered for start and stop is shown if Figure 7.4. The study of the 2^{nd} excited state is significantly easier compared to the 1^{st} as there is only one start event and the two stop transitions 2 – 1 and 2 – 0 can be separated well from the rest. The half-life of this level is too short to be studied with the gamma detector due to its timing resolution.

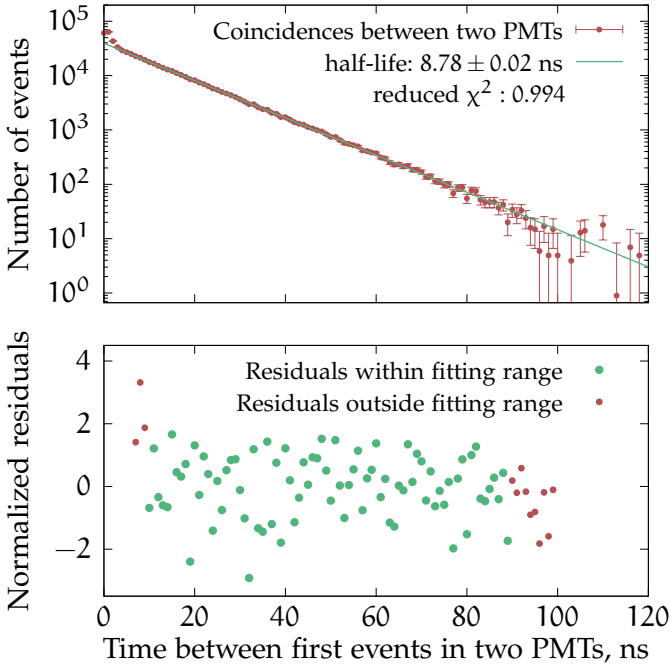

FIGURE 7.7: LS–LS coincidences measurements of the 136.5 keV level of ^{57}Fe. The start signal is given by a low energy event in one PMT and a 122-136 keV event in the other PMT. The time interval distribution is obtained with the 2-PMT system. The normalized residuals are in units of number of standard deviations.

The observed decay curve in such a configuration is shown in Figure 7.7. The fast response of the PMTs in LS–LS technique allows us to study 9.7 half-lives of this state. The half-life obtained from an exponential fit is 8.78(2) ns, where the uncertainty is the statistical uncertainty reported by the fitting algorithm.

7.4 HALF-LIFE OF THE LONG LIVED NEPTUNIUM-237 EXCITED STATE

^{241}Am decays with the emission of an α-particle to the 59.54 keV short-lived isomeric state of ^{237}Np with 84.45% probability (see Figure 7.8). A 1 kBq source of ^{241}Am in UltimaGold (UG) liquid scintillator in a standard 20 ml glass vial was prepared for the purpose of this study. The source was measured for 60 hours with the described measurement system and the events from all LS channels and the γ detector were recorded in list-mode files. The files were analyzed to obtain the time interval distributions for the LS–LS and LS–γ coincidences.

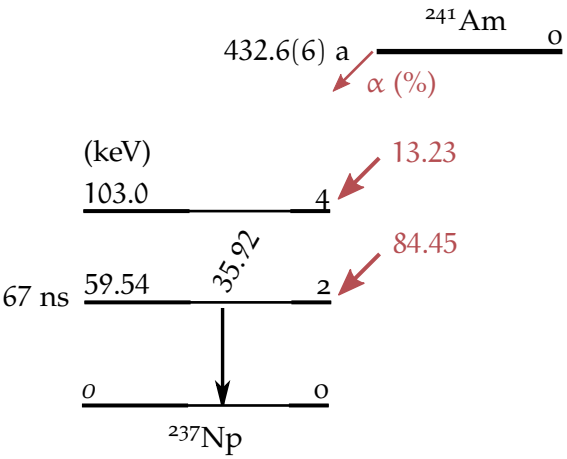

FIGURE 7.8: Simplified decay scheme of ^{241}Am. Only γ emissions with intensities above 3% are shown. Data and figure taken from [121].

For the usual applications of the LS detectors the PMTs are working in single photon mode with gain in the order of 10^7. At such high gain the light from the alpha particles of ^{241}Am would produce large signals with significant afterpulses spanning several microseconds. Thus, single photon mode would be unsuitable to detect the signal from the 59.54 keV de-excitation as the detectors will be saturated. This saturation can be avoided by reducing the PMT high-voltage, from 2100 V to 1700 V for the used XP2020Q PMTs, thereby reducing the gain to approximately 10^5. This is sufficient to reduce the afterpulses to a negligible level and gives the opportunity to use the ^{241}Am α-particle in the LS as a start signal and a 59.54 keV conversion electron or γ, again in the LS, as a stop. The obtained decay curve with such a configuration is shown in Figure 7.10. A major advantage of the LS–LS coincidences with the 2-PMT detector over using a γ detector is the 100% efficiency for α-particles and close to 100% efficiency for the 59.54 keV emissions.

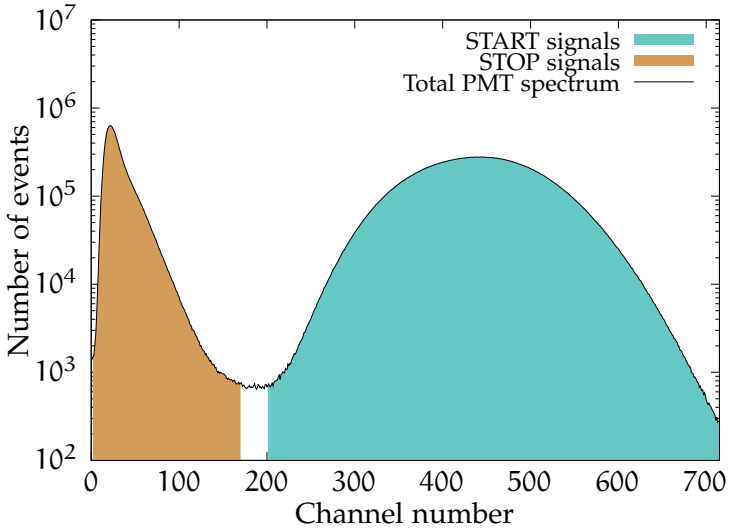

FIGURE 7.9: Spectrum of the ^{241}Am LS–sample obtained with the 2-PMT system. The ^{241}Am α peak is shown in green and the events from the 59.5 keV transition of ^{237}Np in red.

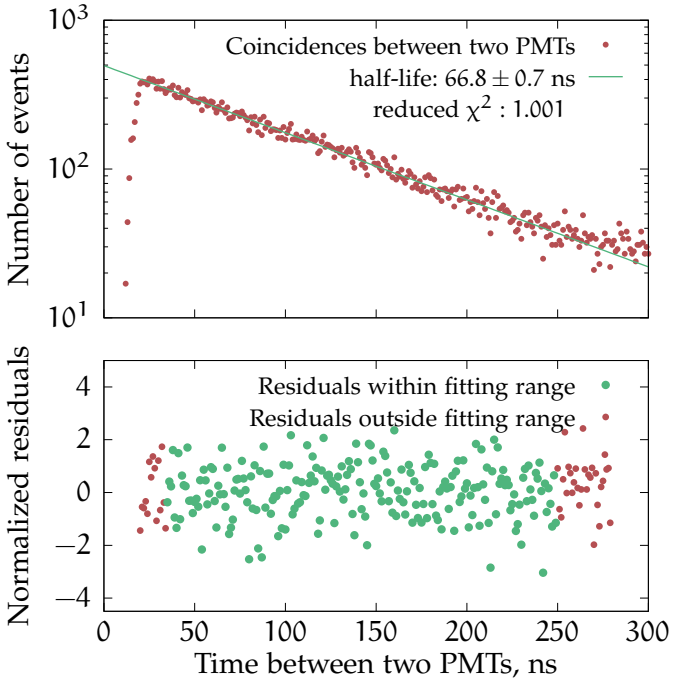

FIGURE 7.10: LS–LS coincidences measurement of the 59.5 keV level of ^{237}Np. The start signal is given by events in the alpha peak of the LS spectrum and the stop signal is given by a low energy event from the 59.5 keV transition. The time interval distribution is obtained with the 2-PMT system. The normalized residuals are in units of number of standard deviations.

The result from the LS–LS coincidences was compared with the half-life obtained with LS–γ coincidences using the 3-PMT TDCR-γ detector. In this case the start signal is given by an α event in the LS and the stop event is given by an event in the 59.54 keV peak in the CdTe detector.

The alpha particle coming from the decay ^{241}Am is detected in the scintillator with 100% efficiency. The 59.54 keV gamma can then be detected in the CdTe detector with a geometrical efficiency of about 0.35%. The performed measurement is 136 hour long and the total number of recorded coincidences is 4×10^5. The distribution of the time interval between a PMT event and the CdTe detector event in the 59.54 keV peak is displayed in Figure 7.11. The number of events per bin are normalized by the total number of detected events. The bottom graph shows the residuals of the fit within the fitting range of 175 ns to 700 ns in green and outside the fitting range in red. The points before 175 ns are excluded in order to remove effects of the gaussian timing response of the CdTe and events after 700 ns are excluded due to too low statistics. The reduced χ^2 statistic of the fit is 1.037. The observed half-life is 67.60(22) ns, where the uncertainty is the statistical uncertainty reported by the fitting algorithm.

7.5 ANALYSIS OF THE RESULTS AND UNCERTAINTY EVALUATION

An overview of the uncertainty budgets is presented in Table 7.1. The factors that could influence the half-life assessment considered in this work are: the uncertainty associated with the fitting algorithm, the corrections for accidental coincidences, the choice of boundaries for the fitting and possible contribution from other excited states in the case of LS–LS coincidences. The fits of the decay curves were performed with

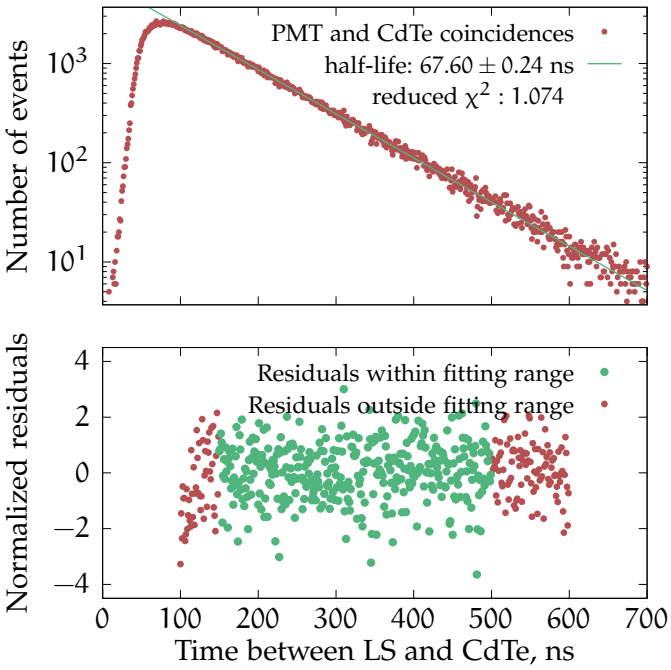

FIGURE 7.11: LS–γ coincidences measurement of the 59.5 keV level of ^{237}Np. The start signal is given by the alpha particle in the LS and the stop is given by an event in the 59.5 keV peak in the CdTe. The normalized residuals are in units of number of standard deviations.

non-linear least squares Levenberg-Marquardt algorithm. The fit uncertainties are taken from the output of the fitting algorithm. The uncertainty associated with the correction for accidental coincidences was estimated by a manual change of their amplitude until a visible change in the residuals was observed; similar to the technique described in [122]. The uncertainty coming from the choice of fitting boundaries was evaluated by choosing different low and high limits and studying the effect on the final value for the half-life. For the LS–LS coincidences there is some uncertainty due to the choice of the parts of the PMT spectrum that are taken for start and stop signals. The estimate of this uncertainty was performed by analyzing the decay curves obtained with different parts of the spectra for the start and stop energy windows.

Due to the poor energy resolution of the LS detector it is important to consider that the studied excited states could be populated by higher-lying states. Their half-life is in some cases unknown and should not be readily assumed to be instant compared to the half-life of the studied state. In the case of the 136.5 keV level of ^{57}Fe there are two higher energy excited states from which it could be populated. The 3 – 2 and the 4 – 2 transition have 0.0004% and 0.015% probability respectively and would give negligible contribution to the decay curve observed in Figure 7.7. For the 14.4 keV level of ^{57}Fe the 3 – 1 transition has 0.0032% probability and according to the literature the half-life of the 3rd excited state is less than 4 ns. Therefore, this transition will have a negligible influence on the decay curve observed in Figure 7.5. The 4 – 1 transition, however, occurs with 0.159% probability and is 692.4 keV. The half-life of the 4th excited state is, however, unknown. The maximum deviation in the obtained decay time due to this transition would be less than 0.05% if we assume that the 4th excited state has close to 50 ns half life. No such considerations are needed in the case of the ^{237}Np decay curve from LS–γ coincidences as the start and stop levels are well-defined.

Due to the finite sampling rate of the digitizer there is a time jitter which could be worth considering when dealing with short half-lives, such as that of the 136.5 keV excited state of ^{57}Fe. Considering that inside a 1 ns time interval, the pulse could happen anywhere with the same probability. So, taking into account a uniform distribution for the start signal, and the same for the stop signal, the total time distribution would be a triangular distribution (convolution of two square distributions) with a standard deviation of $1/\sqrt{6}$ ns, thus about 0.4 ns. For a sample of N start/stop couples, there is an averaging, so this standard deviation is divided by $\sqrt{N}$. For the LS–LS measurements of the 136.5 keV level of ^{57}Fe this effect should be the most pronounced. The timing uncertainty in the bins with the least amount of detected events is 0.03 ns or 3%. This uncertainty is considered negligible, compared to the statistical uncertainty due to the number of detected events in those bins (around 18%), which is already included in the uncertainty of the fit.

The final values obtained for the half-lives of the two ^{57}Fe states and the ^{237}Np state, after taking into account the factors contributing to the uncertainty, are shown in Table 7.1. Due to the low counting statistics the ^{237}Np LS–LS and the ^{57}Fe LS–γ measurements were not considered for the final result report.

TABLE 7.1: Measured half-life values and uncertainty budgets. The uncertainty values are the standard uncertainties.

	136.5 keV ^{57}Fe	14.4 keV ^{57}Fe	59.5 keV ^{237}Np
Uncertainty from fit	0.22%	0.13%	0.33%
Corrections for accidental coincidences	0.25%	0.15%	0.15%
Fitting boundaries	0.22%	0.24%	0.10%
Contribution from higher excited states	$\leqslant$0.01%	0.05%	—
Choice of gates in the spectrum	0.10%	0.25%	$\leqslant$0.01%
Total	0.41%	0.40%	0.37%
Final result	8.780(36) ns	97.90(40) ns	67.60(25) ns

7.6 COMPARISON WITH EXISTING DECAY DATA

The Decay Data Evaluation Project (DDEP) data on ^{57}Co provides 98.0(4) ns for the half-life of the 14.4 keV level of ^{57}Fe [85]. It is taken as the weighted average of 7 measurements:

1. In [123] from 1961 Clark reports 97.9(2) ns via two NaI detectors.
2. In [124] from 1965 Kistner and Sunyar report 98(1) ns.

3. In [125] from 1966 Eckhause et al. report 97.7(2) ns via two NaI detectors.
4. In [126] from 1969 Hohenemser et al. report 99.3(5) ns via Time-differential perturbed angular correlation.
5. In [127] from 1978 Alikov et al. report 97.8(14).
6. In [128] from 1995 Ahmad et al. report 99.2(4) ns via two HPGe detectors.
7. In [129] from 2006 Morozov et al. report 94(4) via autocorrelation single-crystal scintillation time spectrometer with plastic scintillators and a single XP2020 PMT.

It should be noted that there is a significant discrepancy between the different measurements. The obtained half-life value in this work is 97.90(40) ns which is in agreement with reports 1 and 3 within the estimated uncertainties, but not with reports 4 and 6; reports 2, 5 and 7 have large uncertainties, and thus are in agreement.

The DDEP data on ^{57}Co states 8.6(4) ns for the half-life of the 136.5 keV level of ^{57}Fe. It is taken as the weighted average of 5 measurement, which are consistent within their stated uncertainties. The result from this study, 8.780(36) ns, has the lowest uncertainty compared to previous measurements and is consistent with the already provided average value.

The Nuclear Decay Sheets (NDS) state 68.1(2) ns for the half-life of the 59.54 keV level of ^{237}Np [130]. The value is the weighted average of 5 measurements, the most recent of which is from 1972. The value obtained in this study does not agree with the stated average value which could be caused by the very low uncertainty of the 1972 measurement 68.3(2) ns [131]. This low uncertainty is increased to 0.7 ns (1%) by the evaluator in the ENSDF[2] dataset and the obtained weighted average value is 67.2(7) ns, which is consistent with the result obtained in this work.

CONCLUSIONS

The half-lives of two excited nuclear states in ^{57}Fe and one in ^{237}Np were measured by means of LS–LS and LS–γ coincidences. The half-life of the 59.54 keV level of ^{237}Np was measured by LS–γ coincidences and the result is 67.60(25) ns, which is in good agreement with already published decay data. The half-life of the 14.4 keV level of ^{57}Fe was measured by LS–LS coincidences and the result is 97.90(40) ns which is consistent with some of the published results, however a significant discrepancy exist between the values found in the literature. The half-life of the 136.47 keV level of ^{57}Fe was measured also by LS–LS coincidences and the result is 8.780(36) ns, which is consistent with the published data and comes with a significant improvement in the uncertainty.

Liquid scintillation fast timing measurements can be a useful tool to refine some already known decay times. Another advantage over more-commonly used methods is the relatively short measurement time that is needed, due to the 4π geometrical

2 Evaluated Nuclear Structure Data File from Brookhaven National Laboratory

efficiency. This could allow more precise studies of half-lives of excited states of short-lived nuclides where long measurements are difficult to perform and to isotopes in liquid phase. The method employing LS–LS coincidences is shown be useful for precise measurements of half-lives as short as 8 ns. The results from this study are published in *Applied Radiation and Isotopes* [132].

8

EVALUATION OF ACCIDENTAL COINCIDENCES IN TDCR COUNTING

Liquid scintillation counters with three PMTs as well as electronics with coincidence circuits and extending type dead-time are needed to properly apply the TDCR method to radioactivity measurements. What is usually recorded are the coincidences between three PMTs (triple coincidences) and between pairs of PMTs (double coincidences). As with all other systems working in coincidence, there exists the possibility for two or more unrelated events to occur within the same coincidence window which will result in an *accidental coincidence* (also known as chance or random coincidence).

Accidental coincidences were mostly ignored in the past due to the usually short coincidence windows that are fixed in analogue TDCR counting modules (commonly 40 ns). Another method to minimize the influence of chance coincidences that is commonly employed is to measure sources with not so high activity. With the recent advancement in the field of digital electronics the possibility to use longer, user-selectable coincidence windows has been opened. As an effect, an emergence of systems can be seen recently that use fast digitizers [133] or FPGA-based devices [101, 102, 134].

The rate of random coincidences increases with increasing coincidence resolving time and thus their accurate assessment is necessary to study long coincidence windows. Another field of study where chance coincidences cannot be neglected is the *in situ* metrology of LS-sources used in the nuclear energy and medical fields, where the sources could have considerable activities. In such cases the accidental coincidences cannot be neglected. There has been a recent trend towards the development of miniature portable TDCR counters whose aim is to be used for *in situ* metrology [104, 135].

In this chapter a method for the experimental evaluation of accidental coincidences is presented. The method is complemented with analytical expressions that can be used to calculate the chance coincidences in any TDCR system that provides information about the single, double and triple counting rates. The methods and equations are validated with artificially generated data using a Monte Carlo approach.

8.1 EXPERIMENTAL EVALUATION OF ACCIDENTAL COINCIDENCES

Due to the stochastic nature of the light emission from scintillators, the individual scintillation events are spread out in time with respect to the initial interaction of an ionizing particle with the medium. For high-energy emitters the events are grouped within a short period of time, e. g., 16 ns for ^{18}F with 633 keV maximum energy of the β particles [134]. For lower-energy emitters, one example being ^{3}H with 18.6 keV

maximum β-spectrum energy, the spread of events could be much larger. Studies in the past decade suggest that the necessary coincidence resolving time to gather all scintillation events is as high as 250 ns [82]. From the studies presented in Chapter 4 it can be seen that even 300 ns might be insufficient. The incidence of true events decreases with the time elapsed from the initial radioactive decay and after a few microseconds the probability for occurrence becomes negligible. Therefore, primary events with a difference in time of arrival longer than several microseconds can be considered uncorrelated.

The analysis of the distribution $\theta_i(t)$ of the time differences Δt between the first and last primary event in a given coincidence channel ($i = AB, BC, AC, D, T$) can give information about correlated and uncorrelated events. This distribution and its analysis are the basis of the experimental method for evaluation of random coincidences. An important step in the method is to construct the proper time interval distributions for each coincidence channel. This is straightforward in a two PMT detector where the distribution of interest is the distribution of the absolute time difference between one PMT and the other. For a three PMT detector the proper procedure to construct the time interval is more sophisticated. In a TDCR detector there are many possible coincidences, including complex logic such as for the logical sum of double coincidences D. The calculation of the time differences Δt for the AB, D and T channels is coded in the LIST_MODE_ANALYSIS program as described in Chapter 3. A schematic of the logic is shown in that chapter in Figure 3.1.

Let us consider a common dead-time detector with counting logic as used in the MAC3 module [100]. For such a detector the distribution of the rate of events $f_i(t)$ with a given time difference t for a given coincidence channel i can be defined as:

$$f_i(t) = \frac{\theta(t)}{L}, \tag{8.1}$$

where L is the live-time of the detector. The distribution $f_i(t)$ will be referred to as a *time interval distribution* from here on. It is defined in such a way that:

$$n_i = \int_0^\tau f_i(t)dt, \tag{8.2}$$

where n_i is the counting rate in channel i. The definition is such that if the n_i is calculated from the time interval distribution for a specified coincidence resolving time τ, the same counting rate would be reported by a TDCR detector for the same coincidence window length.

The time interval distribution that is observed in practice consists of two parts: the distribution of true coincidences f_{tc} and the distribution of accidental coincidences f_{acc}. An illustration of the concept is given in Figure 8.1. If it can be assumed that the detection of accidental coincidences is a Poisson process, then the time interval between the events is exponentially distributed. The total time distribution can then be expressed as:

$$f_{tot}(t) = f_{tc}(t) + a_0 e^{-\lambda t}, \tag{8.3}$$

where a_0 is the rate of accidental coincidences at $t = 0$ and λ is the rate of detected events in the coincidence channel.

If a large enough time difference t is considered, the probability of true coincidences will be close to zero. The total distribution in this time interval will be dominated only by the distribution of chance coincidences:

$$f_{tot}(t) = a_0 e^{-\lambda t} \text{ for } t > t_c, \tag{8.4}$$

where t_c is the cut-off time difference. The cut-off time should be selected such that for longer times the probability for true coincidences can be considered negligible.

In most measurements done in practice, the exponential nature of accidental coincidences can be simplified as the observed counting rates are not high enough. For example, the commonly measured counting rates are lower than 10^4 s^{-1} and the width of the analytical time interval distribution (t_e) is less than 2×10^{-6} s. The exponent in equation (8.4) can be approximated well with a linear function as the argument will be less than 2×10^{-6}:

$$f_{acc}(t) = a_0(1 - \lambda t). \tag{8.5}$$

In the case of even lower counting rates the equation can be simplified further:

$$f_{acc}(t) = a_0 \text{ for } t < t_e, \tag{8.6}$$

where t_e should be short enough for λt_e to be considered negligible.

The distribution of the accidental coincidences has two parameters, λ and a_0. They can be estimated by fitting f_{acc} from equations (8.4), (8.5) or (8.6) to the experimentally obtained time interval distribution in the interval (t_c, t_e). If the parameters of the distribution are known, then the counting rate of the random coincidences can be evaluated from the integral of the distributions within the coincidence resolving time:

$$a_i = \int_{t=0}^{\tau} f_{acc}^{(i)}(t)dt. \tag{8.7}$$

where $f_{acc}^{(i)}(t)$ is the distribution of accidental coincidences of the i^{th} coincidence channel (AB, BC, AC, D or T). This approach assumes that the parameters of the distribution are the same for the time interval where the fit was performed and within the coincidence window. The assumption holds if random coincidences are Poisson distributed.

The experimental approach towards the evaluation of random coincidences is advantageous because the only assumptions made are that primary event separated by several µs are uncorrelated and that random coincidences are Poisson distributed. The validity of those assumptions can be checked by analyzing the time interval distribution.

8.2 ANALYTICAL CALCULATION OF ACCIDENTAL COINCIDENCES

A major disadvantage of the experimental method is that it requires a fast digitizer and a lot of computational power in order to construct the time distribution of events in

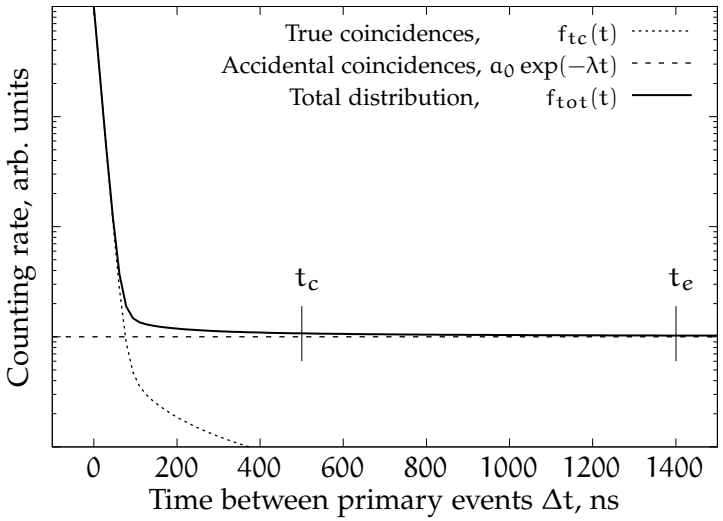

FIGURE 8.1: The measured distribution of the time between first and last primary event in a given coincidence channel is a linear combination of the distribution of the true and accidental coincidences. Note the logartithmic scale on the y axis.

each coincidence channel. This is undesirable in some cases. Therefore, an analytical approach to the problem of random coincidences in TDCR counting was also developed. It is based on the conditional probabilities for the occurrence of uncorrelated events within the same coincidence window.

In a detector with three PMTs one can define many channels of scintillation events – with or without coincidences. The structure of channels that is commonly used in TDCR counting is given in the work of Broda et al. [2]:

- three single event channels (A, B, C)
- logical sum of singles ($S = A \vee B \vee C$)
- three double coincidence channels ($AB = A \wedge B, BC = B \wedge C, AC = A \wedge C$)
- logical sum of the double coincidences channel ($D = AB \vee BC \vee AC$)
- triple coincidence channel ($T = A \wedge B \wedge C$)

Here $\wedge$ denotes the logical "and" operator and $\vee$ the logical "or" operator. Within this convention there is a correlation between the various channels, e. g., all T channel events are also included in all other channels, all BC events are also B, C and S events, etc.

To simplify the coincidence logic, a set of uncorrelated channels can be devised:

- three pure single event channels that exclude doubles and triples:
  $PA = A \wedge \neg(B \vee C)$; $PB = B \wedge \neg(A \vee C)$; $PC = C \wedge \neg(A \vee B)$
- three pure double coincidence channels that exclude triples:
  $PAB = AB \wedge \neg C$; $PBC = BC \wedge \neg A$; $PAC = AC \wedge \neg B$
- the logical sum of the pure single events channel:
  $PS = PA \vee PB \vee PC$

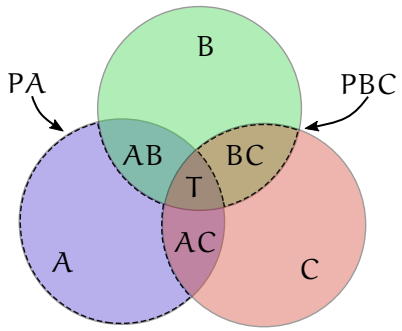

FIGURE 8.2: Venn diagram of the uncorrelated and correlated coincidence channels. The areas representing PA and PBC are surrounded with dashed lines.

- the logical sum of pure double coincidences channel:
  $PD = PAB \vee PBC \vee PAC$
- pure triple coincidence channel:
  $PT = T$.

Here $\neg$ is the logical "not" operator. The PA channel, for example, contains all A events that are not B or C events. This excludes all A events that are correlated to other single or coincidence channels. As a visual example, the pure channels PA and PBC are outlined by dashes in Figure 8.2.

The counting rates p_i in the newly constructed uncorrelated set of channels can be estimated as:

$$\begin{aligned}
p_A &= n_A - n_{AC} - n_{AB} + n_T \\
p_B &= n_B - n_{AB} - n_{BC} + n_T \\
p_C &= n_C - n_{AC} - n_{BC} + n_T \\
p_{AB} &= n_{AB} - n_T \\
p_{BC} &= n_{BC} - n_T \\
p_{AC} &= n_{AC} - n_T \\
p_S &= p_A + p_B + p_C = n_S - n_D \\
p_D &= p_{AB} + p_{BC} + p_{AC} = n_D - n_T \\
p_T &= n_T
\end{aligned} \tag{8.8}$$

where n_i are the counting rates in the commonly used set, for which a correlation exists between the channels.

There exists a well known formula for the rate of random coincidences N_a between two uncorrelated detectors. One of the earliest occurrences in the literature is given by Janossy [136]:

$$N_a = 2\tau(N_1 N_2). \tag{8.9}$$

Here, with the coincidence resolving time of the detector is denoted with τ.

The accidental coincidence counting rate between two uncorrelated channels can be calculated by using equation (8.9). For example, PA and PB detected within the same coincidence window would result in an accidental AB coincidence. The sum of all such coincidences between uncorrelated channels, which result in a signal in the given channel, give the total number of random coincidences in that channel.

We can roughly distinguish two types of accidental coincidences that can be observed. The first type of coincident events are more obvious and consists of two signals, that when detected simultaneously, fall into another channel. For example, a PAC and a PAB event coming in the same coincidence window will be falsely attributed to the T channel. The same pair of uncorrelated events will result in a BC coincidence as well. It is important here to note that the same train of thought cannot be used for the AC and AB channels, as some of these events could be true T coincidences.

The second type of random coincidences could evade the analysis at first sight. It consists of events in the channel of interest that are detected during the resolving time started by another channel. The logic is better illustrated with an example: if a PA event is the first event in a coincidence window and an event in the PBC channel is also detected in the same window afterwards, then the PAB event will contribute to the accidental coincidences in channel AB. Despite PAB being a legitimate AB event, it is still considered an accidental coincidence due to the fact that it is detected within the window started by an uncorrelated event. The order of the time of arrival of events in this type of random coincidences is important however. Regarding channel AB, a PAB coincidence detected after a PC single event is accidental, but the reverse does not hold true. A PC single event detected after a PAB coincidence would not lead to an invalid AB coincidence. Thus, the factor of 2 must be omitted in (8.9).

Let us consider a full example of how to calculate the chance coincidences in a channel. This can be done by summing all possible variants from the two types of accidental coincidence. Taking the AB channel as an example, the contributions belonging to the first type are:

1. PA within the same resolving time as PB: $2\tau(p_A p_B)$,
2. PA within the same resolving time as PBC: $2\tau(p_A p_{BC})$,
3. PB within the same resolving time as PAC: $2\tau(p_B p_{AC})$,
4. PAC within the same resolving time as PBC: $2\tau(p_{AC} p_{BC})$.

The contributions that are of the second type are:

1. PAB in the window started by a non PAB event:
   $\tau(p_A + p_B + p_C + p_{BC} + p_{AC})p_{AB}$
2. PT in the window started by a non PAB event:
   $\tau(p_A + p_B + p_C + p_{BC} + p_{AC})p_T$

The counting rate of the random coincidences a_i in the remaining channels can be calculated by following similar logic. They are expressed as:

$$\begin{aligned}
a_{AB} &= \big[2\,(p_A p_B + p_A\, p_{BC} + p_B p_{AC} + p_{AC} p_{BC}) \\
&\quad + (p_S + p_D - p_{AB})\,(p_{AB} + p_T)\big]\tau \\
a_{BC} &= \big[2\,(p_B p_C + p_B\, p_{AC} + p_C p_{AB} + p_{AB} p_{AC}) \\
&\quad + (p_S + p_D - p_{BC})\,(p_{BC} + p_T)\big]\tau \\
a_{AC} &= \big[2\,(p_A p_C + p_A\, p_{BC} + p_C p_{AB} + p_{AB} p_{BC}) \\
&\quad + (p_S + p_D - p_{AC})\,(p_{AC} + p_T)\big]\tau \\
a_D &= \big[2\,(p_A\, p_B + p_B\, p_C + p_C\, p_A) + p_S(p_D + p_T)\big]\tau \\
a_T &= \big[2\,(p_A\, p_{BC} + p_B\, p_{AC} + p_C\, p_{AB}) + (p_S + p_D)\,p_T \\
&\quad + 2\,(p_{BC}\, p_{AB} + p_{AC}\, p_{BC} + p_{AC}\, p_{AB})\,\big]\tau
\end{aligned} \tag{8.10}$$

Equations (8.8) and (8.10) are a large milestone as they can be applied to all already used TDCR systems that output the single, double and triple counting rates. The estimate of the accidental coincidences using the analytical equations must be applied with care as there are a few assumptions that are involved. Firstly, the coincidences n_{AB}, n_{BC}, n_{AC} and n_T that the detector outputs are the total, i. e., true as well as accidental coincidences. For low enough counting rates this would not be a hindrance, but it would be if the contribution of random coincidences is a significant fraction of the total. To minimize the effect, the measurements should be performed with a coincidence resolving time that is large enough not to miss true coincidences, but not larger, as this would increase the contribution of accidentals unnecessarily. Another point that has to be mentioned is that second order (or higher) random coincidences are not included in equation (8.10) because it is considered that they have negligible contribution. This means random coincidences of the type PA, PB and PC events detected in the same coincidence window and producing an erroneous T coincidence. These approximations do not concern the experimental method for evaluation, and thus equation (8.10) should be used only when the contribution of random coincidences is not overwhelming. The uncertainty of the evaluated accidental coincidences is not derived so far, but as this correction is expected to be small in the usual use cases, then its uncertainty would be insignificant.

8.3 VALIDATION OF THE METHODS

Measurements of four LS-sources were used to validate the developed methods. The sources are: two samples of ^{3}H – UltimaGold in Polyethylene vial, one ^{55}Fe – UltimaGold in Polyethylene vial and one ^{14}C – UltimaGold in glass vial. One of the ^{3}H sources and the ^{55}Fe source were prepared with high activity ($\approx$ 23 kBq) in order to emphasize the contribution of random coincidences. The same pair of sources was also measured by placing a 75% transparent grey filter between the vial and PMTs.

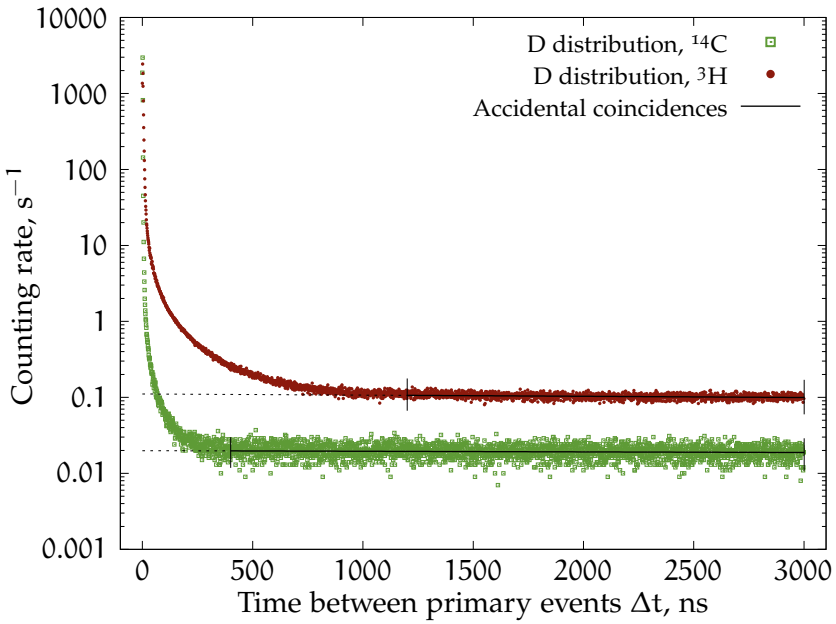

FIGURE 8.3: Time distributions in the D channel of ^{3}H and ^{14}C sources. The mean value of the coincidences between uncorrelated events is shown with a solid line.

The measurements were done with a portable TDCR detector (*miniTDCR*). The outputs of the PMTs were connected to a CAEN DT5751 digitizer with 1 GS/s sampling rate. The digitizer was set up to record the timestamp of incoming event in a *list-mode* file. The files recorded in each measurement were analyzed off-line by the LIST_MODE_ANALYSIS software described in Chapter 3. The program was used to calculate the coincidence counting rates as well as the time distributions in each channel.

APPLICATION OF THE EXPERIMENTAL METHOD The following paragraph presents an example of the application of the experimental method. The D time distributions from the measurements of the 23 kBq ^{3}H source and the 6.2 kBq ^{14}C source are shown in Figure 8.3. In these examples the large time spread of events is evident. The necessary time to gather all ^{3}H events seems to be as high as 1300 ns. The signals from ^{14}C are better grouped in time, but still the needed window is close to 400 ns. For the proper application of the experimental method, the distribution of random coincidences must be well separated from the true coincidences. As the counting rates in the sources are not very large, a uniform distribution of the random coincidences was assumed instead of the expected exponential distribution. In this case equation (8.6) was fitted to the experimental data in the interval 1300 ns – 3000 ns for the ^{3}H source and 400 ns – 3000 ns for the ^{14}C source. The random coincidence counting rate per nanosecond of coincidence window is evaluated at 0.107 s^{-2} for the ^{3}H source and at 0.018 s^{-2} for the ^{14}C source. For a 100 ns coincidence resolving time the counting rates of the accidental coincidences in the two samples are 10.7 s^{-1} and 1.8 s^{-1}, respectively. In order to obtain the counting rates in the other coincidence channels the same analysis can be performed on the respective time distributions.

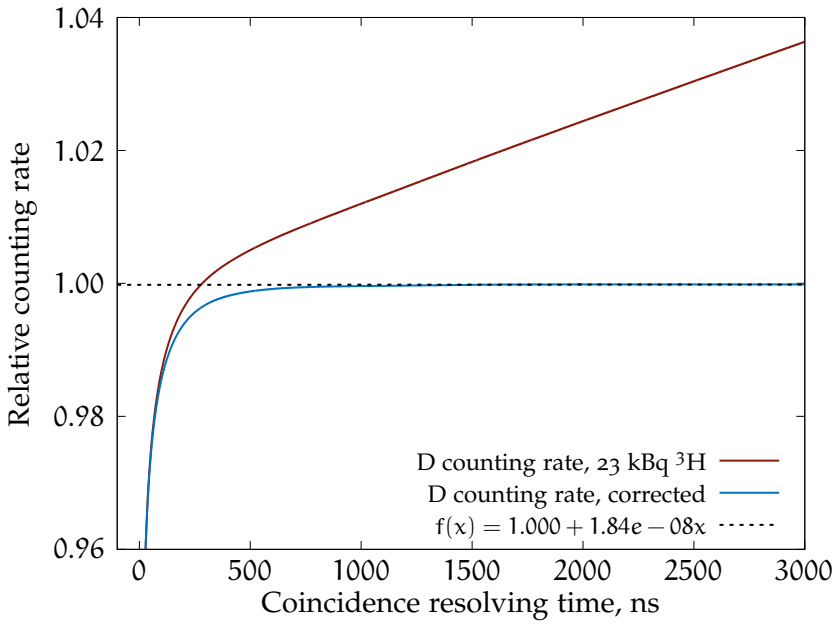

FIGURE 8.4: D counting rate as a function of the coincidence window for the high-activity ^{3}H source without and with correction for accidental coincidences using the experimental method. The counting rates are normalized by the corrected value at 2 µs. A linear fit on the data after 1.3 µs is shown with a dashed line.

By integrating the time distribution in a channel from $t = 0$ to $t = \tau$, one obtains the counting rate in that channel as if a normal measurement with coincidence window τ was performed. Figure 8.4 shows the counting rate in the D channel of the ^{3}H measurement with respect to the coincidence resolving time (shown with a solid red line). The counting rate is normalized by the value corrected for accidentals at 2 µs. For coincidence windows less than 500 ns a significant loss of coincidences can be seen. This is due to the large spread of scintillation events for the low-energy β-emitter that is ^{3}H. For larger coincidence windows the counting rate increases even further. The increase is due to the larger probability for accidental coincidences. The already determined counting rate of random coincidences was used in order to perform a correction. The corrected counting rate as a function of the resolving time can be seen in the same figure with a solid blue line. After the correction for accidental coincidences the counting rate is constant, provided the coincidence window is sufficient to include all true coincidences.

COMPARISON OF EXPERIMENTAL AND ANALYTICAL METHODS The analytical approach towards the calculation of random coincidences relies on several assumptions. While they should be appropriate in most practical cases, it is reasonable to compare the analytical approach to the experimental method. The assumptions in the latter are less constraining and are easily satisfied in practice. Thus, the correctness of the analytical equations can be validated by comparing the evaluated random coincidence counting rates to the ones obtained by the experimental approach. To do so, the

Nuclide	TDCR	Correction method	Accidental coincidences, s^{-1}			Corrected counting rate, s^{-1}		
			AB*	T	D	AB*	T	D
^{3}H 23 kBq **	0.3998	Calc.	84.74	85.82	83.49	5986.8	4055.9	10145.2
		Expt.	85.24	86.34	83.59	5986.3	4055.4	10145.1
		Δ	−0.59%	−0.60%	−0.12%	0.01%	0.01%	0.00%
		a_i/n_i				1.40%	2.08%	0.82%
	0.2080 (with filter)	Calc.	54.63	37.43	83.52	2209.8	981.5	4719.5
		Expt.	54.44	37.09	83.29	2210.0	981.8	4719.7
		Δ	0.36%	0.93%	0.27%	−0.01%	−0.04%	0.00%
		a_i/n_i				2.4%	3.64%	1.73%
^{3}H 2.4 kBq	0.4018	Calc.	2.57	1.67	4.39	548.5	370.2	921.4
		Expt.	2.57	1.72	4.63	548.5	370.2	921.2
		Δ	0.00%	−3.27%	−5.15%	0.00%	0.02%	0.03%
		a_i/n_i				0.47%	0.46%	0.50%
^{55}Fe 24 kBq **	0.2809	Calc.	40.07	38.98	41.99	3300.1	1806.0	6429.4
		Expt.	40.24	39.04	42.69	3300.0	1806.0	6428.7
		Δ	−0.42%	−0.14%	−1.63%	0.01%	0.00%	0.01%
		a_i/n_i				1.20%	2.12%	0.66%
	0.1248 (with filter)	Calc.	25.65	14.03	48.80	989.1	299.5	2399.6
		Expt.	25.26	13.63	47.24	989.5	299.9	2401.1
		Δ	1.54%	2.93%	3.30%	−0.04%	−0.13%	−0.06%
		a_i/n_i				2.49%	4.35%	1.93%
^{14}C 6 kBq	0.9315	Calc.	1.93	1.82	1.94	5651.3	5513.3	5918.6
		Expt.	1.93	1.82	1.94	5651.3	5513.3	5918.6
		Δ	0.00%	0.00%	0.00%	0.00%	0.00%	0.00%
		a_i/n_i				0.03%	0.03%	0.03%

* The results for the BC and AC channels were found to be similar and were omitted for brevity.
** The same source was measured twice, first without a filter (upper row) and a second time with a 75% transparent gray filter (lower row).

TABLE 8.1: Comparison of the analytical (Correction method: Calc.) and the experimental (Correction method: Expt.) methods.

same list-mode files with measurements of the four LS-sources were analyzed with the LIST_MODE_ANALYSIS software. The selected dead-time base duration was 40 µs. The coincidence window width was chosen such as to include all true coincidences. Contrary to the usually used short coincidence resolving times, the values were found to be 100 ns for ^{14}C and 800 ns for ^{3}H and ^{55}Fe.

The resolving time that is needed to collect all true coincidences was determined by analyzing the corrected counting rates in each of the coincidence channels. From the example in Figure 8.4, in order to miss 0.1% of the D coincidences the necessary resolving time is 550 ns. To reach the same accuracy in the T channel it would be necessary to use 800 ns coincidence window. A major finding from the initial studies on the correction for accidental coincidences was the significant dependence of the counting rates on the coincidence window width. The full analysis of the time spread of events in commercial LS cocktails will be presented in the next chapter.

The experimental method was applied using the time distributions obtained from the same list-mode data that was used to calculate the counting rates for the esitmate with the analyical aproach. The random coincidences counting rates were calculated using equation (8.7) with the assumption for a uniform distribution in the interval from 2 µs to 2.5 µs. The time interval was chosen conservatively to ensure that the probability for true coincidences is negligible for all studied LS-sources. The obtained accidental coincidence counting rates a_i are shown in Table 8.1. The corrected counting rates were calculated by subtracting the estimate chance coincidence rate from the measured counting rates. The difference between the two methods Δ is calculated as:

$$\Delta = N_{calc}/N_{expt} - 1, \tag{8.11}$$

where N_{calc} is accidental coincidence counting rate from equation (8.10) and the same quantity from the experimental method N_{expt}.

The random coincidences estimates provided by the two methods agree within 3.30% for the measurements of the ^{55}Fe and ^{3}H sources with high activities. The differences seem to be larger when the measurements were performed with a filter, thus lowering the detection efficiency, compared to the measurements without a filter. The agreement between the methods is satisfactory for the 2.4 kBq ^{3}H source. In that case, the counting rate of the chance coincidences is low and is subject to relatively large statistical fluctuations. The agreement between the two methods is perfect for the ^{14}C source.

The two methods do not give identical results for the counting rate of the accidental coincidences. Nevertheless, the agreement between the corrected counting rates is very good. The relative deviations are below 0.13% in all performed measurements and below 0.02% if only the higher efficiency measurements without a filter are considered. It is important to note here that the increase in the accidental coincidences is not linear with the activity of the source. For the two ^{3}H sources that were studied, a 10 times increase in the activity results in 50 times increase in the triple and 20 times increase in the logical sum of doubles random coincidences counting rates.

If the 23 kBq ^{3}H source measurements are considered, the relative contribution of the accidental coincidences in the D channel increases from 0.82% to 1.73% when the detection efficiency is reduced. Similarly, for the ^{55}Fe measurements: without a filter the contribution of the accidental coincidences is 0.66% and with a filter it increases to 1.93%. It can be concluded that the contribution of random coincidences is significantly affected by the detection efficiency. This is understandable as the reduced efficiency would lead to more single events being detected at the expense of double and triple coincidences. Thus, the useful signal is decreased and the noise events are increased, which leads to a higher probability to register uncorrelated events in coincidence.

DEPENDENCE OF THE ANALYTICAL ESTIMATE ON THE COINCIDENCE WINDOW

In order to calculate the counting rate of random coincidences, the analytical equations use the measured counting rates. These, however, already include accidental coincidences. It presents interest to check, whether there is a significant effect on the cal-

culation based on the fraction of the total coincidences that are accidental. By increasing the coincidence resolving time to a higher value than the one needed to collect all true coincidences, the contribution of random coincidences to the measured counting rates will rise. Conversely, if a very short coincidence window is used, it will lead to a loss of true coincidences which could possibly influence the estimate of chance coincidences. As the experimental estimation does not depend on the used coincidence window, but only on the obtained time interval distributions, it can be used as a reference to compare the analytical approach.

A comparison of the two methods was performed by analyzing the data from the 23 kBq ^{3}H LS-source with various coincidence windows from 200 ns to 3 µs. The results from the experiment are presented in Table 8.2. Equations (8.8) and (8.10) to calculate counting rates of random (Method: Calc.) as well as true coincidences. The latter is calculated by subtracting the contribution of chance coincidences from the measured counting rates. The experimental approach was applied to the D and T time distributions. Equation (8.7) was used to evaluate the accidental coincidences (Method: Expt.), assuming uniform distribution in the interval between 2 µs and 2.5 µs. The difference between the two methods is calculated using equation (8.11). While there are some minor differences in the estimated counting rates of random coincidences, no significant difference in the true counting rates can be seen. In the latter case the two methods agree within 0.1% for all studied coincidence windows. The comparison shows that the analytical approach at the estimation of accidental coincidences does not depend significantly on the choice of resolving time and can be used freely even in cases where a fraction of the true coincidences is lost.

MONTE CARLO SIMULATION The validations performed on the methods thus far suffer from a significant drawback and that is the lack of knowledge of the true counting rates. This can be circumvented, however, by using artificially generated data using the Monte Carlo code for generation of realistic time sequence of PMT detection events, which is briefly presented in [103]. The same code was also used for validation of the comparison between common and individual dead-time counting logics used in TDCR (see Chapter 4). A brief recap of the function of the code follows: the activity of the source whose measurement would be simulated and the single and coincidence counting rates are used as an input. The time to next decay is sampled from exponential distribution with a decay constant calculated from the input activity. The time between PMT detection events in a given decay is sampled from an approximation of a real time interval distribution. The code outputs list-mode data with timestamps and PMT number, similar to a measurement with a digitizer. The generated files were analyzed with the same software used for the experimental measurements, thus eliminating possible differences from the analysis technique. The defining feature of the Monte Carlo approach is that it can output the simulated counting rates in the single and coincidence channels. This gives a concrete reference to which the two methods can be compared.

Resolv. time, ns	Corr. method	D acc., s^{-1}	D true, s^{-1}	T acc., s^{-1}	T true, s^{-1}
200	Calc.	21.3	10056.5	21.3	3994.2
	Expt.	20.9	10056.8	21.6	3993.9
	Δ	1.69%	0.00%	-1.38%	0.01%
800	Calc.	83.5	10145.2	85.8	4055.9
	Expt.	83.6	10145.1	86.3	4055.4
	Δ	-0.12%	0.00%	-0.60%	0.01%
1000	Calc.	104.1	10148.5	107.4	4057.8
	Expt.	104.5	10148.1	107.9	4057.3
	Δ	-0.41%	0.00%	-0.49%	0.01%
2000	Calc.	205.4	10155.0	215.8	4059.3
	Expt.	209.0	10151.5	215.8	4059.2
	Δ	-1.71%	0.04%	0.00%	0.00%
3000	Calc.	304.2	10158.2	325.0	4055.8
	Expt.	313.5	10149.0	323.8	4057.1
	Δ	-2.94%	0.09%	0.39%	-0.03%

TABLE 8.2: Comparison between the analytically calculated (Calc.) and experimentally (Expt.) obtained D and T accidental and true coincidence counting rates at different resolving times.

List-mode files for a ^{3}H sample with activities from 2 kBq to 200 kBq were generated with the code. Contrary to a real measurement, the output does not contain noise or PMT after-pulses. Thus, the chosen dead-time base duration for the analysis was 10 µs. The coincidence resolving time was set to 800 ns. The same window was used for the real ^{3}H measurements. The measured counting rates (Correction method: None) were compared to the reference given by the Monte Carlo code (see Table 8.3). It should be emphasized here, that, by using artificial data, it is possible to know the *exact* true coincidences counting rate. A significant discrepancy can be observed between the measured and reference counting rates, a discrepancy which increases with the simulated activity. For example, the discrepancy in the T channel is 0.14% for the 2 kBq simulation and increases up to 15.28% for the 200 kBq simulation.

Equations (8.8) and (8.10) were used in order to estimate the contribution of random coincidences according to the analytical method. The contribution of the accidental coincidences was subtracted from the measured counting rates giving the counting rates of true coincidences. These were then compared to the reference (Correction method: Calc.). For simulations up to 60 kBq, the discrepancy between the corrected and reference counting rates is less than 0.12%. For 100 kBq and 200 kBq there is an increase in the discrepancy. It could be attributed to the large contribution of the accidental coincidences to the measured counting rates, which are used to calculate the correction. Another possibility is the low number of recorded events, due to the huge global dead-time close to 100%. Nevertheless, even for activities as high as 100 kBq, the

TABLE 8.3: Comparison of the uncorrected and corrected by the two methods (Calc. and Expt.) counting rates with the Monte Carlo generated reference counting rates.

Activity	Correction method	Difference from Monte Carlo reference, %		
		AB*	D	T
2 kBq	None	0.11	0.06	0.14
	Calc.	−0.01	−0.02	−0.02
	Expt.	−0.01	−0.02	−0.02
10 kBq	None	0.59	0.42	0.76
	Calc.	−0.03	0.00	−0.05
	Expt.	−0.01	0.01	−0.04
20 kBq	None	1.23	0.85	1.59
	Calc.	−0.01	0.01	−0.03
	Expt.	−0.02	0.03	−0.06
40 kBq	None	2.43	1.64	3.13
	Calc.	−0.07	−0.01	−0.12
	Expt.	0.01	0.04	−0.02
60 kBq	None	3.69	2.50	4.78
	Calc.	−0.04	0.02	−0.10
	Expt.	−0.03	−0.01	−0.06
100 kBq	None	6.07	4.11	7.90
	Calc.	−0.12	0.08	−0.29
	Expt.	0.10	0.16	0.13
200 kBq	None	11.71	7.91	15.28
	Calc.	−0.61	0.20	−1.31
	Expt.	0.08	0.21	−0.18

* The results for the BC and AC channels were similar and were omitted for brevity.

corrected counting rates are within 0.29% from those simulated by the Monte Carlo code.

The same artificially generated list-mode data was used to obtain the time distributions in the coincidence channels. Up to 40 kBq the assumption for uniform distribution of accidental coincidences in the interval between 1500 ns and 2000 ns was deemed valid. For the larger activities, above 60 kBq and up to 200 kBq, the assumption does not hold due to the very high counting rates. Therefore, the accidental coincidence counting rates were obtained by fitting the linear equation (8.5) to the time interval distribution in the same time interval. The corrected for coincidence counting rates were compared to the Monte Carlo reference (Correction method: Expt. in Table 8.3). For activities up to 60 kBq, the results from the experimental method are within 0.06% of the reference. For larger activities (100 kBq and 200 kBq) the discrepancy is higher, but still within 0.21%.

CONCLUSIONS

In this chapter, an experimental method to evaluate the counting rate of accidental coincidences in TDCR measurements was proposed. The method was used to derive and validate analytical expressions that can be used to directly calculate corrections for random coincidences with data from standard TDCR systems. The work was published in the journal *Nuclear Instruments and Methods, Section A* [103].

The analysis of the list-mode data shows that the analytical and experimental evaluations provide comparable results for ^{3}H, ^{55}Fe and ^{14}C measurements. The contribution of random coincidences increases with reduction of the counting efficiency. The counting rate of true coincidences does not seem to depend significantly on the choice of coincidence resolving time for the studied 23 kBq ^{3}H LS-source if the analytical approach is used.

Both methods were used to evaluate corrections for accidental coincidences for Monte Carlo generated ^{3}H measurements with activities from 2 kBq to 200 kBq. The correction according to the analytical method is consistent with the Monte Carlo reference to within 0.29% up to 100 kBq. The experimental method deviates less than 0.06% from the reference counting rates up to 60 kBq and less than 0.21% up to 200 kBq.

A note should be made here, that the corrections for accidental coincidences should be applied not only to the measurements of the radioactive source, but also to the measurements of the blank sample that is used for background correction. Due to the usually low counting rates in the coincidence channels of the blank sample, the single counting rates are relatively high. For example, a typical blank measurement with a TDCR detector at Sofia University has 12 cps in the double coincidences channels and around 400 cps in the single channels. Therefore, the contribution of the accidental coincidences to the double counting rates is significant.

The analytical equations can be used to evaluate the rate of accidental coincidences in measurements performed with most existing TDCR acquisition systems, the only requirement being that they output the single, double and triple coincidence counting rates. The correction for random coincidences provides the opportunity to study long coincidence windows. The corrected time distributions indicate that the use of short resolving times leads to a loss of coincidences in low-energy radionuclides. The accidental coincidences corrections will improve the non-linearity of TDCR systems used for studies of short half-life medical nuclides line ^{11}C, ^{15}O or ^{18}F. They will allow TDCR measurements of sources with high activities, where the contribution of accidental coincidence cannot be neglected.

9

THE DELAYED FLUORESCENCE AND THE TDCR METHOD

The maximum difference in the time of arrival of two events that are considered in coincidence is the coincidence resolving time or the coincidence window. It is set in accordance with the used scintillator and, usually, the goal is to catch most of the true coincidences, while avoiding unnecessary increase of accidental coincidences. While the loss of a fraction of true coincidences may not be so critical for a two PMT detector, it could skew the results from a three PMT system such as a TDCR counter. The reason behind this difficulty is that the TDCR method uses the ratios of the triple to double coincidences to calculate the detection efficiency [2]. If the used coincidence window is too short, a fraction of coincidences could be missed. This fraction may well be different for the doubles and triples, leading to a bias in the efficiency and, therefore, activity calculated by the method.

The commonly used coincidence resolving time in TDCR counting is the one set in the MAC_3 acquisition module [100] – 40 ns. As seen in the previous chapter, this may be insufficient to gather all true coincidences for low-energy nuclides such as ^{3}H and ^{55}Fe. In addition, a study of the time dependence of scintillation light of a commonly used solvent/fluor combination diisopropylnaphtalene (DIN) and 2,5-diphenyloxyzole (POP) reports scintillation events up to 1.5 µs [17]. Such findings raise the question: *Is it not necessary to increase the used coincidence resolving time?*

As already mentioned in Chapter 1, there are predominantly two types of luminescence which can occur in organic molecules: prompt and delayed fluorescence. The prompt component is the result of transitions from singlet S_1 to S_0 states of the solvent. Its intensity decays exponentially with time and its lifetime is in the order of a few nanoseconds [7]. The delayed component emissions are more spread in time and can occur up to a few µs after the excitation of the solvent. Its origin are triplet-triplet interactions resulting in S_1 excitations, e. g., $T_1 + T_1 \rightarrow S_1 + S_0$ [7].

Reports on the influence of the coincidence window on the activity determined by the TDCR method can already be found in the literature, however, the studies usually encompass a few hundred nanoseconds. No corrections for accidental coincidences were performed previously as well. In one study of ^{3}H in Insta-Gel [137] the studied coincidence windows are at maximum 200 ns and in another study of ^{3}H in HionicFluor and UltimaGold cocktails [138], coincidence resolving times up to 400 ns were analyzed. Such resolving times should be sufficient to collect all events due to prompt fluorescence. Delayed fluorescence events, however, could be missed, and they may have a non-negligible contribution to the overall light emission [7].

An increase in the number of in-house made TDCR acquisition systems can be seen due to the recent advancements in the field of digital electronics. They all have the possibility

to use arbitrarily long resolving times [101, 102, 104, 134, 135]. Moreover, the constraint on the coincidence window due to possible contribution from increased accidental coincidences is removed with the presented correction methods (see Chapter 8 or [139]).

These circumstances give the opportunity to expand the maximum coincidence window to be long enough to register all scintillation light, including delayed fluorescence. Care must be taken, however, because, as previously stated, delayed fluorescence could have different ionization quenching properties than prompt fluorescence. The latter is the only type of fluorescence considered in Birks' ionization quenching formula [7]. In addition, the TDCR model has been shown to be very sensitive to the parameters used to describe the ionization quenching for low-energy β emitters like ^{3}H [80].

The objective of the work presented in this chapter is to stress the dependence of the measured counting rate and calculated activity on the used coincidence resolving time. The emphasis is on the use of long enough coincidence windows that do not miss correlated scintillation events and the influence of delayed fluorescence in that case is also discussed. The main novelty lies in the fact that the results are corrected for accidental coincidences, which cannot be neglected when using long resolving times.

9.1 MEASUREMENT OF TIME DISTRIBUTIONS OF LS-SOURCES

EXPERIMENTAL SETUP AND SOURCES The understanding of the influence of the delayed fluorescence on TDCR measurements starts with the acquisition of time interval distributions. This was done using a miniature 3D-printed miniTDCR counter connected to a fast digitizer. The counter is equipped with three Hamamatsu R7200U-200 PMTs [91] connected to a CAEN DT5751 digitizer [109] with 1 GS/s sampling rate. The system records all incoming events in list-mode file for off-line analysis with the LIST_MODE_ANALYSIS software (see Chapter 3 for details). In one experiment, the French primary TDCR counter (RCTD1) [140] was also used to verify results obtained with the miniTDCR. The RCTD1 is equipped with three Burle 8850 PMTs connected to a nanoTDCR device [101] after an amplifier and a discriminator.

TABLE 9.1: Composition of the studied sources.

Source name	Nuclide	Avg. TDCR	ε_D	Activity, Bq	LS cocktail	Vial type	m_{H_2O}/m_{tot}, g
H3-UG	^{3}H	0.399	0.43	23000	UG	PE	0.1/10
H3-LLT	^{3}H	0.435	0.47	3070	UG LLT	PE	0.1/10
H3-Tol	^{3}H	0.582	0.64	470	Tol. + PPO	G + DT	0.0/10
H3-UGQ (1–7)	^{3}H	0.4–0.2	0.44–0.18	2600	UG	PE	0.1/10
Fe55-UG	^{55}Fe	0.280	0.48	13300	UG	PE	0.1/10
Fe55-HF	^{55}Fe	0.185	0.31	13700	HF	PE	0.1/10
Ni63-UG	^{63}Ni	0.760	0.75	1100	UG	G + DT	0.1/10
C14-UG	^{14}C	0.931	0.94	6300	UG	G + DT	0.1/10

The studies of the time distributions were performed on seven LS-sources whose composition is presented in Table 9.1. The vial type PE refers to Polyethylene vials and G

+ DT to glass vials with a layer of diffusive tape. The last column shows the approximate mass of the aqueous solution (m_{H_2O}) and the total mass of the scintillation cocktail (m_{tot}) The ^{3}H and ^{63}Ni sources were measured with a set of home-made optical gray filters in order to perform the efficiency variation method (see Section 2.2) to select the optimal kB parameter. The H_3-UGQ sources are a set of seven 10 ml UltimaGold LS-sources. The sources were quenched with an increasing weight of nitromethane, from 0 mg to 70 mg.

The net time distribution of all channels for each measurement was obtained after analysis of the list-mode data. The net time distribution refers to the time distributions corrected for the contribution of accidental coincidences. The correction was made automatically by the LIST_MODE_ANALYSIS software after fitting the distribution in the interval [2.5 µs, 3 µs] with a linear function. More information on the analysis of list-mode data is given in Chapter 3.

The Monte Carlo code presented in Appendix A was used to gain a better understanding of the influence of the delayed component on the measured activity. The performance of the code can be illustrated by fitting one of the experimental time distributions. The D channel of the H_3-UG source was chosen for this purpose. The adjustment of the parameters was done by the Nelder-Mead method [141]. The optimized values for the parameters are shown in Table 9.2.

Parameter	Value
λ_p	0.57 ph.e$^-$/keV
λ_d	0.08 ph.e$^-$/keV
τ_p	0.28 s^{-1}
τ_d	0.09 s^{-1}
σ	1.25 ns
kB	100 µm/MeV

TABLE 9.2: Optimal parameters obtained from the Monte Carlo code for the H_3-UG source. The free parameters λ_d and λ_p are given in number of photoelectrons per keV effective energy released in the cocktail (ph.e$^-$/keV).

As a reference, the FOM obtained with the TDCR method for the same measurement is λ = 0.68 ph.e$^-$/keV. The ratio between the delayed and total (prompt + delayed) fluorescence is 0.12. A similar ratio 0.14 was reported for DIN + PPO (1.5 g/l) cocktail in the work of Lombardi et al. [17]. The experimental and simulated time interval distributions are shown in Figure 9.1. It should be noted here, that the equation that is used for the time dependence of the delayed fluorescence is only approximate. Nevertheless, a good agreement between the experiment and simulation is observed.

9.2 RESULTS

The analysis of the data is structured in the following way: first, the coincidence counting rates as a function of the used coincidence resolving time are obtained. They

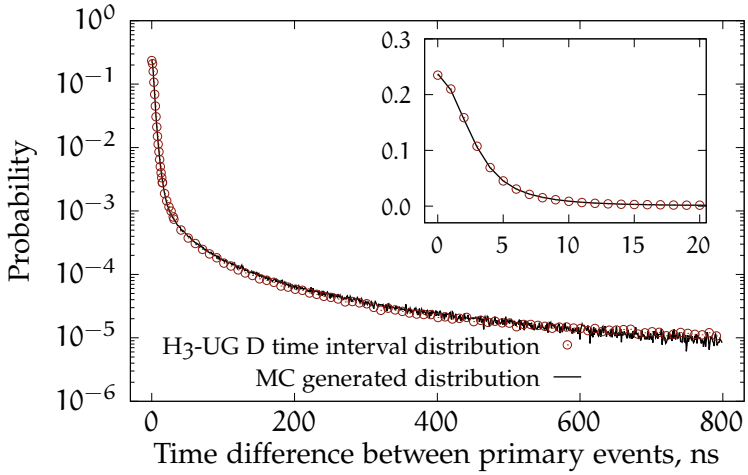

FIGURE 9.1: An example of the D time distribution of the H3-UG source and the Monte Carlo generated distribution. The insert shows the same distributions in linear scale from 0 to 20 ns.

give information on what is the necessary coincidence window that needs to be used in order to gather the bulk of true coincidences. All counting rates are corrected for accidental coincidences. This procedure is done for each nuclide and cocktail. The data was then used to calculate the activity of the samples according to the TDCR method for counting rates at various coincidence windows. This allows the study of the influence of the loss of true coincidences or the inclusion of delayed fluorescence events on the calculated activity. The results were interpreted with the aid of Monte Carlo simulations of TDCR measurements with the ability to separate prompt and delayed fluorescence events. Finally, a comprehensive discussion on the results is given.

DEPENDENCE OF THE COUNTING RATE ON THE RESOLVING TIME As the activities of the sources are more or less arbitrary, it is useful to scale all counting rates to the rate at a particular coincidence window. Here it is assumed that above 1.5 µs the contribution of true coincidences should be insignificant. As a conservative approach, all counting rates were scaled to the counting rate at 2 µs and are presented as relative counting rates. This coincidence window should be long enough to include all true coincidences and thus, a comparison with that counting rate would give the fraction of missed coincidences. The relative counting rate R is calculated as:

$$R = \frac{n_i^{true}(\tau)}{n_i^{true}(2\ \mu s)} - 100\% \tag{9.1}$$

The relative counting rates in the D channels for the tritium sources are shown in Figure 9.2. Figure 9.3 shows the same relationship, but for the D and T channels of the ^{55}Fe LS-sources. From the results it is clearly visible, that the commonly used 40 ns coincidence resolving time would be insufficient for UltimaGold, UltimaGold LLT and Toluene+PPO cocktails if measurements of ^{3}H or ^{55}Fe are performed. In these cases the time that is needed to acquire 99.9% of true coincidences is close to 1 µs. The loss of true coincidences is the largest for ^{55}Fe in UltimaGold where 25% of T coincidences are

missed at 40 ns coincidence window. A few important takeaways must be extracted from these results:

- The loss of triple coincidences is larger than the loss of double coincidences.
- UltimaGold LLT has the most significant contribution of delayed events
- The ^{55}Fe and ^{3}H results with the same cocktail (UltimaGold) show that the counting rate as a function of the coincidence window depends on the nuclide and the energy spectrum.
- HionicFluor is the fastest tested cocktail, and it has the lowest contribution of delayed events.
- If measurements of ^{3}H and ^{55}Fe are performed, the necessary resolving time to gather 99.9% of true coincidences is close to 1 µs.

The first point is particularly important as it suggests that the T/D ratio also depends on the used coincidence window. Thus, the loss of coincidences will not only decrease the counting rate, but it may also skew the results from the application of the TDCR method. As presented in Section 2.2, to calculate the detection efficiency, the TDCR method relies on the triple to double coincidence ratios.

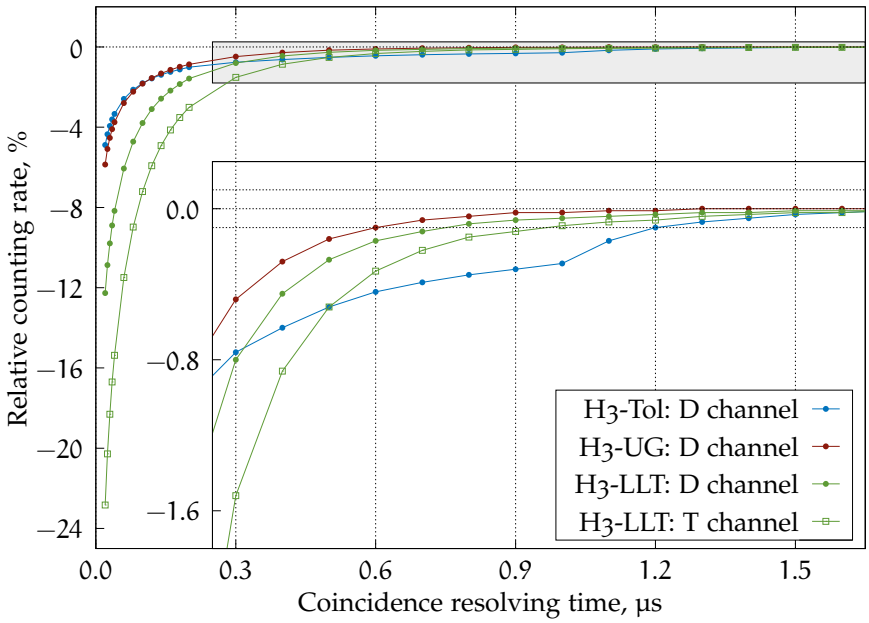

FIGURE 9.2: Relative counting rate, compared to the counting rate at 2000 ns coincidence resolving time. The grey box shows the region that is enlarged in the inlet graph.

For the higher energy nuclides ^{63}Ni and ^{14}C, the counting rate converges significantly faster to the value at 2 µs. The relative counting rate as a function of the coincidence window for these sources is presented in Figure 9.4. For ^{14}C, a coincidence window of 100 ns is necessary to include 99.9% of D and T events and for ^{63}Ni source the necessary

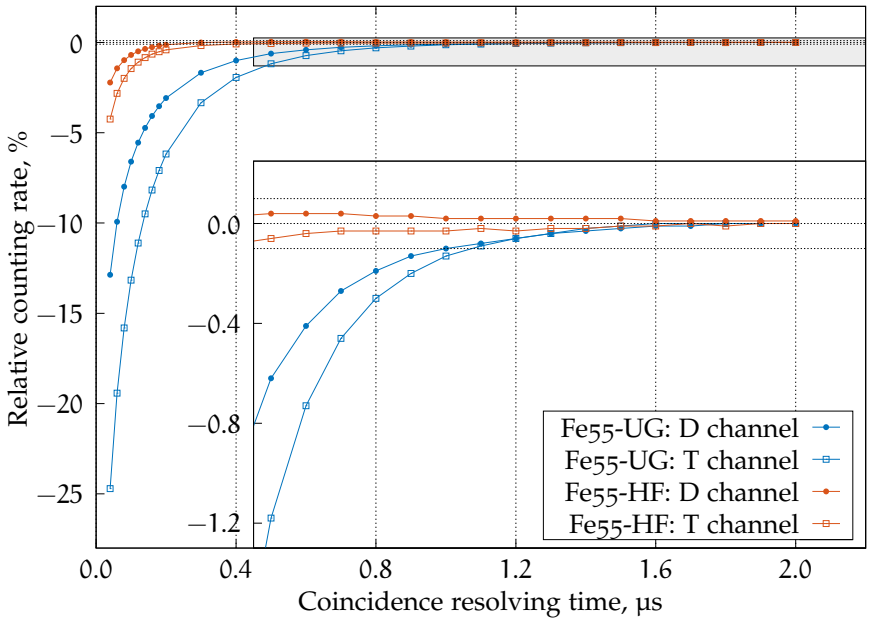

FIGURE 9.3: Relative counting rate in the D and T channels as a function of the coincidence resolving time for the Fe55-UG and Fe55-HF sources.

time is 600 ns. Despite the higher detection efficiency for these sources, there is still significant contribution of delayed fluorescence photons to the total counts.

Note that all measurements were performed without optical grey filters. Thus, the achieved detection efficiency is the maximum for this detector. If filters are used, e. g., for the efficiency variation method, the decreased efficiency will lead to a larger spread in the time distributions. Lowering the efficiency could also increase the contribution of delayed fluorescence.

The results in this section show that the commonly used short resolving times are insufficient to collect all true coincidences. However, increasing the coincidence window too much could be undesirable due to the larger contribution of delayed fluorescence. Moreover, it is possible that Birks' ionization quenching formula does not properly account for the delayed component. A solution could be found in selecting a coincidence window that includes all prompt fluorescence, but still the contribution of delayed fluorescence is negligible. The impediment is that it is not precisely known what is the level of overlap between the delayed and prompt fluorescence, especially considering that some singlet states could diffuse before interacting with a fluor molecule [7]. It is thus important to also study the calculated activity with respect to the coincidence window. It may give insight on the influence of the delayed fluorescence on TDCR measurements.

DEPENDENCE OF THE CALCULATED ACTIVITY ON THE COINCIDENCE RESOLVING TIME The LIST_MODE_ANALYSIS program was used to get the T/AB, T/BC and T/AC ratios at different coincidence windows, from 40 ns to 2 µs. The TDCR18 program,

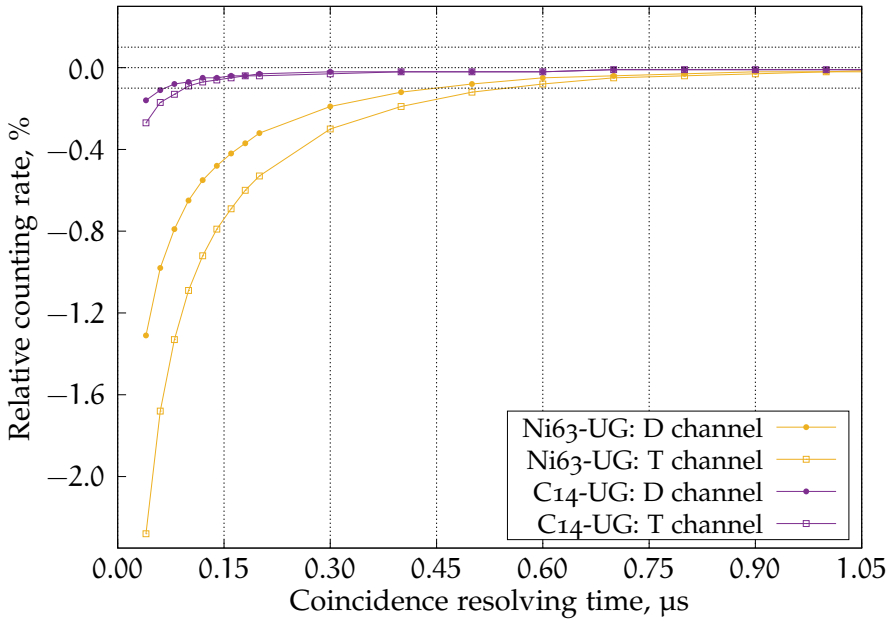

FIGURE 9.4: Relative counting rate of the D and T channels for the C14-UG and Ni63-UG sources. The dashed horizontal lines indicate relative counting rates −0.1%, 0.0% and 0.1% respectively.

developed by Ph. Cassette, was used to calculate the activity. It is an updated version of TDCR07 [93]. The updates include new data for more LS cocktails and also the option to calculate the stopping power using the dataset published by Tan and Xia [94]. The activity of the measured sources with respect to the coincidence window is shown in Figure 9.5. The relative activity is calculated using (9.1).

The ^{3}H sources have a similar behaviour at short coincidence windows as the calculated activity decreases with decrease of the resolving time down to 30 ns. A sharp increase in the calculated activity is seen for shorter coincidence resolving times. The high overestimation for very short coincidence resolving times can be explained by the higher loss of triple coincidences than double coincidences leading to a lower TDCR and an underestimation in the efficiency. From the results in the previous section it was shown that Toluene+PPO and UltimaGold have a significantly less pronounced delayed scintillation component compared to UltimaGold LLT. Intuition suggests that the dependence of the calculated activity on the coincidence resolving time would be lower for cocktails exhibiting low amount of delayed fluorescence. The experiments contradict this — the calculated activity of the H3-LLT source is less dependent on the coincidence window than that for the H3-Tol and H3-UG sources. A possible explanation for this behaviour is given in the next subsection.

Similar relationships to the ^{3}H sources were observed for the other two pure-β nuclides: ^{14}C and ^{63}Ni. The bias in the calculated activity of the C14-UG source is less than 0.1% for all coincidence windows. The behaviour of the Ni63-UG source is very similar to the ^{3}H source in the same cocktail, however, the dependence on the coincidence window is less pronounced.

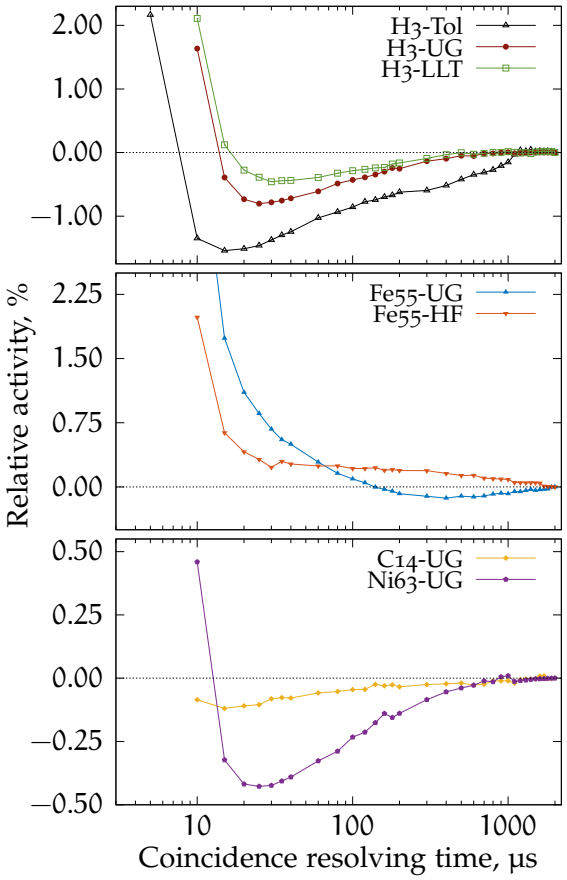

FIGURE 9.5: Activity relative to the activity calculated at 2000 ns coincidence resolving time as a function of the coincidence resolving time. Note that, the activity at 2000 ns coincidence resolving time is taken only as a reference and should not be considered as the true activity of the source.

The electron-capture ^{55}Fe behaves differently with change in the coincidence resolving time. For the Fe55-HF source the difference from the reference activity is positive at all coincidence windows. For Fe55-UG the function has a minimum at around 400 ns. The increase for longer coincidence resolving times is significantly lower in comparison to the ^{3}H sources and could be due to statistical uncertainties.

STUDIES OF THE ACTIVITY AS A FUNCTION OF THE COINCIDENCE RESOLVING TIME USING THE MONTE CARLO CODE The question raised in the previous experiments is what is the possible influence of the delayed fluorescence on the activity calculated with the TDCR method. Here, an advantage of the developed Monte Carlo code compared to real measurements is that the method can be applied to data from a source with precisely known activity. It also gives the possibility to have two separate scintillation components: prompt fluorescence – described by the Birks equation, and delayed fluorescence – presumably not subject to ionization quenching.

An initial step that is needed for the Monte Carlo code is to provide the parameters of the measurement, the cocktail that is simulated, the radionuclide spectrum and the activity. The initial parameters were set to the optimal parameters determined for the H3-UG source (shown in Table 9.1). The standard deviation σ of the gaussian jitter was set to zero to facilitate the interpretation of the results. The code was used to generate

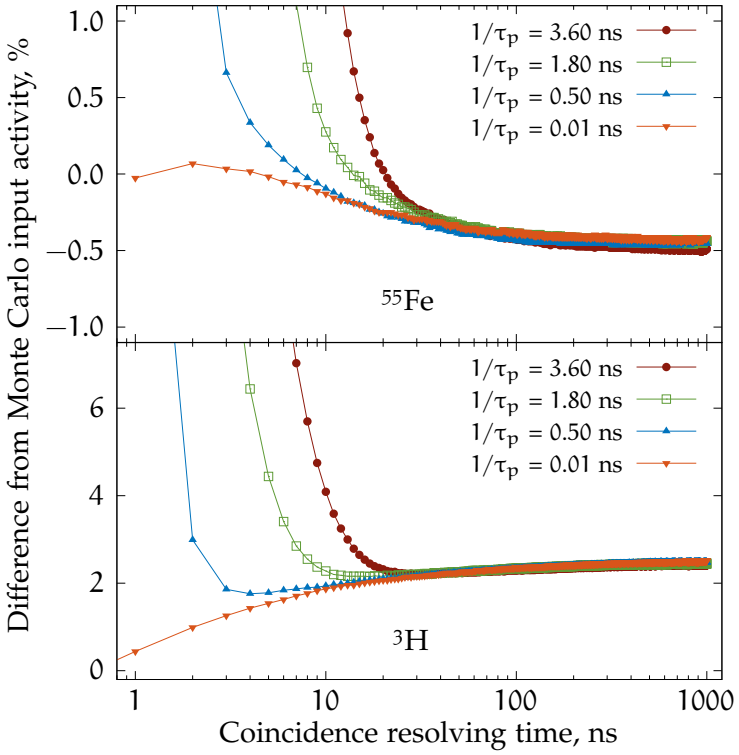

FIGURE 9.6: Dependence of the calculated activity on the coincidence resolving time for Monte Carlo simulated measurements of ^{3}H and ^{55}Fe for various prompt scintillation component decay times.

artificial data for ^{55}Fe and ^{3}H with different prompt scintillation component decay times, keeping all other parameters unchanged. In one of the runs, the decay time was set to 10 ps to separate the prompt from the delayed component, as the separation between prompt events would not be larger than 1 ns. Thus, if such a coincidence window is used, the effects of delayed fluorescence would be suppressed.

The results from the experiment are presented in Figure 9.6. Please note that in the simulation code the prompt and delayed fluorescence time distributions overlap, i. e., there is no coincidence resolving time that would include only prompt events and no delayed events. That is due to the approximate equation used to describe the delayed fluorescence decay time. Nevertheless, other studies [18, 142] report that an overlap between the two is to be expected. The effect of the overlap between the two is negligible for 1 ns coincidence window.

For ^{55}Fe the activity with respect to the coincidence resolving time shows a consistent downward trend which intersects the Monte Carlo input activity at a certain coincidence window. Considering 10 ps prompt decay time simulation, the correct activity can be reconstructed for very short coincidence resolving times due to the low overlap between the prompt and delayed components. However, increasing the coincidence resolving time leads to an underestimation of the activity. An effect most probably caused by the detection of more delayed fluorescence events. For too short resolving times there is a larger loss of T coincidences than D coincidences, leading to a lower TDCR value and

lower estimate of the detection efficiency. This effect is seen as an overestimation of the activity.

The same phenomenon was observed in the ^{3}H simulations. Too short coincidence window and a loss of prompt events leads to significant overestimation of the (T losses are higher than D losses). The difference from ^{55}Fe is that the inclusion of delayed events leads to the overestimation of the calculated activity. Note here, that the difference between prompt and delayed events in the simulation is the lack of ionization quenching for the latter. The only case where the calculated ^{3}H activity does reach the Monte Carlo reference value is for the 10 ps decay time measurement at 1 ns coincidence window. For all other prompt decay times the calculated activity is overestimated by two or more percent.

The calculated activity curves obtained from the simulations closely resemble the results from the measurements with the digitizer (shown in Figure 9.5). After a discussion between the co-authors of [139], the following effects that lead to a bias in the calculated activity were stipulated:

- unequal losses of double and triple coincidences for too short resolving times
- influence of the delayed scintillation component, which has different ionization quenching properties
- difference in the free parameter (mean number of photoelectrons per keV absorbed in the scintillator) for the prompt and the delayed scintillation

The first effect leads to activity overestimation in all cases, because short coincidence windows lead to the loss of more triple than double coincidences. This in turn leads to a decrease of the TDCR value and underestimation of the detection efficiency. The second and third effects lead to activity underestimation in monoenergetic sources and to overestimation in ^{3}H.

The reason for the last bias effect is that the TDCR model considers only one free parameter value. As the emission mechanism is different for the prompt and the delayed fluorescence, however, it seems reasonable to think that the intrinsic light yields of those two processes could be different. In the case of ^{55}Fe the K-shell rearrangement is the predominantly detected process. The emission is quasi-monoenergetic and thus the correctness of the used ionization quenching function is less important. Then, the observed dependence of the calculated activity on the coincidence window is not explained by a different quenching behaviour of prompt and delayed emission. The more probable reason is a difference in the intrinsic light yield of each scintillation component.

From the Monte Carlo results it seems that for a monoenergetic source there is a certain coincidence window that would result in the correct activity calculation. Its width will depend on the prompt and delayed fluorescence decay times and the relative contribution of the two. The ^{3}H results indicate that all bias effects lead to an overestimation and no coincidence window will lead to the correct activity calculation.

Moreover, the difference between the minimum activity and the activity at very long coincidence resolving times would appear lower the shorter the decay time of the prompt fluorescence is. The same phenomenon was observed in the real measurements of Toluene+PPO and UltimaGold LLT cocktails (see Figure 9.5). Toluene+PPO has a faster prompt fluorescence than LLT, thus all the prompt fluorescence light is gathered at shorter coincidence windows, lowering the contribution of delayed fluorescence.

9.2.1 *Delayed fluorescence and the ionization quenching model*

As discussed previously, the TDCR model relies on the proper description of the light output of the scintillator with respect to the deposited energy. This is predominantly done using Birks' ionization quenching formula (1.12) [23, 27]. Thus, the TDCR model has one external parameter, the kB, which should be specific to the used cocktail. The equation of Birks was, however, proposed for the description of prompt fluorescence only and it may not account correctly for the presence of delayed fluorescence. The contribution of the delayed component to the total detected scintillation light depends on the width of the used coincidence window. Thus, it is to be expected that the perceived light output of the scintillator would be different for long and short resolving times – the former including more delayed fluorescence light than the latter. This could introduce a dependence of the value of the kB parameter that best describes the scintillator light output on the used coincidence window.

The main way to determine the optimal kB parameter in TDCR measurements is by the efficiency variation technique, which was described in Section 2.2. For the implementation of the technique, a source or a set of sources with the same specific activity are measured, where all measurements are done at a different detection efficiency. A commonly used way to vary the efficiency is with the use of grey filters. The optimal kB parameter is the parameter that results in the same calculated activity at different detection efficiencies.

OPTIMAL kB PARAMETER AND THE COINCIDENCE WINDOW The efficiency variation technique was performed on three of the sources, H_3-UG, H_3-LLT and Ni_{63}-UG, using optical grey filters. The objective of this study was to determine if there is a dependence on the obtained optimal kB parameter on the coincidence window used to make the measurements. Each measurement of a source and filter was corrected for background with the corresponding measurement of a blank sample. The off-line data for these measurements was analyzed with the LIST_MODE_ANALYSIS program in order to get the counting rates as a function of the coincidence window. All measurements, including blank measurements were corrected for accidental coincidences.

The activity of the samples are calculated for coincidence windows $20, 40, 60, 80, 200$ and 1000 ns. The kB values that are used for calculation are from 70 µm/MeV to 160 µm/MeV with a 5 µm/MeV step. The kB value that is considered optimal is the kB

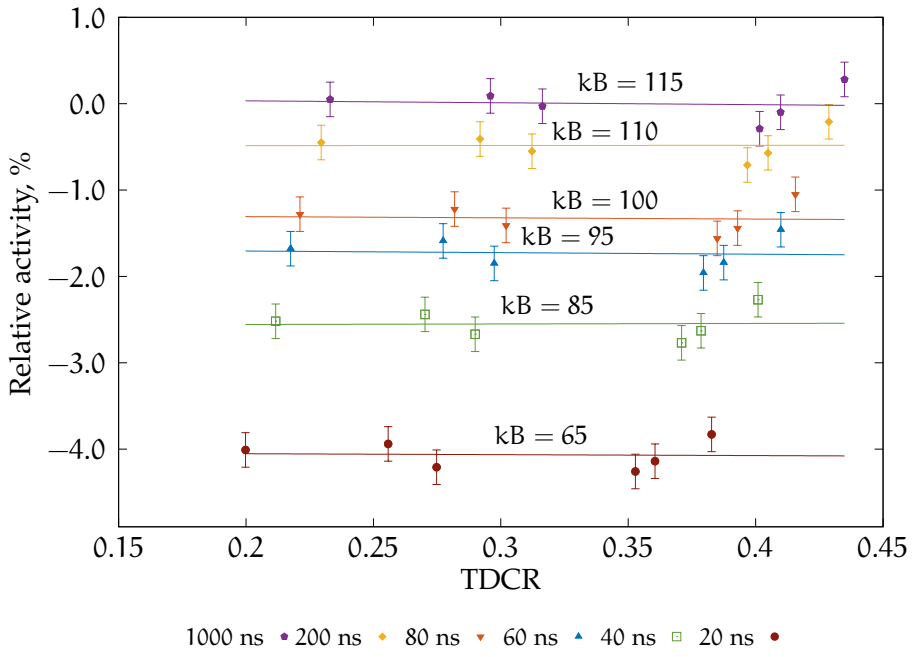

FIGURE 9.7: Relative activity of the H_3-LLT as a function of the TDCR value at the optimal kB value for different coincidence resolving times. The kB value is given in units µm/MeV.

for which the slope of the linear fit of the activity as a function of the TDCR is closest to zero.

For two of the sources, H_3-UG and Ni_{63}-UG, the optimal kB parameter does not seem to depend significantly on the coincidence window. It was found out to be 100 µm/MeV for all studied coincidence resolving times. For the H_3-LLT source, however, such a dependence was observed. The calculated activity, relative to the average of the values for 1000 ns coincidence resolving time, as a function of the TDCR value for the studied coincidence resolving times is shown in Figure 9.7. The kB parameter that results in the smallest slope for 40 ns coincidence window is at 85 µm/MeV and for 1000 ns it is 115 µm/MeV.

Another source (H_3-LLT2) from the same LLT cocktail and tritiated water solution was prepared and measured on the RCTD1 [140] detector at LNHB. The PMTs of the counter were directly connected to the nanoTDCR [101], a device dedicated to TDCR measurements. The nanoTDCR is capable of simultaneous measurements with two different coincidence windows which makes it a particularly suitable device to test the effect of the used coincidence window time on the kB parameter. The H_3-LLT2 source and its blank sample were measured with a series of optical grey filters. All measurements were performed simultaneously with coincidence windows 40 ns and 200 ns and 10 µs dead-time base duration. The results of the experiment are shown in Figure 9.8. The measurements of the H_3-LLT2 source confirm the observed behaviour of the H_3-LLT source. The kB value that results in the smallest slope (fit shown with solid line) for 40 ns coincidence resolving time is 90 µm/MeV and for 200 ns it is 120 µm/MeV. The wider coincidence

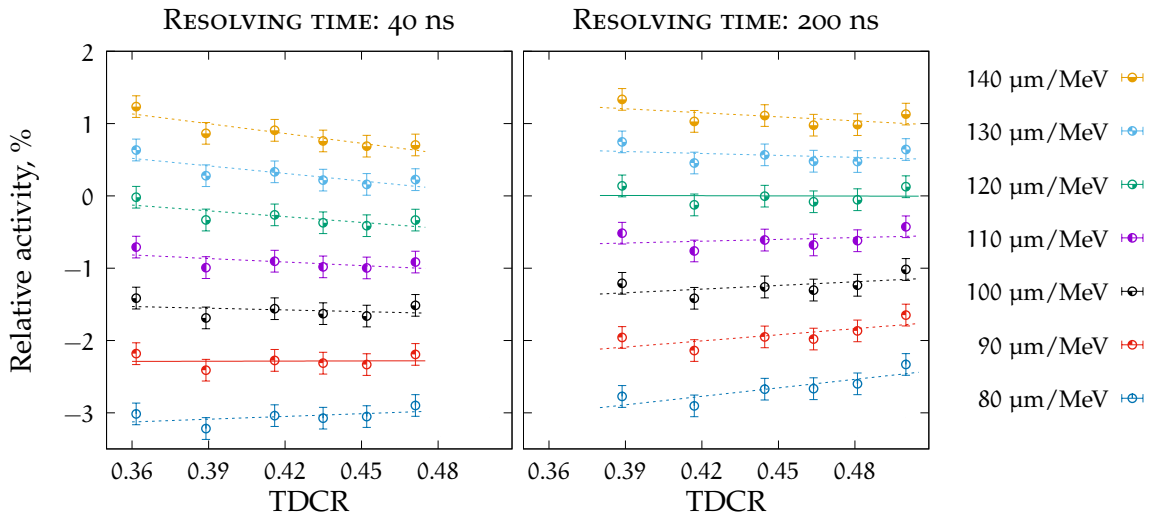

FIGURE 9.8: Relative activity of the H_3-LLT2 as a function of the TDCR value. The linear fit with the smallest slope is shown with a solid line. The values on the right are the kB parameter given in units µm/MeV. The measurements were carried out on the RCTD1 system and nanoTDCR device.

resolving time also leads to a significant increase in the detection efficiency for all measurements.

The results from the previous section imply that the delayed component in the LLT cocktail is more pronounced compared to UltimaGold. This could explain why increasing the coincidence window and including more delayed fluorescence photons leads to some dependence of the optimal kB parameter. It is possible that it compensates for some dependence of the calculated activity on the amount of detected delayed fluorescence photons that are not included in the model.

Note here the large difference between the kB parameters obtained for H_3-LLT at 20 ns and 40 ns coincidence resolving time (see Figure 9.7). That is the range that should include a resolving time which is long enough not to miss prompt fluorescence events, but short enough to minimize the contribution of delayed fluorescence. The strong dependence of the optimal kB value and calculated activity in this range would prevent the selection of such a coincidence resolving time. These results suggest that UltimaGold LLT is unsuitable for standardization of ^{3}H LS-samples with the TDCR method using the Birks formula, due to its large delayed fluorescence contribution.

COMPARISON OF EFFICIENCY VARIATION WITH GRAY FILTERS AND CHEMICAL QUENCHING Besides the use of grey filters, another common way to vary the detection efficiency in TDCR is to use chemical quenching. The idea is to create a set of sources with the same specific activities, but with increasing concentrations of a quenching agent such as nitromethane. In the context of delayed fluorescence, the two methods may not be identical. The grey filter absorbs light emitted from the vial and thus affects both prompt and delayed fluorescence in the same way. Note that both types of scintillation light are emitted from S_1 excited states and have the same emission

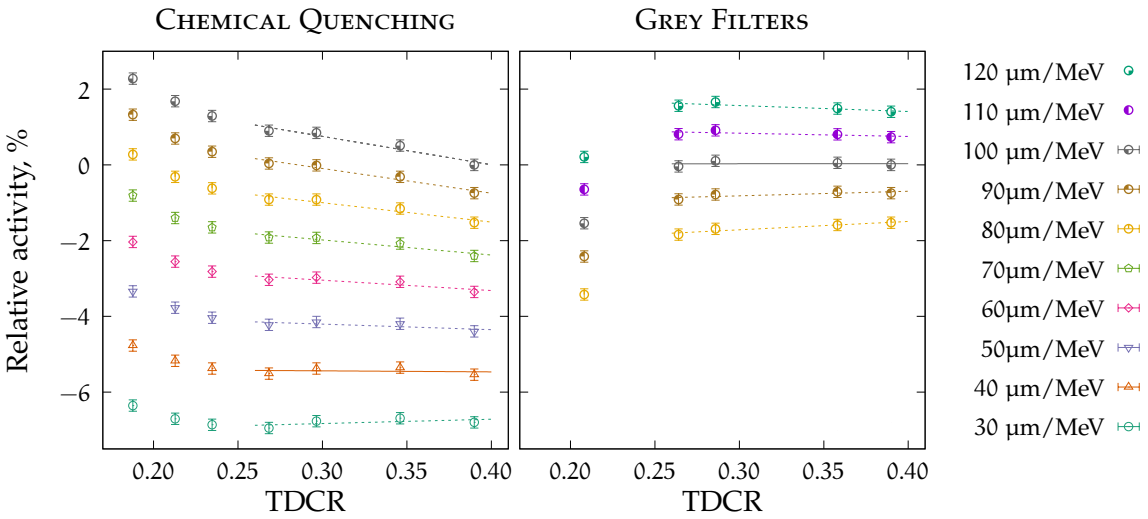

FIGURE 9.9: Relative activity of the H3-UG as a function of the TDCR value. The linear fit with the smallest slope is shown with a solid line. The values on the right are the kB parameter given in units µm/MeV. The two plots have the same scale and range on the abscissa. The measurements were performed using the miniTDCR system and the CAEN digitizer.

spectra. The chemical quenching is achieved by introducing chemical scavengers of excited solvent molecules, which leads to a decrease in the light emission yield [80]. The quenching agent could affect the two types of scintillation light differently, thus changing their relative contributions.

The influence of delayed fluorescence on the calculated activity with the two efficiency variation methods was performed using a set of seven ^{3}H in UltimaGold LS-sources with added nitromethane (H3-UGQ in Table 9.1). The unquenched source was also measured with a set of grey filters. All measurements were performed using the miniTDCR with the CAEN DT5751 digitizer and the LIST_MODE_ANALYSIS software. The coincidence resolving time was set to 40 ns.

The results of the experiment are shown in Figure 9.9. In the left and right plots, the highest efficiency data points are from the same measurements of the unquenched sample. The left plot shows the experiments with chemical quenching and the right with grey filters. The optimal kB value is 40 µm/MeV for the former and 100 µm/MeV for the latter. It is interesting to note here that for TDCR values lower than 0.25 there is an upward trend in the calculated activity when using chemical filters. This is contrary to the downward trend observed for grey filters in the same range of TDCR values.

One possible explanation for the different behaviour of chemical quenching and grey filters is that the added nitromethane does not quench delayed fluorescence in the same manner as prompt fluorescence. A comparison of the time interval distributions with grey filters and chemical quenching is shown in Figure 9.10. The solid black line is the D time interval distribution of the unquenched H3-UGQ1 source. The dashed lines are the distributions of the chemically quenched samples and the dash/dot lines are the distributions of the unquenched sample with gray filters.

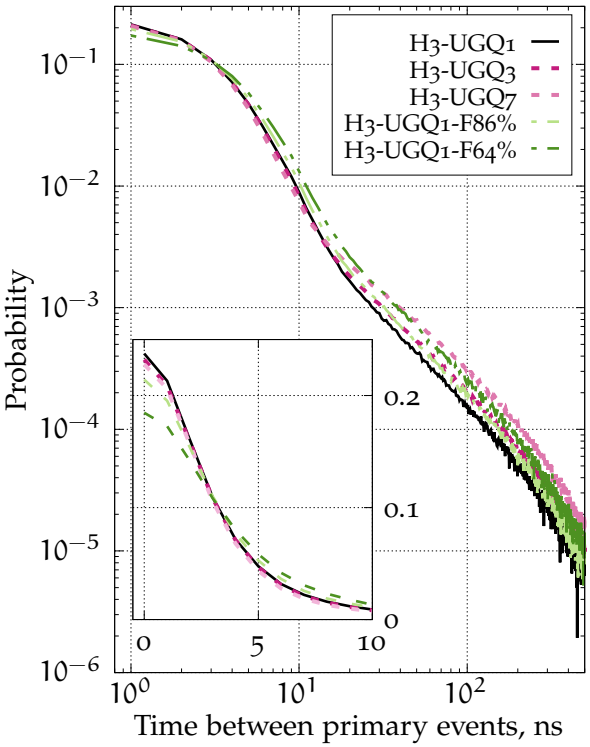

FIGURE 9.10: Time interval distributions in the D channel of the H3-UGQ set of sources. The H3-UGQ1 LS-source is unquenched, UGQ3 and UGQ7 are quenched with nitromethane and F86%and F64%are the unquenched source with gray filters.

The time interval distributions suggest that chemical quenching with nitromethane does not affect delayed fluorescence significantly. The probability for events with more than 20 ns time difference is higher compared to the unquenched sample. In the first 10 ns the distributions of all chemically quenched samples closely resemble the distribution of the unquenched sample. In the same time interval the distribution is changed significantly if filters are used. Note the insert in Figure 9.10 which has linear scale on the y axis.

When the total number of photons is reduced, the probability for the detection of a delayed fluorescence photon increases. As an illustration, if the average number of photons is high, then the primary events in each PMT would be prompt events as delayed events are slower on average. If the average number of prompt fluorescence photons is 1 or lower, then some delayed photons should be detected in order to have a double or triple coincidence. Another effect of the reduction of the mean number of photons is on the shape of the time distribution. When the number of detected photons is reduced, the average time interval between two photons increases. This leads to a decrease of the height of the distribution at $\Delta t = 0$ as well as an increase in probability in the tails. These effects are predicted by the theory presented in Chapter 5 and are also clearly seen for the grey filter measurements in Figure 9.10. The latter effect should be present also in the time interval distributions with chemical quenching. The fact that the distribution is not significantly changed in the first few nanoseconds suggests that nitromethane quenches prompt fluorescence predominantly.

From the theory of the scintillation process in organic materials there are two paths that lead to energy transfer between the solvent and fluor molecules: non-radiative

transfer to the fluor from an excited solvent molecule (Förster process) and diffusion controlled non-radiative transfer [7]. The non-radiative transfer between solvent and solute can be interrupted if the excited solvent molecule interacts with a molecule of the quencher before reaching the fluor. Thus, solvent molecules that are excited in the immediate vicinity of a fluor molecule would produce scintillation light promptly. If, however, solvent molecules need to undergo diffusion before interacting with a fluor molecule, then the probability for interaction with a quencher molecule increases with time. Such process could possibly explain the reduced probability for events between 5 and 15 ns with nitromethane compared to grey filters.

The selective quenching of the prompt fluorescence by nitromethane would lead to increased overestimation of activity for higher concentrations. This introduces a dependence of the calculated activity from the detection efficiency which is compensated by a lower kB parameter. Further studies are needed to quantify the magnitude of the possible underestimation of the kB value when applying the efficiency variation method with chemical quenching. Moreover, further studies on the prompt and delayed components are necessary as well in regard to TDCR measurements.

9.3 THE EFFECT OF DELAYED FLUORESCENCE ON TDCR MEASUREMENTS

The results described in this chapter show that there could be a significant dependence of the measured coincidence counting rates on the used coincidence resolving time. The necessary coincidence resolving times in order to detect 99.9% of coincidences for the studied LS-sources were found to be 700 ns for the ^{3}H in UltimaGold source, 1 µs for the ^{3}H in UltimaGold LLT source and 1.2 µs for the ^{3}H in Toluene+PPO source. Both studied ^{55}Fe sources also show a large time spread of the coincidences where for the ^{55}Fe in HionicFluor source the necessary coincidence resolving time is 300 ns and for the same nuclide in UltimaGold cocktail it is 1.1 µs. The observed losses at short coincidence resolving times for the studied ^{14}C and ^{63}Ni sources are lower than for the other nuclides. The necessary coincidence resolving time to achieve a bias in the coincidence counting rates lower than 0.1% is 100 ns for the ^{14}C in UltimaGold source and 600 ns for ^{63}Ni in UltimaGold source.

The TDCR model for the calculation of detection efficiency seems to compensate well for the large loss of coincidences at short coincidence resolving times, nevertheless, a significant dependence of the calculated activity on the coincidence resolving time was observed for ^{3}H, ^{55}Fe and ^{63}Ni. A large overestimation of the calculated activity can be observed for these nuclides at coincidence resolving times shorter than 20 ns. For the pure-β sources, the relationship has a minimum between 15 ns and 30 ns.

The Monte Carlo code (see Appendix A) was used to simulate TDCR measurements of ^{3}H and ^{55}Fe with assumptions of exponentially decaying prompt fluorescence and delayed fluorescence that does not experience ionization quenching. The calculated activity as a function of the coincidence window is very similar for simulated data and

true measurements. For short coincidence resolving times the activity is overestimated for both nuclides. This is explained with the larger loss of T coincidences compared to D coincidences which leads to a lower TDCR and underestimation of the detection efficiency. When delayed fluorescence is considered, there is a difference in the behaviour of the two nuclides. The calculated activity is underestimated in the case of ^{55}Fe and overestimated in the case of ^{3}H. This suggests that no coincidence resolving time exists that results in the correct ^{3}H activity calculation, as both bias effects (loss of T and D and delayed fluorescence) lead to an overestimation. For the simulated ^{55}Fe measurements a coincidence resolving time can be found for which the calculated activity is equal to the true activity. It is difficult to be found in practice as it depends on the prompt and delayed fluorescence decay time and their relative contribution.

The Monte Carlo studies indicate that, for ^{3}H and nuclides with a similar spectrum, the minimum calculated activity would be closest to the real one. Increasing the coincidence resolving time beyond that which results in the minimum calculated activity, would only introduce more delayed fluorescence photons and increase the overestimation of the activity. However, if the delayed fluorescence is not negligible in comparison with the prompt, then it is possible that even the minimum activity is still significantly overestimated. Thus, it would seem that the use of LS cocktails that exhibit lower delayed fluorescence contribution is preferable. In this regard, the TDCR method could benefit if the chemists produce LS cocktails with enhanced prompt and suppressed delayed scintillation components.

The efficiency variation method for obtaining the optimal kB parameter used in the TDCR model was applied to two of the ^{3}H sources and the ^{63}Ni source. No dependence of the optimal kB value on the used coincidence resolving time was observed for the ^{3}H in UltimaGold and the ^{63}Ni sources. A significant dependence was observed for the ^{3}H in UltimaGold LLT source; the kB value that leads to the smallest dependence on the calculated activity from the TDCR value is 85 µm/MeV for 40 ns coincidence resolving time and 115 µm/MeV for 1 µs coincidence resolving time. A similar source, ^{3}H in UltimaGold LLT, was measured on a different TDCR counter with the nanoTDCR device using its feature for simultaneous measurements with coincidence resolving times 40 ns and 200 ns. The optimal kB parameter for the shorter coincidence resolving time was found out to be 90 µm/MeV and for the longer one: 120 µm/MeV. These experiments imply that if the delayed fluorescence contribution is significant, as is the case for ^{3}H in UltimaGold LLT, then efficiency variation could be an unreliable method to determine the optimal kB parameter.

A set of ^{3}H in UltimaGold LS-sources chemically quenched with different amounts of nitromethane were measured to determine the optimal kB parameter. An unquenched source from the set was measured also with a set of gray filters in order to compare the kB parameters obtained by the two approaches. The kB parameter obtained from chemical quenching is 40 µm/MeV and from gray filters is 100 µm/MeV. A possible explanation for this discrepancy is that nitromethane quenches singlet states more so than triplet states, thus increasing the relative contribution of the delayed fluorescence

leading to a higher overestimation of activity. This introduces a dependence of the calculated activity on the efficiency which is compensated by the kB parameter, being the only adjustable parameter in the TDCR model. Thus, the kB parameter may not be regarded as a property of the cocktail.

When it was observed that, for low-energy radionuclides, some real coincidences are lost when a coincidence resolving time of 40 ns is used, it made sense to admit that the coincidence resolving time must be extended to record the maximum number of events. In fact, this is only a reasonable approach if the physics describing the prompt and delayed emission is modelled in the TDCR calculation. A closer look at the physics reveals that the ionization quenching phenomenon described by the Birks law only concerns the prompt light emission. Moreover, due to the difference in the light emission process, the intrinsic light yield of the scintillator and thus the figure of merit used to calculate the detection efficiency is likely to be different for the two components. This is also the case for the effects of the chemical quenching, which generally occurs in LS sources because of the presence of oxygen.

From these considerations, four approaches could be used:

1. Use a short coincidence resolving time, in order to avoid a big influence of the delayed light emission. A value of about 50 ns, close to the 40 ns used in the MAC_3 module [100] seems to be a good compromise, but this value does not completely suppress the effects of the delayed fluorescence and it should be noted that it is only an approximation.

2. Use a newly developed or already existing LS cocktail that strongly diminishes the undesirable influence of delayed fluorescence.

3. Include a model of the delayed fluorescence in the TDCR calculation. This would include a term for the ionization quenching of T excited states, but also a kinetic model of triplet annihilation reactions considering the initial spatial inhomogeneity and the molecular diffusion phenomena together with the energy transfer mechanisms between the excited molecules. Of course, such a model would not be straightforward and would involve more parameters than only the kB value (e. g., kB for T states, diffusion coefficients, different figures of merit. . .). These parameters could not be determined from the TDCR value of a single counting experiment and more characterisations would be needed, e. g., from pulses time distributions.

4. Possibly the most satisfactory approach is to determine the light output of the scintillator as a function of the deposited energy experimentally using the Compton coincidences method. This approach is described in Section 2.3 and new developments towards it were made in the framework of this thesis (see Chapter 10).

The findings from the quest for the optimal coincidence resolving time in TDCR measurements are published in [143].

10

A NEW COMPTON-TDCR SYSTEM – FIRST RESULTS

From the results in Chapter 9 it was seen that the TDCR method may encounter problems when there is a non-negligible presence of delayed fluorescence in the detected scintillation light. This is likely so, because the used description of the ionization quenching phenomenon, the equation proposed by Birks, holds well only for the prompt fluorescence component. A few remedies to the problem are possible, such as, using LS cocktails that exhibit little to no delayed fluorescence or changing Birks' equation with a more complete model of the scintillation light. The former option seems not to be available yet, and, moreover, the current trend of LS cocktail development is in the direction of increasing delayed fluorescence contribution, as it enhances the pulse-shape discrimination capabilities of the scintillator. The latter option would require a much more complex model with a number of unknown parameters like the ratio between delayed and prompt fluorescence as a function of the deposited energy, the ionization quenching behaviour of delayed fluorescence and possibly others. Perhaps, one of the best solutions is to forego the model for the light output as a function of the deposited energy altogether and replace it with an experimentally obtained one. This can be done using the Compton coincidences and TDCR (C-TDCR) method which was proposed by Ph. Cassette and Phuc Do [97], following the work done by M. N. Péron and Ph. Cassette in 1994 [95]. Its basics are described shortly in Section 2.3.

What is needed for the application of the C-TDCR method is a TDCR detector, a γ detector with good spectroscopic capabilities and a monoenergetic γ-ray source. A new such system was designed and developed at LNHB by B. Sabot and Ph. Cassette. Regarding the electronics and the analysis algorithms, the detectors of the system are connected to a CAEN digitizer and the analysis of the data is performed with the LIST_MODE_ANALYSIS software[1]. In this chapter, the characterization of the new C-TDCR system is presented. It was also used for comparison between the C-TDCR and existing activity measurement techniques. The application of the C-TDCR approach to standardization of low-energy β emitters is discussed in the context of the observed problems with the TDCR method.

10.1 DESIGN AND SETUP OF THE SYSTEM

The C-TDCR system consists of a miniature TDCR detector similar in design to detectors in operation at ENEA[2], Italy [135] and Sofia University, Bulgaria [104]. The counter consists

1 see Chapter 3 for more information on the software.

2 ENEA – The Italian National Agency for New Technologies, Energy and Sustainable Economic Development

of three Hamamatsu R7200U-200 PMTs positioned in a plane with 120° symmetry. The PMTs are aimed at a standard 20 ml LS vial that contains the sample that is to be measured. A CdTe X-ray detector sits between two of the PMTs, as close as possible to the sample. An external ^{241}Am source is located below the sample and is housed in a lead shielding that has the possibility to rotate and move along one horizontal axis. A sliced view of the detector is shown in Figure 10.1.

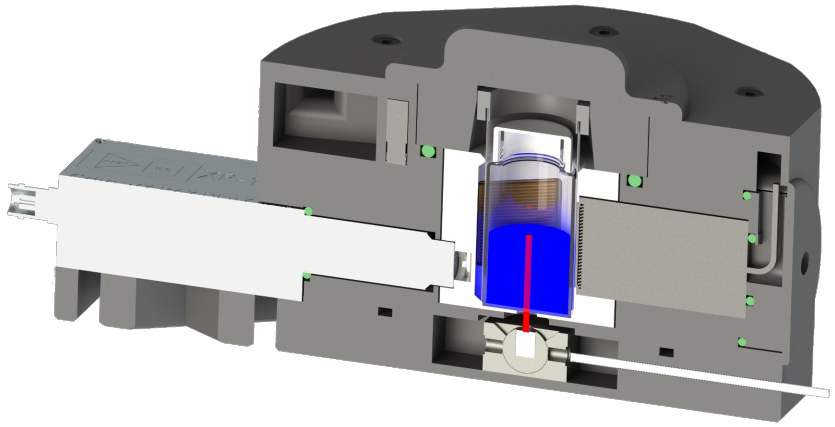

FIGURE 10.1: Sliced view of the C-TDCR detector. The red line shows the beam of the external γ-ray source. The figure was kindly provided for use in this thesis by Benoît Sabot, (LNHB).

There are several important design considerations that are introduced in this system. Firstly, the external source is placed below the scintillation vial. This ensures that the symmetry that exists between the PMTs is preserved, i. e., there is no one PMT that would be directly irradiated by the γ-rays of the source. The CdTe detector is placed as close as possible to the LS vial which ensures high geometrical efficiency. Another feature is the ability to change the position of the external source. By rotating the source, one can change the angle between the collimated beam and the CdTe detector. This will change the Compton scattering probability distribution with respect to the angle, e. g., at 90° between the source and detector, the probability for the detection of 90° Compton interactions will be the highest and will fall rapidly for higher or lower angles.

The acquisition system of the C-TDCR detector is a CAEN DT5751 digitizer with four 10 bit channels and 1 GS/s sampling rate. The three PMTs of the TDCR system are connected to the inputs of the digitizer through a fast amplifier. The CdTe detector is connected to an Amptek PX2T-CdTe shaper and amplifier. The output of the shaper is connected to the fourth channel of the digitizer. The digital pulse processing firmware of the DT5751, however, is unable to process pulse-height information and can only record the area of the integrated pulse. As the precise knowledge of the energy of the scattered γ is critical for the C-TDCR method, a good energy calibration of the digitizer is needed.

The CdTe detector as connected with the CAEN digitizer was calibrated with 15 lines from four spectrometric point sources: ^{241}Am, ^{133}Ba, ^{129}I and ^{55}Fe. In each measurement the source was placed in front of the CdTe detector at a 5 cm distance. The spectra were

acquired until at least 10^4 events per peak were recorded. The centroid of each peak was determined using the Colegram software developed and maintained at Laboratoire National Henri Becquerel, France. The peaks were fitted with an exponentially modified Gaussian with one left tail. A satisfactory fit was observed for each of the peaks. The energy calibration can be seen in Figure 10.2. The data was fitted with a linear function and the linearity of the detector is very good in the range from 0.6 keV to 60 keV.

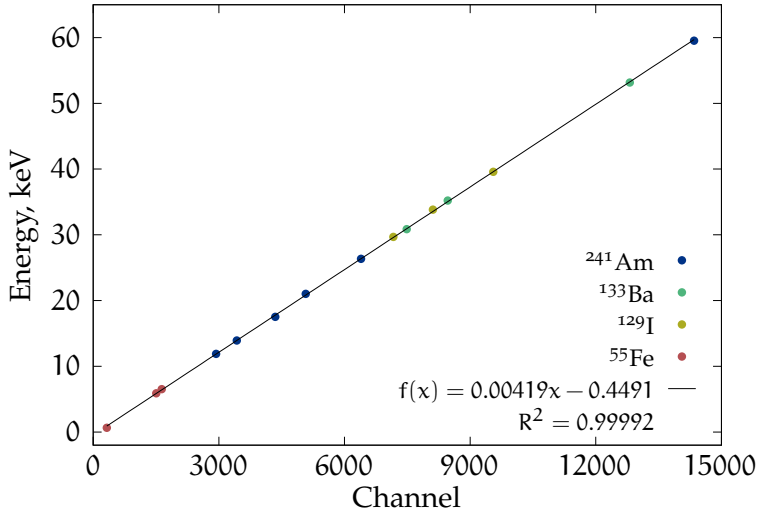

FIGURE 10.2: Energy calibration of the CdTe detector with four spectrometric point sources. An excellent linearity of the detector response is observed.

10.1.1 *Data analysis*

For each measurement the CAEN digitizer outputs *list-mode* files that contain the time-stamp and the deposited in the detector energy. The files are processed with the in-house developed LIST_MODE_ANALYSIS software. The code applies the common dead-time logic with user-defined coincidence window and dead-time base duration. It outputs the single and coincidence counting rates in all channels in coincidence with the γ detector (AG, ..., ABG, ..., ABCG, DG) for each energy bin in the G channel. The off-line data analysis and the developed code give the possibility to obtain the relative light output of the scintillator as a function of the energy for arbitrarily long coincidence resolving time and with a single measurement.

In order to obtain reasonably high counting rate in coincidence with the γ channel, the activity of the external source and thus the counting rate in the LS has to be large. In the present system the typical counting rates in the single LS channels is in the order of 5000 to 10000 s^{-1}. It is thus necessary to perform corrections for accidental coincidences, especially when studying long coincidence resolving times. The correction for accidental coincidences in the presented studies was performed using the experimental method

described in Chapter 8. The true counting rate $N_t^{(i)}(\tau)$ in a coincidence channel i for coincidence window τ is calculated as:

$$N_t^{(i)}(\tau) = N_m^{(i)}(\tau) - \left(\frac{N_m^{(i)}(2500\ \text{ns}) - N_m^{(i)}(2000\ \text{ns})}{500\ \text{ns}} \right) \tau, \tag{10.1}$$

where $N_m^{(i)}$ is the measured coincidence counting rate in channel i. The assumption here is that above 2000 ns coincidence window the increase in counting rate with increase in the coincidence window is due only to accidental coincidences. It is also assumed the distribution of accidental coincidences can be approximated with a linear function.

The mean number of detected photons $\bar{n}$ in a given PMT for a given energy E was calculated using the equation derived in [97]:

$$\bar{n}_X(E) = -3 \ln \left(1 - \frac{TG(E)}{YZG(E)} \right), \qquad X = (A, B, C),\ YZ = (AB, BC, AC),\ X \neq Y \text{ or } Z. \tag{10.2}$$

TG and YZG are the counting rates in the respective coincidence channels in coincidence with the γ-detector at a certain energy E. Equation (10.2) holds for monoenergetic events, so in practice a narrow energy gate must be used in the γ channel. If the width of the energy gate is sufficiently small, equation (10.2) can be used. In the present studies the width of a channel of the γ-detector is 270 eV, which will be considered narrow enough in order to use the monoenergetic approximation. Another assumption that was made in order to apply equation (10.2) is that the three PMTs of the detection system are independent. This may not be the case when using clear glass vials, however, for all presented studies, the used vials are PTFE coated PE vials which are diffusive and scatter significantly the light emitted from the cocktail. The mean number of detected photons in all three PMTs is the sum of the mean number of detected photons in each:

$$\bar{n} = \bar{n}_A + \bar{n}_B + \bar{n}_C. \tag{10.3}$$

10.2 RESULTS WITH VARYING ANGLES

The external source holder is designed in such a way as to allow translation along a horizontal axis and rotation in order to change the angle between the source and detector. By changing the angle it is possible to select the Compton electron energy that would have the highest probability to be detected in the gamma channel. The spectra in the CdTe detector without and with coincidences with the D channel of the TDCR detector are shown in Figure 10.3 for two different angles between the beam of the source and the CdTe detector. At 40° the Compton peak is shifted towards the higher energies thus there is a higher probability for low-energy Compton electrons in the sample.

A possible problem in Compton coincidences systems is the increased asymmetry of the PMTs due to one PMT being irradiated directly by the source. Such a bias could

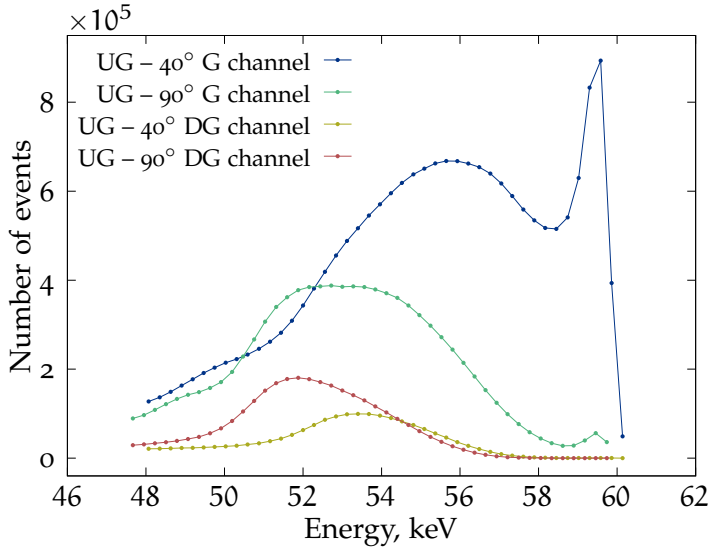

FIGURE 10.3: Energy spectrum in the CdTe without and with coincidences with the D channel of the TDCR detector.

also occur if a larger part of the interactions in the LS happen near one side of the vial. This would increase the detection probability of one or two PMTs at the expense of the others. Both problems will depend highly on the position of the source compared to the measured sample and on the angle between the source and the detector. In a well-designed system the measured light output for a given energy should be the same at different source positions and angles.

Figure 10.4 shows two measurements of the relative light output of the same UltimaGold sample at two different angles between the source and detector. At 90° the external source is placed directly below the center of the vial. At 40° it is located 1 cm off the center and so the beam is kept in the middle of the vial. The light output obtained with the two measurements agrees very well in the interval from 3 to 6 keV deposited energy. The contribution of multiple Compton scattering events becomes large above 6 keV at 40° as single Compton events will have small probability to enter the γ detector at this angle. Similarly, below 3 keV, the probability for small angle scattering is much lower for 90° compared to 40° and thus the divergence.

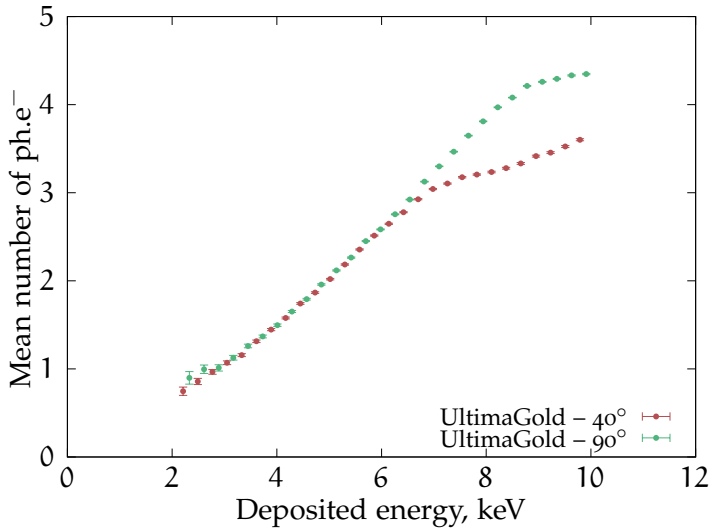

FIGURE 10.4: Relative light output of 10 ml UltimaGold in PTFE coated PE vial measured at 40° and 90° between the source and detector.

The agreement between the results from the two measurement geometries is a good indicator that the system is not biased towards a certain PMT. It also shows that the calculations made with equations (10.2) and (10.3) and the assumptions associated with them hold well event with significantly different energy spectra between the two measurements (see Figure 10.3).

10.3 LIGHT OUTPUT OF COMMERCIAL COCKTAILS

The C-TDCR system was used to measure three commonly used commercial LS cocktails: UltimaGold, UltimaGold LLT and HionicFluor. Measurements were made also on a Toluene + PPO + POPOP cocktail. The amount of dissolved PPO is 3% w/V and the POPOP is 0.015% w/V. The cocktails were used to prepare four 10 ml samples, one per each cocktail, in PTFE[3] coated polyethylene (PE) vials. The PE vials ensure good light diffusion and the plastic has lower probability for interaction with γ-rays compared to vials made of glass.

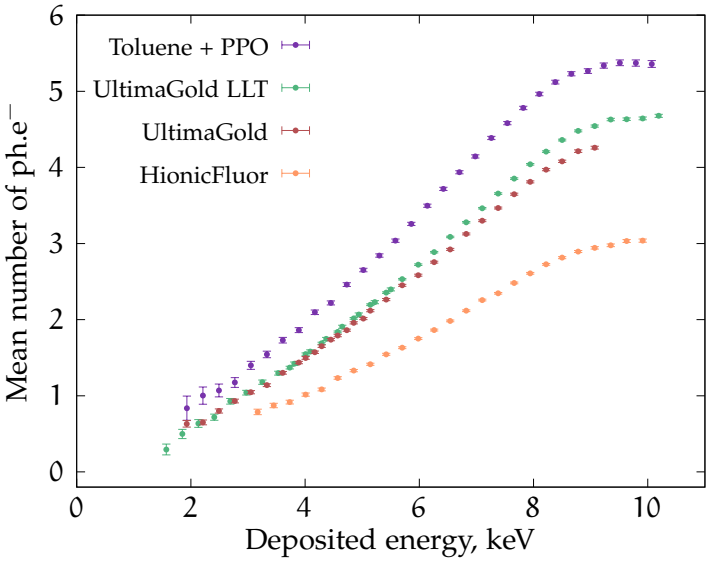

FIGURE 10.5: Relative light output of UltimaGold, UltimaGold LLT, Toluene + PPO and HionicFluor cocktails.

The mean number of detected photoelectrons as a function of the deposited in the cocktail energy is shown in Figure 10.5. The in-house made Toluene + PPO cocktail has the largest light output of all measured samples. The light output of the HionicFluor cocktail is significantly lower than the of the other samples. The curves of UltimaGold and UltimaGold LLT are obtained as a combination of two measurements, one at 40° and the other at 90° between the source and detector, in order to increase the studied energy range. For both samples the light output is very similar between 2 keV and 4 keV, but it increases faster for LLT than for UltimaGold with increasing deposited energy. This indicates higher non-linearity for the UltimaGold LLT cocktail.

Overall the system can be used to obtain the relative light output of cocktails for energies in the range from 2 keV to 7.5 keV. The Compton electron energies that lead to less than one detected photo-electron on average cannot be studied due to the very low

3 Polytetrafluoroethylene – commonly known by the brand name Teflon

counting rate in coincidences between the TDCR and γ detectors. For energies above 7.5–8 keV the contribution of double or multiple Compton scattering events becomes significant. Nevertheless, this energy range is useful for studying the response of LS cocktails for measurements of low-energy emitters such as ^{3}H or ^{55}Fe.

10.4 REVISITING BIRKS' IONIZATION QUENCHING FORMULA FOR THE LIGHT OUTPUT

Birks' semi-empirical ionization quenching formula is the most widely used equation for the description of the non-linearity of organic scintillators. The relationship between the light output of the scintillator L and the deposited energy E is given by:

$$Q(E) = \frac{1}{E}\int_0^E \frac{dE'}{1 + kB(dE'/dx)}, \tag{10.4}$$

where dE'/dx is the stopping power of the electron for energy E' and kB is Birks' ionization quenching factor which is specific to the cocktail and is measured in units µm/MeV. The stopping power is calculated using the recommended equation from the ICRU report №37 [25]. The mean number of detected photons (those producing photoelectrons on the photocathodes of the PMTs) is then:

$$\bar{n}(E) = \varphi Q(E) E, \tag{10.5}$$

where φ is called figure of merit (FOM) and is equal to the average number of detected photons per keV effective energy released in the cocktail, i.e., after taking into account the ionization quenching. It is expressed in units keV^{-1}.

The FOM is a parameter that depends on the measurement geometry and the quantum efficiency of the PMTs. The kB parameter depends only on the LS cocktail and should be constant for different measurement conditions. Assuming that the Birks model is applicable, it is interesting to fit equation (10.4) to the experimentally obtained light output and to attempt to estimate the FOM and kB parameters. The challenge is that, for a single measurement, both parameters are relatively highly correlated and thus the uncertainty of the estimates is high. In order to reduce the correlation between the two free parameters it is possible to make several measurements of the same sample but in different measurement geometries. In the current study the geometry was varied by placing optical grey filters between the LS vial and PMTs. This way, all the properties of the cocktail are kept constant and only a change in the FOM should be observed.

All the LS samples, except the HionicFluor one, were measured without and with grey filters with 85%transparency. The UltimaGold sample was measured with a second filter with 74%transparency. The off-line analysis of the data was performed with 40 ns coincidence window and 20 µs dead-time base duration. The results of the measurements are shown in Figure 10.6. All measurements for each sample were fitted with equation (10.5) with a shared kB parameter for all measurements without and with filters. The FOM parameters in each measurement were free. The stopping power was

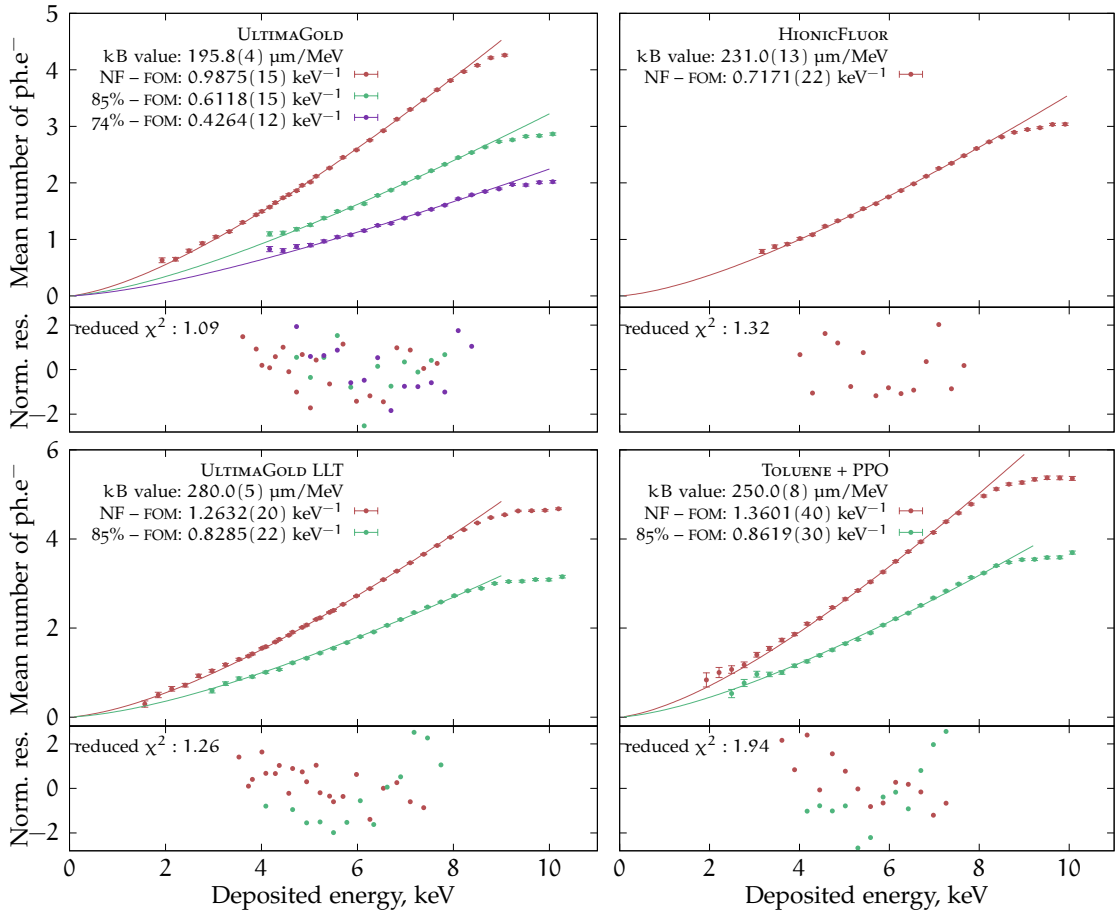

FIGURE 10.6: Mean number of detected photoelectrons (ph.e$^-$) as a function of the deposited energy for four samples in different LS cocktails. The first measurements were performed without optical filters (NF) and some of the samples were measured again with optical grey filters. The lines are Birks' ionization quenching formula with parameters shown in the legend. The normalized residuals are in units of standard deviations.

calculated using the Bethe formula with data from Tan and Xia [94] for energies below 20 keV. The data for the composition of the commercial cocktails was taken from [26].

Very good fits are obtained for the UltimaGold, UltimaGold LLT and HionicFluor cocktails. The reduced χ^2 statistic for these measurements is between 1.09 and 1.32. A poor fit was observed for the Toluene + PPO sample (reduced $\chi^2 = 1.94$). It is possible that the simple Birks equation does not hold for that cocktail leading to an apparent dependence between the FOM and the kB. The kB parameters obtained from the fit are in the range from 195 µm/MeV for UltimaGold to 280 µm/MeV for UltimaGold LLT. It should be noted here, that the fix of a common kB parameter and fitting several measurements with different detection efficiencies leads to a very low correlation between the fit parameters and their precise determination.

The common practice to determine the kB parameter associated with a given cocktail is to apply efficiency variation techniques [80], e.g., grey filters, chemical quenching or PMT defocusing. The basis of the methods is to vary the detection efficiency and calculate the activity of a sample for each measurement with different values of the

kB parameter. The assumption is that the optimal value of kB will result in the same calculated activity for each detection efficiency as discussed previously in Section 2.2. The usual values of the kB parameter that are reported in the literature vary between 75 and 140 µm/MeV. There is a clear discrepancy between the results obtained in this study and the commonly accepted kB parameters.

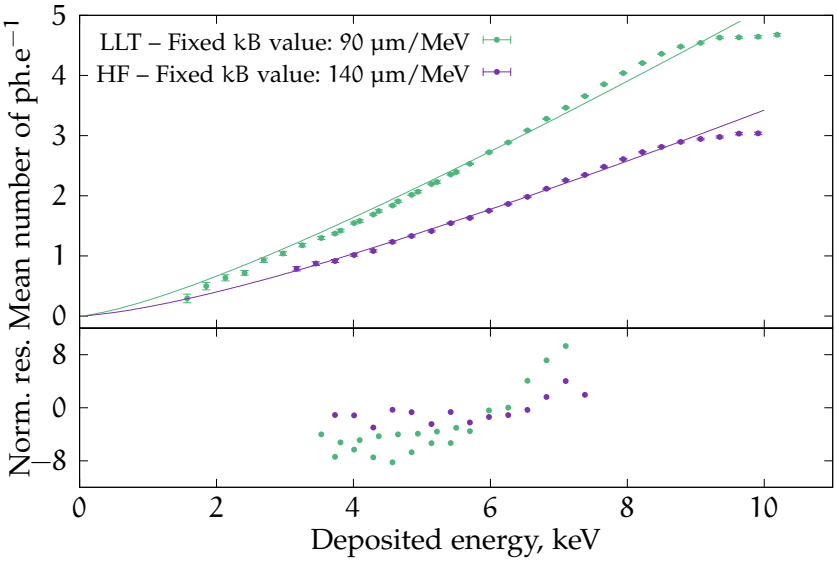

FIGURE 10.7: Relative light output of UltimaGold LLT and HionicFluor for kB parameters fixed from efficiency variation with grey filters.

In order to emphasize the discrepancy, Figure 10.7 shows the measurements of the UltimaGold LLT and HionicFluor samples fitted with fixed kB parameters. The parameters were obtained by the TDCR efficiency variation technique using the same samples with added 100 µl of tritiated water. It should be noted that the results from the efficiency variation are similar to what was obtained during past experiments and what is commonly reported in the literature for these cocktails. While the HF fit is somewhat satisfactory, the fit of the UltimaGold LLT data, with a fixed kB parameter 90 µm/MeV, is poor. The results for the UltimaGold sample are similar to the UltimaGold LLT, but are omitted from the figure as they significantly overlap with the UltimaGold LLT data. Note that the lower kB parameters obtained from the efficiency variation lead to lower than observed mean number of photoelectrons for energies between 6 keV and 8 keV. This discrepancy cannot be explained by interference from double Compton events as their effect is to reduce the detected light.

10.5 COMPARISON BETWEEN TDCR, CSET AND C-TDCR

All measured samples thus far are pure LS cocktails without radioactive sources. One large advantage of the C-TDCR system is that it allows the measurement of the relative light output of scintillators containing radionuclides, provided that they do not emit γ or X-rays in the considered energy range. This is possible because the counting rates

used to obtain the mean number of detected photons for a given deposited energy are in coincidence with the γ-detector, thus pure β events will not interfere.

The main uncertainty, when measuring the activity of ^{3}H LS-sources using the TDCR method, comes from the used model of the light output of the scintillator. As it can be directly measured using the C-TDCR system, the experimentally obtained mean number of detected photons as a function of the deposited energy can be used instead of models of the ionization quenching, as proposed first in [97] and later used in the ZoMBieS method by Bignell et al. [98] The C-TDCR system can be used as a classical TDCR system as well by removing the external γ-ray source. A third method for activity calculation also exists when measurements with an external source are performed. The method is called Compton Efficiency Tracing CSET and is described in detail in [97]. Thus, with tho measurements with a single detection system it is possible to compare the three activity calculation methods in exactly the same geometrical conditions. The digitizer approach also allows the use of arbitrary coincidence resolving times and correlations for accidental coincidences.

In order to perform the comparison a ^{3}H LS-source was measured using the C-TDCR system. The measured source is ^{3}H in 10 ml UltimaGold cocktail in a PTFE coated plastic vial. The source was measured for 48 hours using the CAEN digitizer and all events were recorded in list-mode files. The counting rate in the single channels of the TDCR is around 8000 cps and the counting rate in the CdTe detector in the whole spectrum around 60 cps. This gives about 5 – 8 cps of useful events in the double coincidence channels with the γ channel (ABG, BCG, ACG). There are in the order of 5×10^4 useful events per channel and the channel width is 270 eV. Just after this measurement the same source was measured in the same detector with the external source removed and placed in a lead shielding. The second measurement is 40 minutes long and was again performed with the CAEN digitizer. With these two measurements we can estimate the activity of the source using the three different methods:

- The classical TDCR method with Birks' ionization quenching formula and a kB parameter obtained from efficiency variation curves
- The Compton Efficiency Tracing method, which is similar to the CIEMAT/NIST tracing but with several advantages
- The TDCR method, but using the light output of the scintillator that is obtained experimentally using the C-TDCR system

10.5.1 *TDCR method*

In order to obtain the activity using the classical TDCR method, the measurement of the source without the external source was analyzed. The list-mode files were processed off-line with the common dead-time logic, same as in the commonly used MAC$_3$ module [100]. The coincidence window is 40 ns and the dead-time base duration

20 µs. A blank sample with the same cocktail and in the same type of LS vial, but without a radioactive source was also measured in the system in order to subtract background counting rates. The T/AB, T/BC and T/AC ratios were used as an input to the TDCR18 code to obtain the detection efficiency and activity of the source as a function of the kB parameter. The TDCR18 program is an updated version of TDCR07 [93]. The updates include the data for more LS cocktails and also the option to calculate the stopping power using the dataset published by Tan and Xia [94]. The optimal kB parameter was estimated at 100 µm/MeV from efficiency variation with grey filters.

It should be noted here that a previous study revealed that 40 ns coincidence resolving time is insufficient to collect all true coincidences for UltimaGold cocktails [105]. In the study it was also observed that the activity calculated using the TDCR method depends on the choice of resolving time. Despite the loss of coincidences for short coincidence windows, the study concludes that the use of 40 ns is still a good compromise if Birks' ionization quenching formula is used.

10.5.2 *CSET method*

In order to obtain the activity of the source using the CSET method we followed the method described in the article of Cassette and Do [97]. The events in the γ detector corresponding to Compton electron energies between 3.5 keV and 7.5 keV are considered to be purely single Compton scattering events. Below 3.5 keV deposited energy there could be influence of the 59.54 keV peak of ^{241}Am and there are a low number of events at 90° between the source and detector. Above 8 keV we begin to observe the effect of the multiple Compton scattering and thus the 7.5 keV upper limit is taken conservatively. The CSET method for detection efficiency calculation is the following:

- From all recorded events in the TDCR channels, only those are considered which are in coincidence with the γ channel in the range which corresponds to Compton electron energies between 3.5 keV and 7.5 keV.
- The spectrum in the γ channel within this range is regarded as a spectrum of a virtual source that is created in the LS cocktail.
- The TDCR counting logic is applied to the events which are in coincidence with the γ channel and fall within the specified energy range. The result is the ABG, BCG, ACG, DG and TG counting rates.
- The TDCR18 code is used with the experimental spectrum and the obtained TG/ABG, TG/BCG, TG/ACG ratios to calculate the FOM.
- The FOM is calculated for a set of kB parameters from 70 to 200 µm/MeV.
- A classical TDCR measurement of the ^{3}H source without the external γ source is performed and the double coincidences efficiency for each kB parameter is calculated by using the FOMs predetermined from the previous step.

By using the CSET method the dependence of the calculated activity on the kB parameter is significantly reduced. A possible explanation for this effect is given in the original article [97] and it states that it is probably due to the fact that Birks' formula is used twice: once to calculate the FOM in the measurement of the virtual source and a second time to calculate the detection efficiency of the classical TDCR measurement, thus some of the unknowns in the ionization quenching are cancelled.

10.5.3 *TDCR with experimentally obtained light output*

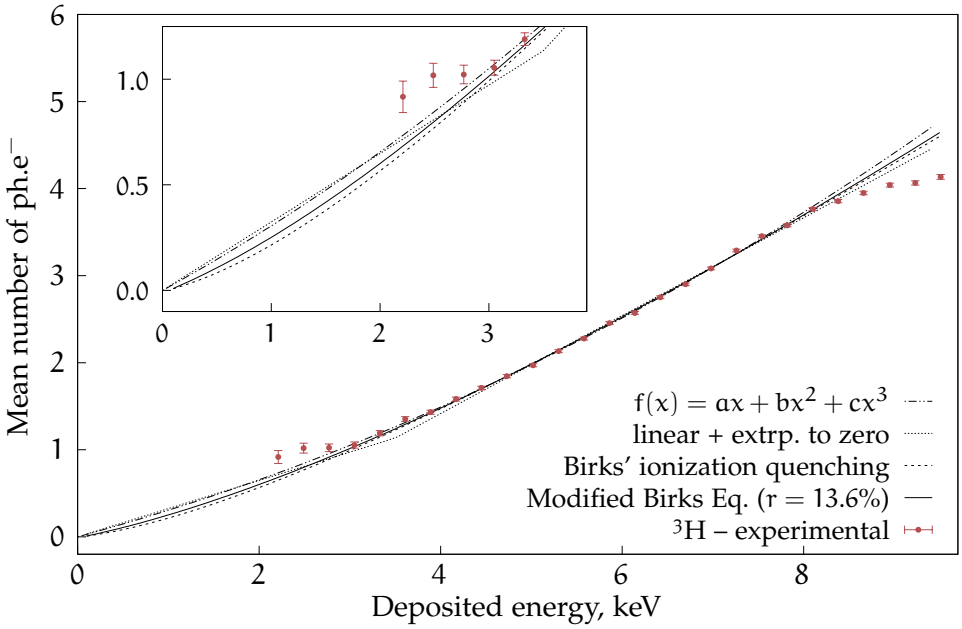

FIGURE 10.8: Light output of the ^{3}H LS-source approximated with several models: Cubic polynomial as used by Bignell et al.[98], linear fit with linear extrapolation to zero below 3.5 keV, Birks' ionization quenching formula and a modified Birks equation with a fraction r that does not experience ionization quenching. The measurement is done with 200 ns coincidence window.

The experimentally obtained light output of the scintillator can be used instead of equation (10.5) with optimized FOM and kB parameters. This approach was proposed by Bignell et al. and is described in [98]. The original setup used a ^{51}Cr source as external monoenergetic source. The system allows the study of energies between 5 keV and 40 keV and was used to determine the activity of a ^{63}Ni source (66.98 keV maximum β spectrum energy). The response of the scintillator for energies lower than 5 keV and higher than 40 keV must be extrapolated from the available data, which does not lead to significant uncertainties in the case of ^{63}Ni, but would be unsuitable for measurement of low energy nuclides such as ^{3}H and ^{55}Fe.

The system presented here allows the study of scintillator non-linearity in the range of energies from 3 keV to 7.5 keV which encompasses a significant part of the ^{3}H β spectrum and the ^{55}Fe emissions. It was used for the determination of the relative light output of a ^{3}H in UltimaGold LS-source. The mean number of photons as a

function of the deposited energy is shown in Figure 10.8. Previous studies of the distribution of scintillation events from ^{3}H in UltimaGold samples show that 40 ns coincidence window is insufficient to collect all true coincidences [105], thus a 200 ns coincidence resolving time was chosen for this study. The choice of this coincidence window is a compromise between the loss of true coincidences and the influence of accidental coincidences. It should be noted here that for the Compton measurements the accidental coincidences are not at all negligible. For example, for 200 ns resolving time the accidental coincidences are 1.7% of the TG counting rate and 0.7% of the DG counting rate. Corrections for accidental coincidences in all channels were performed using equation (10.1).

Tritium has 18.64 keV maximum energy of the β spectrum, thus it is necessary to extrapolate the experimentally obtained light output above 7.5 keV and below 3 keV. As activity measurements of ^{3}H are very sensitive to the model describing the scintillator non-linearity it is important to choose a good model and access the uncertainties associated with that choice. Four different models were chosen to describe the light output of the LS-source: sum of two linear models, a cubic polynomial as used by Bignell et al. in [98], Birks' ionization quenching formula and a modified Birks equation with a term accounting for delayed fluorescence.

The sum of two linear models consists of a linear function fitted to the experimental data points between 4 keV and 7.5 keV. As this function gives less than zero photons for zero deposited energy it is cut at 3.5 keV and is connected to the point $(0,0)$ with another linear function. The rationale behind this model is to be as simple as possible. If using Birks' equation as a reference, the linear model will underestimate the light output of high energy events and will give a lower boundary for the detection efficiency. On the other hand, the cubic model was already used to describe light output of a liquid scintillator. As seen from Figure 10.8 it seems to overestimate the light output of events above 8 keV and thus can be used as an upper limit of the estimated detection efficiency.

The modified Birks equation $B_{mod}(E,r)$ is proposed in the framework of this thesis. It accounts for a fraction r of the scintillation light that does not experience ionization quenching and is given by:

$$B_{mod}(E,r) = \varphi\left((1-r)Q(E)E + rE\right). \tag{10.6}$$

Such a modification to Birks' formula may be necessary as the latter was proposed by Birks as a description of the prompt fluorescence only. Delayed fluorescence could experience little to no ionization quenching [7]. For some scintillators delayed fluorescence could have non-negligible contribution in the order of 10 – 15%[7, 17]. This contribution should increase with the coincidence resolving time [105].

The uncertainty of the measurement was taken as the standard deviation of a uniform distribution with a lower boundary defined by the linear model and an upper boundary defined by the cubic model. The relative uncertainty of the measurement, considering only the dispersion of results with the different models, is 0.7% at k = 1.

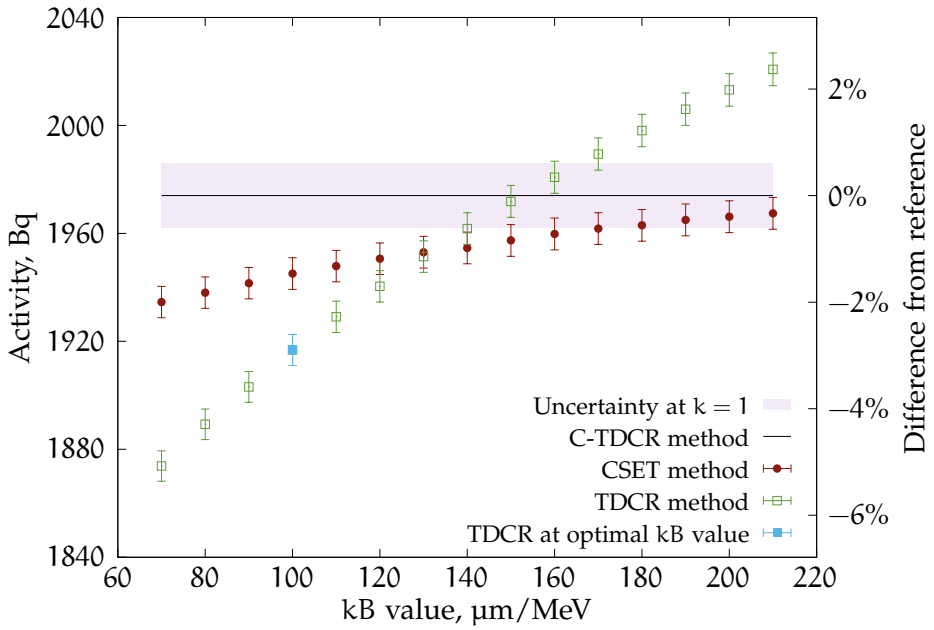

FIGURE 10.9: Activity of a ^{3}H in UltimaGold LS-source calculated using the three methods. The optimal value for the kB parameter 100 µm/MeV was obtained by efficiency variation using grey filters on the same source.

10.5.4 *Comparison and discussion*

The results for the calculated activity of the LS-source using the three methods is shown in Figure 10.9. All activities are relative to the one obtained by the C-TDCR method using the experimental light output, which is 1976 Bq. The comparison with this method should be the closest to knowing the true activity of the source as there are no assumptions for the cocktail composition, ionization quenching parameters and FOM. The activity calculation is however dependent on the extrapolations below 3 keV and above 7.5 keV. This range encloses 50% of the spectrum of ^{3}H.

There are a few interesting features that can be noted from this study. The CSET obtained activity is much less dependent on the choice of the kB parameter than the classical TDCR method. Both the CSET and TDCR methods give the same activity value if the kB is chosen to be 140 µm/MeV. The activity at this point is 1% lower than the activity obtained by the C-TDCR method. The results seem to agree well with the hypothesis given in [105]. There, from the Monte Carlo simulations it is shown that if there is some contribution of scintillation light that does not experience ionization quenching the TDCR method would overestimate the activity for the true kB parameter. In the Monte Carlo simulation the true kB parameter is the one selected by the user. In this case if we assume that the fit of the light output could give the real kB parameter (200 µm/MeV), then the classical TDCR would overestimate the activity by approximately 2% This is similar to what was reported from the Monte Carlo simulation in the article. Another observation is that the usually chosen kB parameter could be underestimated. Such an underestimation could occur due to problems with the efficiency variation

technique. That is, when changing the detection efficiency, if there is more than one scintillation component present, then it is possible to change the ratio between the components. As the TDCR model assumes only one scintillation component following the Birks light output equation, a bias in the calculated activity could be introduced.

11

APPLICATIONS OF THE TDCR METHOD AT THE MIL LABORATORY AT SU

This chapter presents the validation of the TDCR system developed and operated at Sofia University through a participation in an international key comparison of ^{3}H activity measurements organized by the BIPM. It is also concerned with the validation of the nanoTDCR, a TDCR acquisition device developed by the labZY company. The chapter also describes shortly some of the practical applications of the TDCR technique for the purposes of the studies performed at the "Metrology of Ionizing Radiation" laboratory at Sofia University (MIL), namely the standardization of ^{222}Rn activity.

A TDCR counter has been developed in the Faculty of Physics of Sofia University. The counter, called TDCR-SU, is an in-house built detector with three PMTs, whose purpose is to perform primary measurements of activity of liquid scintillation samples at the MIL laboratory and thus to provide reference sources for the calibration of the other LS instruments used in the laboratory. The performance of the TDCR-SU detector was validated by comparisons with the French primary TDCR counter at LNHB. These studies were done before the research in this thesis, and are described in detail in [104].

11.1 STANDARDIZATION OF PURE BETA-EMITTERS USING THE NANOTDCR

An important part of the TDCR-SU detector is the nanoTDCR device. At the time of development of the TDCR-SU detector, the nanoTDCR device was brand new, and one of the first produced units was purchased to be used at Sofia University. Due to this, the nanoTDCR required extensive validation of its performance. The validity of the nanoTDCR device was tested, within the scope of the thesis, by comparisons with the widely used MAC$_3$ TDCR acquisition module. The studies were performed in partnership and collaboration with the labZY company and with LNHB.

The possibility to use the nanoTDCR acquisition system for TDCR activity standardization of pure β-emitters was demonstrated by comparisons with the MAC$_3$ module. For the purpose of this study, the logical outputs of the three channels of RCTD1 were connected to the inputs of the MAC$_3$ and nanoTDCR. The experimental setup was used for measurements of ^{3}H and ^{90}Sr/^{90}Y in UltimaGold cocktails.

The results of the comparison demonstrate excellent agreement between the MAC$_3$ and nanoTDCR units, and are shown in the work of Jordanov et al. [101]. The comparison shows that the nanoTDCR system has excellent metrological capabilities, and can be used within the TDCR-SU system for the standardization of radionuclides.

11.2 VALIDATION OF TDCR-SU IN THE CCRI(II)-K2 H-3 KEY COMPARISON 2018

In 2018 a key comparison of the measurement of the activity concentration of a tritiated water solution was organized by the LNHB under the patronage of the Consultative Committee for Ionizing Radiation (CCRI from the French *Comité Consultatif pour les Rayons Ionisants*), part of the BIPM. The purpose of key comparisons is to measure the degree of equivalence of national standards, and are usually multiyear efforts, where a pilot laboratory finds a suitable transfer standard, circulates it between participants, processes data, and writes a comparison report that is posted on the BIPM key comparison data base [144].

The ^3H_2O solution was sent to ten national metrology institutes[1], and to the MIL laboratory. All the participating laboratories used the TDCR method to measure the specific activity of the solution. At our laboratory, we have used the TDCR-SU detector for the measurements, which serves as a validation of the capabilities of the system to perform ^3H activity measurements that are consistent with laboratories around the world.

It should be mentioned here, that ^3H was chosen because it is a good tracer of nuclear activity, thus it is widely monitored. Moreover, it is also used as a tracer for the implementation of the CNET method, and it is widely used for quality control in LS counters [34]. The mean energy of the β-spectrum of ^3H is low (5.6 keV), and it is difficult to measure by LS counting due to the low detection efficiency that is usually achieved. Therefore, if there are problems present with a given TDCR detector, they will be the best visible when measuring ^3H.

The tritiated water sample provided by the LNHB was used to make ten LS samples. Half of the samples are with UltimaGold cocktail and the other half with UltimaGold LLT cocktail. All samples contain roughly 7 µl of tritiated water and 10 ml cocktail. Two blank samples were made in the same manner as the others, but with distilled and deionized water instead of ^3H_2O.

The samples and blanks were measured on the TDCR-SU detector. Each sample was measured once, where the measurement consists of eleven one-hour repetitions. The blank samples were measured in the same way, with one measurement of the corresponding blank for each sample. For example, the first ^3H in UltimaGold sample was measured for 11 hours (eleven repetitions, one hour each). The distilled water in UltimaGold sample was also measured in the same way after. The first repetition of each measurement is discarded. This is done, because it is possible to excite the PMTs with ambient light when opening the optical chamber to place the sample in the detector. This could increase the single counting rate in the first repetition and lead to accidental coincidences.[2]

1 CENTIS (Cuba), CIEMAT (Spain), ENEA (Italy), IRA-METAS (Switzerland), LNE-LNHB (France), NIM (China), NPl (UK), NRC (Canada), POLATOM (Poland), PTB (Germany)

2 The corrections for accidental coincidences developed in this thesis were not yet available at the time of the experiments.

The activity of the ^{3}H sample was calculated for each repetition. To do so it is necessary to obtain the net (background corrected) double and tripple counting rates n_{net}. This was done by subtracting the blank counting rate b in a given coincidence channel for each repetition i from the corresponding repetition from the sample measurement n_{meas}:

$$n^X_{net,i} = \frac{n^X_{meas,i}}{b^X_i}, \tag{11.1}$$

where X denotes the coincidence channel AB, BC, AC, D or T. The triple to double coincidences ratios, T/AB, T/BC, T/AC and T/D, are calculated from the net counting rates for each repetition. The TDCR07c code [93] was then used to calculate the activity for each repetition, and the activity of the source is taken as the average of the activities calculated for the ten repetitions. The kB parameter that was used for the samples measured in UltimaGold was determined by the efficiency variation technique (see Section 2.2) performed with a set of 3D printed mesh filters. The mesh filters are described in detail in [145]. The same method was used for the UltimaGold LLT samples. The optimal kB parameter for UltimaGold was found to be 130 µm/MeV and for UltimaGold LLT 100 µm/MeV.

TABLE 11.1: Uncertainty budget of the activity measurement.

Source of uncertainty	Relative standard uncertainty, %
Counting rates	0.06
Weighing	0.05
Dead time	0.05
Blank	0.14
Resolving time	0.32
kB parameter	0.60
Sample variability	0.09
FINAL VALUE	0.69

The final result for the activity of the sample was determined from the average value from all measured samples, and is 52.68(36) kBq/g (reference date: 1st February 2018. The relative standard uncertainty is 0.69%. The uncertainty budget is shown in Table 11.1.

The final result was submitted to the laboratory organizing the intercomparison (LNHB), that compiles the reports from all participants. The results were published in [34]. The final conclusion from the intercomparison is that the results from all laboratories are compatible, within the reported uncertainties, and that the values of

the arithmetic mean, the weighted mean, the power-moderated mean and the median are very consistent [34]. The key comparison reference value is 53.16(13) kBq/g. This is consistent with the specific activity determined at the MIL laboratory using the TDCR-SU detector. The successful participation of the laboratory in the BIPM key comparison shows that the TDCR-SU detector, and the TDCR analysis methods employed at the MIL laboratory are comparable to the methods used in the leading metrology institutes for measurements of the activity of tritiated water.

11.3 PRIMARY ACTIVITY STANDARDIZATION OF RN-222 USING TDCR COUNTING

Radon is a radioactive noble gas without stable isotopes. Measurements and standardization of the activity of ^{222}Rn are of practical interest because it poses a risk to human health as it can be accumulated in people's homes and, when inhaled, it and its short-lived progeny damage the lungs. ^{222}Rn is the second leading cause of lung cancer in the world [146, 147]. Therefore, accurate measurements of the activity of ^{222}Rn, and the metrological assurance of these measurements, are necessary.

The calibration of LS counting instruments for ^{222}Rn measurements is typically performed with standardized ^{226}Ra solutions. However, this type of calibration is prone to errors as, with the ageing of the solution, there is a build-up of ^{210}Pb, which interferes with the measurements of the LS sample and is difficult to account for [148]. For this reason the TDCR method was chosen as a method to prepare reference sources for ^{222}Rn calibration in the MIL laboratory.

^{222}Rn is produced by the decay of ^{226}Ra and in turn decays with a half-life of 3.8232(8) days through a decay chain containing two $\alpha-$emitters (^{218}Po and ^{214}Po and two $\beta-$emitters (^{214}Bi and ^{214}Pb) to ^{210}Pb which has a much longer half-life (22.2 years). Due to the relatively long half-life of ^{210}Pb, ^{222}Rn reaches equilibrium with its short-lived progeny after a period of around five hours. The activity of ^{210}Pb is negligible during the first few days after the production of ^{222}Rn.

The standardization of ^{222}Rn by TDCR counting was proposed and developed by Ph. Cassette et al. in 2006 [74]. The method is based on the measurement of a LS sample containing ^{222}Rn in equilibrium with its short-lived daughter products. Due to its very short half-life of 165 µs, ^{214}Po can decay during the dead-time of the detector [74]. This will result in a reduced detection efficiency for that radionuclide. The counting rate, calculated for the live time of the detector and taking into account the correction for decays of ^{214}Po during the effective dead-time of the detector τ_{eff}, is [74]:

$$\begin{aligned} R =& \varepsilon_{Rn222} S_{Rn222} A_{Rn222} + \varepsilon_{Po218} S_{Po218} A_{Po218} + \varepsilon_{Pb214} S_{Pb214} A_{Pb214} + \\ & \varepsilon_{Bi214} S_{Bi214} A_{Bi214} + \varepsilon_{Po214} S_{Po214} A_{Po214} e^{\lambda \tau_{eff}}, \end{aligned} \tag{11.2}$$

where ε are the detection efficiencies of the radionuclides which are, 100%for the $\alpha-$emitters and nearly 100%for the high-energy $\beta-$emitters, S are the corresponding emission probabilities, which are practically 100%for all nuclides in the chain, and A are the activities of ^{222}Rn and its daughter products. As the imposed dead-time in

TDCR measurements is of the extending type, the effective dead-time of the detector is considered as the average of the dead-times imposed after the decay of ^{214}Bi, including extensions from sporadic signals or uncorrelated decays. Note that it is an open research question whether or not τ_{eff} should be used in equation (11.2), or the dead-time base duration should be used instead. If we take into account also the relations between the activity of ^{222}Rn and activities of its daughters after they reach secular equilibrium, which according to the Bateman equations are [149]:

$$\frac{A_{Po218}}{A_{Rn222}} = 1.000558; \quad \frac{A_{Pb214}}{A_{Rn222}} = 1.00547; \quad \frac{A_{Bi214}}{A_{Rn222}} = 1.00910; \quad \frac{A_{Po214}}{A_{Rn222}} = 1.00910 \tag{11.3}$$

Equation (11.2) can be written as:

$$R = A_{Rn222}\left(1.0091\varepsilon_{Bi214} + 1.00545\varepsilon_{Pb214} + 2.000558 + 1.0091e^{\lambda\tau_{eff}}\right) \tag{11.4}$$

The efficiencies of the high-energy $\beta-$emitters, ε_{Po-214} and ε_{Bi-214} , can be calculated with the TDCR model using their respective energy spectra. The proper choice of kB value is insignificant, because the detection efficiencies are very close to 100%and can be chosen in the middle of the range of possible kB values for the used cocktail. By far, of the largest importance to the correct calculation of the activity of ^{222}Rn is the correction for ^{214}Po, decaying during the effective dead-time of the detector τ_{eff} [74].

The practical realization of these calculations is done by a computer program developed by Ph. Cassette. The program assumes that τ_{eff} is equal to the dead-time base duration and the kB parameter is equal to 100 µm/MeV. The program requires the β spectra of ^{214}Bi and ^{214}Po, the TDCR parameter of the measurement and the dead-time base duration as inputs, and it outputs the detection efficiency for ^{222}Rn. The software was used in the ^{222}Rn measurements described hereafter.

11.4 VALIDATION OF TDCR-SU FOR PRIMARY ACTIVITY MEASUREMENTS OF RADON IN WATER

The TDCR-SU detector has been validated for primary activity measurements of the activity of ^{222}Rn in water through participation in two international intercomparisons. These will be described hereafter.

JRC INTERNATIONAL INTERCOMPARISON A large scale Europe-wide proficiency test (REM 2018 PT) on the determination of the specific activity of ^{222}Rn in drinking water was organized by the Joint Research Centre (JRC) of the European Commission. The 101 participating environmental radioactivity monitoring laboratories were either nominated by their corresponding national authorities or invited by JRC to participate [150]. The MIL laboratory was also invited to participate.

The proficiency test consists of the determination of the specific activity of ^{222}Rn in a water sample that is sent out by JRC. The water sample is a 1 l bottle containing

Austrian natural spring water. Ten LS sources were made from the water sample in order to perform LS counting measurements of the ^{222}Rn activity. The water was sampled with a large 60 ml syringe attached to a hose that allows sampling from the bottom of the 1 l bottle. The sampling was performed immediately after the first opening of the bottle. When the bottle is opened the ^{222}Rn that is close to the water surface starts to diffuse into the above air, and thus the sampling of the bottom is necessary. After filling the 60 ml syringe, the attached hose was replaced with a needle and the contents of the syringe were distributed to five LS vials that were already filled with 10 ml of UltimaGold LLT cocktail. Eight milliliters of the water were discharged on the bottom of each LS cocktail filled vial. Again, this is done to prevent ^{222}Rn diffusion in the surrounding air. The LS vials were then filled to the brim with UltimaGold LLT. Thus, a homogeneous system is achieved – ^{222}Rn containing water that is fully dissolved in a liquid scintillator. Special precautions were taken in order to avoid the forming of air bubbles in the samples. A total of ten LS samples were prepared this way. Some samples in a LS vial were also prepared that contain only water, i. e., a sample with 20 ml ^{222}Rn water and no LS cocktail.

After the preparation of all ^{222}Rn containing samples, a pump was used to pump clean air in the water remaining in the 1 l bottle. This is done in order to evacuate the radon gas. The remaining radon-free water was used to prepare blank samples that serve as background correction. The use of the same water is important as it can be checked if it contains radium, uranium or other radionuclides that can interfere with the ^{222}Rn LS measurements. This also ensures that the cocktail-water mixture is the same as in the ^{222}Rn samples.

The prepared LS samples were measured on a RackBeta 1219 LS spectrometer. The samples have a relatively low activity and cannot be measured directly on the TDCR-SU detector, as it does not have passive shielding and has a high background counting rate that would interfere. In the RackBeta detector, the sample and the PMTs are contained in a lead box, therefore significantly decreasing the background counting rate. The RackBeta spectrometer is not a primary measurement device and it requires calibration. It was calibrated using a standardized ^{222}Rn-in-water LS sample. The standardization of the LS sample was performed with the TDCR-SU detector. The LS sample was prepared using the water remaining in the 1 l bottle. The water was exposed to air with high ^{222}Rn concentration and the radon gas diffuses into the water. A radon-in-water source with relatively high activity concentration can be produced in this way. The newly produced radon containing water was used to prepare a sample to be measured on the TDCR system.

The sample was measured on the TDCR-SU and its activity was estimated using the method outlined above using the radon activity calculation code by Ph. Cassette. The specific activity of ^{222}Rn in the sample was measured at 9.672(48) Bq/g. This sample was measured on the RackBeta for calibration. The detection efficiency of the RackBeta spectrometer for ^{222}Rn and its progeny is 4.999(22). Note that the maximum achievable

detection efficiency is 5.012 as there are on average 4.012 decays of short-lived daughter nuclides for every ^{222}Rn decay.

The final value for the specific activity of ^{222}Rn in the spring water samples is 273.4(91) Bq/kg with a coverage factor $k = 1$. The reference ^{222}Rn specific activity value in the REM 2018 proficiency test samples with it combined uncertainty with a coverage factor $k = 1$ is $A_{ref} = 318(16)$ Bq/kg. The final reported result of our laboratory falls within the acceptance range set by the organizers of the intercomparison which is $A_{ref} \pm 20\%$ [150]. Thus, the participation of the MIL laboratory was deemed successful.

After the end of the proficiency test, it was found out that a small amount of ^{222}Rn activity was caught in the hose attached to the syringe during the sampling of the 1 l spring water bottle. This in part explains the discrepancy between our reported result and A_{ref}. Another source of discrepancy is that A_{ref} is calculated as the average of many reported values, where some measurements were performed with HPGe detectors. A problem may occur if the HPGe detector is calibrated for efficiency with a uniform source, and the calibration factor is then used on the ^{222}Rn-in-water measurements. Even though ^{222}Rn itself is uniformly distributed in a water sample, its daughter products are heavy metals that can easily attach on the glass surface of the bottle. Thus, if the source is measured close to the HPGe detector it cannot be readily assumed to be a uniform activity source.

IRSN INTERNATIONAL INTERCOMPARISON A proficiency test for the measurement of ^{222}Rn in water samples was organized by the Environmental Analysis and Metrology Department of the French radiation protection and nuclear safety institute (IRSN). Twenty laboratories (twelve French and eight foreign laboratories) took part in the test, including the MIL laboratory. The results reported by the laboratories are collected by the IRSN, compared to the reference values, statistically studied and distributed to participating laboratories, to ASN (French Radiation & Nuclear Safety Authority) and to the members of the French accreditation committee for environmental radioactivity measurement [151].

The test items are 1.2 l aluminum flasks with polypropylene screw cap and aluminum cap seal, filled to the brim with water spiked with radon under laboratory conditions. In order to measure the specific activity of ^{222}Rn in the water samples a similar method was used as in the previous proficiency test. An important difference is that this time the plastic syringe with a plastic hose was replaced with a glass syringe with a wide metallic needle. This prevents unwanted ^{222}Rn absorption and loss of activity when sampling. A total of eight water samples, 10 ml each, were taken from the 1.2 l aluminum flask. The water was carefully transferred below the surface of UltimaGold LLT LS cocktail in 20 ml high performance glass vials. The water and cocktail were mixed by vigorous shaking by hand. The LS samples were measured on a RackBeta 1219 LS counting spectrometer. The spectrometer was calibrated using one of the samples whose activity was certified by the TDCR-SU detector. The blank samples were prepared in the same

way as for the previous proficiency test, i. e., using the same water from the test item after bubbling for enough time to evacuate the ^{222}Rn.

The standardization of the sources was done by primary activity measurements on the TDCR-SU detector and the new TDCR-LNHB-SU detector. One of the sources was measured on the TDCR-SU and the other on the TDCR-LNHB-SU. The latter detector is very similar to TDCR-SU and uses the same model of PMTs. The only differences are in the designs of the optical chambers and the construction material – polytetrafluoroethylene (PTFE, commercial name: Teflon) in the TDCR-SU and polylactic acid (PLA) in the TDCR-LNHB-SU.

The specific activity of ^{222}Rn in the two LS sources measured in the two detectors are 0.660(7) Bq/g for the source in the TDCR-SU and 0.656(7) Bq/g for the source in the TDCR-LNHB-SU. There is an excellent agreement between the two detectors within the estimated uncertainties. The difference between the two specific activities is 0.54%. Thus, the new TDCR-LNHB-SU detector is shown to be equivalent to the TDCR-SU for the standardization of the activity of ^{222}Rn in water LS sources.

The final reported value by the MIL laboratory for the specific activity of the proficiency test water sample is 666 ± 40 Bq/l with a coverage factor $k = 2$. The assigned value of the proficiency test is established at 677 ± 55 Bq/l [151]. There is an excellent agreement between the official assigned value and the result obtained at the MIL laboratory.

The successful participation in both proficiency tests affirms that the calibration, sampling and measurement techniques at the MIL laboratory at Sofia University provide accurate and unbiased estimates of the ^{222}Rn-in-water activity concentration.

11.5 MEASUREMENT OF THE PARTITION COEFFICIENT OF RN-222 IN POLYMERS

The ability of some polymers like polypropylene [152], polyethylene [153], polystyrene [154], polycarbonates [155], plastic scintillators [149] and others to absorb radionuclide noble gases was shown recently. This property allows for some materials to be used as radon samplers that dissolve in a liquid scintillator and can be measured by LS counting. Moreover, plastic scintillators could be used for direct scintillation measurements of ^{222}Rn activity. Also, most of the passive or active devices used for radon and thoron (^{220}Rn) measurements are sensitive to both isotopes [156]. To discriminate between the two they typically use a diffusion barrier or are packed in polymer bags. Thus, a proper description of the process of diffusion of the radon gas through a polymer barrier or into a plastic scintilla cor is needed. The sorption and desorption of radioactive noble gases in polymers is described adequately by the diffusion equation [155]. Two parameters are needed in order to model the behavior of ^{222}Rn in the material – the diffusion length, i. e., the mean distance that a ^{222}Rn atom passes through the polymer before decaying, and the partition coefficient, i. e., the ratio of the concentration of the gas on the surface of the polymer to the concentration of the gas in the surrounding medium. With these two parameters it is possible to describe

the behavior of ^{222}Rn and ^{220}Rn for arbitrary size of the polymer for which they are determined, arbitrary activity concentration in the external medium and for arbitrary sorption and desorption durations.

To determine the diffusion length and the partition coefficient of ^{222}Rn in a given polymer, a several hundred micrometers thick sample of the material is prepared. The sample is then placed in a chamber with air containing ^{222}Rn with a known activity concentration. In order to determine the diffusion length, the sample is left to desorb in radon free air and the activity concentration of ^{222}Rn that is still inside is monitored in time [157]. In order to determine the partition coefficient it is necessary to determine the activity of ^{222}Rn that is contained inside the polymer just after it is removed from the radon containing atmosphere. A good way to measure the activity of radon in polymer samples is by dissolving them in a liquid scintillator and performing LS counting measurements.

The partition coefficients and diffusion lengths of ^{222}Rn in some polymers[3] at different temperatures were measured in the MIL laboratory. One of the experiments was dedicated to the estimation of the counting efficiency of the RackBeta 1219 LS spectrometer for LS counting of Makrofol N in a Toluene + PPO cocktail. In order to do this calibration, a foil was exposed to radon; then, it was dissolved in the toluene cocktail and measured on the RackBeta and on the TDCR-SU detector. The detection efficiency for ^{222}Rn of the RackBeta was estimated as the ratio of the counting rate of the LS counter and the TDCR-determined activity in the vial. The obtained value was $4.946(29)$ and was used further for the determination of the activity that was absorbed in the polymers. The results for the partition coefficients and diffusion length of the polymers are given in [156]. From practical point of view, the TDCR-SU detector appears to be an excellent reference instrument for the calibration of LS instruments for the measurement of the activity of ^{222}Rn sources.

3 polypropylene, low-density polyethylene, low-density polyethylene with antislip coating, high density polyethylene, Makrofol N, Makrofol DE and Makrofol DE for compact disks

SUMMARY OF PART III

SUMMARY The main focus in the third part of the thesis falls on the studies of the applications of the time distribution of scintillations, and digital list-mode acquisition in general, to radionuclide metrology using LS counting.

Chapter 7 explores the possibility for precise measurements of short half-lives of nuclear isomeric states using LS counting. The half-lives of two excited nuclear states in ^{57}Fe and one in ^{237}Np were measured by means of LS-LS and LS-γ coincidences. The half-life of the 59.54 keV level of ^{237}Np obtained by LS-γ coincidences is 67.60(25) ns, which is in good agreement with already published decay data. The measured half-life of the 14.4 keV level of ^{57}Fe is 97.9(3) ns which is consistent with some of the published results, however a significant discrepancy exist between the values found in the literature. The half-life of the shorter-lived 136.47 keV level of ^{57}Fe was measured also by LS-LS coincidences and the result is 8.78(4) ns. The result is consistent with the published data and comes with a significant improvement in the uncertainty.

The studies presented in Chapter 7 show that liquid scintillation fast timing measurements can be a useful tool to refine some already known decay times. The LS-LS coincidences method could allow more precise studies of half-lives of excited states of short-lived nuclides, where long measurements are difficult to perform. It could be valuable also when measuring isotopes in liquid phase. The studies show that LS-LS coincidences could be used for precise measurements of half-lives as short as 8 ns.

Off-line analysis of TDCR measurements allowed the development of an experimental method to evaluate the counting rate of accidental coincidences. These studies were central to the derivation of a set of analytical equations that can be used to evaluate random coincidences in any existing TDCR counter. The analytical method developed in this thesis was adapted in the extended international reference system for pure β-emitting radionuclides operated by the BIPM [158].

In Chapter 9 it is shown that both the detected coincidences and the TDCR estimated activities depend significantly on the choice of coincidence window. This dependence is attributed to the unequal loss of double and triple coincidences as well as to the different ionization quenching properties of the delayed scintillation component. Studies of Monte Carlo generated data shows that if the used cocktail has a non-negligible delayed fluorescence contribution, then, even for short coincidence resolving times, the activity of a low energy β-emitter would be overestimated. Despite the developed corrections for accidental coincidences in TDCR counting, the obtained results show that it is not yet advisable to use longer coincidence resolving times in TDCR measurements of low energy β-emitters. A primary method, different from the TDCR method, would be needed to measure the activity of a sample, so as to have a reference value. A good

candidate for such a method is the Compton coincidences and TDCR method discussed in Chapter 10.

The characterization and first results with a new C-TDCR system are shown in Chapter 10. The detector was designed in such a way as to allow changing the angle between the external source and the detector, thus changing the useful energy range of Compton electrons. An excellent agreement between the experimentally obtained scintillation response at 40° and at 90°. This is a good indication that the system is not biased towards a certain PMT. The system was used to measure the light output as a function of deposited energy for three commercial cocktails – UltimaGold, UltimaGold LLT and HionicFluor, and a home-made Toluene + PPO cocktail. The response of the cocktails was approximated with Birks' ionization quenching formula and a good agreement was observed. The measurements were made also with a set of grey filters, which allows to fix the kB parameter in the ionization quenching function more precisely. The results, however, lead to a much larger kB parameter than is commonly used in the TDCR method and what is found by the efficiency variation technique.

The C-TDCR system was also used to perform a comparison between three primary activity measurement methods – TDCR, CSET and C-TDCR. The activity obtained by the C-TDCR method was evaluated with four different assumptions for the function describing non-linearity of the light output of the scintillator in order to estimate the uncertainty on the calculated detection efficiency. The comparison between the three methods shows a large discrepancy between the TDCR activity at the kB parameter found by efficiency variation with grey filters and the C-TDCR activity. The results confirm the expectations laid out in Chapter 9, that the kB parameter could be underestimated by the efficiency variation technique due to the influence of the delayed fluorescence.

Chapter 11 summarizes some applications of the TDCR method for calibration and quality assurance of the activity measurements performed in the MIL laboratory at Sofia University.

12

CONCLUSIONS

In conclusion, the cross-correlation distribution, that describes the time intervals between the first detected events in each PMT within a given coincidence window, has been derived. The feasibility of using the derived theoretical model to fit experimental cross-correlation distributions and extract information about the FOM was evaluated. The preliminary results show that, if the decay constant of the scintillator is known, it would be possible to calculate the FOM and, from there, the activity of the sample. This constitutes a new approach at primary activity measurements using LS counting.

Perhaps the largest contribution of the thesis to radionuclide metrology using the TDCR method are the derived corrections for accidental coincidences. They can be used in any existing TDCR LS system that reports the single and coincidence counting rates. The corrections allow the measurement of radioactive sources with high activity, which can be encountered when performing *in situ* measurements of medical radioisotopes. Removing the influence of accidental coincidences gives the possibility to use long coincidence resolving times and study the time dependence of delayed fluorescence, which was shown to have a non-negligible effect on the TDCR calculated activity.

The studies of the influence of the coincidence window on TDCR measurements showed that, for some LS cocktails, there is a significant dependence of the calculated activity on the resolving time. Moreover, as the influence of delayed fluorescence depends also on the detection efficiency, the efficiency variation technique was shown to be potentially unreliable to determine the kB parameter of the ionization quenching function. This was emphasized by a discrepancy that was observed between the kb parameters obtained with efficiency variation with grey filters, as well as with chemical quenching.

As a possible solution to the problems related to the uncertainties regarding the light output of the scintillator, a Compton coincidences and TDCR system was investigated. It was shown that the non-linearity of the scintillator response can be studied in the interval between 2 keV and 8 keV energy of Compton electrons. The light output of several commercial scintillation cocktails was obtained and the optimal kB parameters in all cases were significantly higher that what is usually used in TDCR measurements. This indicates that conventional TDCR measurements of low-energy emitters such as ^{3}H and ^{55}Fe could underestimate the activity of the sample by as much as two or three percent. Perhaps, the accuracy of the standardization of low-energy emitters can be improved by the use of the Compton coincidences and TDCR technique.

Within this work, it was shown that LS counting and off-line data analysis can be useful tools for the study of half-lives of nuclear excited states as short as 8 ns. The half-lives of the long-lived excited states in ^{57}Fe and ^{237}Np were measured by LS-LS coincidences with 0.4% uncertainty.

Some applications of the TDCR method for calibration and quality assurance of the activity measurements performed in the MIL laboratory at Sofia University were shown.

A program called LIST_MODE_ANALYSIS was developed to analyze CAEN digitizer data, and it was used throughout the thesis. A Monte Carlo code to simulate the timing of detected scintillation events in a three-PMT detector was also developed. The code was used to validate a theoretical model of the timing of the prompt fluorescence. A fast software for the calculation of the model was developed in order to be able to fit the equations to real-world data.

CONTRIBUTIONS TO NEW KNOWLEDGE IN THE FIELD OF ACTIVITY MEASUREMENTS USING LS COUNTING

- Methods for the evaluation of accidental coincidence counting rates in TDCR measurements were proposed for the first time [P1].
- The cross-correlation distribution of the time intervals between detected scintillation events was derived, and it was shown how it can be used to determine the detection efficiency and activity of the sample [P2].

CONTRIBUTIONS TO METHODICAL ASPECTS IN THE FIELD OF LS COUNTING

- The effect of the delayed fluorescence on the activity calculated using the TDCR method has been demonstrated [P3].
- A comparison of two counting algorithms for TDCR measurements has been performed [P4]. The comparison demonstrates their advantages and disadvantages.
- The possibility to use digitized LS measurements for the precise determination of the half-life of some excited nuclear states has been demonstrated [P5].
- A software for the analysis of digitizer data has been developed. It has applications for TDCR measurements, cross-correlation measurements and C-TDCR measurements.
- A Monte Carlo code has been developed that gives the possibility to simulate the time interval distribution and the number of detected scintillation events in LS measurements.

PUBLICATIONS

PUBLICATIONS ON THE TOPIC OF THE THESIS

[P1] C. Dutsov, P. Cassette, B. Sabot, and K. Mitev. "Evaluation of the accidental coincidence counting rates in TDCR counting". In: *Nuclear Instruments and Methods in Physics Research, Section A: Accelerators, Spectrometers, Detectors and Associated Equipment* 977 (2020), p. 164292. DOI: 10.1016/j.nima.2020.164292 (cit. on p. 176).

[P2] Krasimir Mitev, Chavdar Dutsov, Philippe Cassette, and Benoît Sabot. "Time-domain based evaluation of of detection efficiency in liquid scintillation counting". In: *Scientific Reports, Nature Research* 11 (2021), p. 12424. DOI: 10.1038/s41598-021-91873-1 (cit. on p. 176).

[P3] C. Dutsov, P. Cassette, K. Mitev, and B. Sabot. "In quest of the optimal coincidence resolving time in TDCR LSC". In: *Nuclear Instruments and Methods in Physics Research, Section A: Accelerators, Spectrometers, Detectors and Associated Equipment* 987 (2021), p. 164846. DOI: 10.1016/j.nima.2020.164846 (cit. on p. 176).

[P4] C. Dutsov, K. Mitev, P. Cassette, and V. Jordanov. "Study of two different coincidence counting algorithms in TDCR measurements". In: *Applied Radiation and Isotopes* 154 (2019), p. 108895. DOI: 10.1016/j.apradiso.2019.108895 (cit. on p. 176).

[P5] Chavdar Dutsov, Benoît Sabot, Philippe Cassette, and Krasimir Mitev. "Measurement of the half-life of excited nuclear states using liquid scintillation counting". In: *Applied Radiation and Isotopes* 176 (Oct. 2021), p. 109845. DOI: 10.1016/j.apradiso.2021.109845 (cit. on p. 176).

[P6] V. Jordanov, P. Cassette, Ch. Dutsov, and K. Mitev. "Development and applications of a miniature TDCR acquisition system for in-situ radionuclide metrology". In: *Nuclear Instruments and Methods in Physics Research Section A: Accelerators, Spectrometers, Detectors and Associated Equipment* 954 (Feb. 2020), p. 161202. DOI: 10.1016/j.nima.2018.09.037.

[P7] Ph Cassette, A Arinc, M Capogni, P De Felice, C Dutsov, R Galea, E Garcia-Torano, K Kossert, J Liang, K Mitev, et al. "Results of the CCRI (II)-K2. H-3 key comparison 2018: measurement of the activity concentration of a tritiated-water source". In: *Metrologia* 57.1A (2020), p. 06004. DOI: 10.1088/0026-1394/57/1A/06004.

[P8] M. Hamel, B. Sabot, C. Dutsov, G. H. V. Bertrand, and K. Mitev. "Tuning the decay time of liquid scintillators". In: *Journal of Luminescence* 235 (2021), p. 118021. DOI: 10.1016/j.jlumin.2021.118021.

[P9] S. Georgiev, K. Mitev, C. Dutsov, T. Boshkova, and I. Dimitrova. "Partition coefficients and diffusion lengths of ^{222}Rn in some polymers at different temperatures". In: *International Journal of Environmental Research and Public Health* 16.22 (2019). URL: https://doi.org/10.3390/ijerph16224523.

OTHER PUBLICATIONS

[O1] K. Mitev, P. Cassette, D. Pressyanov, S. Georgiev, C. Dutsov, N. Michielsen, and B. Sabot. "Methods for the experimental study of ^{220}Rn homogeneity in calibration chambers". In: *Applied Radiation and Isotopes* 165 (2020), p. 109259. DOI: 10.1016/j.apradiso.2020.109259.

[O2] R. Merín, A. Tarancón, K. Mitev, S. Georgiev, C. Dutsov, H. Bagán, and J. F. García. "Evaluation of synthesis conditions for plastic scintillation foils used to measure α- and β-emitting radionuclides". In: *Journal of Radioanalytical and Nuclear Chemistry* 319.1 (2019), pp. 135–145. DOI: 10.1007/s10967-018-6341-z.

BIBLIOGRAPHY

[1] Bureau International des Poids et Mesures. *The International System of Units (SI)*. https://www.bipm.org/documents/20126/41483022/SI-Brochure-9-EN.pdf/2d2b50bf-f2b4-9661-f402-5f9d66e4b507. Accessed on 16.06.2021. BIPM, 2019 (cit. on p. 1).

[2] Ryszard Broda, Krzysztof Pochwalski, and Tomasz Radoszewski. "Calculation of liquid-scintillation detector efficiency". In: *International Journal of Radiation Applications and Instrumentation. Part A. Applied Radiation and Isotopes* 39.2 (1988), 159–164. DOI: 10.1016/0883-2889(88)90161-x (cit. on pp. 7, 116, 129, 199).

[3] A. Grau Malonda and Bert M. Coursey. "Calculation of beta-particle counting efficiency for liquid-scintillation systems with three phototubes". In: *International Journal of Radiation Applications and Instrumentation. Part A. Applied Radiation and Isotopes* 39.12 (Jan. 1988), pp. 1191–1196. DOI: 10.1016/0883-2889(88)90098-6 (cit. on pp. 7, 199).

[4] Donald L. Horrocks. *Applications of Liquid Scintillation Counting*. Elsevier, 1974. DOI: 10.1016/b978-0-12-356240-1.x5001-x (cit. on pp. 7, 20).

[5] J A B Gibson and H J Gale. "Absolute standardization with liquid scintillation counters". In: *J. Phys. E: Sci. Instrum.* 1.2 (Feb. 1968), pp. 99–106. DOI: 10.1088/0022-3735/1/2/305 (cit. on p. 7).

[6] V. Kolarov, Y. Le Gallic, and R. Vatin. "Mesure absolue directe de l'activité des emetteurs β purs par scintillation liquide". In: *The International Journal of Applied Radiation and Isotopes* 21.8 (Aug. 1970), pp. 443–452. DOI: 10.1016/0020-708x(70)90090-6 (cit. on p. 7).

[7] J. B. Birks. *The Theory and Practice of Scintillation Counting*. Oxford: Pergamon Press, 1964 (cit. on pp. 8, 11–13, 15, 129, 130, 134, 144, 159, 199).

[8] G. F. Knoll. *Radiation detection and measurement*. Wiley, 1989. ISBN: 978-047-181-5-0-4-4. URL: https://books.google.bg/books?id=dyBRAAAAMAAJ (cit. on p. 8).

[9] Mordechai Bixon and Joshua Jortner. "Intramolecular Radiationless Transitions". In: *The Journal of Chemical Physics* 48.2 (Jan. 1968), pp. 715–726. DOI: 10.1063/1.1668703 (cit. on p. 10).

[10] R. Voltz, J. Lopes da Silva, G. Laustriat, and A. Coche. "Influence of the Nature of Ionizing Particles on the Specific Luminescence of Organic Scintillators". In: *The Journal of Chemical Physics* 45.9 (Nov. 1966), pp. 3306–3311. DOI: 10.1063/1.1728106 (cit. on pp. 11, 15).

[11] G. T. Wright. "Scintillation Response of Organic Phosphors". In: *Phys. Rev.* 91.5 (Sept. 1953), pp. 1282–1283. DOI: 10.1103/physrev.91.1282.2 (cit. on pp. 11, 15).

[12] Ayataka Endo, Mai Ogasawara, Atsushi Takahashi, Daisuke Yokoyama, Yoshimine Kato, and Chihaya Adachi. "Thermally Activated Delayed Fluorescence from Sn^{4+}-Porphyrin Complexes and Their Application to Organic Light Emitting Diodes - A Novel Mechanism for Electroluminescence". In: *Advanced Materials* 21.47 (Aug. 2009), pp. 4802–4806. DOI: 10.1002/adma.200900983 (cit. on p. 11).

[13] Ayataka Endo, Keigo Sato, Kazuaki Yoshimura, Takahiro Kai, Atsushi Kawada, Hiroshi Miyazaki, and Chihaya Adachi. "Efficient up-conversion of triplet excitons into a singlet state and its application for organic light emitting diodes". In: *Applied Physics Letters* 98.8 (Feb. 2011), p. 083302. DOI: 10.1063/1.3558906 (cit. on p. 11).

[14] Hiroki Uoyama, Kenichi Goushi, Katsuyuki Shizu, Hiroko Nomura, and Chihaya Adachi. "Highly efficient organic light-emitting diodes from delayed fluorescence". In: *Nature* 492.7428 (Dec. 2012), pp. 234–238. DOI: 10.1038/nature11687 (cit. on p. 11).

[15] R. Voltz and G. Laustriat. "Radioluminescence des milieux organiques I. Étude cinétique". In: *Journal de Physique* 29.2-3 (1968), pp. 159–166. DOI: 10.1051/jphys:01968002902-3015900 (cit. on pp. 11, 12).

[16] J. B. Birks and J. C. Conte. "Excimer Fluorescence. XI. Solvent-Solute Energy Transfer". In: *Proceedings of the Royal Society of London. Series A, Mathematical and Physical Sciences* 303.1472 (1968), pp. 85–95. ISSN: 00804630. URL: http://www.jstor.org/stable/2415866 (cit. on pp. 11, 12).

[17] Paolo Lombardi, Fausto Ortica, Gioacchino Ranucci, and Aldo Romani. "Decay time and pulse shape discrimination of liquid scintillators based on novel solvents". In: *Nuclear Instruments and Methods in Physics Research Section A: Accelerators, Spectrometers, Detectors and Associated Equipment* 701 (Feb. 2013), pp. 133–144. DOI: 10.1016/j.nima.2012.10.061 (cit. on pp. 13, 129, 131, 159).

[18] G. Laustriat. "The luminescence decay of organic scintillators". In: *Molecular Crystals* 4.1-4 (June 1968), pp. 127–145. DOI: 10.1080/15421406808082905 (cit. on pp. 14, 137, 198).

[19] T. A. King and R. Voltz. "The time dependence of scintillation intensity in aromatic materials". In: *Proceedings of the Royal Society of London. Series A. Mathematical and Physical Sciences* 289.1418 (Jan. 1966), pp. 424–439. DOI: 10.1098/rspa.1966.0021 (cit. on pp. 13, 197, 198).

[20] C. N. Chou. "Saturation Effect of Plastic Scintillators". In: *Phys. Rev.* 87.5 (Sept. 1952), pp. 903–904. DOI: 10.1103/physrev.87.903 (cit. on p. 15).

[21] W. H. Bragg and R. Kleeman. "XXXIX. On the α particles of radium, and their loss of range in passing through various atoms and molecules". In: *The London, Edinburgh, and Dublin Philosophical Magazine and Journal of Science* 10.57 (Sept. 1905), pp. 318–340. DOI: 10.1080/14786440509463378 (cit. on p. 16).

[22] N. Bohr. "II. On the theory of the decrease of velocity of moving electrified particles on passing through matter". In: *The London, Edinburgh, and Dublin Philosophical Magazine and Journal of Science* 25.145 (Jan. 1913), pp. 10–31. DOI: 10.1080/14786440108634305 (cit. on p. 16).

[23] M. F. L'Annunziata. *Editor, Handbook of Radioactivity Analysis.* Third. Amsterdam, The Netherlands: Academic Press, Elsevier., 2012 (cit. on pp. 16, 99, 139).

[24] H. Bethe. "Bremsformel für Elektronen relativistischer Geschwindigkeit". In: *Zeitschrift für Physik* 76.5-6 (May 1932), pp. 293–299. DOI: 10.1007/bf01342532 (cit. on p. 16).

[25] M. J. Berger, M. Inokuti, H. H. Anderson, H. Bichsel, J. A. Dennis, D. Powers, S. M. Seltzer, and J. E. Turner. "Report 37". In: *Journal of the International Commission on Radiation Units and Measurements* os19.2 (Dec. 1984), NP–NP. DOI: 10.1093/jicru/os19.2.report37 (cit. on pp. 16, 32, 153).

[26] *Elemental composition of some LS cocktails produced by Perkin Elmer*. http://www.nucleide.org/ICRM_LSC_WG/icrmlsdata.htm. LNE-LNHB (cit. on pp. 17, 154).

[27] Ryszard Broda, Philippe Cassette, and Karsten Kossert. "Radionuclide metrology using liquid scintillation counting". In: *Metrologia* 44.4 (2007), S36 (cit. on pp. 17, 20–22, 26–31, 83, 139).

[28] *Photomultiplier tubes - basics and applications*. Third edition. Accessed on 16.05.2021. Hamamatsu photonics. 2007. URL: https://www.hamamatsu.com/resources/pdf/etd/PMT_handbook_v3aE.pdf (cit. on pp. 17–19, 31).

[29] Philippe Cassette and Jacques Bouchard. "The design of a liquid scintillation counter based on the triple to double coincidence ratio method". In: *Nuclear Instruments and Methods in Physics Research Section A: Accelerators, Spectrometers, Detectors and Associated Equipment* 505.1-2 (June 2003), pp. 72–75. DOI: 10.1016/s0168-9002(03)01023-4 (cit. on pp. 18, 31, 32).

[30] Xiaolin Hou and Xiongxin Dai. "Environmental liquid scintillation analysis". In: *Handbook of Radioactivity Analysis: Volume 2*. Elsevier, 2020, pp. 41–136. DOI: 10.1016/b978-0-12-814395-7.00002-7 (cit. on p. 20).

[31] Stefanie N. Smith and John G. Learned. "Liquid scintillation detectors for high energy neutrinos". In: *Progress in Particle and Nuclear Physics* 64.2 (Apr. 2010), pp. 384–389. DOI: 10.1016/j.ppnp.2009.12.055 (cit. on p. 20).

[32] Henry A Polach. "Evaluation and Status of Liquid Scintillation Counting for Radiocarbon Dating". In: *Radiocarbon* 29.1 (1987), pp. 1–11. URL: https://doi.org/10.1017/s0033822200043502 (cit. on p. 20).

[33] L. Liong Wee Kwong, J. J. La Rosa, S. H. Lee, and P. P. Povinec. In: *Journal of Radioanalytical and Nuclear Chemistry* 248.3 (2001), pp. 751–755. DOI: 10.1023/a:1010657131856 (cit. on p. 20).

[34] Ph Cassette, A Arinc, M Capogni, P De Felice, C Dutsov, R Galea, E Garcia-Torano, K Kossert, J Liang, K Mitev, et al. "Results of the CCRI (II)-K2. H-3 key comparison 2018: measurement of the activity concentration of a tritiated-water source". In: *Metrologia* 57.1A (2020), p. 06004. DOI: 10.1088/0026-1394/57/1A/06004 (cit. on pp. 20, 164–166).

[35] R. Galea, C. Michotte, M. Nonis, K. Moore, I. El Gamal, J. Keightley, and A. Fenwick. "The first official measurement of ^{11}C in the SIRTI". In: *Applied Radiation and Isotopes* 154 (Dec. 2019), p. 108834. DOI: 10.1016/j.apradiso.2019.108834 (cit. on p. 20).

[36] Yasushi Sato, Hidetake Ishizu, and Takahiro Yamada. "Standardization of ^{14}C by CIEMAT-NIST Method and TDCR Method". In: *RADIOISOTOPES* 65.1 (2016), pp. 1–5. DOI: 10.3769/radioisotopes.65.1 (cit. on p. 20).

[37] Miguel Roteta, Eduardo García-Toraño, and Leonor Rodríguez Barquero. "Standardization of ^{18}F by coincidence and LSC methods". In: *Applied Radiation and Isotopes* 64.10-11 (Oct. 2006), pp. 1199–1202. DOI: 10.1016/j.apradiso.2006.02.077 (cit. on p. 20).

[38] R. Fitzgerald, B. E. Zimmerman, D. E. Bergeron, J. C. Cessna, L. Pibida, and D. S. Moreira. "A new NIST primary standardization of ^{18}F". In: *Applied Radiation and Isotopes* 85 (Feb. 2014), pp. 77–84. DOI: 10.1016/j.apradiso.2013.11.116 (cit. on p. 20).

[39] O. Nähle, K. Kossert, and R. Klein. "Activity standardization of ^{22}Na". In: *Applied Radiation and Isotopes* 66.6-7 (June 2008), pp. 865–871. DOI: 10.1016/j.apradiso.2008.02.028 (cit. on p. 20).

[40] F. Jaubert and P. Cassette. "Standardization of a ^{32}P solution containing pure-beta impurities using the TDCR method in liquid scintillation counting". In: *Applied Radiation and Isotopes* 60.2-4 (Feb. 2004), pp. 601–606. DOI: 10.1016/j.apradiso.2003.11.084 (cit. on p. 20).

[41] B. R. S. Simpson and W. M. Morris. "The standardization of ^{33}P by the TDCR efficiency calculation technique". In: *Applied Radiation and Isotopes* 60.2-4 (Feb. 2004), pp. 465–468. DOI: 10.1016/j.apradiso.2003.11.060 (cit. on p. 20).

[42] JM Calhoun, BM Coursey, D Gray, and L Karam. "The standardization of ^{35}S methionine by liquid scintillation efficiency tracing with ^{3}H". In: *Liquid Scintillation Counting and Organic Scintillators*. Citeseer, 1991, p. 317 (cit. on p. 20).

[43] Karsten Kossert, Gerhard Jörg, and Christoph Lierse v. Gostomski. "Activity standardization of ^{41}Ca by means of liquid scintillation counting". In: *Radiochimica Acta* 97.1 (Jan. 2009), pp. 1–8. DOI: 10.1524/ract.2009.1571 (cit. on p. 20).

[44] B. E. Zimmerman and R. Colle. "Standardization of Ni-63 by 4πβ liquid scintillation spectrometry with H-3-standard efficiency tracing". In: *J. Res. Natl. Inst. Stand. Technol.* 102.4 (July 1997), p. 455. DOI: 10.6028/jres.102.031 (cit. on p. 20).

[45] B. M. Coursey, L. L. Lucas, A. Grau Malonda, and E. Garcia-Toraño. "The standardization of plutonium-241 and nickel-63". In: *Nuclear Instruments and Methods in Physics Research Section A: Accelerators, Spectrometers, Detectors and Associated Equipment* 279.3 (July 1989), pp. 603–610. DOI: 10.1016/0168-9002(89)91310-7 (cit. on p. 20).

[46] Denis E Bergeron, Jeffrey T Cessna, Ryan Fitzgerald, Leticia Pibida, and Brian E Zimmerman. "Standardization of ^{64}Cu activity". In: *Applied Radiation and Isotopes* 139 (2018), pp. 266–273 (cit. on p. 20).

[47] A. C. Razdolescu, Ph. Cassette, and M. Sahagia. "Measurement of ^{55}Fe solution activity by LSC-TDCR method". In: *Applied Radiation and Isotopes* 66.6-7 (June 2008), pp. 750–755. DOI: 10.1016/j.apradiso.2008.02.013 (cit. on p. 20).

[48] E. Günther. "Standardization of ^{59}Fe and 131I by liquid scintillation counting". In: *Nuclear Instruments Meth. Phys. Res. Section A: Accelerators, Spectrometers, Detectors and Associated Equipment* 339.1-2 (1994), pp. 402–407. DOI: 10.1016/0168-9002(94)91840-6 (cit. on p. 20).

[49] J. Steyn. "Special problems involved in liquid scintillation counting". In: *Nuclear Instruments and Methods* 112.1-2 (Sept. 1973), pp. 137–141. DOI: 10.1016/0029-554x(73)90787-8 (cit. on p. 20).

[50] B. E. Zimmerman, J. T. Cessna, and R. Fitzgerald. "Standardization of ^{68}Ge/^{68}Ga Using Three Liquid Scintillation Counting Based Methods". In: *J. Res. of the Nat. Institute of Standards Technology* 113.5 (2008), p. 265. DOI: 10.6028/jres.113.020 (cit. on p. 20).

[51] K. Kossert. "Activity standardization by means of a new TDCR-Čerenkov counting technique". In: *Applied Radiation and Isotopes* 68.6 (June 2010), pp. 1116–1120. DOI: 10.1016/j.apradiso.2009.12.038 (cit. on p. 20).

[52] K Kossert and H Schrader. "Activity standardization by liquid scintillation counting and half-life measurements of 90Y". In: *Applied radiation and isotopes* 60.5 (2004), pp. 741–749 (cit. on p. 20).

[53] K. Kossert and X. Mougeot. "Improved activity standardization of ^{90}Sr/^{90}Y by means of liquid scintillation counting". In: *Applied Radiation and Isotopes* 168 (2021), p. 109478. DOI: 10.1016/j.apradiso.2020.109478 (cit. on pp. 20, 27).

[54] B. Coursey, J. Gibson, M. Heitzmann, and J. Leak. "Standardization of technetium-99 by liquid-scintillation counting". In: *The Int. J. Appl. Radiation Isotopes* 35.12 (1984), pp. 1103–1112. DOI: 10.1016/0020-708x(84)90142-x (cit. on p. 20).

[55] A. Grau Malonda and B. Coursey. "Standardization of isomeric-transition radionuclides by liquid-scintillation efficiency tracing with hydrogen-3: Application to technetium-99m". In: *International Journal of Radiation Applications and Instrumentation. Part A. Applied Radiation and Isotopes* 38.9 (1987), pp. 695–700. DOI: 10.1016/0883-2889(87)90249-8 (cit. on p. 20).

[56] A. Chylinski and T. Radoszewski. "Standardization of ^{109}Cd by a 4π(LS)e-x coincidence method". In: *International Journal of Radiation Applications and Instrumentation. Part A. Applied Radiation and Isotopes* 38.10 (Jan. 1987), pp. 777–780. DOI: 10.1016/0883-2889(87)90172-9 (cit. on p. 20).

[57] K. Kossert, H. Janßen, R. Klein, M. K. H. Schneider, and H. Schrader. "Activity standardization and nuclear decay data of ^{109}Cd". In: *Applied Radiation and Isotopes* 64.9 (Sept. 2006), pp. 1031–1035. DOI: 10.1016/j.apradiso.2006.04.008 (cit. on p. 20).

[58] E. García-Toraño, M. Roteta, and L. Rodríguez Barquero. "Standardization of ^{110m}Ag by liquid scintillation and 4πβ–γ coincidence counting". In: *Applied Radiation and Isotopes* 52.3 (Mar. 2000), pp. 637–641. DOI: 10.1016/s0969-8043(99)00223-7 (cit. on p. 20).

[59] B. M. Coursey, D. B. Golas, D. H. Gray, D. D. Hoppes, and F. J. Schima. "Liquid-scintillation standardization of ^{123m}Te". In: *Nuclear Instruments and Methods in Physics Research Section A: Accelerators, Spectrometers, Detectors and Associated Equipment* 312.1-2 (Feb. 1992), pp. 121–123. DOI: 10.1016/0168-9002(92)90140-y (cit. on p. 20).

[60] Carlos J. da Silva, A. Iwahara, R. Poledna, E. M. de Oliveira, M. A. R. R. de Prinzio, José U. Delgado, and Ricardo T. Lopes. "Standardization of ^{241}Am, ^{124}Sb and ^{131}I by live-timed anti-coincidence counting with extending dead time". In: *Applied Radiation and Isotopes* 66.6-7 (June 2008), pp. 886–889. DOI: 10.1016/j.apradiso.2008.02.029 (cit. on p. 20).

[61] D. Bergeron, J. Cessna, R. Fitzgerald, L. Pibida, and B. Zimmerman. "Standardization of I-124 by three liquid scintillation-based methods". In: *Appl. Radiation Isotopes* 154 (2019), p. 108849. DOI: 10.1016/j.apradiso.2019.108849 (cit. on p. 20).

[62] P Cassette, J Bouchard, and B Chauvenet. "Standardization of iodine-129 by the TDCR liquid scintillation method and 4π β-γ coincidence counting". In: *Nuclear Instruments and Methods in Physics Research Section A: Accelerators, Spectrometers, Detectors and Associated Equipment* 339.1-2 (Jan. 1994), pp. 339–342. DOI: 10.1016/0168-9002(94)91828-7 (cit. on p. 20).

[63] E. García-Toraño, L. Rodrıguez Barquero, and M. Roteta. "Standardization of ^{134}Cs by three methods". In: *Applied Radiation and Isotopes* 56.1-2 (Jan. 2002), pp. 211–214. DOI: 10.1016/s0969-8043(01)00190-7 (cit. on p. 20).

[64] Karsten Kossert, Justyna Marganiec-Gałązka, and Ole J. Nähle. "Primary activity standardization of ^{134}Cs". In: *J Radioanal Nucl Chem* 314.2 (June 2017), pp. 545–553. DOI: 10.1007/s10967-017-5338-3 (cit. on p. 20).

[65] R. Broda, M. N. Péron, P. Cassette, T. Terlikowska, and D. Hainos. "Standardization of ^{139}Ce by the liquid scintillation counting using the triple to double coincidence ratio method". In: *Applied Radiation and Isotopes* 49.9-11 (Aug. 1998), pp. 1035–1040. DOI: 10.1016/s0969-8043(97)10016-1 (cit. on p. 20).

[66] B. M. Coursey, D. D. Hoppes, F. J. Schima, and M. P. Unterweger. "The standardization of samarium-153". In: *International Journal of Radiation Applications and Instrumentation. Part A. Applied Radiation and Isotopes* 38.1 (Jan. 1987), pp. 31–34. DOI: 10.1016/0883-2889(87)90232-2 (cit. on p. 20).

[67] N. E Bowles, S. A Woods, D. H Woods, S. M Jerome, M. J Woods, P de Lavison, S Lineham, J Keightley, and I Poupaki. "Standardization of ^{153}Sm". In: *Applied Radiation and Isotopes* 49.9-11 (Aug. 1998), pp. 1345–1347. DOI: 10.1016/s0969-8043(97)10071-9 (cit. on p. 20).

[68] B. E Zimmerman, M. P Unterweger, and J. W Brodack. "The standardization of ^{177}Lu by 4πβ liquid scintillation spectrometry with ^{3}H-standard efficiency tracing". In: *Applied Radiation and Isotopes* 54.4 (Feb. 2001), pp. 623–631. DOI: 10.1016/s0969-8043(00)00316-x (cit. on p. 20).

[69] B. M. Coursey et al. "The standardization and decay scheme of rhenium-186". In: *International Journal of Radiation Applications and Instrumentation. Part A. Applied Radiation and Isotopes* 42.9 (Jan. 1991), pp. 865–869. DOI: 10.1016/0883-2889(91)90226-q (cit. on p. 20).

[70] F. Jaubert. "Standardization of a ^{186}Re sodium perrhenate radiochemical solution using the TDCR method in liquid scintillation counting". In: *Applied Radiation and Isotopes* 66.6-7 (June 2008), pp. 960–964. DOI: 10.1016/j.apradiso.2008.02.065 (cit. on p. 20).

[71] Brian E Zimmerman, Jeffrey T Cessna, and Michael P Unterweger. "The standardization of ^{188}W/^{188}Re by 4πβ liquid scintillation spectrometry with the CIEMAT/NIST ^{3}H-standard efficiency tracing method". In: *Applied Radiation and Isotopes* 56.1-2 (Jan. 2002), pp. 315–320. DOI: 10.1016/s0969-8043(01)00207-x (cit. on p. 20).

[72] A. Cristina Razdolescu and P. Cassette. "Standardization of tritiated water and ^{204}Tl by TDCR liquid scintillation counting". In: *Appl. Radiation Isotopes* 60.2-4 (2004), pp. 493–497. DOI: 10.1016/j.apradiso.2003.11.065 (cit. on p. 20).

[73] L. Laureano-Pérez, R. Collé, R. Fitzgerald, I. Outola, and L. Pibida. "A liquid-scintillation-based primary standardization of ^{210}Pb". In: *Appl. Radiation Isotopes* 65.12 (2007), pp. 1368–1380. DOI: 10.1016/j.apradiso.2007.06.012 (cit. on p. 20).

[74] P. Cassette, M. Sahagia, L. Grigorescu, M. C. Lépy, and J. L. Picolo. "Standardization of ^{222}Rn by LSC and comparison with α- and γ-spectrometry". In: *Applied Radiation and Isotopes* 64.10-11 (Oct. 2006), pp. 1465–1470. DOI: 10.1016/j.apradiso.2006.02.068 (cit. on pp. 20, 50, 166, 167).

[75] J. Cessna and B. Zimmerman. "Standardization of radium-223 by liquid scintillation counting". In: *Appl. Radiation Isotopes* 68.7-8 (2010), pp. 1523–1528. DOI: 10.1016/j.apradiso.2009.11.068 (cit. on p. 20).

[76] RFP Simões, CJ da Silva, RL da Silva, LV de Sá, R Poledna, AE de Oliveira, A Iwahara, PAL da Cruz, and JU Delgado. "Standardization of ^{223}Ra by live-time anticoincidence counting and gamma-ray emission determination". In: *Applied Radiation and Isotopes* 170 (2021), p. 109559 (cit. on p. 20).

[77] E. Napoli, J. T. Cessna, R. Fitzgerald, L. Pibida, R. Collé, L. Laureano-Pérez, B. E. Zimmerman, and D. E. Bergeron. "Primary standardization of ^{224}Ra activity by liquid scintillation counting". In: *Applied Radiation and Isotopes* 155 (2020), p. 108933. DOI: 10.1016/j.apradiso.2019.108933 (cit. on p. 20).

[78] J. M. Lee, K. B. Lee, M. K. Lee, P. J. Oh, T. S. Park, and H. Y. Hwang. "Standardization of ^{125}I and ^{238}Pu". In: *Applied Radiation and Isotopes* 60.2-4 (Feb. 2004), pp. 397–401. DOI: 10.1016/j.apradiso.2003.11.048 (cit. on p. 20).

[79] C. Balpardo, M. E. Capoulat, D. Rodrigues, and P. Arenillas. "Standardization of ^{241}Am by digital coincidence counting, liquid scintillation counting and defined solid angle counting". In: *Applied Radiation and Isotopes* 68.7-8 (July 2010), pp. 1358–1361. DOI: 10.1016/j.apradiso.2009.12.010 (cit. on p. 20).

[80] P Cassette, R Broda, D Hainos, and T Terlikowska. "Analysis of detection-efficien-cy variation techniques for the implementation of the TDCR method in liquid scintillation counting". In: *Applied Radiation and Isotopes* 52.3 (Mar. 2000), pp. 643–648. DOI: 10.1016/s0969-8043(99)00224-9 (cit. on pp. 21, 31, 33, 34, 130, 142, 154).

[81] A. Grau Malonda. "Poissonian And Binomial Models In Radionuclide Metrology By Liquid Scintillation Counting". In: *CIEMAT* (1990). URL: http://www.iaea.org/inis/collection/NCLCollectionStore/_Public/22/081/22081242.pdf (cit. on p. 24).

[82] C. Bobin, C. Thiam, B. Chauvenet, and J. Bouchard. "On the stochastic dependence between photomultipliers in the TDCR method". In: *Applied Radiation and Isotopes* 70.4 (Apr. 2012), pp. 770–780. DOI: 10.1016/j.apradiso.2011.12.035 (cit. on pp. 25, 114).

[83] Ph. Cassette. *Programme de calcul du spectre en énergie des électrons émis par des radionucléides émetteurs bêta*. LPRI/92/307/Juillet (cit. on pp. 26, 32).

[84] Xavier Mougeot. "BetaShape: A new code for improved analytical calculations of beta spectra". In: *EPJ Web of Conferences* 146.12015 (Sept. 2017). DOI: 10.1051/epjconf/201714612015 (cit. on p. 27).

[85] M. A. Kellett and O. Bersillon. "The Decay Data Evaluation Project (DDEP) and the JEFF-3.3 radioactive decay data library: Combining international collaborative efforts on evaluated decay data". In: *EPJ Web Conferences* 146 (2017). Ed. by A. Plompen, F.-J. Hambsch, P. Schillebeeckx, W. Mondelaers, J. Heyse, S. Kopecky, P. Siegler, and S. Oberstedt, p. 02009. DOI: 10.1051/epjconf/201714602009 (cit. on pp. 27, 110).

[86] Karsten Kossert and Xavier Mougeot. "The importance of the beta spectrum calculation for accurate activity determination of 63 Ni by means of liquid scintillation counting". In: *Applied Radiation and Isotopes* 101 (July 2015), pp. 40–43. DOI: 10.1016/j.apradiso.2015.03.017 (cit. on p. 27).

[87] X. Mougeot. "Towards high-precision calculation of electron capture decays". In: *Applied Radiation and Isotopes* 154 (Dec. 2019), p. 108884. DOI: 10.1016/j.apradiso.2019.108884 (cit. on p. 27).

[88] P Cassette. "Evaluation of the influence of wall effects on the liquid scintillation counting detection efficiency for the standardization of high-energy beta and alpha radionuclides". In: *Proc. of the Int. Conf. on Advances in Liquid Scintillation Spectrometry (Karlsruhe, Germany, 7–11 May 2001)*. 2001 (cit. on p. 27).

[89] R Broda. "A review of the triple-to-double coincidence ratio (TDCR) method for standardizing radionuclides". In: *Applied Radiation and Isotopes* 58.5 (May 2003), pp. 585–594. DOI: 10.1016/s0969-8043(03)00056-3 (cit. on p. 29).

[90] O. Nähle, K. Kossert, and J. Brunzendorf. "Study of the light emission process for the design of liquid scintillation counters". In: *LSC 2008, Advances in liquid scintillation spectrometry* (2009), pp. 87–95. URL: http://citeseerx.ist.psu.edu/viewdoc/download?doi=10.1.1.658.1144 (cit. on p. 30).

[91] Hamamatsu. *Photomultiplier tubes R7600U series*. R7600U-200. Accessed on 16.05.2021. Hamamatsu photonics. 2016. URL: https://www.hamamatsu.com/eu/en/product/type/R7600U-20/index.html (cit. on pp. 31, 75, 99, 130).

[92] Ryszard Broda and Krzysztof Pochwalski. "The enhanced triple to double coincidence ratio (ETDCR) method for standardization of radionuclides by liquid scintillation counting". In: *Nuclear Instruments and Methods in Physics Research Section A: Accelerators, Spectrometers, Detectors and Associated Equipment* 312.1-2 (Feb. 1992), pp. 85–89. DOI: 10.1016/0168-9002(92)90133-o (cit. on p. 32).

[93] *Detection efficiency calculation for pure-beta radionuclides, program with short tutorial*. http://www.nucleide.org/ICRM_LSC_WG/icrmsoftware.htm. Accessed on 16.05.2021. LNHB, 2021 (cit. on pp. 32, 33, 52, 85, 135, 157, 165).

[94] Zhenyu Tan and Yueyuan Xia. "Stopping power and mean free path for low-energy electrons in ten scintillators over energy range of 20 – 20 000 eV". In: *Applied Radiation and Isotopes* 70.1 (Jan. 2012), pp. 296–300. DOI: 10.1016/j.apradiso.2011.08.012 (cit. on pp. 32, 135, 154, 157).

[95] M. Péron and P. Cassette. "COCO, a Compton coincidence experiment to study liquid scintillator response in the 1–20 keV energy range". In: *Nuclear Instruments Meth. Phys. Res. Section A: Accelerators, Spectrometers, Detectors and Associated Equipment* 353.1-3 (1994), pp. 41–45. DOI: 10.1016/0168-9002(94)91598-9 (cit. on pp. 35, 147).

[96] M. N. Peron and P. Cassette. "A Compton coincidence study of liquid scintillator response to low-energy electrons". In: *Nuclear Instruments and Methods in Physics Research Section A: Accelerators, Spectrometers, Detectors and Associated Equipment* 369.2-3 (Feb. 1996), pp. 344–347. DOI: 10.1016/s0168-9002(96)80006-4 (cit. on p. 35).

[97] P. Cassette and P. Do. "The Compton source efficiency tracing method in liquid scintillation counting: A new standardization method using a TDCR counter with a Compton spectrometer". In: *Appl. Radiation Isotopes* 66.6-7 (2008), pp. 1026–1032. DOI: 10.1016/j.apradiso.2008.02.062 (cit. on pp. 35–37, 147, 150, 156–158).

[98] L. J. Bignell, L. Mo, T. Steele, and S. Reza Hashemi-Nezhad. "The Zero Model by Using Coincidence Scintillation (ZoMBieS) Method of Absolute Radioactivity Measurement". In: *IEEE Transactions on Nuclear Sci.* 60.5 (2013), pp. 4007–4014. DOI: 10.1109/tns.2013.2275990 (cit. on pp. 36, 156, 158, 159).

[99] Agustín Grau Malonda and Eduardo Garcia-Toraño. "Evaluation of counting efficiency in liquid scintillation counting of pure β-ray emitters". In: *The International Journal of Applied Radiation and Isotopes* 33.4 (Apr. 1982), pp. 249–253. DOI: 10.1016/0020-708x(82)90022-9 (cit. on p. 36).

[100] J. Bouchard and P. Cassette. "MAC3: an electronic module for the processing of pulses delivered by a three photomultiplier liquid scintillation counting system". In: *Applied Radiation and Isotopes* 52.3 (Mar. 2000), pp. 669–672. DOI: 10.1016/s0969-8043(99)00228-6 (cit. on pp. 42, 47, 114, 129, 146, 156).

[101] V. Jordanov, P. Cassette, Ch. Dutsov, and K. Mitev. "Development and applications of a miniature TDCR acquisition system for in-situ radionuclide metrology". In: *Nuclear Instruments and Methods in Physics Research Section A: Accelerators, Spectrometers, Detectors and Associated Equipment* 954 (Feb. 2020), p. 161202. DOI: 10.1016/j.nima.2018.09.037 (cit. on pp. 42, 47, 113, 130, 140, 163).

[102] T. Steele, L. Mo, L. Bignell, M. Smith, and D. Alexiev. "FASEA: A FPGA Acquisition System and Software Event Analysis for liquid scintillation counting". In: *Nuclear Instruments and Methods in Physics Research Section A: Accelerators,*

Spectrometers, Detectors and Associated Equipment 609.2-3 (Oct. 2009), pp. 217–220. DOI: 10.1016/j.nima.2009.07.045 (cit. on pp. 44, 81, 113, 130).

[103] Ch Dutsov, K. Mitev, P. Cassette, and V. Jordanov. "Study of two different coincidence counting algorithms in TDCR measurements". In: *Applied Radiation and Isotopes* 154 (Dec. 2019), p. 108895. DOI: 10.1016/j.apradiso.2019.108895 (cit. on pp. 47, 50, 58, 93, 124, 127).

[104] K. Mitev, P. Cassette, V. Jordanov, H. R. Liu, and Ch. Dutsov. "Design and performance of a miniature TDCR counting system". In: *Journal of Radioanalytical and Nuclear Chemistry* 314.2 (Sept. 2017), pp. 583–589. DOI: 10.1007/s10967-017-5451-3 (cit. on pp. 50, 113, 130, 147, 163).

[105] Chavdar Dutsov, Philippe Cassette, Krasimir Mitev, and Benoît Sabot. "In quest of the optimal coincidence resolving time in TDCR LSC". In: *Nuclear Instruments and Methods in Physics Research Section A: Accelerators, Spectrometers, Detectors and Associated Equipment* (Nov. 2020), p. 164846. DOI: 10.1016/j.nima.2020.164846 (cit. on pp. 57, 157, 159, 160).

[106] A. G. Malonda. *Free Parameter Models in Liquid Scintillation Counting*. Colección Documentos CIEMAT. CIEMAT, 1999. ISBN: 978-8478-34-3-5-0-8. URL: https://books.google.ch/books?id=YR5EQwAACAAJ (cit. on p. 70).

[107] X. Mougeot. "Reliability of usual assumptions in the calculation of β and ν spectra". In: *Physical Review C* 91.5 (May 2015). DOI: 10.1103/physrevc.91.055504 (cit. on pp. 70, 200, 206).

[108] X. Mougeot. "Erratum: Reliability of usual assumptions in the calculation of β and ν spectra [Phys. Rev. C91, 055504 (2015)]". In: *Physical Review C* 92.5 (Nov. 2015). DOI: 10.1103/physrevc.92.059902 (cit. on pp. 70, 200, 206).

[109] CAEN. *CAEN DT5751 digitizer manual*. https://www.caen.it/products/dt5751/. Accessed on 16.05.2021. CAEN, 2020 (cit. on pp. 76, 100, 130).

[110] Joseph R. Lakowicz, ed. *Principles of Fluorescence Spectroscopy*. Springer US, 2006. DOI: 10.1007/978-0-387-46312-4 (cit. on p. 84).

[111] Yannick Lecompte, Martine Rosset, Jérôme Loess, Nadine Chianea, Flora Jourquin, Alain Cazoulat, and Philippe Cassette. "Tritium analysis in urine by the Triple-To-Double Coincidence Ratio Method with the Hi-dex 300 SL liquid scintillation Counter". In: *Radiation Protection Dosimetry* 188.2 (Dec. 2019), pp. 148–161. DOI: 10.1093/rpd/ncz270 (cit. on p. 91).

[112] Karsten Kossert, Gerhard Jörg, Ole Nähle, and Christoph Lierse v. Gostomski. "High-precision measurement of the half-life of ^{147}Sm". In: *Applied Radiation and Isotopes* 67.9 (Sept. 2009), pp. 1702–1706. DOI: 10.1016/j.apradiso.2009.03.013 (cit. on p. 99).

[113] Karsten Kossert, Gerhard Jörg, and Christoph Lierse v. Gostomski. "Experimental half-life determination of ^{176}Lu". In: *Applied Radiation and Isotopes* 81 (Nov. 2013), pp. 140–145. DOI: 10.1016/j.apradiso.2013.03.033 (cit. on p. 99).

[114] Jérôme Chmeleff, Friedhelm von Blanckenburg, Karsten Kossert, and Dieter Jakob. "Determination of the ^{10}Be half-life by multicollector ICP-MS and liquid scintillation counting". In: *Nuclear Instruments and Methods in Physics Research Section B: Beam Interactions with Materials and Atoms* 268.2 (Jan. 2010), pp. 192–199. DOI: 10.1016/j.nimb.2009.09.012 (cit. on p. 99).

[115] Karsten Kossert. "Half-life measurement of ^{212}Pb by means of a liquid scintillator-based ^{220}Rn trap". In: *Applied Radiation and Isotopes* 125 (July 2017), pp. 15–17. DOI: 10.1016/j.apradiso.2017.03.026 (cit. on p. 99).

[116] Karsten Kossert, Marcell Péter Takács, and Ole Nähle. "Determination of the activity of ^{225}Ac and of the half-lives of ^{213}Po and ^{225}Ac". In: *Applied Radiation and Isotopes* 156 (Feb. 2020), p. 109020. DOI: 10.1016/j.apradiso.2019.109020 (cit. on p. 99).

[117] Amptek. *AMPTEK, X-Ray and gamma ray detector high resolution CdTe Cadmium Telluride, XR-100T-CdTe*. http://www.amptek.com. Accessed on 16.05.2021. AMPTEK, 2020 (cit. on p. 99).

[118] J. Radeloff, N. Buttler, W. Kesternich, and E. Bodenstedt. "Measurement of lifetimes up to one second of isometric nuclear states populated in the decay of radioactive sources". In: *Nuclear Instruments and Methods* 47.1 (Jan. 1967), pp. 109–115. DOI: 10.1016/0029-554x(67)90170-x (cit. on p. 101).

[119] gnuplot. *gnuplot fitting algorithms manual*. http://gnuplot.sourceforge.net/docs_4.2/node82.html. Accessed on 16.05.2021. gnuplot, 2020 (cit. on p. 102).

[120] J.-P. Briand, B. d'Etat Ban, D. Schneider, M. A. Briere, V. Decaux, J. W. McDonald, and S. Bardin. "Time for the emptyLshell of a hollow atom to be filled". In: *Physical Review A* 53.4 (Apr. 1996), pp. 2194–2199. DOI: 10.1103/physreva.53.2194 (cit. on p. 102).

[121] M. M. Bé et al. *Table of Radionuclides*. Vol. 8. Monographie BIPM-5. Pavillon de Breteuil, F-92310 Sèvres, France: Bureau International des Poids et Mesures, 2016. ISBN: 978-928-222-2-6-4-5. URL: http://www.bipm.org/utils/common/pdf/monographieRI/Monographie_BIPM-5_Tables_Vol8.pdf (cit. on pp. 103, 107).

[122] G. Suliman et al. "Half-lives of ^{221}Fr, ^{217}At, ^{213}Bi, ^{213}Po and ^{209}Pb from the ^{225}Ac decay series". In: *Applied Radiation and Isotopes* 77 (July 2013), pp. 32–37. DOI: 10.1016/j.apradiso.2013.02.008 (cit. on p. 109).

[123] M. A. Clark. "Atomic Energy of Canada Limited Report AECL-1337". In: (1961), p. 40 (cit. on p. 110).

[124] O. C. Kistner and A. W. Sunyar. "Excited States of ^{57}Fe Populated in ^{57}Co Decay". In: *Physical Review* 139.2B (July 1965), B295–B299. DOI: 10.1103/physrev.139.b295 (cit. on p. 110).

[125] M Eckhause, R J Jr Harris, W B Shuler, and R E Welsh. "A measurement of the lifetime of the 14.4 keV level of ^{57}Fe". In: *Proceedings of the Physical Society* 89.1 (Sept. 1966), pp. 187–188. DOI: 10.1088/0370-1328/89/1/130 (cit. on p. 111).

[126] C. Hohenemser, R. Reno, H. C. Benski, and J. Lehr. "Time-Differential Perturbed Angular-Correlation Experiment for ^{57}Fe in a Ni Host and a Comparison with the Mössbauer Effect". In: *Physical Review* 184.2 (Aug. 1969), pp. 298–302. DOI: 10.1103/physrev.184.298 (cit. on p. 111).

[127] B. A. Alikov, Ya. Babryshchuk, G. I. Lizurei, K. M. Muminov, T. M. Muminov, Yu.S. Salikhbaev, and R. R. Usmanov. In: *Journal of the Joint Institute for Nuclear Research* 13.P13 (1978), p. 10911 (cit. on p. 111).

[128] I. Ahmad, K. E. Rehm, E. P. Kanter, W. Kutschera, W. R. Phillips, and A. R. Barnett. "Half-lives of isomeric states in ^{57}Fe and ^{83}Kr". In: *Physical Review C* 52.4 (Oct. 1995), pp. 2240–2241. DOI: 10.1103/physrevc.52.2240 (cit. on p. 111).

[129] V. A. Morozov, N. V. Morozova, T. Badica, Gh. Cata-Danil, D. Ghita, and I. V. Popescu. "Measurement of the half-life for two ^{57}Fe excited states by a single-crystal scintillation time spectrometer". In: *Nuclear Instruments and Methods in Physics Research Section A: Accelerators, Spectrometers, Detectors and Associated Equipment* 566.2 (Oct. 2006), pp. 448–451. DOI: 10.1016/j.nima.2006.06.059 (cit. on p. 111).

[130] M. S. Basunia. "Nuclear Data Sheets for A = 237". In: *Nuclear Data Sheets* 107.8 (Aug. 2006), pp. 2323–2422. DOI: 10.1016/j.nds.2006.07.001 (cit. on p. 111).

[131] G. H. Miller, P. Dillard, M. Eckhause, and R. E. Welsh. "Determinations of nuclear level half-lives in ^{85}Rb and ^{237}Np and their use as timing standards". In: *Nuclear Instruments and Methods* 104.1 (Oct. 1972), pp. 11–12. DOI: 10.1016/0029-554x(72)90290-x (cit. on p. 111).

[132] Chavdar Dutsov, Benoît Sabot, Philippe Cassette, and Krasimir Mitev. "Measurement of the half-life of excited nuclear states using liquid scintillation counting". In: *Applied Radiation and Isotopes* 176 (Oct. 2021), p. 109845. DOI: 10.1016/j.apradiso.2021.109845 (cit. on p. 112).

[133] Giuliano Mini, Francesco Pepe, Carlo Tintori, and Marco Capogni. "A full digital approach to the TDCR method". In: *Applied Radiation and Isotopes* 87 (May 2014), pp. 166–170. DOI: 10.1016/j.apradiso.2013.11.103 (cit. on p. 113).

[134] C. Bobin, J. Bouchard, and B. Censier. "First results in the development of an on-line digital counting platform dedicated to primary measurements". In: *Applied Radiation and Isotopes* 68.7-8 (July 2010), pp. 1519–1522. DOI: 10.1016/j.apradiso.2009.11.067 (cit. on pp. 113, 130).

[135] Marco Capogni and Pierino De Felice. "A prototype of a portable TDCR system at ENEA". In: *Applied Radiation and Isotopes* 93 (Nov. 2014), pp. 45–51. DOI: 10.1016/j.apradiso.2014.03.021 (cit. on pp. 113, 130, 147).

[136] L. Jánossy. "Rate of n-fold Accidental Coincidences". In: *Nature* 153.3875 (Feb. 1944), pp. 165–165. DOI: 10.1038/153165a0 (cit. on p. 117).

[137] L. Mo, L. J. Bignell, T. Steele, and D. Alexiev. "Activity measurements of ^{3}H using the TDCR method and observation of source stability". In: *Applied Radiation and Isotopes* 68.7-8 (July 2010), pp. 1540–1542. DOI: 10.1016/j.apradiso.2009.11.059 (cit. on p. 129).

[138] E. Halter, C. Thiam, C. Bobin, J. Bouchard, D. Chambellan, B. Chauvenet, M. Hamel, L. Rocha, M. Trocmé, and R. Woo. "First TDCR measurements at low energies using a miniature x-ray tube". In: *Applied Radiation and Isotopes* 93 (Nov. 2014), pp. 7–12. DOI: 10.1016/j.apradiso.2014.03.007 (cit. on p. 129).

[139] Chavdar Dutsov, Philippe Cassette, Benoît Sabot, and Krasimir Mitev. "Evaluation of the accidental coincidence counting rates in TDCR counting". In: *Nuclear Instruments and Methods in Physics Research Section A: Accelerators, Spectrometers, Detectors and Associated Equipment* 977 (Oct. 2020), p. 164292. DOI: 10.1016/j.nima.2020.164292 (cit. on pp. 130, 138).

[140] P. Cassette and R. Vatin. "Experimental evaluation of TDCR models for the 3 PM liquid scintillation counter". In: *Nuclear Instruments and Methods in Physics Research Section A: Accelerators, Spectrometers, Detectors and Associated Equipment* 312.1-2 (Feb. 1992), pp. 95–99. DOI: 10.1016/0168-9002(92)90135-q (cit. on pp. 130, 140).

[141] J. Nelder and R. Mead. "A Simplex Method for Function Minimization". In: *Comput. J.* 7 (1965), pp. 308–313 (cit. on p. 131).

[142] C. Fuchs, F. Heisel, and R. Voltz. "Formation of excited singlet states in irradiated aromatic liquids". In: *The Journal of Physical Chemistry* 76.25 (Dec. 1972), pp. 3867–3875. DOI: 10.1021/j100669a033 (cit. on p. 137).

[143] C. Dutsov, P. Cassette, K. Mitev, and B. Sabot. "In quest of the optimal coincidence resolving time in TDCR LSC". In: *Nuclear Instruments and Methods in Physics Research, Section A: Accelerators, Spectrometers, Detectors and Associated Equipment* 987 (2021), p. 164846. DOI: 10.1016/j.nima.2020.164846 (cit. on p. 146).

[144] Consultative Committee for Mass and Related Quantities. *Key Comparison Report Template*. https://www.bipm.org/documents/20126/2071009/CCM+Key+Comparison+Report+Template.pdf/cf0a4b60-2ece-819c-e50f-f91972f29901. Accessed on 16.06.2021. BIPM, 2019 (cit. on p. 164).

[145] Chavdar Dutsov, Krasimir Mitev, and Philippe Cassette. "Characterization of filters for efficiency variation in TDCR". In: *2018 IEEE Nuclear Science Symposium and Medical Imaging Conference Proceedings (NSS/MIC)*. IEEE. 2018, pp. 1–3. DOI: 10.1109/nssmic.2018.8824752 (cit. on p. 165).

[146] World Health Organization. *WHO Handbook on Indoor Radon - A Public Health Perspective.* http://www.who.int/en/ (cit. on p. 166).

[147] United Nations Scientific Committee on the Effects of Atomic Radiation. *UNSCEAR 2000 Report to the General Assembly, with Scientific Annexes. Sources and effects of ionizing radiation.* New York, NY, USA: UN Publications, 2008 (cit. on p. 166).

[148] Laina Salonen. "Calibration of the direct LSC method for radon in drinking water: Interference from 210Pb and its progenies accumulated in 226Ra standard solution". In: *Applied Radiation and Isotopes* 68.1 (Jan. 2010), pp. 131–138. DOI: 10.1016/j.apradiso.2009.08.006 (cit. on p. 166).

[149] Krasimir K. Mitev. "Measurement of ^{222}Rn by absorption in plastic scintillators and alpha/beta pulse shape discrimination". In: *Applied Radiation and Isotopes* 110 (2016), pp. 236–243 (cit. on pp. 167, 170).

[150] European Commission. Joint Research Centre. *Technical report on the REM 2018 radon-in-water proficiency test.* Publications Office, 2020. DOI: 10.2760/805627 (cit. on pp. 167, 169).

[151] Vadim Tsoupko-Sitnikov. *Results of the Proficiency Test 163 RN 300*. Environmental Analysis and Metrology Department, IRSN, 2020 (cit. on pp. 169, 170).

[152] H. Möre and L. M. Hubbard. "^{222}Rn Absorption in Plastic Holders for Alpha Track Detectors: A Source of Error." In: *Rad. Prot. Dosim.* 74 (1997), pp. 85–91 (cit. on p. 170).

[153] Wolfgang Rau. "Measurement of radon diffusion in polyethylene based on alpha detection." In: *Nuclear Instrments and Methods in Physics Research A* 664 (2012), pp. 65–70 (cit. on p. 170).

[154] Masaaki Saito, Yoshlyuki Tanizaki, and Shlgeru Takata. "A New Monitor for Radon in Water Using Absorptive Plastic Scintillation Counting". In: *Radioisotopes (Tokyo)* 55.2 (2006). in Japanese, pp. 55–60 (cit. on p. 170).

[155] D. Pressyanov, A. Van Deynse, J. Buysse, A. Poffijn, and G. Meesen. "Polycarbonates: A New Retrospective Radon Monitor." In: *Proceedings of IRPA Regional Congress on Radiation Protection in Central Europe.* International Radiation Protection Association. Cedex, France, 1999, pp. 716–722 (cit. on p. 170).

[156] S. Georgiev, K. Mitev, C. Dutsov, T. Boshkova, and I. Dimitrova. "Partition coefficients and diffusion lengths of ^{222}Rn in some polymers at different temperatures". In: *International Journal of Environmental Research and Public Health* 16.22 (2019). URL: https://doi.org/10.3390/ijerph16224523 (cit. on pp. 170, 171).

[157] Krasimir K. Mitev, P. Cassette, S. Georgiev, I. Dimitrova, B. Sabot, T. Boshkova, and I. Tartes. "Determination of ^{222}Rn absorption properties of polycarbonate foils by liquid scintillation counting. Application to ^{222}Rn measurements". In: *Applied Radiation and Isotopes* 109 (2016), pp. 270–275 (cit. on p. 171).

[158] Romain Coulon, Steven Judge, Haoran Liu, and Carine Michotte. "The international reference system for pure beta-particle emitting radionuclides: an evaluation of the measurement uncertainties". In: *Metrologia* 58.2 (Mar. 2021), p. 025007. DOI: 10.1088/1681-7575/abe355 (cit. on p. 173).

[159] Pauli Virtanen et al. "SciPy 1.0: Fundamental Algorithms for Scientific Computing in Python". In: *Nature Methods* 17 (2020), pp. 261–272. DOI: 10.1038/s41592-019-0686-2 (cit. on p. 208).

APPENDICES

A

A MONTE CARLO CODE FOR THE SIMULATION OF LS MEASUREMENTS

In order to gain more insight on the nature of the time distribution between photons in a LS measurement, a Monte Carlo simulation code was developed. The main influence to design the software is the Monte Carlo code for TDCR measurements developed by K. Mitev, which was used in chapters 4 and 8. It uses already measured time distributions as an input from which the timing of events in a TDCR detector are sampled. The aim of the newly developed code is rather to simulate the timing of events with as few as possible fundamental parameters and models describing the system. It is capable of accurate simulations of the number and time properties of detected photons created in a two or three PMT detection system. The code was written in the Rust programming language which is a systems programming language, similar to C++, but with improved memory safety. It was chosen because it is fast and strongly typed. Another benefit is the ease with which parallel code can be written.

A.1 CODE BASICS

The code assumes that for each decay there are two types of scintillation light that could be emitted from the scintillation cocktail: prompt and delayed fluorescence. The photons of the prompt fluorescence are assumed to follow an exponential distribution with decay time τ_p:

$$P_p(t) = \tau_p e^{-\tau_p t}, \tag{A.1}$$

where $P_p(t)$ is the probability to observe a prompt photon at time t. This assumption will be good for cocktails with a short rise time of the scintillation light, which is controlled by the non-radiative transfer between the solvent and the primary fluorophore. The sampling from exponential distribution is done using the inverse transform method. The delayed fluorescence is more complex and will be discussed in the following section.

A.1.1 *Modeling the delayed component*

In practice the delayed fluorescence intensity has a complex dependence on time as it is controlled by the diffusion of triplet states. A comprehensive description of the dependence of delayed fluorescence intensity with time is given in the work of King and Voltz [19]. It is also described briefly in subsection 1.1.1. Due to the large number of unknown parameters, there is a difficulty in comparing the proposed equation with

real data. It was therefore not used in this study and an approximate equation for the time dependence of delayed fluorescence was utilized instead. The approximate equation is also proposed by King and Voltz and is derived in the same paper [19]. The simplified equation is:

$$P_d(t) = \frac{\tau_d}{4(1+\tau_d t)^{\frac{3}{2}}}, \tag{A.2}$$

where $P_d(t)$ is the probability to observe a delayed fluorescence photon at time t and τ_d is the delayed fluorescence decay time. Note that, with this equation the probability for delayed fluorescence does not go to zero at $t = 0$ as expected. Delayed fluorescence is produced by interaction of two triplet states yielding a singlet emission and should have some non-negligible rise time [18]. Thus, the used simplified equation could lead to increased probabilities for delayed events in the first nanoseconds after a decay.

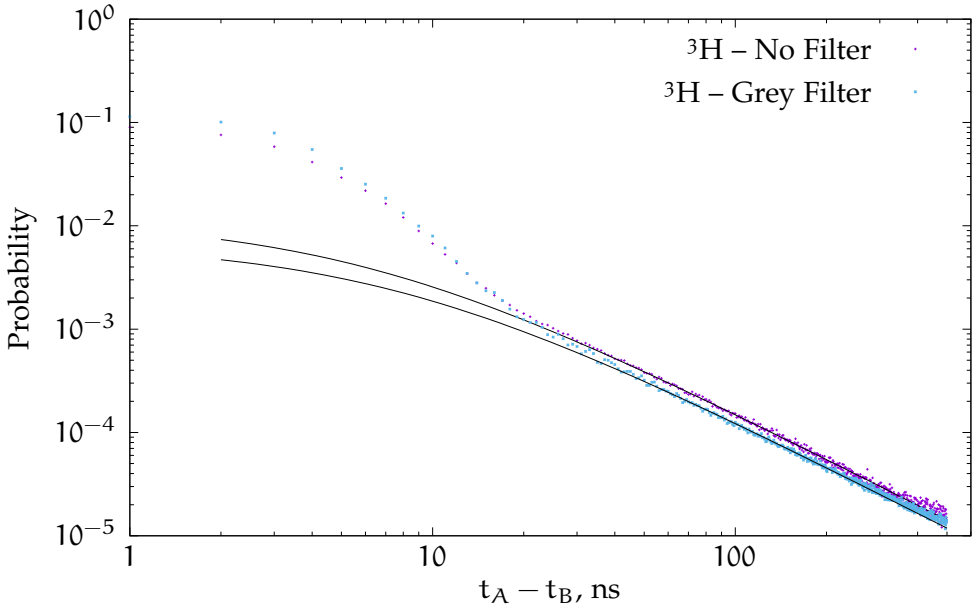

FIGURE A.1: Distribution of the time between two PMTs for two ^{3}H measurements, with and without filter. The black line represents the fit with equation (A.2). The graph is in log-log scale so that the delayed component is better visible.

Due to the approximations and general uncertainties regarding the delayed fluorescence component it is interesting to use the simplified model to fit real data. Consider the time distribution between the primary events in two PMTs that is for times longer than 100 ns. It should be expected with a high probability that, for such long delays, the photon giving the stop signal is a delayed photon. The start trigger could be either from prompt or a delayed photon, but it should be a good approximation to consider that the first photon is prompt, as in general there are not many detected delayed photons. As the typical decay time of the prompt photons is in the order of 3 ns it could be expected that almost all prompt photons arrive in the first ten nanoseconds after the decay. Thus, as time differences of more than 100 ns are considered, the time distribution of the first photon can be considered a δ function. The long tailing of the distribution of the time

between photons in two PMTs in this case should be modeled as the cross-correlation between a δ function and the probability density function of delayed fluorescence given by equation (A.2), which is equal to the probability density function of the delayed fluorescence only. In short, the simplified model should describe the time distribution after a long enough time that the distribution of prompt fluorescence can be deemed negligible.

In Figure A.1 two measurements of ^{3}H with and without a filter are shown. The time distributions are fitted using equation (A.2). A very good agreement between the data and the model can be observed after time differences larger than 50 ns.

In the Monte Carlo code, the sampling from the delayed fluorescence distribution is done by the inverse transform method. The inverse of equation (A.2) is:

$$X = \frac{(1-2R)^{-2}-1}{\lambda_d}, \tag{A.3}$$

where R is a uniformly distributed random number in the interval $[0,1]$, λ_d is the decay constant of delayed fluorescence, and X has the probability distribution of the delayed component.

A.1.2 *Ionization quenching in the Monte Carlo code*

In order to calculate the number of detected photons from the energy deposited in the cocktail, the Monte Carlo code uses the free parameter model described in [2, 3]. The scintillator non-linearity is accounted for using Birks' ionization quenching formula [7]:

$$Q(E) = \frac{1}{E}\int_0^E \frac{dE}{1+kB(dE/dx)}, \tag{A.4}$$

where dE/dx is the electron stopping power for the given cocktail parameters and kB is the Birks parameter. The semi-empirical ionization quenching formula describes the prompt fluorescence intensity as a function of the deposited in the scintillator energy. Note that, the intensity of delayed fluorescence has been reported to have less or even no dependence on the deposited energy [7]. Thus ionization quenching was considered only for prompt fluorescence.

A.2 INPUT OF THE CODE

The input currently is given as command line arguments to the executable code. The parameters which are given to the code are:

- Number of Monte Carlo runs
- Prompt fluorescence FOM in units photoelectrons per keV
- Delayed fluorescence FOM in units photoelectrons per keV

- Prompt fluorescence decay constant in units s^{-1}
- Delayed fluorescence decay constant in units s^{-1}
- Gaussian jitter standard deviation in units ns
- Relative efficiencies of the PMTs
- Spectrum file with two columns: energy in eV and probability

A.2.1 *Simulation*

After the code is started it reads the spectrum file and the effective energy (after ionization quenching is taken into account) is calculated and stored into a list for quick access later. The flow of the MC simulation is the following:

1. An energy E is sampled from the spectrum of the nuclide, as provided by the BetaShape code [107, 108].
2. The average number of prompt fluorescence photons for the sampled energy E is calculated as:

$$\bar{n}_p = EQ(E)\varphi_p, \tag{A.5}$$

   where φ_p is the free parameter measured in photoelectrons per keV effective energy released in the cocktail.
3. The average number of the delayed fluorescence photons for the sampled energy E is calculated as:

$$\bar{n}_d = E\varphi_d, \tag{A.6}$$

   where φ_d is the free parameter for the delayed fluorescence.
4. The number of delayed fluorescence photons n_d and the number of prompt fluorescence photons n_p for the current decay are sampled from Poisson distributions with averages $\bar{n}_d$ and $\bar{n}_p$, respectively.
5. The timestamps of each of the prompt and delayed photons is sampled from the appropriate distribution, equations (A.1) and (A.2) respectively. The PMT that was hit is sampled from a uniform distribution, where the parts are the relative PMT efficiencies.
6. The detected photons are sorted according to their timestamp and the primary event in each PMT is identified.
7. A value is sampled from Gaussian distribution with mean μ and standard deviation σ for each of the three channels and is added to the timestamps of the primary events. The purpose of this step is to model the time jitter introduced by the detection system in the timing of the events.

8. The timestamps of the primary events are saved in list-mode files (one for each PMT channel), similar to the comma-separated values files produced by a CAEN digitizer, i. e., one entry per line containing the timestamp of the event in picoseconds after the start.

9. The time to the next decay is sampled from an exponential distribution with the decay time of the simulated nuclide as a parameter.

10. The loop returns to step one and the steps are repeated until the number of requested decays is reached.

The list-mode files produced by the Monte Carlo code can later be analyzed by the same LIST_MODE_ANALYSIS software used for the CAEN digitizer files. A short summary of the code is presented in Chapter 3.

A.3 COMPARING THE MONTE CARLO CODE TO REAL DATA

Studies on two LS sources have been performed, in order to compare the Monte Carlo simulation to real measurements. The sources are ^{3}H and ^{14}C in a Toluene + PPO cocktail. The measurements were performed on a three-PMT LS detector connected to a CAEN DT5751 digitizer. The list-mode files were analyzed with the dedicated software to obtain the distribution of the time differences between PMTs A and B.

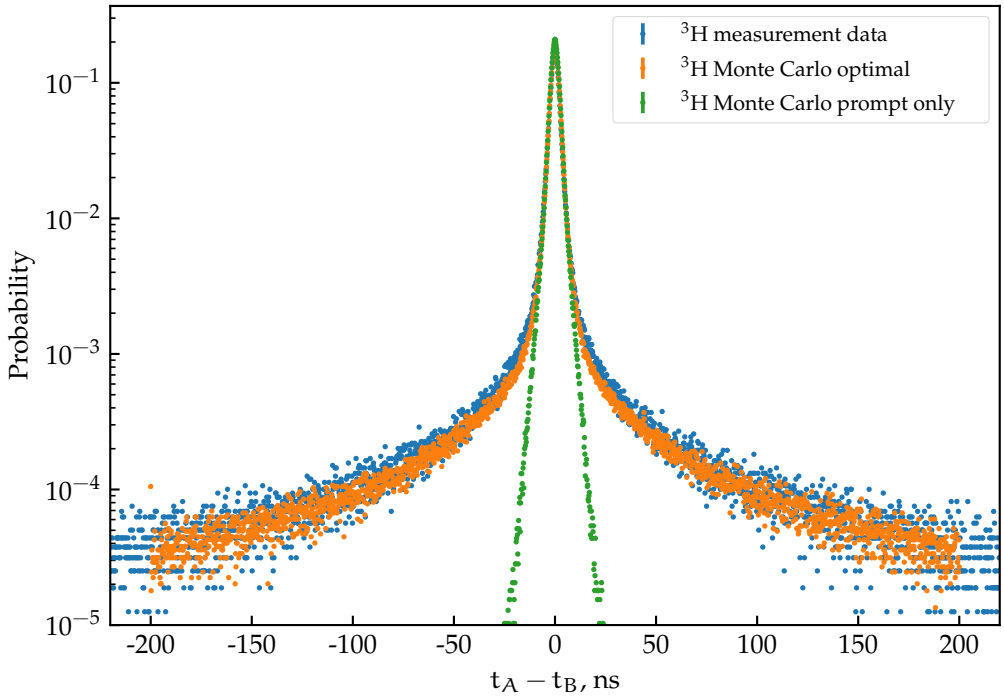

FIGURE A.2: Comparison between the Monte Carlo simulation and a real measurement of ^{3}H. The data in green is a Monte Carlo simulation of the prompt component only.

In order to compare the simulation and real ^{3}H measurements, the Monte Carlo code was used to generate artificial data with various input parameters. Both the Monte Carlo and real measurement data were visualized on the same graph, and the parameters of the simulation were varied until a satisfactory agreement was reached. The optimal parameters of the code that produced the best agreement between the two sets of data are: FOM equal to 1.0 ph.e^{-}/keV for the prompt fluorescence and to 0.25 ph.e^{-}/keV for the delayed fluorescence, 2.5 ns prompt decay constant, 10 ns delayed decay constant and 1.2 ns standard deviation of the gaussian jitter. The optimal Monte Carlo simulation and the real data are shown in Figure A.2. Another artificial set of data was produced with the same parameters, but with a FOM of the delayed fluorescence equal to zero, i. e., removing its contribution. It is interesting to note that for ^{3}H it seems that all the signals that come after 20 ns are due to the delayed fluorescence.

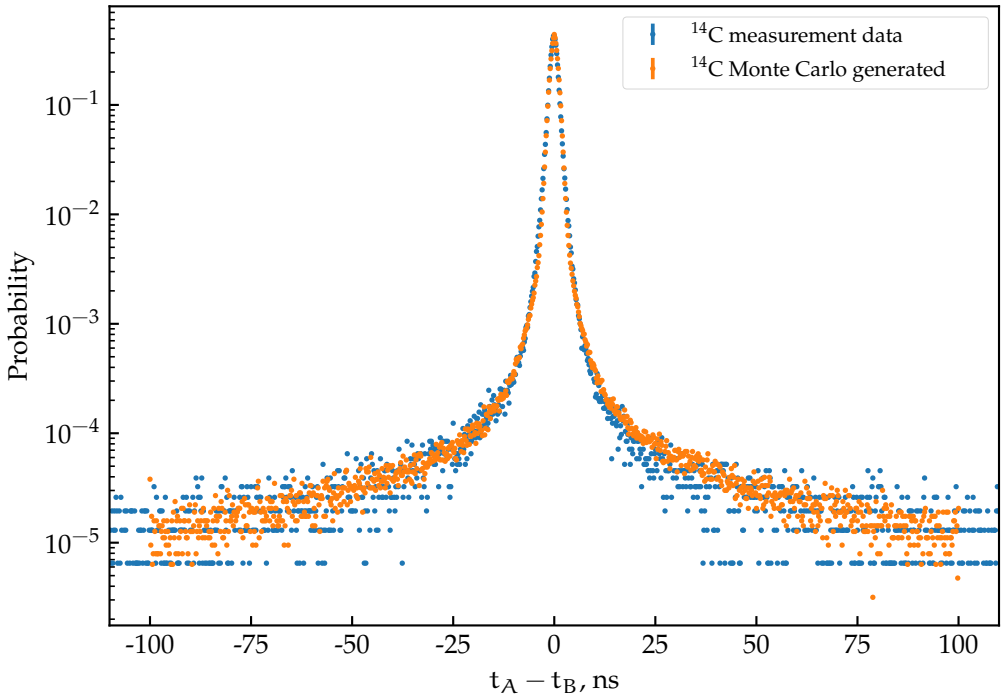

FIGURE A.3: Comparison between the Monte Carlo simulation and a real measurement of ^{14}C.

The same comparison was done for the ^{14}C source. The Monte Carlo parameters were optimized manually until the following was reached: FOM equal to 0.7 ph.e^{-}/keV for the prompt fluorescence and to 0.25 ph.e^{-}/keV for the delayed fluorescence, 3.0 ns prompt decay constant, 10 ns delayed decay constant and 0.8 ns standard deviation of the gaussian jitter. In fact, the only difference with the ^{3}H source is a slightly lower gaussian time jitter and prompt FOM, and a longer prompt decay constant. The optimal parameters found for ^{3}H and ^{14}C seem reasonable and do not contradict with what we have seen in practice thus far.

A.4 DISCUSSION ON THE MONTE CARLO CODE

The main purpose of the Monte Carlo code is to provide artificial data with exactly known physics and parameters. It was used to test the ability of the TDCR model to reconstruct the input activity under various conditions, e. g., changing the ratio of delayed and prompt fluorescence. The results from this study are shown in Chapter 9. The code was also used to validate a theoretical derivation that aims to describe the prompt fluorescence time distribution analytically.

B

CODE FOR THE CALCULATION OF THE CROSS-CORRELATION EQUATION

The cross-correlation equation consists of a sum of two exponentially modified gaussian distributions summed through a cascade of a binomial distribution, Poisson distribution and the nuclide spectrum. In order to use the cross-correlation distribution to fit real data, equation (5.2) has to be calculated for a number of different times from $-20\ldots-30$ to $20\ldots30$ ns with a step of $0.1\ldots1$ ns. The fitting would also require the evaluation of the analytical equation for different parameters which could easily go to ≈ 1000 iterations for a single fit. Such calculations require the use of a fast computer program.

One such computer program was developed in the Rust programming language. Due to the complexity of the cross-correlation distribution, without any optimizations, one calculation of the equations takes 10 – 20 seconds for ^{3}H and more than a minute for ^{14}C on a relatively powerful laptop with Intel i7-7700HQ 3.8 GHz 4-physical/8-logical core processor. In order to calculate the distribution in a reasonable time, however, the code must be optimized to increase the execution speed.

B.1 OPTIMIZATION OF THE CODE

The first optimization that was done was to parallelize the computer code. To output the whole distribution, i. e., the distribution in a set of points from $\Delta t = \Delta t_{min}$ to $\Delta t = \Delta t_{max}$, the code has to calculate equation (5.34) for each Δt with a given step. As the individual calculations are independant, it is relatively straightforward to parallelize the calculations. The total bins in which the cross-correlation distribution is to be calculated are distributed among a number of threads and each thread calculates the value of equation (5.2) and stores the value in an array – one element per bin. At the end of the execution the arrays from all threads are combined into one and the total distribution is given. On the same laptop, the parallel code reduces the execution time by a factor of 8. It is important to note that no information is lost by the parallelization and thus this optimization comes "for free".

The next possible time reduction can be made in the poissonian sum. As the sum in the Poisson distribution goes to infinity, the calculation has to be cut short somewhere. In order to see where would be the optimal trade-off between the execution time and producing the correct time distribution, tests with different cut-offs of the terms in the sum were performed. The meaning of the cut-off is to skip all calculations for which the Poisson coefficient is less than a given value, e. g., 10^{-10}, 10^{-6}, 10^{-3}, 10^{-2}, etc. To test the optimal cut-off, the time distributions of ^{3}H and ^{63}Ni were calculated for different

cut-offs. The ^{3}H results are shown in Figure B.1. The figure on the left shows the whole range of the distribution in log-scale.

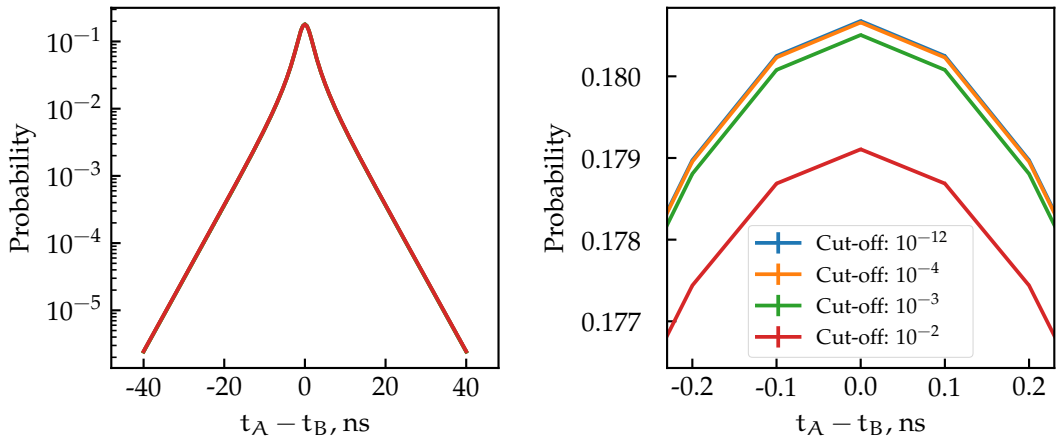

FIGURE B.1: Calculation of the analytical equation at different cut-offs of the infinite sum of the Poisson distribution. The figure on the left is the calculated distribution in log-scale. On the right the same distributions are shown, emphasizing the vicinity of the peak.

No obvious difference between cut-offs from 10^{-12} to 10^{-2} can be seen. Zooming near the peak shows that at 10^{-2} a discrepancy can be seen, however, all other points are well grouped together. The best acuracy compared to the execution time seems to be at a cut-off of 10^{-3}. The results for ^{63}Ni are very similar and not shown here. With these settings the calculation of a typical ^{3}H distribution takes about 0.8 s to finish and for ^{63}Ni — 5.3 s. The improvement with this optimization is already around 20× compared to the non-optimized parallel code, but still needs to be better to be practical.

The other possibility to reduce the computation time is to reduce the resolution of the spectrum input file. Thus far, the spectra that have been used are provided by the BetaShape program [107, 108]. The resolution of the output of the program is such that the spectrum is divided in around 320 bins. In order to simplify the spectrum a small program was developed that takes the BetaShape spectrum and divides into a given number of variable sized bins. The bin size is proportional to the derivative of the function in that region. The value in the bin, assigned to the center of the bin, is the average value of the BetaShape spectrum within the bin. A few examples with different number of bins are shown in Figure B.2 where the simplified spectrum is shown in orange and the original ^{3}H spectrum with blue. An extreme case with only 8 bins can be seen on the bottom.

The idea behind is to keep as much information from the original spectrum as possible. By using variable sized bins the spectrum will be discribed better where it changes rapidly. In order to test the optimal trade-off between execution speed and the number of bins in the spectrum, simplified spectra with 5 to 312 (the maximum number) bins were generated. The analytical equation was calculated with all different spectra to see the influence of the number of bins on the shape of the distribution. The

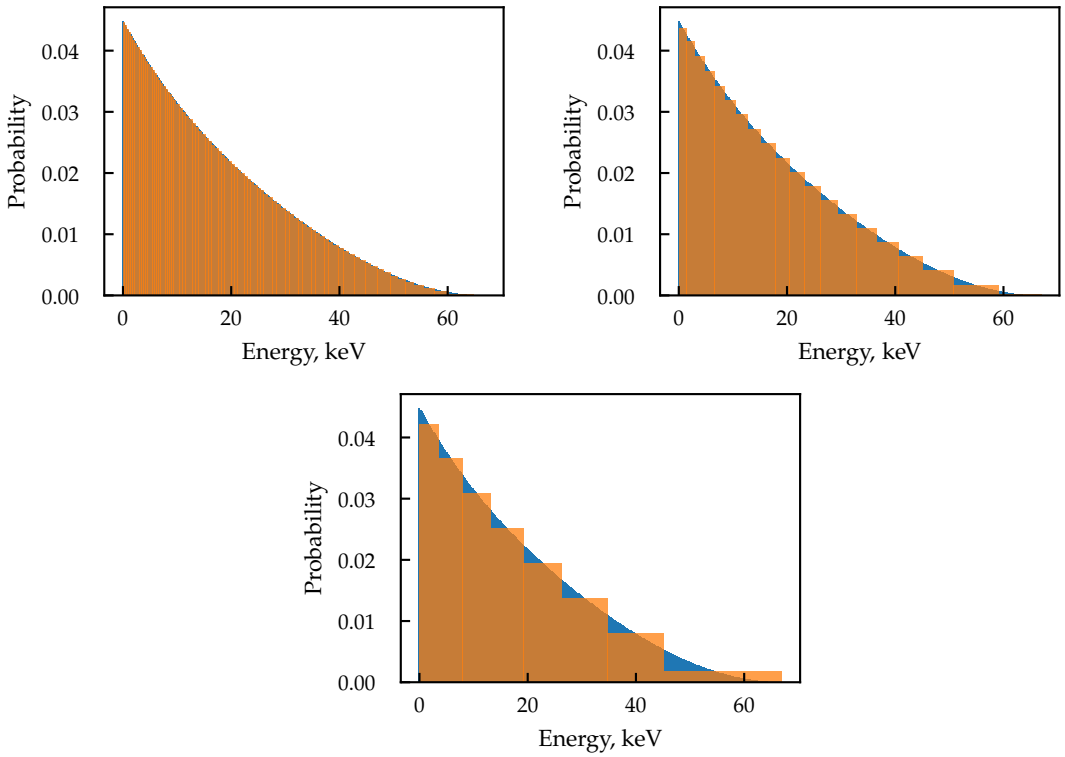

FIGURE B.2: Re-binning of the spectrum of ^{63}Ni into a smaller number of variable sized bins. The original spectrum (blue) has 320 bins. The resulting spectra with reduced number of bins are shown in orange as follows: top left – 100 bins, top right – 20 bins, bottom – 8 bins.

tests were performed with ^{3}H and ^{63}Ni spectra and were done for −40 to 40 ns time distribution and 30 ps bin size. No optimizations on the Poisson cut-off were used, i. e., the cut-off is 10^{-12}.

Some of the results for ^{3}H are shown in Figure B.3. The left subfigure shows the entire time distribution and the right subfigure shows a zoom in on the peak area. The spectrum with 20 bins seems to be the optimal as it overlaps with the reference spectrum with 312 bins. Similar results were obtained for ^{63}Ni. The execution time decreases from 4 s for the original spectrum to 0.3 s for 20 bins, a reduction of 12. For ^{63}Ni the execution time decreases from 72 s to 1.7 s.

The final optimizations of the code that calculates equation 5.2 are: 10^{-4} cut-off of the Poisson sum and a simplified spectrum with 20 variable size bins. One calculation of a ^{3}H time distribution from −40 to 40 ns with 0.1 ns bin size takes approximately 0.09 seconds. The same calculation for ^{63}Ni requires 0.32 seconds. These final values are acceptable for the use of the code for fitting experimental spectra. The final version of the code including the stated optimizations will be referred to as XCORR_CALC.

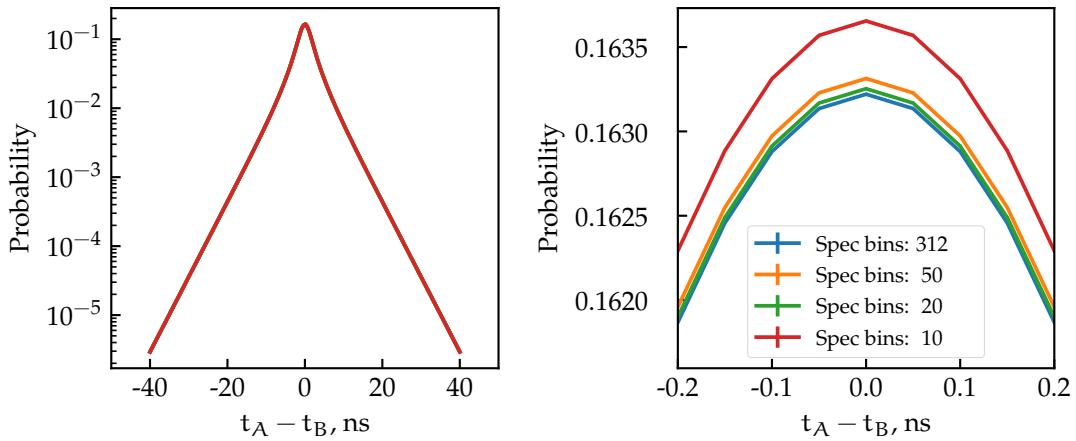

FIGURE B.3: Effect of the re-binning of the spectrum of ^{3}H on the shape of the time distribution. The spectrum with 312 bins was used as a reference. On the left figure, where the total distribution is shown, all distributions overlap. The difference is more visible if the peak area is zoomed (right).

B.2 FITTING A MONTE CARLO GENERATED DISTRIBUTION

The analytical equations and Monte Carlo were compared with using exactly the same parameters in both. Thus far, the agreement between the two has been exceptional. In a more realistic scenario, the optimized XCORR_CALC code has to be used, however, due to its faster execution time. Despite that the accuracy of the calculation was always kept in mind when optimizing the code, it is possible that some discrepancy was introduced in comparison with the Monte Carlo code. This was checked by comparison between the optimized XCORR_CALC and the Monte Carlo, which is described hereafter.

The Monte Carlo code was used to generate the time distribution of ^{3}H with parameters: $1/\lambda = 4.0$ ns, $\sigma = 0.6$ ns, $\mu = 0.0$ ns and a FOM = 0.6 keV^{-1}. In order to fit the analytical distribution to experimental data, a small routine that varies the input parameters of the XCORR_CALC code was developed. The routine uses the Nelder-Mead (downhill-simplex) optimization method from the SciPy Python package [159]. The cross-correlation equation (5.2) was fitted to the data with the same fixed λ, σ and μ parameters. The FOM was left as a free parameter. The purpose of this comparison is twofold: one to test the accuracy of the optimized code for the calculation of the analytical equation XCORR_CALC, and two to test the code that fits the equation to experimental data. The results of the fit are shown in Figure B.4.

An excellent agreement between the XCORR_CALC code and the Monte Carlo simulation can be seen. The minimization algrorithm reports a value for the FOM $\varphi = 0.6006(12)$ keV^{-1}. This agrees well with the input of the Monte Carlo code. The comparison shows that the optimized code for the calculation of equation (5.2) and the associated fitting routine are able to reconstruct the FOM parameter generated by the Monte Carlo code, by fixing all other parameters.

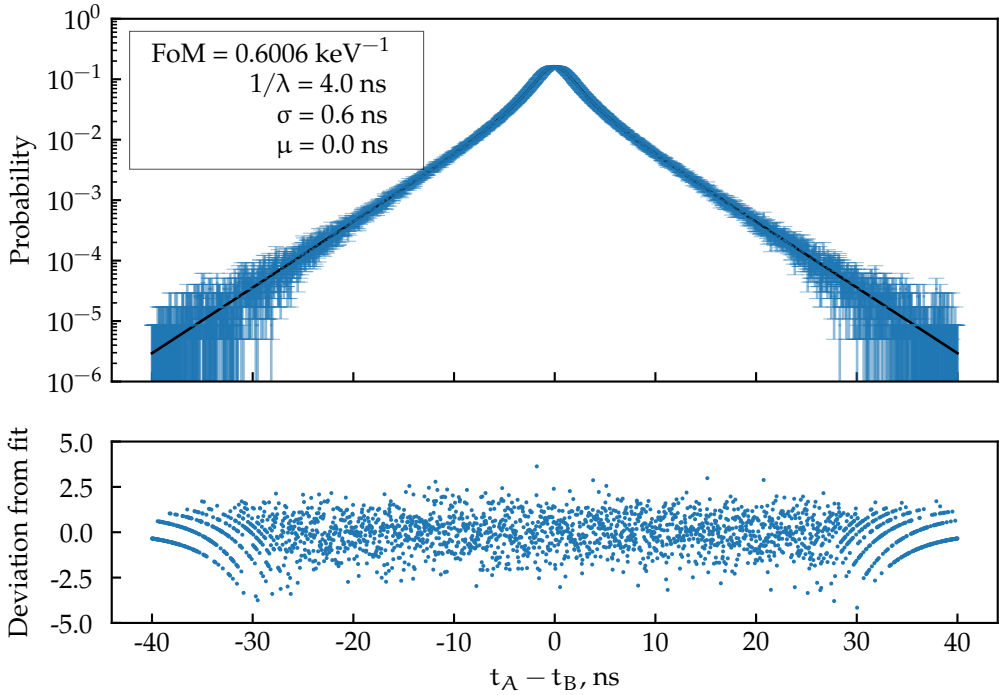

FIGURE B.4: Fit of a ^{3}H cross-correlation spectrum using equation (5.2), as calculated by the XCORR_CALC code, using the downhill-simplex optimization algorithm. The data points are generated using the Monte Carlo code. The input FOM parameter is 0.6 keV^{-1}.

The Monte Carlo simulated data could provide more information on how to optimally fit experimental spectra. In the fit in Figure B.4, all parameters except the FOM were fixed. It is interesting to test wether if all fit parameters are left to vary freely, their correct values can be obtained. The artificial data has a great advantage here, because the exact values of all parameters are known, and the cross-correlation distribution can be obtained with a very high resolution for a high number of events.

The Monte Carlo code was used to simulate a measurement of ^{63}Ni with parameters: $1/\lambda = 4.0$ ns, $\sigma = 0.6$ ns, $\mu = 0.0$ ns and a FOM $\varphi = 0.5334$ keV^{-1}. The generated list mode file was processed with the LIST_MODE_ANALYSIS program with 31 ps bin size and the total number of processed coincidences are 10^8. The obtained cross-correlation distribution is with higher quality than what is experimentally possible, so fitting it with equation 5.2 would give an upper bound on what accuracy can be expected from the obtained optimal fit parameters. The distribution was fitted and all parameters were left to vary. The best fit is shown in Figure B.5

There are several observations that can be made from the fit with all parameters left as free parameters. The residuals of the fit show a slight pattern, but, nevertheless, most residuals stll fall well within $\pm 3\sigma$. The parameters σ and μ that were optimized by the minimization algorithm agree well with the input Monte Carlo parameters. The other two parameters of interest, however, are significantly different than their true value. The decay constant of the scintillator is 4% lower, and the FOM 5.5% lower, than what

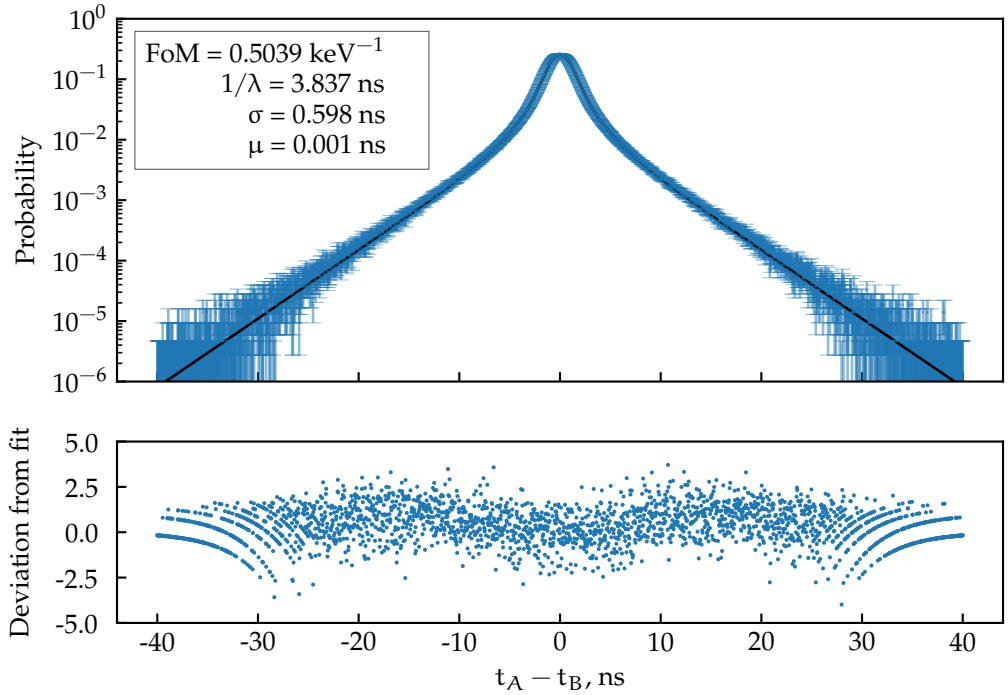

FIGURE B.5: Fit of a ^{63}Ni cross-correlation spectrum using equation (5.2), as calculated by the XCORR_CALC code, using the downhill-simplex optimization algorithm. The data points are generated using the Monte Carlo code. The input parameters are FOM = 0.5334 keV^{-1}, $1/\lambda = 4$ ns and $\sigma = 0.6$ ns.

was generated by the simulation. The fitting algorithm reports an 88.8% correlation between the two parameters. In comparison, the correlation between the FOM and σ is 43.1%. From this comparison it seems that a fit of a single experimental cross-correlation distribution will not be sufficient to obtain all of the distribution's parameters. What is posiible is to obtain the centroid and standard deviation of the gaussian response function of the detector. The FOM and decay constant of the scintillator are highly correlated, however, and one of the two parameters must be fixed from another method or measurement in order to obtain the other.

C

SUPPLEMENTARY INFORMATION

C.1 AVAILABLE OPTIONS OF THE LIST_MODE_ANALYSIS SOFTWARE

The help output of the LIST_MODE_ANALYSIS software is shown in listing C.1. On the command line it is invoked by `list_mode_analysis -h`. The options with values in pink should be input by the user. The options with a single dash can be stacked, thus `list_mode_analysis -c -s -P -e` is equivalent to `list_mode_analysis -csPe`. The order of the options does not matter except for the `-paths` option which should always be last and it sholud contain all paths to folders containing list-mode files that need to be analyzed.

Listing C.1: LIST_MODE_ANALYSIS software – list of command line options. The options with associated text in triangular brackets require a number or a list of numbers, e. g., `-ref-channel B` or `-sca 10 250`. All other options are flags that are false by default.

```
Usage:
  list_mode_analysis [OPTIONS] [PATH] CW

Rust program that can be used to analyze \textsmaller{CAEN} list-
    mode files

Positional arguments:
  path                  Path to \textsmaller{CAEN} files folder
  cw                    Coincidence window duration (default 200),
       ns

Optional arguments:
  -h,--help                     Show this help message and exit
  -V,--version                  Show version
  -d,--dt DT                    Dead-time duration (default 10 000),
       ns
  --energy-hist-size SIZE       Gamma Energy upper limit (default
     2^14), LSB
  --energy-bin-size SIZE        Gamma energy bin size (default 1),
     LSB
  -L,--hw HW                    Histogram size in channels (default:
      1000)
  -b,--bin-size SIZE            Bin size in nanoseconds (default: 1)
     , ns
  -l,--time-limit TIME          Break analysis early (default: 0 [
     whole file]), s
```

```
-g,--gamma-veto                 Gate on gamma channel (default:
    false)
--gamma-only                    Analyze Gamma channel only (default:
     false)
-c,--correct-acc                Correct for accidental coincidences
    (default: false)
-s,--show-time-hist             Show time distribution histogram
-P,--show-pmt-energy            Show the PMT energies histogram
-e,--show-energy-hist           Show gamma energy spectrum
--hide-config                   Hide the output the configuration of
     the run
-r,--hide-tdcr                  Hide TDCR output
-T,--triples                    Show time dist histogram for T
    events
-D,--doubles                    Show time dist histogram for D
    events
-i,--ignore-third               Ignore the third channel. Set
    reference and secodary

                                channels if using this option
-a,--asym-doubles               One sided doubles histogram
--triple-veto                   Count only pure double coincidences
    for histogram
-n,--no-live                    Disable live cps printing (prints
    only end result)
--ref-channel CHANNEL           Reference channel for time
    difference histogram
--sec-channel CHANNEL           Secondary channel for time
    difference histogram
--sca-A CHANNEL                 PMT A energy range (default: 0
    16385), channels
--sca-B CHANNEL                 PMT B energy range (default: 0
    16385), channels
--sca-C CHANNEL                 PMT C energy range (default: 0
    16385), channels
--sca CHANNEL                   Gamma energy range (default: 0
    16385), channels
--gain GAINS                    Gain multiplier per channel (default
    : 1 1 1 1)
--paths PATHS                   Paths to analyze. Should be last
    option.
```

C.2 ADDITIONAL FIGURES FOR THE CROSS-CORRELATION METHOD

Results from the Compton coincidences experimental setup on cross-correlation measurements of Toluene+PPO (Figure C.1) and HionicFluor (Figure C.2) cocktails. Compared to the UltimaGold and UltimaGold LLT cocktails, these two have a significantly shorter prompt fluorescence decay constant, close to 2 ns.

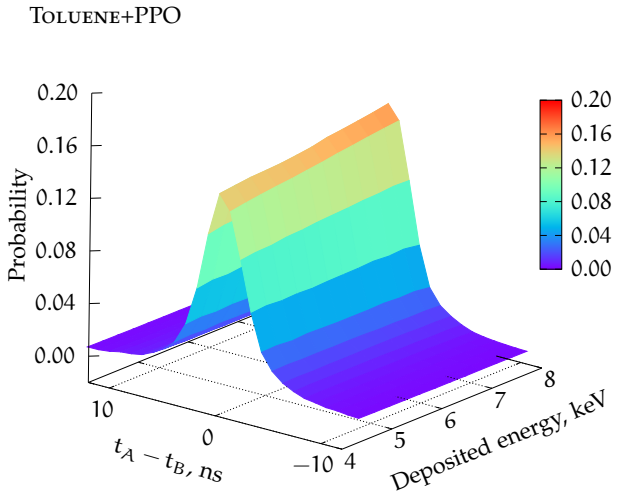

FIGURE C.1: Cross-correlation spectra D(Δt) of Toluene + PPO LS cocktail acquired by the Compton coincidences method.

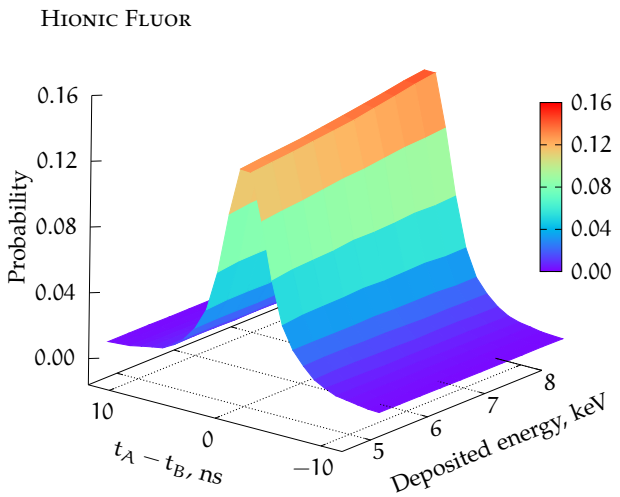

FIGURE C.2: Cross-correlation spectra D(Δt) of HionicFluor LS cocktail acquired by the Compton coincidences method.

FUNDING

The work on this thesis was supported by:

- The Bulgarian National Scientific Research Fund under contract № KP–06–H38/9 from 06.12.19 (TDCX).
- The French "Laboratoire National de Métrologie et d'Essais" (LNE).
- The Scientific Research Fund of Sofia University "St. Kliment Ohridski" under contract № 80-10-16/18.03.2020.
- The European Metrology Program for Innovation and Research, JRP-Contract 16ENV10 (MetroRADON).
- The Bulgarian Science Fund under contract DFNI T02/13 (Polyrad).

The financial support is gratefully acknowledged.